Role of the unstructured N-terminus of the centromere binding protein ParG in mediating segregation of the multidrug resistance plasmid TP228

Madhuri Tanaji Barge

PhD

University of York

Biology

January 2015

Abstract

TP228 is a large low copy number plasmid harbouring the *parFGH* partition cassette. The centromere-like site *parH* is located upstream of the *parFG* genes. ParF is a Walker-type ATPase of the ParA superfamily. ParG is a centromere binding protein and a transcriptional repressor of the *parFG* genes. ParF associates with ParG bound to *parH* forming the segrosome complex. It has been recently observed that ParF oscillates over the nucleoid in the presence of the entire *parFGH* system and oscillation is responsible for plasmid segregation. ParG is a dimeric protein: each monomer consists of a folded ribbon-helix-helix domain and an unstructured N-terminal tail. ParG enhances ParF ATPase activity and promotes ParF self-assembly through its flexible N-terminus.

In the present study, the role of the ParG N-terminus in plasmid partition was dissected. Residues crucial for plasmid partition were identified and found to form three clusters within the tail. One cluster is located at the extreme tip of the N-terminus that is the most flexible region. The second cluster is present in a linker-type region around amino acids 11-12-13 and the third is positioned in the arginine finger loop. When ParG mutant proteins were purified and characterised, they were all found to be efficient in DNA binding, transcriptional repression and in enhancing ParF polymerization. However, all the ParG mutants were impaired in stimulating ParF ATPase activity. Alteration of the residues in the tip and linker region resulted into a weaker interaction with ParF. The mutants were further investigated by using confocal and super resolution microscopy to visualize protein and plasmid positioning in the cell. Time-lapse experiments showed plasmids were static over time and that ParF oscillation over the nucleoid was abolished in the presence of mutant proteins. All the three clusters of the N-terminal tail are responsible for stimulating ParF ATPase activity and failure to do so may lead to lack of ParF oscillation. It is possible that the residues in the ParG N-terminus are strategically placed to carry out interaction and activation functions towards the common goal of coordinated interplay with ParF for efficient plasmid segregation. The data indicate that, a functional ParG N-terminal tail is a prerequisite for ParF oscillation and plasmid segregation. Based on these findings, a novel plasmid partition model is proposed which may apply to ParA-mediated partition in other plasmid systems.

Table of Contents

List of Figures

List of Tables

List of accompanying material

1. **CD for microscopy movies S1-S18**

2. **Publication-** Schumacher, M. A., Q. Ye, M. T. Barge, M. Zampini, D. Barillà and F. Hayes (2012) . Structural mechanism of ATP induced polymerization of the partition factor ParF: implications for DNA segregation. *J Biol Chem*.

Acknowledgements

First and foremost, I wish to thank my supervisor Dr. Daniella Barillà for giving me the opportunity to work on a fantastic project in her equally fantastic lab. She encouraged and challenged me intellectually throughout this project, never accepting anything less than my best efforts. Her great support, both on personal and professional level, at every stage of this PhD made this journey possible and pleasant.

I would also like to thank my TAP members Prof. Neil Bruce and Prof. Jennifer Potts. Thanks to the Overseas Research Scholarship for awarding me this prestigious studentship that made this PhD possible. As an international student, I cannot thank enough the Biology graduate office for their support, especially Ms. Julie Knox. I would also like to thank Dr. Finbarr Hayes for timely help, Dr. Marcus Posch for super resolution microscopy support, Dr. Andrew Leech for running the SEC-MALLS experiment and Dr. Massimiliano Zampini, for guiding me with CDO reporter assay. My earnest thanks to Ganesh, Pamji, Irene, Kate, David and Birgit for reading drafts and suggesting corrections at various stages of writing. A big thanks to all the present and past members of the Daniella Barillà lab (Fernando, Anne, Brett, Gina and Ben) and people on L1 corridor (especially Judith) because of whom my time in the lab and in York was memorable.

I also want to express my gratitude to all my teachers, friends and family. A warm thanks to my siblings Mithila, Minakshi and Raviraj for being always by my side. This thesis would have been written in half the time had it not been for my daughter, but I would not have been so content person so thanks Siya for being the joy of our life. I would like to express my gratitude to my father-in-law Mr. Suresh Kanase for keeping me motivated and encouraged throughout this time. Huge thanks to my beloved husband Dr. Nilesh Kanase who endured every moment of this journey with great patience, love and care. Last but not the least my greatest thanks to my parents Mrs. Saraswati and Mr. Tanaji Barge who regularly sacrificed their comforts for the good future of their children. This thesis is dedicated to you “aai” and “kaka”, as this PhD is your dream more than mine.

Author’s declaration

I hereby declare that the data presented in this thesis is the result of my own work. The contributions from others are clearly specified wherever required. No material contained in this thesis has yet been presented anywhere else.

Chapter 1: Introduction

1.1 Plasmids

Plasmids are extra-chromosomal genetic elements (Lederberg, 1952) present mostly in bacteria and some lower eukaryotes. Most plasmids are double-stranded circular entities, which are physically separated from the host chromosome. Plasmids are not essential for the growth of the host under normal conditions, so they can be accommodated or removed from the cell without any lethal effect (Clowes, 1972). Plasmids can be divided into conjugative and non-conjugative types. Conjugative plasmids encode *tra* genes that can induce conjugation and the transfer of plasmids to bacteria. There are various types of plasmids depending upon the functions. R plasmid encodes antibiotics, F plasmid facilitates transfer of chromosomal DNA, col plasmid produces bacteriocin and the virulence plasmid causes diseases in its host. Plasmids sizes range from 1 to 1000 kilobase pairs (kbp). Plasmids also vary in their copy numbers. Low copy number plasmids like P1 and F are maintained at one to two per cell whereas in medium to high copy number plasmids like ColE1 over 50-100 copies per cell are found. Plasmids exhibit organized and independent replication machinery and are stably transferred to the daughter cells. The plasmid has to replicate its DNA once per cell cycle to transfer its copy to the daughter cells on cell division. Irrespective of its independent replication system, plasmids also use host components during replication.

1.2 Multidrug resistance plasmids

Among the many interests in the study of plasmids, one is the fact that plasmids are small and relatively simple in their genetic composition and can be easily modified and used in recombinant DNA technology. Another important feature of plasmids is their ability to confer crucial properties like virulence and antibiotic resistance to bacteria. Concern about antibiotics resistance was imminent since the discovery of penicillin in 1928, but a marked increase in this phenomenon has been seen in the last three decades. Antibiotics act on bacteria by using different modes like impairing or inhibiting cell wall synthesis, protein synthesis and targeting the DNA (Neu, 1992). Resistance to antibiotics can be developed through different mechanisms, for example, by utilizing changes in bacterial chromosomes and/or more rarely, by changing expression of some of the chromosomal genes. Another method is by acquisition of mobile genetic elements such as transposons, which can

integrate in the chromosome and can harbour resistance genes. But the most widely occurring mode is the presence of drug resistant plasmid (Johnson and Nolan, 2009). Plasmids can transfer the resistance laterally or horizontally i.e. intra and inter transfer both in species and genera is widely seen (Carattoli, 2009) and is found in Gram-positive as well as Gram-negative bacteria. Plasmid mediated resistance is observed in a number of antibiotic classes ranging from β-lactams (e.g. penicillin, ampicillin and cephalosporin), amino glycosides (e.g. gentamycin), various tetracycline drugs, macrolides and chloramphenicol (Williams and Hergenrother, 2008). The presence of antibiotic selective pressure for longer duration in bacterial environment results in emergence of drug resistance. Increase in the prevalence of drug resistance may be attributed to various factors such as generous use of antibiotics, inconsistent prescription practices among physicians worldwide, patient demands for antibiotics in viral illness and extensive utilization of antibiotics in animal feeds. The study of the drug resistance plasmid has thus becomes a very important approach to control infection. These studies will help to devise a strategy for restraining the occurrence of drug resistance and reduce the limitation of antibiotic chemotherapy.

1.3 Plasmid replication

Similar to chromosome, plasmids also contain an origin of replication, *ori* which is a *cis*-acting region where replication starts and proteins involved in replication bind (Bramhill and Kornberg, 1988). Most of the plasmids employ Rep proteins which are specific to the plasmid origin and which are encoded on plasmid DNA (Actis *et al.*, 1999). The Rep protein has two motifs, a leucine zipper like (LZ) motif for protein-protein interaction which regulates monomer-dimer equilibrium and a DNA binding helix-turn-helix motif (HTH) (Garcia de Viedma *et al.*, 1996, Garcia de Viedma *et al.*, 1995b). Rep protein along with the *ori* region also binds to the inverted repeats of the *rep* promoter region where it acts as an auto-regulator (Garcia de Viedma *et al.*, 1995a). There are three general mechanisms involved in plasmid replication which are theta, rolling circle and strand displacement (del Solar *et al.*, 1998).

The system under investigation in this project is of plasmid TP228. The partition cassette *parFGH* of plasmid TP228 is cloned into a vector pFH450. This vector contains two origins of replication i.e. P1 for low and pMB1 for medium copy number. P1 and R2 exhibit theta type replication (Kiewiet et al., 1993). P1 type ori sites contain directly repeated sequences, termed iterons. Iterons mediated replication is established in many unit or a low copy number plasmid replicons. Iterons contain binding sites for the plasmid-encoded Rep proteins and have properties essential for plasmid replication and its control. Plasmid P1 replication is dependent on the initiator protein RepA and the chromosome encoded DnaA protein. RepA-DNA binding is stimulated by heat shock chaperones. The heat shock chaperons convert RepA dimers into monomers and activate monomeric RepA, which recognizes the iterons in the *ori* site and results in wrapping of the DNA around RepA. DnaA melts the DNA and stimulates the RepA-DNA binding. DnaB favourably loads on to one of the DNA strands and replication proceeds into the unidirectional mode. Efficient replication of P1 requires adenine methylation of the five GATC sites of the origin (del Solar et al., 1998). The pMB1 origin of replication is similar to ColE1 type, which is extensively studied. Replication of ColE1-type plasmids is commenced at a distinctive *ori* site and unlike other plasmid families, instead of plasmid-encoded protein for replication initiation; ColE1 requires the host encoded DNA Polymerase I (PolI), RNA polymerase and ribonuclease RNase H. During the replication process upstream of *ori* region synthesis of an RNA molecule, called RNA II is occurred first. This RNA II extends from its initiation and its 3' end forms a duplex with the template plasmid DNA. RNase H, which digests the RNA II at the replication origin, recognizes RNA II-DNA duplex and generates free 3'-hydroxyl group which acts as primer for DNA synthesis. Once PolI begins the DNA strand synthesis, RNase H digests the remaining part of RNA II, which is still complexed to the template DNA. ColE1 DNA replication proceeds unidirectionally in the θ-shaped manner with the initiation of the lagging strand synthesis at specific ColE1 sites (Actis *et al.*, 1999).

1.4 Plasmid maintenance

After replication, the plasmid copy has to be transferred to the daughter cell stably. There are a number of mechanisms utilised by plasmids to carry out effective

transfer of plasmid copies. Medium to high copy number plasmids are usually transferred to daughter cells by passive diffusion to avoid mis-segregation of plasmids. At the replication level, the copy numbers are maintained for stability. The addiction system, which involves the toxin-antitoxin (TA) encoding genes, helps to kill daughter cells that lack plasmids. Virulence and antibiotic resistance genes encoded by plasmids, force bacteria to retain plasmids for survival. Most importantly, plasmids also harbour dedicated partition mechanisms to ensure their stable inheritance. Importantly, all these mechanisms provide potential targets to fight bacterial infection.

1.4.1 Replication control

It is important for plasmid stability that the copy number is maintained at its standard level. Plasmid copy numbers are controlled at the replication level by two mechanisms, antisense RNA and DNA iterons (Actis *et al.*, 1999). Antisense RNA controls the replication either by keeping Rep protein synthesis in check or by reducing the RNA primer activity. In plasmid R1, CopA which is antisense RNA interacts with CopT, an mRNA for Rep protein and thus produces inhibition of the Rep protein synthesis (Blomberg *et al.*, 1990). Whereas in the plasmid ColE1 (in which antisense RNA was discovered for the first time) the antisense RNA I interacts with the RNA primer, RNA II, and the duplex formed inhibit initiation of replication (Lacatena and Cesareni, 1981). Iterons are repeated sequences present within the plasmid replicons and are found in a variety of plasmids. Rep proteins interact with iterons and exhibit negative control on replication. In plasmid P1, the copy control locus *incA* contains iteron. When bound to *incA,* RepA is proposed to create a steric hindrance at origin of replication, *oriR* which leads to a negative effect on replication (Abeles *et al.*, 1995).

1.4.2 Multimer resolution system

Homologous recombination in circular DNA gives rise to dimers during the crossover process and the multimerization of DNA can cause plasmid instability also called as “dimer catastrophe” (Summers *et al.*, 1993). The site-specific recombination system has been shown to act on the dimers to convert them to monomers and thus helps in maintaining plasmid copy number (Sherratt *et al.*,

1984). These multimer resolution systems are found in both high and low copy number plasmids (Summers and Sherratt, 1984). In multi-copy plasmids like ColE1, the host encoded recombinase proteins XerCD act on plasmid *cer* (resolution) site to convert dimers into monomers. The low copy number P1 plasmid is efficiently maintained owing to its *loxP-cre* site-specific recombination system. P1 Cre recombinase mediates the site-specific recombination between two *loxP* sites on dimer (Austin *et al.*, 1981).

1.4.3 Toxin-antitoxin system

Plasmid maintenance is also ensured by the toxin-antitoxin system, which is also referred to as post-segregational cell killing or addiction system. The principle behind this mechanism is that bacterial cells are killed due to the deleterious effects of plasmid removal. The TA system is based on two components; one is a toxin gene, which encodes a stable protein, and the other encodes an antitoxin. If plasmid-free cells are generated because of any error, the TA complex is still transferred to the bacterial cell. The toxin can cause detrimental effect on bacteria as the neutralising antitoxin is short lived and the source of antitoxin is removed in the plasmid-free environment (Hayes, 2003). TA cassettes are classified into five types (Hayes and Kedzierska, 2014). In type I TA system, small but stable protein acts as a toxin whereas antisense RNA is the antitoxin. In type II TA system, both toxin and antitoxin are small proteins but toxin protein is stable and antitoxin is labile. In type III, RNA acts as an antitoxin and directly interacts with the toxin protein. In type IV, both toxin and antitoxin are proteins but antitoxin prevents toxin from binding to its target. In the last type of TA system, mRNA acts as a toxin on which antitoxin protein acts in the form of ribonuclease and impair the mRNA synthesis. Type I and II TA systems are widely present in the prokaryotes. Plasmid R1 exhibits both types of TA systems. The *hok-sok* system encoded by *parB* locus is a type I system in plasmid R1 where the expression of toxin Hok (host killing) is repressed by the antitoxin antisense RNA sok (suppressor of killing) (Gerdes *et al.*, 1986). The *parD (kid, kis*) locus of plasmid R1 is type II TA system. The toxin Kid is an endoribonuclease which is neutralised by the unstable Kis protein (Diago-Navarro *et al.*, 2010). Plasmid F also shows type II TA system, *ccd* in which the toxin CcdB

inactivates DNA gyrase, which leads to DNA lesions and cell death (Critchlow *et al.*, 1997).

1.4.4. Active plasmid partition system

For low copy number plasmids, it is extremely important that the replicated plasmid copies be transferred to the daughter cells with the highest precision. Extensive work carried out recently in the field of plasmid research contradicts the long standing notion that passive transfer is sufficient for plasmid maintenance from one generation to the next. It is now established that plasmid segregation is an active process and utilises a dedicated partition system (Nordstrom and Austin, 1989). A typical *par* system contains *cis*-acting centromere sequences and two partition genes *parA* and *parB.* The plasmid partition system is the basis of this study and will be discussed in detail with respect to all its aspects in the following sections.

ParAB-*parS* system has also been implicated in bacterial chromosome segregation (Reyes-Lamothe *et al.*, 2012). ParAB-*parS* partition system in *C. crescentus* is essential for viability. Chromosomal *par* systems function similarly to plasmid *par* system.

1.5 Plasmid partition systems

Partition systems are indispensable for segregation of low copy number plasmids. Partition systems are composed of three components, a *cis*-acting centromere-like partition site, a Walker or an actin or tubulin type NTPase and a centromere binding protein (CBP) (Hayes and Barillà, 2006b). The centromere-like site performs its function similarly to the eukaryotic centromere, where a partition complex forms. The partition genes generally designated as *parA* and *parB,* are usually present in the same operon and one of the partition proteins act as auto-regulator of this operon (Mori *et al.*, 1989). It is very important to control the transcription of partition genes for plasmid stability. The plasmid partition system also serves as incompatibility determinants as plasmids with similar partition sites cannot co-exist (Austin and Nordstrom, 1990). In 1983 Austin and Hiraga groups reported the partition mechanism of P1 (ParABS) and F plasmid (SopABC) respectively (Austin and Abeles, 1983);(Ogura and Hiraga, 1983). Subsequently in 1986 the Gerdes group

reported the characterization of partition locus of R1 plasmid (ParMRC) (Gerdes and Molin, 1986). These initial studies into active partition systems were instrumental in the field of low copy number plasmid segregation. Depending on the differences between ATPase, plasmid partition systems can be classified into four different types (Schumacher, 2008).

1.5.1 Type I

Type I partition system exhibits a Walker-type ATPase and is further divided into two subtypes, Ia and Ib. There are a number of differences between Ia and Ib systems with respect to the position of centromere, length of ParA and ParB proteins and mode of transcriptional repression (Schumacher, 2008). Type Ia has centromere downstream of the *par* operon and type Ib shows the centromere upstream of the *par* operon. Type Ia ParA proteins (around 251-420 residues) and ParB proteins (182-336) are longer compared to Ib ParA proteins (208-227 residues) and ParB proteins (46-113 residues) (Schumacher, 2008). ParA proteins of type Ia also act as a transcriptional repressor. This is attributed to their HTH motif at the N-terminal end (Schumacher, 2007). In type Ib systems, instead of ParA proteins, ParB proteins act as transcriptional repressors. Type I ParB proteins do not show any sequence homology with each other. CBPs of Ia are complex and usually contain three domains i.e. NTPase binding (N-terminal), DNA-binding (central, HTH motif) and dimerization domain (C-terminal) (Schumacher, 2007). Type Ib CBPs, although not homologues by their amino acid sequences, show a common Ribbon-Helix-Helix (RHH) structural motif (Schumacher, 2007).

1.5.1.1 Partition system of P1 plasmid

P1 is a unit copy number *E. coli* plasmid. Partition cassette *parABS* is responsible for the stable segregation of plasmid P1. The centromere *parS* of P1 is around 80 bp and present downstream of the *parAB* genes (Figure 1.1). The *parS* site contains A boxes which are formed by four hexamers and B boxes, formed by two heptamers present at two different locations on the DNA and the DNA binding protein ParB recognises both these motifs (Martin *et al.*, 1987). The *parS* site is made available for ParB by the action of Integration Host Factor (IHF) on *parS*. For efficient P1 plasmid partitioning, the spacing between A and B boxes and IHF is crucial (Hayes *et al.*,

1994). IHF introduces a bend in *parS* site on binding to its recognition site and by doing this it facilitates the binding of ParB to the A and B box across the bend of each arm (Hayes and Austin, 1994). IHF and ParB binding at *parS* is cooperative as they increase each other's affinity to the *parS* site by modifying protein-DNA interactions. In the resultant partition complex, *parS* wraps around the ParB-IHF core (Funnell, 1991). ParB binds to *parS* site as a dimer. ParB contains three important regions- HTH domain, a flexible linker and a dimerization domain (Schumacher and Funnell, 2005). ParB dimerization domain is made up of antiparallel sheet and coiled-coil structure. ParB binds to hexamer and heptamer motifs in various combinations, hence the A and B boxes incorporate more ParB dimers or pairing of adjacent plasmids (Vecchiarelli *et al.*, 2007). ParB dimers load on *parS* site and ParB-ParB and ParB-DNA interactions lead to the formation of a large nucleoprotein complex (Bouet *et al.*, 2000). ParA, a Walker-type ATPase does not bind directly to *parS* DNA but is recruited by ParB to form a segrosome. ParA structure contains N-terminal region, HTH motif and the large C-terminal domain for the interaction with ParB (Dunham *et al.*, 2009). The ParA N-terminus contains a DNA binding HTH domain which promotes association with the operator and thus acts as transcriptional repressor (Dunham *et al.*, 2009). ParB also enhances this repression activity. ParA performs various functions depending upon its NTP bound form. ParA-ADP is required for *parAB* operon repression (Davis *et al.*, 1992) whereas ParA-ATP is responsible for dimerization (Davey and Funnell, 1994), and interaction with ParB (Bouet and Funnell, 1999). ATP hydrolysis by ParA is essential for segregation and is also responsible for controlling ATP-ADP switch. ParA binds to non-specific DNA and the ATP-bound form is required for this activity (Vecchiarelli *et al.*, 2010). The intracellular studies of the P1 partition proteins showed that ParB forms foci when it is bound to the *parS* site on plasmid and ParA is required for the movement of plasmid to the cell quarter position (Li and Austin, 2002b). Plasmids harbouring ParB mutations were seen as a stagnant foci at the midcell position and produced division defects in the cell. It is possible that the plasmid segregation is linked to the cell division (Li and Austin, 2002a). Contrary to the ParB foci, ParA was found to be diffuse indicating that it is not directly bound to the plasmid (Erdmann *et al.*, 1999).

1.5.1.2 Partition system of F plasmid

The *E. coli* F plasmid is a low copy number plasmid and contains stability of partition (sop) cassette *sopABC* of type Ia. The centromere *sopC* site is located downstream of *sopAB* genes and contains 12 repeats of 43 bp sequences (Figure 1.1) (Austin and Abeles, 1983). Each of the 12 repeats contains 7 bp inverted repeats. SopB recognises the repeats in *sopC* and binds to it as a dimer to form a partition complex. The *sopC* in F plasmid and *parS* in P1 plasmid are different in sequence and their organisation indicating that the partition complexes formed by them are different. When bound to s*opC,* SopB wraps around DNA in a right-handed coil and thus induces overall relaxation of supercoils in F plasmid. The ParB homologues in type Ia partition loci have low sequence similarity but many of them use HTH domain for the DNA binding indicating that even though ParBs recognise different centromere motifs they may employ similar structural domains for DNA binding. A single repeat in the *sopC* is sufficient for the F plasmid partition (Biek and Shi, 1994). SopB binding to the single repeat in *sopC* serves as a nucleating core to which many SopB dimers bind to form a large partition complex (Mori *et al.*, 1989). The SopA is a Walker-type ATPase and binds to SopB to form segrosome at *sopC.* SopA also acts as an auto-repressor of *sopAB* operon and binds to the four repeats within the *sopAB* promoter region (Mori *et al.*, 1989). The ATP binding motif of SopA is important for partition and mutations in this domain change the integrity of Walker motif and results in partition defects (Libante *et al.*, 2001). SopA-ATP complex undergoes polymerization and shows long filaments. SopA polymerization is inhibited by DNA (Bouet *et al.*, 2007). It has been demonstrated by intracellular studies that the SopA filaments extend proportional to the rate of plasmid partition. In the presence of SopB-*sopC* complex, SopA polymers radiate out, a feature which resembles the mitotic spindle in eukaryotes (Lim *et al.*, 2005). SopA was shown to oscillate from pole to pole at nucleoid tip and thus place the plasmid at required position for the segregation. An alternative model for F plasmid partition was also proposed which relies on the SopA gradient and is described in section 1.9.1.1 later in this chapter.

1.5.1.3 Type Ib partition systems

The *Agrobacterium tumefaciens* plasmid pTAR contains *parABS* partition cassette of type Ib. The partition genes *parAB* are situated downstream of the pTAR *parS* site

(Figure 1.1). The ParA protein is a Walker-type ATPase (222 residues) and ParB (94 residues) is a centromere binding protein. ParB acts as a transcriptional repressor and ParA augments this function (Kalnin *et al.*, 2000). Plasmid pSM19035 of *Streptococcus pyogenes* harbours δ/ω/*parS* partition cassette of type Ib. The *parS* site in pSM19035 is made up of six separate DNA sequences. The downstream *par* locus encodes two *trans*-acting genes *δ* and *ω*. Protein δ is Walker-type ATPase. Protein ω is CBP and a transcriptional repressor (Pratto *et al.*, 2008). The focus of this study is the partition locus of plasmid TP228 which is type Ib partition cassette and discussed in detail later in this chapter.

1.5.2 Type II

In the type II segregation cassette, the ATPase protein, ParM, belongs to the actin/Hsp70 superfamily. The partition site *parC* is located upstream of the *par* operon. The type II partition system is similar in organization to type Ib. The plasmid R1 is a well-studied example of the type II system. The centromere binding protein, ParR acts as a transcriptional repressor. The ParM proteins are 276-336 amino acids long whereas ParR proteins are small and range between 46-120 residues.

1.5.2.1 Partition system of R1 plasmid

The partition cassette *parMRC* of plasmid R1 encodes for ParM, an actin type ATPase and ParR, a centromere binding protein (Jensen and Gerdes, 1997). The centromere site *parC* is located upstream of *parMR* genes and comprises 5 tandem repeats of 2 sets of 10 bp sequences (Figure 1.1). The centromere site also contains the promoter sequence for *parMR* operon. ParR acts as a transcriptional repressor of *parMR* operon (Moller-Jensen *et al.*, 2007). ParR binds to *parC* and forms the partition complex. ParR dimerization might be responsible for the plasmid pairing which is proposed to be the first step in plasmid segregation (Moller-Jensen *et al.*, 2007). Plasmid pairing increases in the presence of ParM-ATP complex. ParM is a member of the actin superfamily of proteins and eukaryotic actin and the bacterial MreB are members of this family. ParM forms double helical protofilaments similar to F-actin (van den Ent *et al.*, 2002). But in contrast to F-actin, ParM filaments have a left handed twist and exhibit bidirectional growth. When bound to ATP ParM

undergoes polymerization. ParM can also bind to GTP and its GTPase activity is more efficient than the ATPase activity (Popp *et al.,* 2008). The short and unstable ParM filaments, present throughout the cell get stabilised by the ParR-*parC* complex. The ParM polymers extend by addition of ParM-ATP complex to the stabilised ParM filaments. This process is called insertional polymerization and mediates the movement of plasmid towards the pole (Moller-Jensen *et al.*, 2003). ParM depolymerizes, plasmid is diffused back into the cell and other ParM polymers capture them. This process continues till the plasmid segregation.

1.5.3 Type III

The type III partition system was recently identified and a few plasmids of *Bacillus* species exhibit the partition cassette of type III. The main characteristic of this type is the nucleotide binding protein TubZ, which is part of the tubulin/FtsZ GTPase superfamily (Ni *et al.*, 2010). An example of the type III system is plasmid pBtoxis in *Bacillus thuringiensis* (Tang *et al.,* 2007). The partition site *tubC* contains four 12 bp pseudo-repeats. The TubR encoding gene is found downstream in the *par* locus and TubZ is found downstream (Figure 1.1). TubR is a DNA binding protein with no sequence homology with any other CBP. TubR structure contains HTH motif and acts as a transcriptional repressor of *tubRZ* genes. The TubZ protein, a GTPase, shows GTP dependent polymerization and the polymers formed appear tubulin-like (Larsen *et al.*, 2007).

1.5.4 Type IV

The Type IV partition system is most unusual as it contains only one *par* gene for plasmid stabilization. It was proposed that this single protein plays the role of both centromere binding protein and motor protein. The plasmid pSK1 of *Staphylococcus aureus* is the example of type IV (Simpson *et al.*, 2003). The Par protein (245 residues) of pSK1 performs the segregation function and in the *par* operon no other gene was identified. The Par protein possibly contains an HTH motif and coiled-coiled domain as predicted by structural studies. The N-terminal HTH motif may help in binding the centromere, whereas the central coiled-coiled domain may play a role in polymerization (Schumacher, 2008).

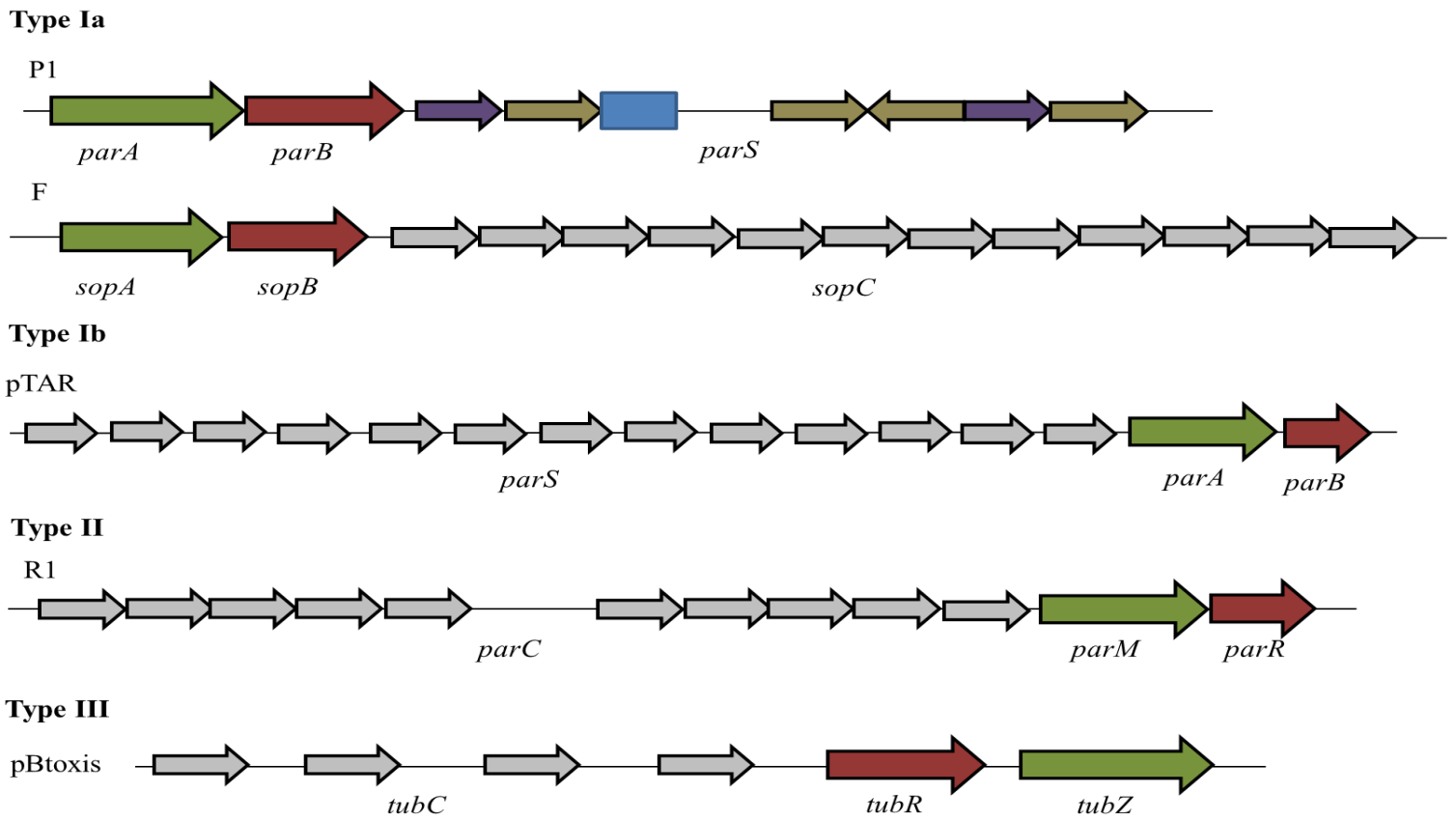

Figure 1.1. Organization of partition loci in various plasmid systems.

Partition genes shown in green are either Walker-type ATPase or actin or tubulin homologues. Centromere binding protein encoding genes are shown in red. The centromere sites containing repeated sequence are shown as grey arrows. P1 centromere site is complex, it contains hexamer (purple) and heptamer (yellow) repeats and an Integration host factor (IHF) binding site (blue). Adapted from (Hayes and Barillà, 2006b).

1.6 Partition system of plasmid TP228

This project involves the study of the molecular mechanisms and dynamics of the segregation of the multidrug resistance plasmid TP228 in *E. coli*. Plasmid TP228 was originally isolated from *Salmonella newport* and confers resistance to a wide range of antibiotics such as aminoglycosides, tetracycline, sulphonamide and some metal ions. Plasmid TP228 falls under the IncX1 incompatibility group. It harbours a well-studied partition system, ParFGH of type Ib, in which ParF is a Walker-type ATPase and ParG is a centromere binding protein (Hayes, 2000). These two *trans*-acting proteins are assembled on the *cis*-acting *parH* centromere site. ParG was shown to bind to the DNA region upstream of the *parF* gene which was speculated to contain the partition site (Barillà and Hayes, 2003). Later on, it was revealed that this site contains repeat elements and part of this region also acts as an operator (Carmelo *et al.*, 2005). ParG binds to both the centromere and the operator site. Thus, ParG acts as the transcriptional repressor of the putative *parFGH* operon. ParF, on ATP binding, undergoes polymerization (Barillà *et al.*, 2005). ParG binds to *parH* and then recruits ParF in this complex to form a segrosome. The typical organization of the TP228 partition system is shown in Figure 1.2A.

1.6.1 Centromere site *parH*

In eukaryotes, the centromere is a region to which mitotic spindle-like microtubules associate. It is part of the chromosome and is known as the primary constriction site. Cell division fails to progress properly in the absence of the centromere and leads to chromosome instability. In bacteria, like the origin of replication, the centromere site is also speculated to be present as a single copy per chromosome. Although the *B. subtilis* has multiple *parS* sites. In plasmids, centromere site provides the foundation to which ParB proteins bind and form the partition complex known as segrosome. Plasmids exhibit diverse centromeres, which are variable in sequence, positioning, numbers, lengths and direction (Hayes and Barillà, 2006a). Centromere sites are specific for each partition system and are optimised to ensure that the ParB proteins from the same partition system bind to them (Hayes and Austin, 1993). The centromere site is present downstream of the two partition genes in case of the large *parA* operons, and upstream of the genes for the small *parA* operons.

The DNA sequence upstream of the *parF* translation start codon contains direct and indirect repeat motifs. During initial efforts to study the region upstream of the *parFG* genes, the 80 bp DNA sequence immediately upstream of *parF* gene was analysed. An inverted repeat (IR) was identified in this region, which consisted of imperfect 16 bp half-sites separated by a 4 bp spacer. These 16 bp half-sites were shown to be the operator site for the *parFG* genes (Carmelo *et al.*, 2005). Subsequent analysis of this region showed that the operator site (O_F) consists of 8 tetramer repeats 5'-ACTC-3' (three direct and five inverted) separated by AT-rich 4 bp spacers (Zampini *et al.*, 2009). ParG does bind a single tetramer box of 5'-ACTC-3' but two adjacent tetramer boxes are required to form a nucleoprotein complex. Thus the entire operator site is coated by eight ParG dimers (Zampini *et al.*, 2009). Recent analysis examining regions further upstream of O_F site revealed that the DNA sequence about 160 bp upstream of *parF* translation start codon contains in total 20 direct and indirect repeat motifs of 5'-ACTC-3' separated by 4 bp AT-rich spacers (Figure 1.2B). A boundary between the partition site and operator site in this region was drawn. Out of the 20 repeats, eight repeats adjacent to the *parF* gene constitute the operator site and a cluster of 12 repeats further up from this site acts as the partition site of plasmid TP228, denoted as *parH* (Wu *et al.*, 2011a). The partition site *parH* and the operator site, O_F, are both able to act as a centromere, although the efficiency of operator site is more modest than that of the *parH* site (Wu *et al.*, 2011a).

All the twelve repeats in the *parH* site (Figure 1.2C) are essential as the sequential deletion of tetramers reduces centromere function. Changes in the tetramers by inserting base variations did not show any adverse effect on the centromere activity, suggesting that the *parH* site is elastic *in vivo* (Wu *et al.*, 2011a). Along with the invert repeats in the *parH* site, the spacers also play an important role for proper binding of ParG to the entire centromere. It was also reported that *parH* site lacks the intrinsic curvature found in other centromere sites (Wu *et al.*, 2011a). The lack of bend in *parH* DNA avoids the centromere being locked in a fixed position. Thus during segrosome formation the centromere might become stretched and bind to ParG and ParF.

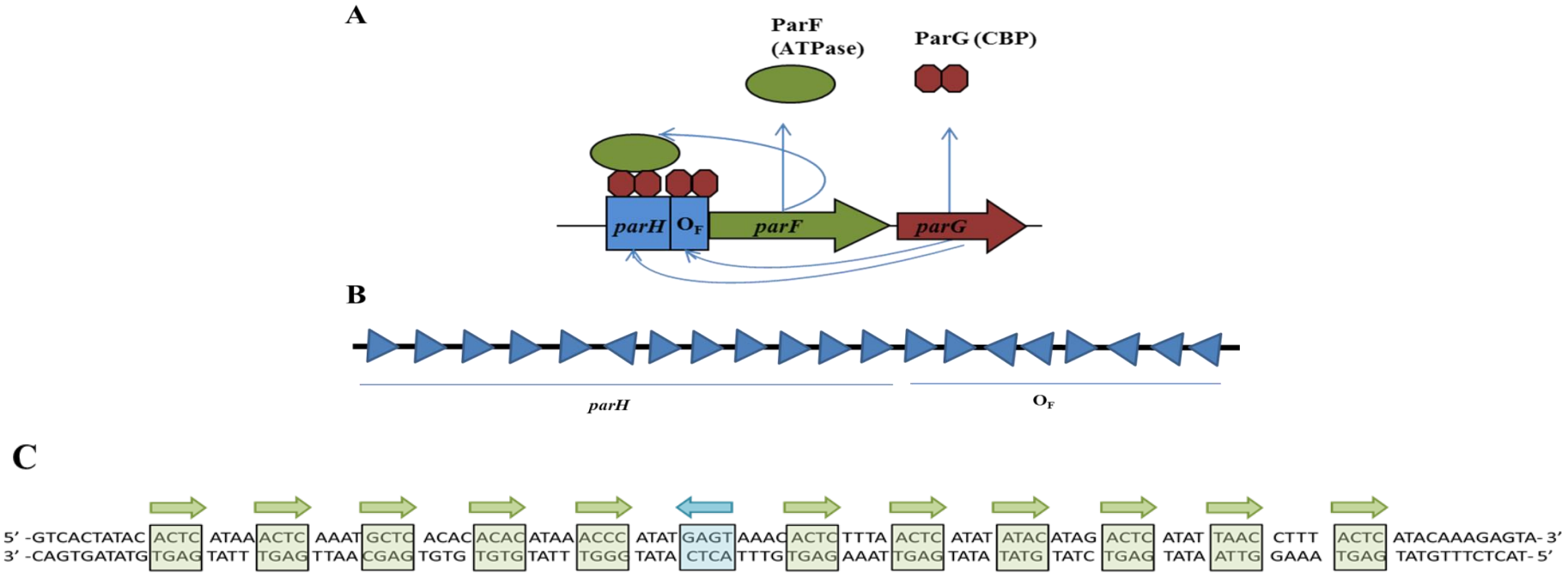

Figure 1.2. The *parFGH* segregation module.

A. The TP228 plasmid partition cassette comprises two genes which encode a Walker-type ATPase ParF (green), a CBP, ParG (brown) and the centromere *parH* (blue), which is located upstream of the segregation locus. ParG binds to operator site and acts as a transcriptional repressor. ParG also assembles on centromere. The ParF is recruited into the segrosome by interactions with ParG. **B.** Organization of the partition site *parH* and operator site upstream of *parF* gene. The partition site is made up of 12 degenerate repeats, while the operator site contains 8 repeats. **C.** DNA sequence of partition site *parH*. 12 degenerate repeats of 5'-ACTC-3' with AT rich spacers constitute the *parH* site of plasmid TP228. The repeats are boxed and denoted by arrows. The green arrows indicate direct repeats and the blue arrow represents the inverted repeat.

1.6.2 Walker-type ATPase ParF

ParF, a 22 kDa protein, is a Walker-type ATPase and is a member of the ParA superfamily of plasmid and chromosome segregation proteins. Proteins that bind and hydrolyse nucleotides are crucial for various cellular processes. These proteins belong to several chain folds, for example the dinucleotide-binding fold and the related tubulin/FtsZ fold, the mononucleotide binding fold (P-loop NTPases), the protein kinase fold, the histidine kinases/HSP90/TopoII fold and HSP70/RNAase H fold (Leipe *et al.*, 2002). Among these, P-loop NTPase are the most widespread. At the sequence level, the P-loop NTPase fold is characterized by the N-terminal Walker motif, which consists of a flexible loop. The loop typically adopts the sequence pattern GXXGXGK (a classic Walker A motif) whose function is to properly position the triphosphate moiety of a bound nucleotide (Walker *et al.*, 1982). The ParA superfamily of ATPases falls under the superclass of P-loop NTPases. The Walker A motif of this family is XKGGXXK, which is known as deviant motif as it differs from the classical motif (Koonin, 1993). ParA ATPases show a conserved lysine in the KGG motif, which interacts with the terminal oxygen atom of the β-phosphate group of ATP across the interface. The conserved lysine suggests that these proteins might be dimers (Lutkenhaus and Sundaramoorthy, 2003). Deviant Walker A motif containing proteins are involved in various functions. MinD, a Walker-type ATPase, is involved in the correct placement of the cell division site in *E. coli* and is ubiquitous in bacteria. The ParA/Soj family ATPases are involved in chromosome and plasmid segregation.

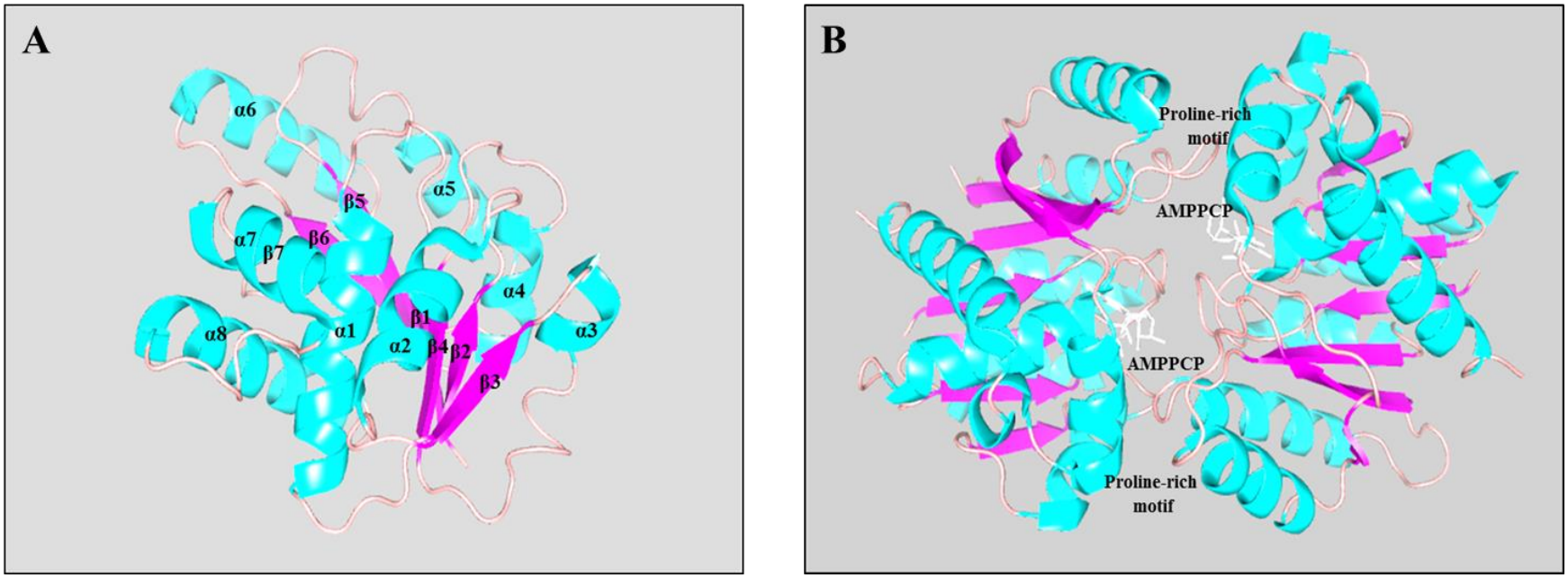

Figure 1.3. Structure of ParF.

A. ParF monomer. Partition protein ParF of plasmid TP228 in the presence of ADP is a monomer. The secondary structures are labelled. The α-helices are aqua, β-sheets are purple and the loops are pink. **B.** ParF dimer. ParF in the presence of non-hydrolysable ATP, AMPPCP is a dimer (Schumacher *et al.*, 2012). ATP is shown as silver sticks. The structures were generated by using PyMol (DeLano, 2002).

Evolutionarily, ParF is more related to the MinD subgroup of cell division proteins than to the archetypical ParA proteins. ParF is shorter than ParA and does not have a DNA binding domain. ParF homologues are found in plasmids pTAR, pVT745 and pB171 (Machón, C., *et al* 2007). The deviant Walker A motif in ParF is PKGGSGKT and it is located at the N-terminal end (residues 9-16). In Walker-type ATPases, the less conserved Walker B motif is also present. In ParF, residues 73-83 constitute the Walker B motif. Recently the crystal structure of ParF was solved in the presence of ADP and phosphomethylphosphonic acid adenylate ester (AMPPCP) (Schumacher *et al.,* 2012). ParF is monomeric when in complexed with ADP and binding to ATP leads to dimerization. The ParF monomer is composed of seven β-sheets and eight α-helices (Figure 1.3A). The lysine at position 10 from the ParF Walker A motif interacts with ATP across the interface and forms the dimers (Figure 1.3B). ParF was shown to be able to self-associate and ATP binding promotes polymerization of ParF (Barillà and Hayes, 2003). Partner protein ParG further enhances this polymerization into extensive multi-stranded filaments (Barillà *et al.*, 2005). ADP is reported as a repressor of ParF polymerization. The cycle of ParF polymerization and depolymerization may drive the partitioning process in plasmid TP228. It has been reported that ParF-K15Q and ParF-G11V mutations in the Walker A motif failed to polymerize and are partition deficient, thus pointing at the connection of polymerization and partition (Barillà *et al.*, 2005).

1.6.2.1 ParF polymerization and its ultrastructure

The crystal structure of ParF revealed a striking feature of ParF. The ParF-ATP complex formed linear ParF polymers within the crystals, with various cross-contacts between ParF dimers (Schumacher *et al.*, 2012). A patch of multiple proline residues (102-112) is responsible for one of the cross-contacts. This proline-rich motif from one unit is inserted next to the nucleotide binding pocket of another unit. The ‘dimer of dimers’ of ParF is shown to be the building block of the linear polymer (Figure 1.4A). The ParF polymer has two interfaces: interface 1 is created by contacts made by residue 61-71 with two separate groups i.e. residues 87-98 and residues 117-129 and interface 2 involves contact made by residues 49-60 and 168-192.

The stages of ParF polymerization were previously investigated by negative-stain electron microscopy (EM). In the absence of ATP, purified ParF appeared as globular particles whose size ranges from 10 to 20 nm (Figure 1.4Bi) (Barillà *et al.*, 2005). When ParF was incubated with ATP, it quickly assembled into needle-like projections (~100 nm long) that soon appeared to increase in length (Figure 1.4Bii). One end of many of the polymers had an uneven, ravelled appearance, whereas the opposite end was more compact. Higher magnification images revealed a multi-stranded ultrastructure of parallel proto-filaments (Figure 1.4Biii). High-magnification EM images show that ParF fibres assembled in the presence of ParG are thicker and longer than those observed in its absence.

Nucleotide-dependent polymerization by NTPases plays an important role in fundamental processes like cell division, which is essential for the survival and propagation of all living species. FtsZ is a tubulin-like protein that self-assembles into linear proto-filaments (termed as 'thick filaments') in a GTP dependent manner by the interaction of the plus end of one subunit with the minus end of another subunit, resulting in a head-to-tail geometry (Tonthat *et al.*, 2011). The ParM protein encoded by the *E. coli* plasmid R1 represents a subfamily of bacterial actins. ParM assembles into two-stranded helical filaments in a nucleotide-dependent manner; these filaments are actin-like in structure, but exhibit the dynamic instability of eukaryotic microtubules. Polymerization of ParM between plasmids has been shown to drive plasmid separation; and ParM is required for the movement of replicated plasmids from mid-cell toward the cell poles (Moller-Jensen *et al.*, 2003). ParA of the *par2* locus of plasmid pB171 has been shown to form cytoskeletal-like structures that dynamically relocated over the nucleoid (Ringgaard *et al.*, 2009). As some ParA proteins have shown polymerization properties and filament-like structure, they are indicated as the bacterial cytoskeleton apparatus.

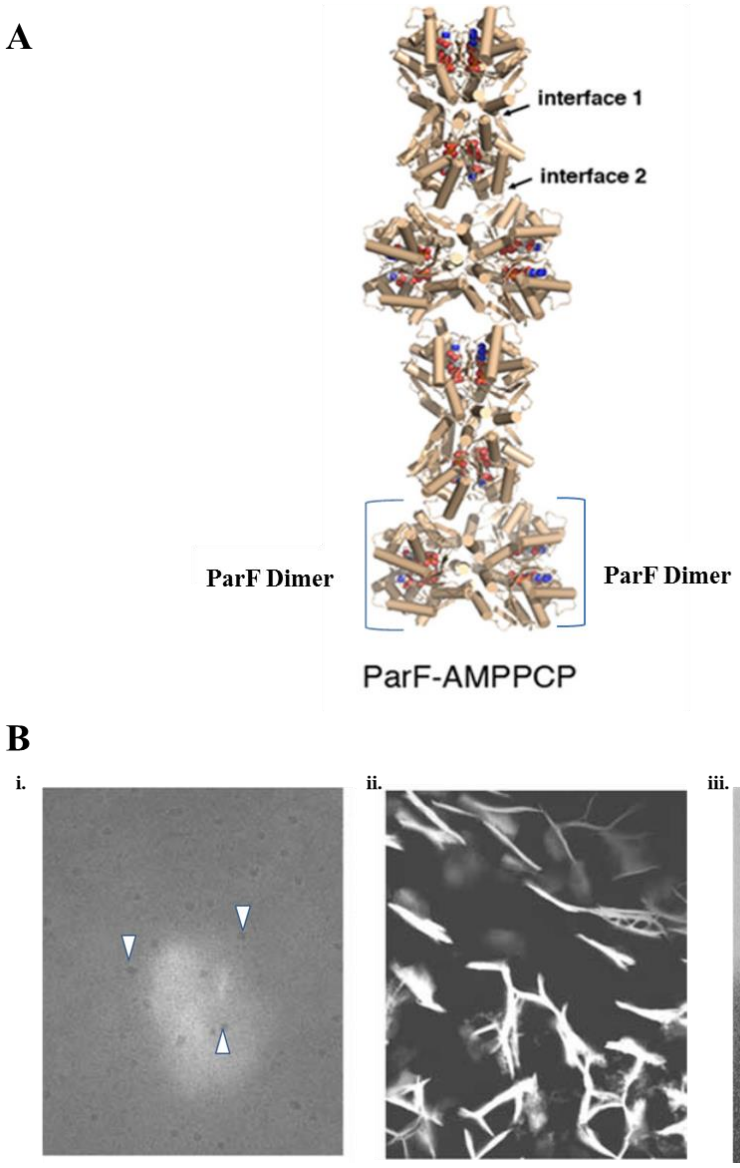

Figure 1.4. ParF-AMPPCP complex leads to ParF polymerization and observed as filaments by EM.

A. The linear ParF polymer is composed of dimer-of-dimer units. The ParF dimers and two polymer interfaces are denoted. The diagram is taken from (Schumacher *et al.*, 2012). **B.** The EM images of ParF filaments. **i.** In the absence of ATP, ParF appeared as globular protein, indicated by white arrow heads. **ii.** In the presence of ATP (2 mM), ParF (2.16 µM) shows polymer formation. **iii.** ParF filaments are observed at higher magnification. Image is reproduced from (Barillà *et al.*, 2005).

1.6.3 Centromere binding protein, ParG

ParG is a 8.6 kDa centromere binding protein and present in monomer-dimer equilibrium in solution. ParG is unrelated to any of the ParB proteins. The ParG dimer consists of two highly interwined C-domains, which form a folded structure, and two mobile N-terminal tails (Figure 1.5) (Golovanov *et al.*, 2003). Residues 34-41 form a β strand, while 42-55 and 60-74 form two α helices thus giving rise to a ribbon-helix-helix (RHH) structure. In the dimer, each of the β strands forms an antiparallel β sheet structure and the four α helices are tightly packed together above the β sheet (Figure 1.5). The folded C-domains have a hydrophobic core formed by side chains of amino acid residues V37, V39, F41, K45, R48, F49, V64, L67, V68, W71 and L72 which are involved in ParG dimerization (Golovanov *et al.*, 2003).
The folded C-terminal domain is involved in three functions:

1. Dimerization of ParG.
2. DNA binding at the centromere and operator site.
3. Interaction with the partner protein ParF and recruiting it to the segrosome complex.

The N-terminal region present at the two ends of the dimer is a flexible tail consisting of amino acid residues 1-32. Two structural characteristics of the tail are: the presence of an arginine finger motif with an arginine at the 19^{th} position (Barillà *et al.*, 2007) and the transient β structure formed by residues 23-29 (Carmelo *et al.*, 2005). The transient β structure interacts with the β sheet of the C-terminal domain, exhibiting an extended β sheet.

1.6.3.1 Role of ParG as a centromere binding protein and transcription factor

Most of the prokaryotic transcription factors have a HTH motif and previously it was assumed that the α-recognition helix from this motif is inserted into the DNA major grove. However, the structures of MetJ and Arc transcriptional repressor proteins have shown that their N-terminal β strand is positioned in the DNA major groove. These structures led to the identification of the new ribbon-helix-helix (RHH) superfamily of transcription factors (Knight *et al.*, 1989). The positively charged amino acids like arginine and lysine from the β strand at the N-terminus in most of the RHH proteins make direct sequence specific contact to the nucleotide bases

(Schreiter and Drennan, 2007). Thus, the RHH superfamily is defined by the feature of DNA binding by β-strands, whereas the HTH superfamily members employ an α-helix to contact DNA at the major groove (Aravind *et al.*, 2005). The N-terminal residues of transcriptional repressors Arc and Mnt determine the operator binding specificity (Knight and Sauer, 1989). This functionally diverse protein superfamily regulates the transcription of genes that are involved in various cellular processes including cell division and control of plasmid copy number (Schreiter and Drennan, 2007). Auto-repressors of the type Ia partition family contain N-terminal HTH fold, whereas type Ib, e.g. ParG, and type II, e.g. ParR, centromere binding proteins contain a RHH fold (Schumacher, 2008). Most of the RHH proteins form dimers of dimers upon DNA binding (Zampini *et al.*, 2009).

Like other RHH family members, ParG binds DNA by inserting a β ribbon i.e. the two β-sheets into the major groove (Figure 1.5). The residues R36, N38 and N40 located on one side of the β strand from each monomer are implicated in making key interactions with DNA (Golovanov *et al.*, 2003). ParG binds to the centromere *parH* and the operator site O_F with equal efficiency. ParG binds differently to the sub-sites of partition site *parH* (Wu *et al.*, 2011a). The tetramer motifs are responsible for the direct contact with ParG whereas the spacer boxes might confer stability to the ParG-DNA complex. The AT-rich spacers might also be responsible for providing flexibility because of which ParG may be able to become associated as a dimer of dimers to coat the entire *parH* site. ParG binds to the eight repeats of the O_F site and acts as a transcriptional repressor of the *parFG* genes. A detailed study of ParG binding to O_F demonstrated that ParG binds with different affinities to the sub-sites of the operator DNA sequence. The operator site tetramers may have evolved with a sequence variation in inverted and direct repeats and different AT contents in the spacer boxes to form a well-organised nucleoprotein complex, which is necessary for transcription control of *parFG* (Zampini *et al.*, 2009).

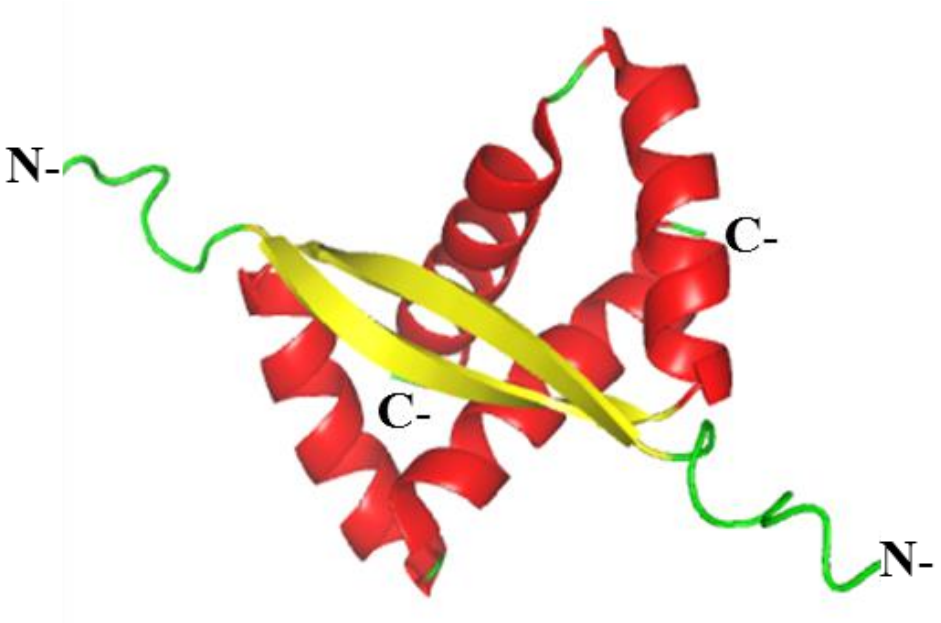

Figure 1.5. Structure of ParG dimer.

ParG dimer- Two ribbons formed by the β-sheets (yellow) in antiparallel position and 4 α-helices compactly arranged (red). N-terminal tails (green) are seen at the left and right side of the structure. The structure was generated by using PyMol (DeLano, 2002).

1.6.3.2 Importance of the ParG N-terminal flexible tail

The ParG N-terminal domain is unstructured but still multifunctional. The N-terminal truncated proteins Δ9 ParG, Δ19 ParG and Δ30 ParG have been instrumental to determine the importance of the N-terminus in various functions of ParG (Carmelo *et al.*, 2005).

The N-terminal flexible tail of ParG is involved in the functions described below:

1. Partition site binding affinity of ParG is altered by the N-terminal end (Wu, M., *et al* 2011). The ParG deletion mutant proteins showed an increase in non-specific DNA binding. The transient secondary structure formed in the N-terminal region by residues 23-29 may provide additional contacts within the partition site conferring the specificity related to the DNA binding (Carmelo *et al.*, 2005).
2. ParG acts as a transcriptional repressor of the *parFG* operon and this function is modulated by the N-terminal end (Carmelo *et al.*, 2005, Zampini *et al.*, 2009). The Δ19 and Δ30 ParG displayed weaker repression of the *parFG* genes, suggesting the requirement of a full-length tail for the regulation of *parFG* cassette.
3. ATP triggers ParF polymerization and addition of ParG further enhances the polymerization. ParG might carry out this function by either bundling the ParF filaments or stabilizing the proto-filaments. The effect of ParG on ParF polymerization is independent of ATP. ParF mutants, defective in ATP-induced polymerization, were shown to be responsive to ParG that was able to induce polymerization (Dobruk-Serkowska *et al.*, 2012). In the absence of ATP, ParG flexible tails may help to wrap around the ParF monomers either on the same or parallel filaments to activate the polymerization process. The truncated ParG mutant proteins were shown to be unable to enhance ParF polymerization beyond the ATP induced polymerization. This indicated that the tail may help to arrange the ParF polymers into filaments (Barillà *et al.*, 2007). This behaviour is similar to that of formin-like factors which act on eukaryotic actin or microtubule-like protein which regulate tubulin kinetics.
4. ParG augments the ATPase activity of ParF by around 30 fold (Barillà *et al.*, 2005). The arginine finger motif present in the ParG flexible N-terminal end has been demonstrated to be responsible to bring out the ATPase activation in ParF (Barillà *et al.*, 2007). Interestingly Δ9 ParG also showed decrease in

the ATPase activation even though the first nine residues do not harbour the arginine finger motif. This provided key evidence for the crucial role for the entire N-terminal tail in stimulating ParF ATPase activity.

1.7 Other ParF related Walker-type ATPases

1.7.1 SopA protein of plasmid F

The *E. coli* F plasmid has its own active segregation mechanism operated by the type Ia partition cassette *sopABC* (Mori *et al.*, 1986). SopA is a Walker-type ATPase and homologous to ParA ATPase of the P1 plasmid. SopB contains an HTH motif and is a centromere binding protein. SopA interacts with SopB and *sopC*. Excess of SopA showed destabilization of the plasmid, hence the role of SopA as a repressor of the *sopAB* operon is important for the segregation of plasmid F (Lemonnier *et al.*, 2000). The N-terminal domain of SopA showed a putative HTH motif which confers specificity during promoter-operator binding (Ravin *et al.*, 2003). The SopA-SopB interaction is also responsible for the proper regulation of the partition locus. The N-terminal domain of SopB was demonstrated to be essential for the strong interaction with SopA (Kim and Shim, 1999). During an intracellular localisation study, SopA was also found to be localised on the nucleoid (Hirano *et al.*, 1998). Mutation K120R, in the ATP-binding motif in SopA resulted in a lack of segregation (Libante *et al.*, 2001). SopA showed ATP-dependent polymerization and DNA appeared to be the inhibitor of the polymerization process. SopB displayed an opposite effect to that of DNA and helped to further enhance SopA polymerization resulting in plasmid displacement and segregation (Bouet *et al.*, 2007). Apart from binding specific DNA sequences at the centromere, SopB also demonstrated non-specific contacts, which bridge the DNA motifs in the centromere site. This way SopB spreads over the DNA and makes it unavailable to antagonise SopA polymerization (Schumacher *et al.*, 2010). The interaction of SopA with the non-specific DNA is attributed to the lysine residue at position 340. Mutation of this residue resulted in plasmid destabilization (Castaing *et al.*, 2008). ATP-dependant non-specific DNA binding is also responsible for the ATP hydrolysis by SopA protein. The partner protein SopB also showed the stimulation of SopA ATPase activity by employing R36 of the arginine finger motif (Ah-Seng *et al.*, 2009). Two different mechanisms are postulated for F plasmid segregation. The cycle of SopA polymerization and depolymerization may

shuttle the plasmid (Lim *et al.*, 2005). On the contrary, it is also proposed that the SopA molecules form a concentration gradient and display a diffusion-ratchet mechanism for plasmid segregation (Vecchiarelli *et al.*, 2013).

1.7.2 ParA protein of plasmid pB171

The *E. coli* plasmid pB171 has two partition loci, *par1*and *par2*. The *par2* locus exhibits a type Ib partition system and the partition cassette encodes Walker-type ATPase ParA and centromere binding protein ParB (Ebersbach and Gerdes, 2001). ParB binds to the *cis*-acting centromere site *parC*2. ParA of pB171 is more related to MinD protein than to the ParA from P1 plasmid. ParA showed interaction with ParB protein. ParA protein also binds to both ATP and ADP. ATP binding results in ParA polymerization (Ebersbach *et al.*, 2006). The intracellular study of fluorescently labelled ParA and ParB proteins showed that, the ParA-GFP protein localised to the nucleoid and in the presence of *parC* and ParB exhibited oscillation from one end of the nucleoid to the other (Ebersbach and Gerdes, 2004). The ParA polymers appeared as spiral-shaped structures and are supposed to provide the force for plasmid segregation. Mutation in the Walker A box abolished the ParA oscillation and also altered the plasmid localisation *in vivo.*

1.7.3 Chromosomal partition protein Soj of *B. subtilis*

In *Bacilus subtilis*, the Soj and SpoOJ proteins are homologues of plasmid partition proteins, ParA and ParB respectively and responsible for chromosome segregation and sporulation (Ireton *et al.*, 1994). Similar to ParA proteins, Soj also binds to DNA and acts as a transcriptional repressor of sporulation gene expression (Quisel *et al.*, 1999). The partner protein Spo0J binds to a number of *parS* sites clustered near the chromosome origin of replication *oriC* (Marston and Errington, 1999). Soj, a Walker-type ATPase, on ATP binding undergoes dimerization. Soj dimer binds to DNA non-specifically and form nucleoprotein filaments (Leonard *et al.*, 2005). Spo0J stimulates the ATPase activity of Soj and the N-terminus of Spo0J is implicated in this role (Autret *et al.*, 2001). The intracellular localisation study of the Soj protein showed that it forms nucleoid associated dynamic structures. The assembly and disassembly of Soj protein over the nucleoid is attributed to the ATP hydrolysis stimulated by Spo0J (Marston and Errington, 1999, Quisel *et al.*, 1999).

Soj mutants do not show segregation defect, but Spo0J null mutants exhibit anucleate cells (Ireton *et al.*, 1994).

The crystal structure of Soj from the Gram-negative hyperthermophile *Thermus thermophilus* was solved in three different forms, opo, ADP-bound and hydrolysis deficient mutant D44A form (Leonard *et al.*, 2005). The opo and ADP-bound forms of Soj are monomeric, whereas ATP-bound Soj is a dimer. Soj contains eight β-strands, seven parallel and one antiparallel. These β-sheets form a twisted arch, twelve α-helices are located outside of the arch (Figure 1.6A) (Leonard *et al.*, 2005). The lysine (K15) in Walker box binds ATP and forms a dimer. The α and γ phosphates of the ATP are stabilised by the lysine residues from each monomer. The ATP dependent dimer is a molecular switch where ATP binding facilitates DNA binding and the Spo0J mediated ATP hydrolysis lead to Soj relocation (Leonard *et al.*, 2005).

1.7.4 Cell division protein MinD of *E. coli*

The MinCDE protein system is responsible for determining the position of the FtsZ-ring in *E. coli* and facilitates selection of division site at mid-cell. MinD protein interacts with other two Min proteins i.e. MinC and MinE. MinD, a Walker-type ATPase dimerises in the presence of ATP and binds to MinC and the membrane (Lutkenhaus and Sundaramoorthy, 2003). The C-terminal amphiphathic helix of MinD is responsible for membrane binding (Zhou and Lutkenhaus, 2003). MinD binds to the membrane at the cell poles and recruits MinC that is an inhibitor of the Z-ring formation. MinE, on the other hand removes MinD from membrane by stimulating its ATPase activity and thus displaces MinC from MinD (Hu *et al.*, 2003). In MinD, the sites for binding to MinC and MinE are overlapping and present at dimer interface (Ma *et al.*, 2004, Park *et al.*, 2011). MinD has been shown to be oscillating from pole to pole *in vivo* (Raskin and de Boer, 1999). The ATPase stimulation by MinE and the membrane association are necessary for MinD oscillation (Hu and Lutkenhaus, 2001). During oscillation, MinE rings follow MinD-MinC complex present at the polar zone. MinE rings travel to the pole and displace the MinD-MinC complex from the membrane, at one pole and the complex reassembles at the opposite pole. Thus, oscillations, which occur several times in a

cell cycle, help to keep MinC away from mid-cell (Ma *et al.*, 2004). Residues R21, L22 and A18 in MinE play important role in ATPase stimulation. MinE, a small protein of 88 amino acids, has been shown to undergo dramatic structural changes on binding to MinD. It has been suggested that MinE releases a membrane targeting sequence (MST) domain and an anti-MinCD domain on binding to MinD (Park *et al.*, 2011). The MST domain contains conserved hydrophobic residues which are not exposed to solvent when MinE is traveling through the cytoplasm thus avoiding the membrane association of MinE in the absence of MinD. This keeps MinE available to interact with MinD and carry out MinD oscillation (Ghasriani *et al.*, 2010). The exact mechanism behind the MinD oscillation is still argued. Formation of MinD filaments in the presence of ATP, membrane and MinE is suggested as one reason for oscillation (Suefuji *et al.*, 2002) A reaction-diffusion mechanism is also suggested for MinD assemblies (Loose *et al.*, 2008), whereas a mechanical stress by tethering MinD and MinE molecules to the membrane is also proposed for the oscillation (Ivanov and Mizuuchi, 2010).

Structures of MinD from various organisms have been reported. The structure of *E. coli* MinD is described here (Figure 1.6B). A hydrolysis deficient MinD D40A mutant protein without its first 10 residues was crystallised (Wu *et al.*, 2011b). Similar to its other homologues like Soj and ParF, MinD also dimerises in the presence of ATP. A lysine at position 11 (K11) in the deviant Walker A box binds to ATP, which leads to MinD dimerization. The orientation of MinD on the membranes has also been described. The C-termini from both monomers are placed on the same face of dimer which comes in close contact with membrane. In the monomer form, amino acids D152, S148 and E146 interact with the conserved lysine (K11), while in the dimer, S148 and E146 also make cross contacts with the adjacent chain at the dimer interface. A glycine at position 12 also make contact with the γ-phosphate across the dimer interface.

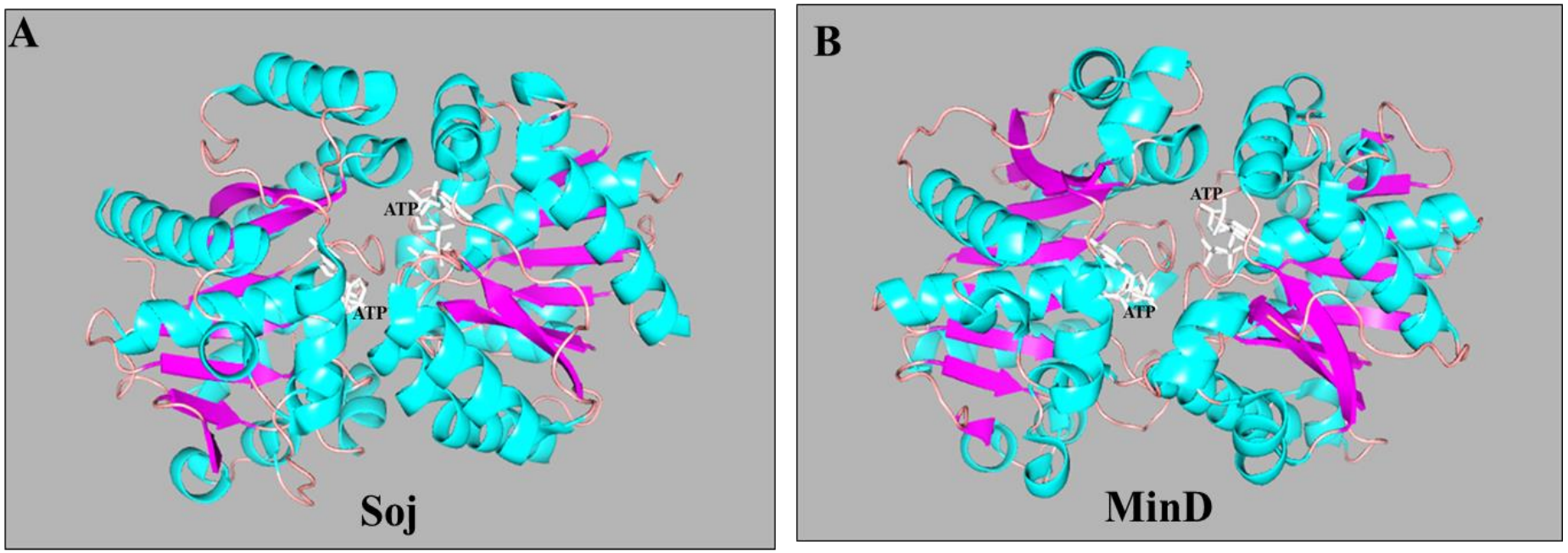

Figure 1.6. Structure of Soj (D44A) and MinD (D40A) dimers.

A. Chromosome partition protein Soj of *Thermus thermophilus* in the presence of ATP forms a dimer. **B.** In the presence of ATP, *E. coil* division site selection protein MinD forms a dimer. The secondary structures are labelled. The α-helices are aqua, β-sheets are purple and the loops are pink. ATP is shown as silver sticks. The structures were generated by using PyMol (DeLano, 2002).

1.8 Other ParG related ParB proteins

1.8.1 Protein ω of plasmid pSM19035

Plasmid pSM19035 from *Streptococcus pyogenes* is a broad-host-range low copy number plasmid of *Inc18* family and is maintained in other Gram-positive bacteria (Lioy *et al.*, 2010). The segregation locus (*Seg2*) of plasmid pSM19035 contains a *cis*-acting *parS* site and two partition genes encoding proteins *δ* and *ω* (Dmowski *et al.*, 2006). Protein δ is a Walker-type ATPase of ParA family from type Ib partition system and forms a dimer (δ_2) in the presence of ATP (Pratto *et al.*, 2008). Protein ω is homo-dimer in solution (ω_2), contains 71 amino acids and acts as a centromere-binding protein. Omega also works as a global regulator as it controls the expression of various genes like *copS,* which is involved in copy number control, segregation genes *δ* and *ω* and toxin-antitoxin proteins encoding genes *ε* and *ζ* (Dmowski *et al.*, 2006). Protein ω_2 acts as a transcriptional repressor that binds to the promoter region upstream of a *copS, δ* and *ω* genes. The centromere site *parS* is made up of the promoter regions of *copS, δ* and *ω* genes and it contains direct and inverted 10, 7 and 9 heptamer repeats respectively. Omega is a member of MetJ/Arc transcriptional repressor family and its crystal structure has revealed that it contains a RHH fold (Murayama *et al.*, 2001). The homodimer ω_2 is made up of 2 β-sheets (residues 28-32) and 4 α-helices (34-46 and 51-66) as shown in Figure 1.7A. The antiparallel β-sheets contact the DNA at a major groove. The arginine at position 31 and threonine at position 29 in β-sheet are involved in interaction with DNA (Murayama *et al.*, 2001). Thr29 has been shown to be necessary for specific DNA binding (Pratto *et al.*, 2008). The N-terminal end contains 20 amino acids, which were not detected in the crystal structure indicating that the N-terminus is a disordered domain (Murayama *et al.*, 2001). The crystal structure of Omega in the presence of DNA has also been solved but without the 19 residues at the N-terminus (Weihofen *et al.*, 2006). The DNA used was a two heptad sequence from the *parS* site. Surprisingly in the absence of the N-terminus region Omega showed binding to the DNA. The *in vitro* analysis revealed that the ω_2 binding to single heptad is poor but increases with addition of more heptad units. Along with the β-sheets, which contact DNA at major groove, the N-termini of helices α2 also lock the phosphate backbone of the DNA sequences. Even though the N-termini is not required for DNA binding, it has been shown that Δ19 ω_2 fails to activate ATP hydrolysis activity of the partner protein δ

(Pratto *et al.*, 2008). Polymerization of δ_2 on DNA is also demonstrated to be dependent on ω_2-*parS* complex (Pratto *et al.*, 2008).

1.8.2 Protein ParR of plasmid pB171

A virulence plasmid pB171 from *E. coli* contains two *par* loci, *par1* and *par2* (Ebersbach and Gerdes, 2001). These loci are placed adjacent but in opposite direction. *par1* locus contains *parMRC* partition cassette of type II whereas *par2* locus exhibits *parABC* cassette of type Ib. The partition site *parC1* is shared between both loci and contains 10 direct hexameric repeats. *parC1* also contains promoter sequences for both the *par1* and *par2* loci. Downstream of *parB* another centromere-like site was observed called *parC2,* which contains 18 direct hexameric repeats. Both, ParR and ParB proteins bind to the *parC1* site and act as repressors of *par1* and *par2* operon respectively. Interestingly ParB was shown to be an efficient repressor of the *par1* operon, exhibiting the cross-talk regulation between two *par* loci (Ringgaard *et al.*, 2007). The crystal structure of ParR has been solved and it was revealed that it is a member of MetJ/Arc transcriptional repressor family having a DNA binding RHH motif (Moller-Jensen *et al.*, 2007). In ParR homodimer, a RHH motif is found at the N-terminus and each monomer contains 1 β-strand and 5/4 α-helices (one monomer contains extra α-helix near the C-terminus). In the ParR dimer, two β-strands are arranged in antiparallel fashion and two α-helices are lined over it, followed by the remaining helices (Figure 1.7B). The 12 dimers of ParR arranged in a helical manner in which N-termini face outward of the helix and C-termini face inward. α-helices 1 and 2 are responsible for stability of DNA interaction whereas α-helices 3, 4 and 5 make inter-dimer interactions. The helical structure of ParR may act as a scaffold on which partition site DNA, *parC1* wraps (Moller-Jensen *et al.*, 2007). Interestingly the C-terminus of ParR is found to be disordered and the DNA binding activity is carried out by the N-terminus. Similar to R1 partition, which is prototype of type II partition system, ParR-*parC1* complex formation might be involved in activating ParM to form dynamic filaments that on ATP hydrolysis push the plasmid copies apart for segregation (Moller-Jensen *et al.*, 2003, Salje *et al.*, 2010).

1.8.3 Protein ParR of plasmid pSK41

The multidrug resistant plasmid pSK41 from *Staphylococcus aureus* exhibits a type II partition cassette, *parMRC* (Moller-Jensen *et al.*, 2002). Upstream of *parM* gene sequence, a centromere site *parC* is located, which contains four 20 bp direct repeats (Schumacher *et al.*, 2007). A centromere binding protein ParR binds to the 20 bp repeats with high affinity and in co-operative manner. The DNA binding residues are present at the N-terminus hence the crystal structure was obtained for the N-terminal region (ParRN) with a 20-mer DNA fragment. The DNA-binding motif was identified as RHH where β strand is made up of resides 5-12, two α-helices are made up of residues 26-25 and 33-47 (Figure 1.7C). Like other RHH proteins the β strands from each monomer is arranged in an antiparallel manner and the α-helices are compactly placed on one side of the β-sheets to form a dimer. The ParR-DNA complex forms a super-helical structure. Six dimer of dimers of ParRN form a helix and the DNA wraps on the convex surface of the helix. The 20 bp DNA has an intrinsic bend and an enlarged major groove, which helps in binding to the ParR. The ParR antiparallel β-sheets inserted into the major groove and the residues K7, K11 and L3 from the β strand are indicated in making DNA contacts. The residues R29, R37, T31 and Y17 are involved in dimer interface interactions. The C-terminal domain of ParR protein is necessary to recruit ParM protein in segrosome. ParM fails to bind to ParRN hence the ParM-ParR interaction is determined by the C-terminus.

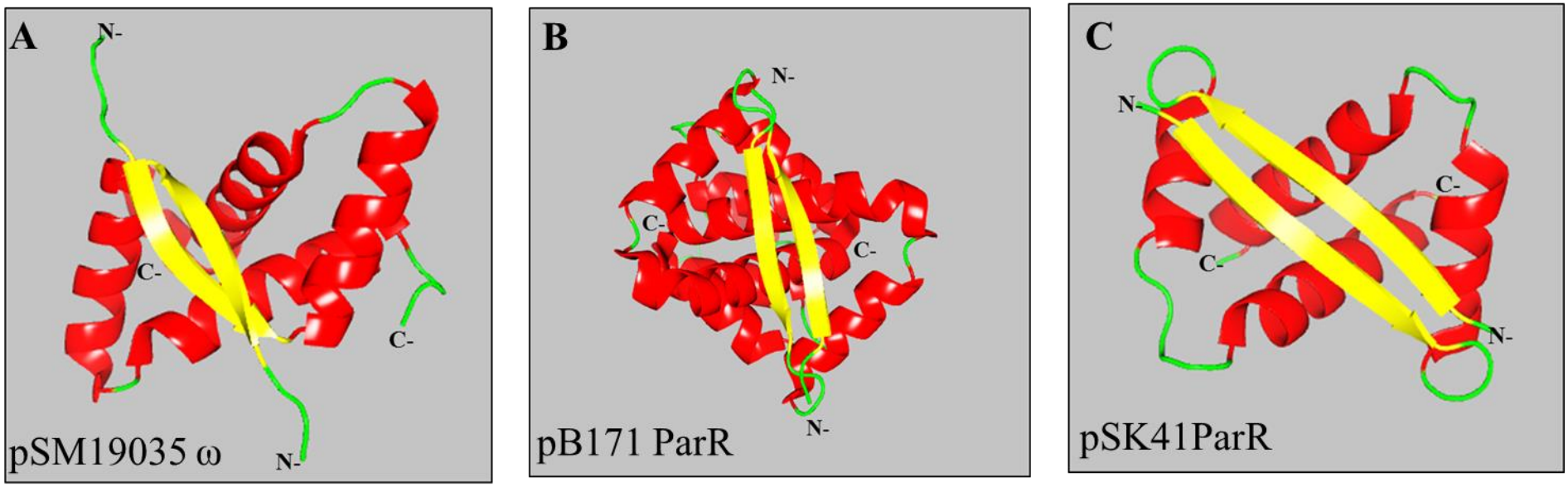

Figure 1.7. Structures of Omega (ω_2) dimer and ParR dimer from pB171 and pSK41.

A. ω_2 protein from *Streptococcus pyogenes* plasmid pSM19035. The ribbon formed by the β-sheets (yellow) in antiparallel position and 4 α-helices compactly arranged (red). N-terminal tails (green) are seen at the left and right side of the structure. **B.** Type II CBP, ParR from *E. coli* plasmid pB171. The ribbon formed by the β-sheets (yellow) in antiparallel position and 9 α-helices compactly arranged (red). **C.** Type II CBP, ParR from *Staphylococcus aureus* plasmid pSK41. The ribbon formed by the β-sheets (yellow) in antiparallel position and 4 α-helices compactly arranged (red). The structures were generated by using PyMol (DeLano, 2002).

1.9 Mechanisms of plasmid segregation

The genetic organization of partition loci is quite similar in all types of plasmid partition systems. The nucleotide binding protein, NTPase provides the force required for DNA segregation, while a repeated DNA sequence either upstream or downstream, acts as a *cis*-acting centromere site. A centromere binding protein plays a role of mediator between the NTPase and the centromere and regulates the expression of partition protein. Interestingly, all these common components together carry out plasmid partition through unrelated mechanisms in the different types of partition systems. The molecular mechanisms involved in plasmid partition are described here.

1.9.1 The ParA mediated plasmid partition mechanisms

ParA driven plasmid segregation has been comprehensively studied (Barillà *et al.*, 2007, Hwang *et al.*, 2013, Ringgaard *et al.*, 2009, Vecchiarelli *et al.*, 2013). ParA protein plays a central role in plasmid partition but as it shows a variation in its structure and change in its functions depending upon its ATP and ADP bound states, researchers have not reached an agreement as to a single mechanism for all types of plasmid partition mediated by the ParA proteins.

1.9.1.1 Diffusion-ratchet mechanism for type Ia plasmid partition system

Partition of plasmid P1 is carried out by Walker-type ATPase ParA, CBP ParB and centromere site *parS* (Erdmann *et al.*, 1999). The HTH motif in ParA is responsible for specific DNA binding and leads to transcriptional regulation of *parAB* operon (Bouet and Funnell, 1999). Unlike most of the other ParA proteins, P1 ParA shows dimerization in apo, and ADP-bound form also (Dunham *et al.*, 2009). The ADP bound form is responsible for specific DNA binding whereas ATP binding facilitates non-specific DNA binding (Vecchiarelli *et al.*, 2010). During plasmid segregation, the initial steps of ParB binding to centromere site and recruiting ParA in the nucleoprotein complex to form the segrosome are similar to those occurring in other systems. However, how the ParB-*parS* cargo is moved to the final destination is debated. The Funnell and Mizucchi groups have proposed a diffusion-ratchet mechanism based on results obtained employing a cell free system (Figure 1.8). For this they used a DNA-carpeted flowcell, which mimics the nucleoid (Hwang *et al.*,

2013, Vecchiarelli *et al.*, 2010). Fluorescently labelled ParA, ParB and *parS* harbouring plasmid were added to the flowcell. Depending upon the findings from the cell free system experiment the P1 plasmid partition model is proposed. ParA when complexed with ATP (activated form), binds to the nucleoid. ParB is bound to plasmid at partition site *parS*. The plasmid becomes bridged to the DNA by ParA-ParB interaction. When ParB stimulates ParA ATPase activity, ParA is released from the nucleoid and diffuses away (ParA-ADP form) before encountering another position on nucleoid to bind. As ParA is removed, the ParB-*parS* complex also detaches from the nucleoid and a ParA depletion zone forms. ParB-*parS* follow the ParA and diffuse towards the high ParA concentration zone. The replicated plasmid complexes move in opposite direction as the ParA-depletion zone inhibits them from coming together again.

A diffusion-ratchet mechanism is also described for F plasmid partition. In a similar cell free system, fluorescently labelled SopA and ATP are added in a flow-cell (Vecchiarelli *et al.*, 2013). In the presence of ATP, SopA attaches to the DNA carpet. Upon introduction of the SopB-SopC complex in the flow cell, SopA-SopB interaction transiently bridges the plasmid to DNA carpet. SopB stimulates the ATPase activity, which leads to release of SopA from the carpet, creating a SopA free zone. The release of SopA from the carpet is quicker than the P1 ParA one hence weak SopA depletion zones are formed. The plasmid remains anchored to the carpet for longer and then dissociates. Based on these observations, it has been proposed that the plasmid may surf on the DNA carpet and follow the wave of SopA ATPase gradients for segregation (Vecchiarelli *et al.*, 2014).

Recently, a DNA-relay mechanism was put forward for chromosome segregation in *Caulobacter crescentus* mediated by ParA. It has been proposed that the elastic nature of nucleoid enables ParA-ATP dimer to bind to the chromosome as a momentary tether. ParB binds to the chromosome via centromere and this nucleoprotein complex attaches to the ParA-ATP tether. The elastic nature of the nucleoid, the ParA-ATP tether and ParA gradient formation contribute to the relay of ParB-chromosome complex within the cell for segregation (Lim *et al.*, 2014).

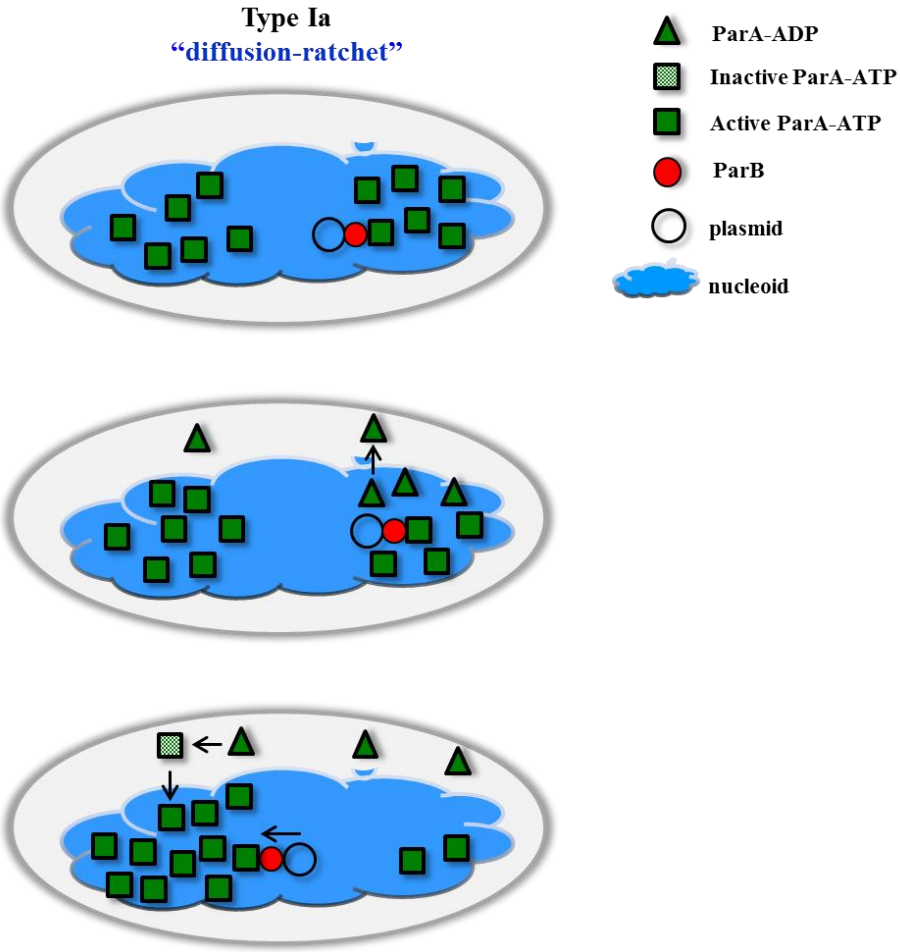

Figure 1.8. Diagrammatic representation of diffusion-ratchet mechanism.
ParB via *parS* forms a plasmid partition complex. ParA-ATP in activated form binds the nucleoid. ParA interacts with ParB and attaches ParB-plasmid complex to nucleoid. ParB stimulates ParA ATPase activity, which leads to ParA-ADP formation. ParA-ADP dissociates from the nucleoid resulting in ParA depletion zone on nucleoid. Slowly ParA diffuses in the cell, binds to ATP and attaches to the nucleoid at the opposite side. Higher ParA concentration results in diffusion of plasmid towards it. Replicated plasmid complexes move in opposite direction as ParA depletion zone pushes them towards higher ParA concentration site. Adapted from (Vecchiarelli *et al.*, 2010).

1.9.1.2 Pulling mechanism for type Ib plasmid partition system

Plasmid partition by a pulling mechanism was proposed by Gerdes group for *par2* locus of plasmid pB171 (Ringgaard *et al.*, 2009). pB171 ParA dimerization in the presence of ATP and polymerization in presence of DNA is consistent with other ParA proteins from various plasmid systems. ParA binds DNA non-specifically and utilises the nucleoid as a scaffold (Ebersbach *et al.*, 2006). ParA also employs plasmids on nucleoid. When fluorescently labelled ParA and ParB were analysed *in vivo*, ParA was found to exhibit a filamentous structure (Ringgaard *et al.*, 2009). ParB binds to *parC2* on plasmid. ParA filament assemblies that are spread on the nucleoid contact ParB-*parC2* complex. On ParA-ParB interaction, ParB stimulates the ATPase activity of ParA, resulting into depolymerization of ParA. This leads to retraction of ParA filaments from the plasmid. ParA appears to shrink and move to the other end of the cell. At this point the plasmid is either released from ParA filaments or dragged behind the shrinking polymers (Figure 1.9A). Eventually ParA depolymerises completely and the filamentous structure disappears. ParA starts assembling into filament at the opposite pole and again contacts the plasmid, undergoes depolymerization and the cycle of assembly/disassembly starts all over again. During this cycle, ParA carries out time-averaged equi-distribution of the plasmid in the cell. The ATP hydrolysis by ParA provides the force required for oscillation in order to pull the plasmid in the cell.

1.9.2 Pushing mechanism by actin-type proteins for type II partition system

Multiple-antibiotic-resistant plasmid R1 from *E. coli*, exhibits type II partition system and so far is the most well-characterized active plasmid partition system (Salje *et al.*, 2010). The *parMRC* partition cassette contains *parM* which encodes an ATPase, *parR* which encodes for ParR, a CBP, and a centromere *parC* (Jensen and Gerdes, 1997). The ParM protein provides force for plasmid segregation hence called motor protein and is a member of actin-type of ATPases. ParM structure shows an ATP-binding pocket with the residues of actin fold located around this pocket (van den Ent *et al.*, 2001). At atomic level, the ParM filaments look like F-actin as they assemble into polar, twisted and double stranded filament but they are bi-directional unlike actin (Moller-Jensen *et al.*, 2002). The ParM filaments traverse

through the entire cell. ParM filaments are dynamic as on ATP binding they polymerize and on ATP hydrolysis they depolymerize. ParR binds to centromere to form partition complex. ParR from the type II plasmid pSK41 and pB171 shows a RHH motif and the centromere DNA wraps around the ParR assembly in helical fashion. ParR from plasmid R1 is also speculated to have the RHH motif and forms super helical partition complex (Schumacher, 2012). ParM filaments search for the plasmid in the cell. The C-terminus of the ParR interacts with ParM. ParM filaments are stabilized by ParR bound to *parC* and the filaments are formed by the addition of ParM-ATP at both ends, giving rise to insertional polymerization (Gerdes *et al.*, 2010). The elongating polymers push the plasmids in opposite direction for segregation (Figure 1.9B) (Garner *et al.*, 2007). On ATP hydrolysis ParR-*parC* dissociates from one end of the polymer.

1.9.3 Tram-like mechanism by tubulin-type proteins for type III partition system

Plasmid pBtoxis from *B. thuringiensis* exhibits the *tubZRC* type III partition locus (Tang *et al.*, 2007). TubR, a CBP is a dimer and acts as a transcriptional repressor. TubR contains a winged-HTH motif. The residues in the wing region might interact with the DNA at minor groove whereas the N-terminal helices bind to the major groove (Ni *et al.*, 2010). Protein TubZ is a GTPase and contains a tubulin fold similar to FtsZ (Ni *et al.*, 2010). TubZ has been shown to polymerize when it binds to GTP (Larsen *et al.*, 2007) and an EM study has shown the formation of double stranded TubZ filaments (Aylett *et al.*, 2010). The C-terminal end of TubZ is flexible and shown to be responsible for interacting with partner protein TubR (Ni *et al.*, 2010). Plasmid segregation was shown to follow a tram-like mechanism (Figure 1.9C) (Schumacher, 2012). In this model, TubR bound to *tubC* site on plasmid interacts with TubZ polymers through the flexible C-terminal domain of TubZ. TubZ filaments show minus and plus ends. GTP binding at the plus end leads to elongation and GTP hydrolysis results in retraction of polymers at the minus end displaying the tread-milling feature (Larsen *et al.*, 2007). This tread-milling helps to move the TubZ filaments with the plasmid-TubR cargo to the pole. The TubZ filaments are speculated to bend at the cell pole, which leads to the dropping off of the plasmid-

TubR cargo. The TubZ filaments may then travel to other side of the cell in search of a new cargo.

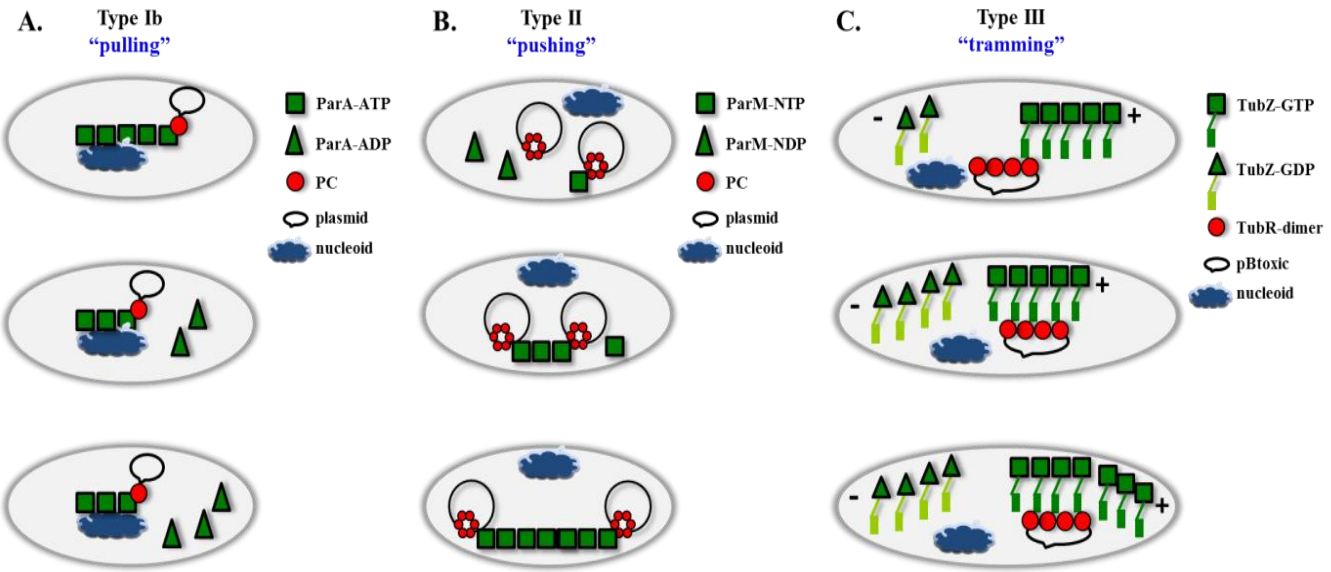

Figure 1.9. Diagrammatic representation of plasmid partition mechanisms.

A. Type Ib pulling mechanism for plasmid pB171. In this system, the nucleoid is used as a scaffold. ParA-ATP binds to nucleoid and undergoes polymerization. When ParA polymers meet ParB-plasmid complex, ParA interacts with ParB. ParB stimulates ParA ATPase activity which leads to ParA depolymerization and formation of ParA-ADP. The retracting ParA polymers pull plasmids in opposite direction. **B.** Type II pushing mechanism for plasmid R1. ParM forms filaments, which are stabilized by ParR-*parC* complex. Centromere DNA wraps around a ring of ParR dimers. ParM interacts with ParR at the inner side of the ring. ParM polymers grow continuously and elongated polymers push plasmids to opposite side in the cell. **C.** Type III tramming mechanism in plasmid pBtoxis. According to this model TubZ forms filaments and through its flexible C-terminal domain, it binds to TubR-*tubC* complex. Treadmilling by TubZ filaments move TubR-plamid complex to the cell pole. These filaments bend at the cell pole and facilitate the dropping-off of TubR-plasmid cargo from the TubR "tram". TubZ filaments then find another cargo and transport it to the opposite side of the cell. Reproduced from (Schumacher, 2012).

1.10 Aim and objectives

Multiple drug resistance is a global health threat. As plasmids play a major role in conferring drug resistance to bacteria, the study of plasmid partition at the molecular level is very important. The aim of this project is to study the molecular mechanism and dynamics of partition of multidrug resistance low-copy plasmids using plasmid TP228 as a model. Plasmid TP228 contains the *parFGH* partition cassette which harbours partition site *parH* and encodes two partition proteins ParF (a ParA type ATPase) and ParG (a CBP). The ParG N-terminal end though flexible, is implicated in various functions. The focus of this project is on the N-terminus of ParG. Given the number of independent functions of the N-terminal region of ParG and its importance in partition, the study of this region will provide an insightful picture of role of ParG in the process of plasmid segregation. This project will also investigate the intracellular activity of ParF and ParG and illuminate the dynamics of the partition system *in vivo*. The objectives of this study are as follows:

1. Generating mutations in individual amino acids of the ParG N-terminal end by using alanine scanning mutagenesis.
2. Determining plasmid partition efficiency of all the ParG N-terminal mutants. This analysis will reveal the residues in this region that are crucial for plasmid segregation.
3. Studying the effect of N-terminal mutations on the DNA binding activity of ParG.
4. Investigating the effect of N-terminal mutations on the transcriptional repressor function of ParG.
5. Characterizing the effect of N-terminal mutations on the polymerization of ParF in the presence and absence of ATP.
6. Examining the effect of N-terminal mutations on the stimulation of the ATPase activity of ParF.
7. Visualizing the localization patterns and dynamics of ParF, wild type and mutant ParG proteins in the cell by fluorescence microscopy. To this end, both conventional and super-resolution fluorescence microscopy will be exploited.

Chapter 2: Materials and Methods

2.1 Media, antibiotics, strains and plasmids

2.1.1 Media

2.1.1.1 Luria-Bertani solid and liquid media

Bacteria were grown in Luria-Bertani (LB) broth (Fisher scientific) or on LB agar (Formedium) media at 37ºC. LB broth or agar media were prepared by dissolving a specified quantity of commercially bought anhydrous mixture in a specified volume of distilled water and sterilising by autoclaving (121ºC for 20 minutes). The composition of media is given in Table 2.1.

Table 2.1 List of components of LB medium.

Components	Concentration g/L
Tryptone	10
Yeast extract	5
Sodium Chloride	10
Agar (for solid medium)	12

2.1.1.2 M9 medium.

A 10x M9 stock salt solution was prepared according to the Table 2.2. All the components were dissolved in distilled water to a final volume of 1 litre and autoclaved at 121ºC for 20 minutes. M9 complete medium was prepared by mixing 1X M9 stock salt solution with remaining ingredients as given in Table 2.3. With the exception of the M9 stock salt solution, all the components of M9 medium were sterilised using a 0.2 µm filter and added according to the requirement in the final media.

Table 2.2 List of components of the 10x M9 stock salt solution.

Components	Quantity (g)
$Na_2HPO_4.7H_2O$	64
KH_2PO_4	15
NaCl	2.5
NH_4Cl	5

Table 2.3 List of components of complete M9 medium.

Components of M9 medium
1X M9 salt solution (table 2.2)
2 mM $MgSO_4$
0.1 mM $CaCl_2$
0.2% Glucose

2.1.2 Antibiotics

Antibiotics were used as and when indicated in specified concentration as given in Table 2.4.

Table 2.4 List of the antibiotics used in this study

Antibiotics	Stock concentration	Working concentration
Chloramphenicol	30 mg/ml in ethanol	30 µg/ml (cloning) 10 µg/ml (partition assay)
Ampicillin	100 mg/ml in dH_2O	100 µg/ml
Kanamycin	50 mg/ml in dH_2O	50 µg/ml

2.1.3 Strains

The *Escherichia coli* strains used in this study are described in Table 2.5.

Table 2.5 List of bacterial strains

Strains	Genotype	Application
DH5α	F–Φ80*lacZ*ΔM15 Δ(*lac*ZYA-*arg*F) U169 *rec*A1 *end*A1 *hsd*R17 (rK–, mK+) *pho*A *sup*E44 λ– *thi*-1 *gyr*A96 *rel*A1	Cloning
BR825	*polA* which has inactivated DNA polymerase gene for supporting only low copy number replication (Ludtke *et al.*, 1989).	Plasmid partition assay
BL21 (DE3)	*fhuA2 [lon] ompT gal (λ DE3) [dcm]* Δ*hsdS*	Gene overexpression and protein production
SP850	*relA1 spoT*Δ(*cya-1400*)::Km *thi-1* e14$^-$λ$^-$	Bacterial two-hybrid assay
BW25113	[Δ(*araD-araB*)*567*Δ(*rhaD-rhaB*)*568 ΔlacZ4787* (::rrnB-3) *hsdR514 rph-1*],	Microscopy

2.1.4 Plasmids

The plasmids used in this study are given in the Table 2.6. Some of the plasmids were available in the laboratory as lab stock; others were constructed during the course of this work.

Table 2.6 List of plasmids used in this study.

Plasmid name	Details	Antibiotic marker
pFH450	A pBR322 derivative having P1 and ColE1 origins of replication without any partition elements (Hayes, 2000).	Chloramphenicol
pFH547	A pBR322 derivative having P1 and ColE1 origins of replication with the wild type partition cassette *parFGH* (Hayes, 2000).	Chloramphenicol
pET22b(+)	A translation vector with the bacteriophage T7 promoter and $(His)_6$-tag at the N-terminal end (Novogen).	Ampicillin
pDM3.0	The reporter gene *xylE* cloned downstream of the *parFG* promoter sequence (Zampini *et al.*, 2009).	Kanamycin
pET.ParG	The plasmid partition gene *parG* cloned into vector pET22b(+) (Barillà *et al.*, 2005).	Ampicillin
pET.ParF	The plasmid partition gene *parF* cloned into vector pET22b(+) (Barillà *et al.*, 2005).	Ampicillin
pT25	A pACYC184 derivative having a T25 fragment corresponding to the amino acids 1–224 of the catalytic domain of adenylate cyclase, CyaA (Karimova *et al.*, 1998).	Ampicillin
pT25ParF	The plasmid partition gene *parF* cloned into pT25 (Barillà and Hayes, 2003).	Ampicillin
pT18	A derivative of pBluescript II KS having a T18 fragment corresponding to the amino acids 225–399 of the catalytic	Chloramphenicol

Table 2.6 contd.

	domain of adenylate cyclase, CyaA (Karimova *et al.*, 1998).	
pT18.ParG	The plasmid partition gene *parG* cloned into pT18 (Barillà and Hayes, 2003).	Chloramphenicol
pBM20	A derivative of pFH547 in which the fluorophore gene *mCherry* is cloned in the frame with the partition gene *parG* (McLeod, B. unpublished data).	Chloramphenicol
pBAD.*parF*	The *egfp* gene which was cloned in the frame with *parF*, under the control of the arabinose-inducible promoter pBAD (McLeod, B. unpublished data).	Ampicillin
pMBS2A	*parGS2A* allele cloned into pFH547 vector by using *Cla*I and *Hpa*I sites (this work).	Chloramphenicol
pMBL3A	*parGL3A* allele cloned into pFH547 vector by using *Cla*I and *Hpa*I sites (this work).	Chloramphenicol
pMBE4A	*parGE4A* allele cloned into pFH547 vector by using *Cla*I and *Hpa*I sites (this work).	Chloramphenicol
pMBK5A	*parGK5A* allele cloned into pFH547 vector by using *Cla*I and *Hpa*I sites (this work).	Chloramphenicol
pMBH7A	*parGH7A* allele cloned into pFH547 vector by using *Cla*I and *Hpa*I sites (this work).	Chloramphenicol
pMBT8A	*parGT8A* allele cloned into pFH547 vector by using *Cla*I and *Hpa*I sites (this work).	Chloramphenicol
pMBK12A	*parGK12A* allele cloned into pFH547 vector by using ClaI and HpaI sites (this work).	Chloramphenicol
pMBS9A	*parGS9A* allele cloned into pFH547 vector by using *Cla*I and *Hpa*I sites (this work).	Chloramphenicol
pMBE17A	*parGE17A* allele cloned into pFH547	Chloramphenicol

Table 2.6 contd.

	vector by using *Cla*I and *Hpa*I sites (this work).	
pMBK11A	*parGK11A* allele cloned into pFH547 vector by using *Cla*I and *Hpa*I sites (this work).	Chloramphenicol
pMBM13A	*parGM13A* allele cloned into pFH547 vector by using *Cla*I and *Hpa*I sites (this work).	Chloramphenicol
pMBT14A	*parGT14A* allele cloned into pFH547 vector by using *Cla*I and *Hpa*I sites (this work).	Chloramphenicol
pMBN18A	*parGN18A* allel cloned into pFH547 vector by using *Cla*I and *Hpa*I sites (this work).	Chloramphenicol
pMBG16A	*parGG16A* allele cloned into pFH547 vector by using *Cla*I and *Hpa*I sites (this work).	Chloramphenicol
pMBL21A	*parGL21A* allele cloned into pFH547 vector by using *Cla*I and *Hpa*I sites (this work).	Chloramphenicol
pMBE22A	*parGE22A* allele cloned into pFH547 vector by using *Cla*I and *Hpa*I sites (this work).	Chloramphenicol
pMBV24A	*parGV24A* allele cloned into pFH547 vector by using *Cla*I and *Hpa*I sites (this work).	Chloramphenicol
pMBV25A	*parGV25A* allele cloned into pFH547 vector by using *Cla*I and *Hpa*I sites (this work).	Chloramphenicol
pMBT26A	*parGT26A* allele cloned into pFH547 vector by using *Cla*I and *Hpa*I sites (this work).	Chloramphenicol
pMBP28A	*parGP28A* allele cloned into pFH547 vector by using *Cla*I and *Hpa*I sites (this work).	Chloramphenicol
pMBV29A	*parGV29A* allele cloned into pFH547 vector by using *Cla*I and *Hpa*I sites (this	Chloramphenicol

Table 2.6 contd.

	work).	
pMBS30A	*parGS30A* allele cloned into pFH547 vector by using *Cla*I and *Hpa*I sites (this work).	Chloramphenicol
pMBS31A	*parGS31A* allele cloned into pFH547 vector by using *Cla*I and *Hpa*I sites (this work).	Chloramphenicol
pMBG32A	*parGG32A* allele cloned into pFH547 vector by using *Cla*I and *Hpa*I sites (this work).	Chloramphenicol
pET-MBL3A	*parGL3A* allele cloned into pET-22b (+) vector by using *Nde*I and *Xho*I sites (this work).	Ampicillin
pET-MBK5A	*parGK5A* allele cloned into pET-22b (+) vector by using *Nde*I and *Xho*I sites (this work).	Ampicillin
pET-MBK12A	*parGK12A* allele cloned into pET-22b (+) vector by using *Nde*I and *Xho*I sites (this work).	Ampicillin
pET-MBK11A	*parGK11A* allele cloned into pET-22b (+) vector by using *Nde*I and *Xho*I sites (this work).	Ampicillin
pET-MBM13A	*parGM13A* allele cloned into pET-22b (+) vector by using *Nde*I and *Xho*I sites (this work).	Ampicillin
pET-MBN18A	*parGN18A* allele cloned into pET-22b (+) vector by using *Nde*I and *Xho*I sites (this work).	Ampicillin
pDB-ParG-R19A	*parGR19A* allele cloned into pET-22b (+) vector by using *Nde*I and *Xho*I sites (Barillà *et al.*, 2007).	Ampicillin
pETMBL21A	*parGL21A* allele cloned into pET-22b (+) vector by using *Nde*I and *Xho*I sites (this work).	Ampicillin
pBART18ParGL3A	*parGL3A* allele cloned into pT18 vector by using *Xho*I and *Hind*III sites (Rodway, B. unpublished data).	Chloramphenicol

Table 2.6 contd.

pBART18ParGK5A	*parGK5A* allele cloned into pT18 vector by using *Xho*I and *Hind*III sites (Rodway, B. unpublished data).	Chloramphenicol
pT18ParGK11A	*parGK11A* allele cloned into pT18 vector by using *Xho*I and *Hind*III sites (this work).	Chloramphenicol
pT18ParGK12A	*parGK12A* allele cloned into pT18 vector by using *Xho*I and *Hind*III sites (this work).	Chloramphenicol
pT18ParGM13A	*parGM13A* allele cloned into pT18 vector by using *Xho*I and *Hind*III sites (this work).	Chloramphenicol
pT18ParGN18A	*parGN18A* allele cloned into pT18 vector by using *Xho*I and *Hind*III sites (this work).	Chloramphenicol
pT25ParGK12A	*parGK12A* allele cloned into pT25 vector by using *kpn*I and *Pst*I sites (this work).	Ampicillin
pT18ParGR19A	*parGR19A* allele cloned into pT18 vector by using *Xho*I and *Hind*III sites (this work).	Chloramphenicol
pT18ParGL21A	*parGL21A* allele cloned into pT18 vector by using *Xho*I and *Hind*III sites (this work).	Chloramphenicol
pBM20-L3A	*parGL3A* allele cloned into pBM20 vector by using *Bst*XI and *Hpa*I sites (this work).	Chloramphenicol
pBM20-K5A	*parGK5A* allele cloned into pBM20 vector by using BstXI and HpaI sites (this work).	Chloramphenicol
pBM20-K11A	*parGK11A* allele cloned into pBM20 vector by using *Bst*XI and *Hpa*I sites (this work).	Chloramphenicol
pBM20-K12A	*parGK12A* allele cloned into pBM20 vector by using *Bst*XI and *Hpa*I sites (this work).	Chloramphenicol
pBM20-M13A	*parGM13A* allele cloned into pBM20 vector by using *Bst*XI and *Hpa*I sites (this	Chloramphenicol

Table 2.6 contd.

	work).	
pBM20-N18A	*parGN18A* allele cloned into pBM20 vector by using *Bst*XI and *Hpa*I sites (this work).	Chloramphenicol
pBM20ParGR19A	*parGR19A* allele cloned into pBM20 vector by using *Bst*XI and *Hpa*I sites (McLeod, B. unpublished data).	Chloramphenicol
pBM20-L21A	*parGL21A* allele cloned into pBM20 vector by using *Bst*XI and *Hpa*I sites (this work).	Chloramphenicol

2.2 Recombinant DNA techniques

2.2.1 Preparation of plasmid DNA

Plasmid DNA miniprep was performed in order to isolate plasmid DNA on small-scale from the bacteria. A bacterial colony was selected and inoculated aseptically in 5 ml of sterile LB medium containing appropriate selective antibiotic for the plasmid. The culture was incubated overnight at 37^{o}C. Following incubation, small scale plasmid DNA isolation was carried out using QIAGEN Miniprep or Machery-Nagel kit according to the manufacturer's instructions. The plasmid DNA was eluted in 100 µl of sterile Milli-Q water by centrifugation of the column for 1 minute at 13000 rpm and stored at -20^{o}C.

2.2.2 Polymerase chain reaction (PCR)

Amplification of genes for cloning was carried out by performing a polymerase chain reaction (PCR). The template DNA was isolated as described in 2.2.1. Primers were designed to anneal to the flanking DNA sequences of the gene of interest with a required alteration in the gene or the insertion of restriction sites. The list of primers obtained from Sigma Aldrich is given in Table 2.7. Milli-Q water was used to resuspend the primers at a concentration of 100 µM. 100 mM stock of each deoxynucleotide triphosphates (dNTPs) (Roche) was also prepared. The PCR reaction was set up as given in Table 2.8 on ice in a 0.2 ml PCR tube. The reaction mixture was quickly spun down in the tube after mixing and transferred to a thermocycler, which was programmed as given in Table 2.9. Instrument lid was

heated to 105^{o}C. On completion, 5 µl aliquot of the PCR was checked on an agarose gel by electrophoresis.

Table 2.7 List of the primers used in this study.

Name	Sequence
ParG S2AForward	5’ GGA GTA GCC TGA ATG GCA CTT GAA AAA GCG 3’
ParG S2AReverse	5’ CGCTTTTTCAAGTGCCATTCAGGCTACTCC 3'
ParG L3A Forward	5’ GTAGCCTGAATGTCAGCTGAAAAAGCGCAT 3’
ParG L3A Reverse	5’ ATGCGCTTTTTCAGCTGACATTCAGGCTAC 3’
ParG E4A Forward	5’ GCCTGAATGTCACTTGCAAAAGCGCATACG 3’
ParG E4A Reverse	5’ CGTATGCGCTTTTGCAAGTGACATTCAGGC 3’
ParG K5A Forward	5’ TGAATGTCACTTGAAGCAGCGCATACGTCA 3’
ParG K5A Reverse	5’ TGACGTATGCGCTGCTTCAAGTGACATTCA 3’
ParG H7A Forward	5’ TCACTTGAAAAAGCGGCTACGTCAGTAAAA-3’
ParG H7A Reverse	5’-TTTTACTGACGTAGCCGCTTTTTCAAGTGA-3’
ParG T8A Forward	5’-CTTGAAAAAGCGCATGCGTCAGTAAAAAAA-3’
ParG T8A Reverse	5’-TTTTTTTACTGACGCATGCGCTTTTTCAAG-3’
ParG S9A Froward	5’-GAAAAAGCGCATACGGCAGTAAAAAAAATG-3’
ParG S9A Reverse	5’-CATTTTTTTTACTGCCGTATGCGCTTTTTC-3’
ParG V10A Forward	5’CATACGTCAGCAAAAAAAATGACCTTTGGT3’
ParG V10A Reverse	5’ ACCAAAGGTCATTTTTTTTGCTGACGTATG 3’
ParG K11A Forward	5’ CATACGTCAGTAGCAAAAATGACCTTTGGT 3’
ParG K11A Reverse	5’ ACCAAAGGTCATTTTTGCTACTGACGTATG 3’
ParG K12A Forward	5’ CATACGTCAGTAAAAGCAATGACCTTTGGT 3’
ParG K12A Reverse	5’ ACCAAAGGTCATTGCTTTTACTGACGTATG 3’
ParG M13A Forward	5’ TCAGTAAAAAAAGCGACCTTTGGTGAAAAC 3’
ParG M13A Reverse	5’ GTTTTCACCAAAGGTCGCTTTTTTTACTGA 3’
ParG T14A Forward	5’ TCAGTAAAAAAAATGGCCTTTGGTGAAAAC 3’

Table 2.7 contd.

ParG T14A Reverse	5’ GTTTTCACCAAAGGCCATTTTTTTTACTGA 3’
ParG E17A Forward	5’ AAAATGACCTTTGGTGCAAACAGAGATCTG 3’
ParG E17A Reverse	5’ CAGATCTCTGTTTGCACCAAAGGTCATTTT 3’
ParG G16A forward	5’GTAAAAAAAATGACCTTTGCTGAAAACAGAGATC T 3’
ParG G16A Reverse	5’ AGATCTCTGTTTTCAGCAAAGGTCATTTTTTTAC 3’
ParG N18A Forward	5’ ATGACCTTTGGTGAAGGCAGAGATCTGGAA 3’
ParG N18A Reverse	5’ TTCCAGATCTCTGCCTTCACCAAAGGTCAT 3’
ParG D20A Forward	5’ GGTGAAAACAGAGCTCTGGAACGAGTAGTA 3’
ParG D20A Reverse	5’ TACTACTCGTTCCAGAGCTCTGTTTTCACC 3’
ParG L21A Forward	5’ GGTGAAAACAGAG ATGCGGAACG AGTAGTA 3’
ParG L21A Reverse	5’ TACTACTCGTTCCGCATCTCTGTTTTCACC 3’
ParGE22A Forward	5’ GAAAACAGAG ATCTGGCACG AGTAGTAACA 3’
ParG E22A Reverse	5’ TGTTACTACTCGTGCCAGATCTCTGTTTTC 3’
ParGV24A Forward	5’ AGAGATCTGGAACGAGCAGTAACAGCACCA3’
ParGV24A Reverse	5’ TGGTGCTGTTACTGCTCGTTCCAGATCTCT 3’
ParGV25A Forward	5’ GATCTGGAACGAGTAGCAACAGCACCAGTA3’
ParGV25A Reverse	5’ TACTGGTGCTGTTGCTACTCGTTCCAGATC 3’
ParGT26A Forward	5’ CTGGAACGAGTAGTAGCAGCACCAGTATCA3’
ParGT26A Reverse	5’ TGATACTGGTGCTGCTACTACTCGTTCCAG 3’
ParGP28A Forward	5’ CGAGTAGTAACAGCAGCAGTATCATCTGGA3’
ParGP28A Reverse	5’ TCCAGATGATACTGCTGCTGTTACTACTCG 3’
ParGV29A Forward	5’ GTAGTAACAGCACCAGCATCATCTGGAAAA3’
ParGV29A Reverse	5’ TTTTCCAGATGATGCTGGTGCTGTTACTAC 3’
ParGS30A Forward	5’ GTAACAGCACCAGTAGCATCTGGAAAAATC3’
ParGS30A Reverse	5’ GATTTTTCCAGATGCTACTGGTGCTGTTAC 3’
ParGS31A Forward	5’ ACAGCACCAGTATCAGCTGGAAAAATCAAA3’
ParGS31A Reverse	5’ TTTGATTTTTCCAGCTGATACTGGTGCTGT 3’

Table 2.7 contd.

ParGG32A Forward	5’ GCACCAGTATCATCTGCAAAAATCAAACGT3’
ParGG32A Reverse	5’ ACGTTTGATTTTTGCAGATGATACTGGTGC 3’
ParF-ClaIupstream-F	5’ ACCGGTGTTAAAGCATTTCGTACA 3’
pET-ParGL3A	5’ GAGGAAACCATATGTCAGCTGAAAAAGCG 3’
pET-ParGK5A	5’ GAGGAAACCATATGTCACTTGAAGCAGCG 3’
InvertRepPromoForBT	5’ [Btn] AACCTTTACTCATACAAAGAGTATG 3’
InvertRepPromoRev	5’ ACCTGAACCCCCTTTCGGATTCAGA 3’
ParFG sequencing Primer	5'GCTTTCTTATCACCCGTAAGATAGAAATGG 3'
ParG2	5' TTCTTTCTCGAGTTCGTTCTCTTTGAG 3'
ParF EGFP primer	5'CGCACTGCAGTAATAAGAAGGAGATATACATATG AAAGTGATCTCAAAAG 3'
pT18 ParG Forward	5' CTTCTTCTCGAGGATGTCACTTGAAAAAGCG 3'
pT18 ParG Reverse	5' TCTCTCAAGCTTTCGTTCTCTTTGAG 3'
pT18 for sequencing	5' ATGACCATGATTACGCCAAGC 3'

Table 2.8 Reaction set up of PCR.

Component	**Volume (µl)**
Template DNA (1:10)	1 µl
Forward primer (5 pmol/ µl)	3 µl
Reverse primer (5 pmol/ µl)	3 µl
dNTPs (dATP, dCTP, dGTP, dTTP) (5 mM)	9.6 µl
10x reaction buffer	6 µl
dH_2O	To 60 µl
Taq/phusion/Pfu polymerase [1]	2 units

1 When a Taq polymerase buffer was used, 3.6 µl of 5 mM $MgCl_2$ was added to PCR reaction.

Table 2.9 Thermocycler programme for the PCR.

Steps	Temperature (^{o}C)	Time (minute)
1. Initial denaturation	93	3
2. Denaturation	92	1
3. Annealing	50/42	1
4. Extension	72	30 seconds
5. Repeat steps 2-4 for 29 cycles		
6. Final extension	72	6
7. Hold	10	∞

2.2.3 Restriction enzyme digestion

Restriction enzyme digestion was performed to analyse the positive clones and for the digestion of DNA fragments for different cloning experiments. Purified DNA was digested in a total volume of 10-40 µl, containing 1 unit of restriction enzyme/ µg of DNA, 1X restriction enzyme buffer, 1X BSA (bovine serum albumin) (if required) and sterile distilled water to make up the final volume of the reaction mixture. The total volume of the digestion reaction was dependent on the use of the digested DNA product. For restriction enzyme analysis of positive clones 10 µl of final volume was used and to produce digested DNA fragments for ligation reactions 40 µl of final volume was used. Restriction digestion was carried out at 37^{o}C for 2 h.

2.2.4 Alkaline phosphatase treatment of DNA

Plasmid DNA after digestion with restriction enzymes was subjected to alkaline phosphatase treatment. Digested DNA mixture was made up to 100 µl volume with 10X phosphatase buffer (NEB), 2 µl (1 unit) of Alkaline Phophatase enzyme (NEB) and water. The mixture was incubated at 37^{o}C for 30 minutes following which another 2 µl (1 unit) of Alkaline Phophatase enzyme was added with further incubation at 37^{o}C for 30 minutes. After incubation 10 µl of 200 mM ethylene glycol tetraacetic acid (EGTA) were added and incubated at 75^{o}C for 10 minutes. The

resulting reaction mixture was cleaned using a QIAGEN gel extraction kit as follows. To the above mixture, 300 µl of QG buffer were added and centrifuged for 1 minute at 13000 rpm. The flow-through was discarded and the column was washed twice with 750 µl PE buffer with incubation at room temperature for 3 minutes before adding the PE buffer for the second time. The PE buffer was removed completely by centrifuging and the sample was eluted in 30 µl of EB buffer.

2.2.5 Ethanol precipitation of plasmid DNA

An ethanol/water mixture with a high concentration of inorganic salt is used to precipitate DNA generated either by PCR or restriction digestion to achieve a high level of purity. To X volume of DNA mixture, 0.1X of Sodium acetate (pH 5.3) and 2X volumes of cold ethanol (100%) was added. The mixture was mixed thoroughly by inverting the tube and incubated at -20^{o}C for over 2 hours. After incubation, the mixture was centrifuged at 4^{o}C for 30 minutes at 14000 rpm. The supernatant was carefully removed with a pipette and 500 µl of 70% ethanol were added. The mixture was again centrifuged at 4^{o}C for 10 minutes. The supernatant was carefully removed with a pipette and any residual supernatant was removed by drying the tubes in a heating block. The precipitated DNA was resuspended in 20-30 µl of sterile Milli-Q water.

2.2.6 Agarose gel electrophoresis

All PCR products and DNA digestions were analysed using 1.2% w/v agarose gel electrophoresis. DNA fragments were visualised following intercalation with a fluorescent dye (SYBR Safe) and UV illumination. Gel was prepared by dissolving the required amount of agarose in 1X TAE buffer (40 mM Tris, 20 mM acetic acid, 1 mM EDTA). Prior to gel electrophoresis, the DNA samples were mixed with a 6X loading dye (10 mM Tris.HCl, pH 7.6, 60% glycerol, 0.3% xylene cyanol, 0.3% bromophenol blue, 60 mM EDTA). To estimate the size of the fragments, a 1 kb DNA ladder, with defined sizes, was run in parallel. DNA samples (5-50 µl) were loaded into the wells of a gel and electrophoresed at 100 V until the DNA fragments separated. The DNA fragments were visualised to confirm the separation of expected DNA fragments using a UV trans-illuminator attached to a gel documentation system.

2.2.7 FlashGel DNA system

Fast electrophoresis was carried out by using the FlashGel™ System (Lonza) which includes disposable precast agarose gel (1.2%) cassettes and a combination electrophoresis and trans-illuminator unit. This highly sensitive electrophoresis system separates DNA in 5-7 minutes. DNA samples were diluted with 1X FlashGel™ loading dye to make volume not less than 5 µl. Appropriate FlashGel™ DNA markers were used. White seals from cassettes were removed and wells were rinsed with distilled water. The cassette was inserted into the dock and samples were loaded. The gel was run at a high voltage power supply of 275 V until anticipated separation was reached. The gel image was captured by using the FlashGel™ Camera.

2.2.8 Gel extraction

DNA samples, either restriction digestion products or PCR products, were purified by electrophoresis on a 1.2% agarose gel and subsequent extraction from the gel using a QIAGEN kit following the manufacturer's protocol.

2.2.9 DNA ligation

A DNA fragment (insert) and vector were digested with same enzymes. The digested insert was gel purified and the plasmid was dephosphorylated to avoid self-ligation. The insert and vector were always used in a 5:1 ratio in the ligation reaction. In a 30 µl reaction volume, 3 µl 5X ligation buffer, 1 µl (2.5 units) T4 DNA ligase (Thermo Scientific) and sterile Milli-Q water (to make up the final volume) were added. The reaction was incubated at room temperature for 3 hours. The ligated DNA mixture was used directly to transform competent *E. coli* cells.

2.2.10 Preparation of competent cells

E. coli competent cells were prepared using rubidium chloride. The strain of *E. coli* was streaked aseptically onto a sterile LB agar plate and incubated overnight in a 37ºC incubator. Following incubation, a single colony was picked from the plate and inoculated into 10 ml of sterile LB broth. The culture was incubated at 37ºC overnight on a shaker. 60 ml of sterile LB broth were inoculated with 0.3 ml of the overnight culture. The bacterial growth was assessed by measuring the absorbance at

600 nm (A_{600}) at 1 h intervals using a spectrophotometer until the culture reached the optimal A_{600} of 0.4 - 0.6. The culture was incubated on ice for 10 minutes. The cells were harvested by centrifugation at 5000 rpm for 5 minutes at 4ºC. The medium was discarded and the cell pellet was resuspended in 20 ml of chilled RF1 buffer (15% glycerol, 100 mM RbCl, 50 mM $MnCl_2$, 30 mM KCH_3CO_2, 10 mM $CaCl_2$, pH 5.8, filter-sterilised and stored at 4ºC). The resuspended cells were incubated on ice for 1 h, then harvested by centrifugation at 5000 rpm for 5 minutes at 4ºC. The medium was removed and the cell pellet resuspended in 4.8 ml of ice-cold RF2 buffer (15% glycerol, 10 mM MOPS, 10 mM RbCl and 75 mM $CaCl_2$, pH 6.8, filter-sterilised and stored at 4ºC). The bacterial suspension was mixed gently followed by chilling on ice for 15 minutes. 400 µl aliquots were transferred into chilled, sterilised microcentrifuge tubes and immediately snap-frozen by immersing the tubes in liquid nitrogen. The tubes were stored at -80ºC until required.

2.2.11 Transformation of competent cells

The frozen competent cells were thawed on ice. For transformation, plasmid DNA (~10 ng) or the ligation mixture was mixed with 100 µl of competent cells in a 1.5 ml micro centrifuge tube. The cells were incubated on ice for 30 minutes. The cells were heat-shocked at 42^{o}C for 90 s. Following the heat shock, 400 µl of LB medium was added and the cells incubated on a shaker at 37^{o}C for 1 h. Following incubation, 100 µl of the transformed cell suspension was spread on LB agar plates containing suitable antibiotic. The plates were incubated at 37^{o}C overnight (18-20 h).

2.2.12 Screening of recombinant plasmids

To check if the cloning of a mutant gene in a plasmid was successful, 10 transformants were inoculated in sterile liquid LB medium with the required antibiotics and incubated at 37^{o}C overnight with shaking. Plasmid DNA was isolated as per 2.2.1 and a restriction enzyme digestion screen was set up with appropriate enzymes (2.2.3). The digestion products were run on gel and plasmids containing the insert of the right size were sent for DNA sequencing.

2.2.13 DNA sequencing

Plasmids harbouring the desired mutations were subjected to DNA sequencing. The primers used in the sequencing are given in the Table 2.7. All sequencing reactions were carried out by GATC Biotech Limited, Constance, Germany. The sequence data was analysed using Chromas software.

2.3 Mutagenesis

2.3.1 Site-directed mutagenesis by overlap extension PCR for *parG* mutagenesis

The ParG N-terminal end comprises of 32 amino acids. To study each amino acid, alanine scanning mutagenesis was carried out changing individual amino acids to alanine. The method used to generate mutations was overlap extension mutagenesis which involves three PCR steps and 4 primers (Figure 2.1). The internal forward and reverse primers were designed to have the flanking *parG* gene sequence with mutation. The forward external primer was designed to have the *parG* upstream sequence and the reverse external primer contained the downstream sequence of the *parG*. Two PCR reactions were performed. In PCR 1, an external forward primer and an internal reverse primer were used. In PCR 2, an internal forward primer and an external reverse primer were used. PCR 1 and PCR 2 were performed according to 2.2.2. Pfu polymerase was the polymerase of choice and pFH547 was used as template DNA. The products from these reactions were purified on agarose gel using gel extraction (2.2.8) and further with ethanol precipitation (2.2.5). The products of PCR 1 and PCR 2 were then combined in a pre-cycle reaction. In a pre-cycle reaction, equal amounts of DNA from PCR 1 and 2 were added to make a total volume of 25 µl. Other components added in the pre-cycle reactions were dNTPs (5 mM each dATP, dCTP, dGTP, dTTP), 10X Taq polymerase buffer, 5 mM MgCl2 to make a final reaction volume of 50 µl. This reaction was assembled in a 0.2 ml PCR tube and denatured at 93^{o}C for 3 minutes in a thermocycler. The tube was removed and 0.5 µl (2.5 units) Taq polymerase (GoTaq Promega) was added. The tube was again returned to the thermocycler and 10 cycles of incubation at 94^{o}C for 40 seconds and at 72^{o}C for 40 seconds were carried out. The pre-cycle step thus helped to promote annealing of the PCR1 and PCR2 fragments as shown in Figure 2.1. After the pre-cycle, extension products incorporating the desired mutations were

amplified in PCR3 using only the external primer pair. Forwards and reverse external primers (both at 25 pmol/ µl) were added to the tube and PCR 3 was carried out. The thermocycler was set up as per Table 2.8 (except the first denaturation step of 93^{o}C for 3 minutes). The PCR product was run on 1.2 % agarose gel and purified by ethanol precipitation. The PCR fragment was digested with *Cla*I (Promega) and *Hpa*I (Thermo Scientific) and cloned into the digested pFH547 vector. The mutation was confirmed by using GATC Biotech sequencing service.

2.3.2 Cloning of the *parG* mutant gene in pET22b and pT18ParG

To clone *parG* mutant allele in vector pET22b, forward primer was designed to have restriction site *Nde*I and the sequence flanking the *parG* gene. Reverse primer with restriction site *Xho*I was available in the lab stock as primer ParG2. For cloning *parG-L3A* and *parG-K5A*, forward primers were designed to have the respective mutant sequences as well. As a template, partition vectors (i.e. pMB series) harbouring mutant *parG* allele were used. The PCR was set up as given in 2.2.2. Pfu DNA polymerase was used and the annealing temperature was set to 42^{o}C. PCR products and pET22b vector were digested with *Nde*I (NEB) and *Xho*I (Fermentas) and further steps were followed similar to 2.3.1. To clone *parG* mutant allele in vector pT18ParG, partition vector harbouring *parG* mutations were isolated as per 2.2.1 and used as a template. The forward primer was designed to have a *Hind*III restriction site and ParG2 with *Xho*I restriction site was used as a reverse primer. PCR was carried out as per 2.2.2 with Taq polymerase and an annealing temperature of 42^{o}C. PCR products and pT18ParG vector were digested with *Hind*III (Thermo Scientific) and *Xho*I, further steps were followed similar to 2.3.1.

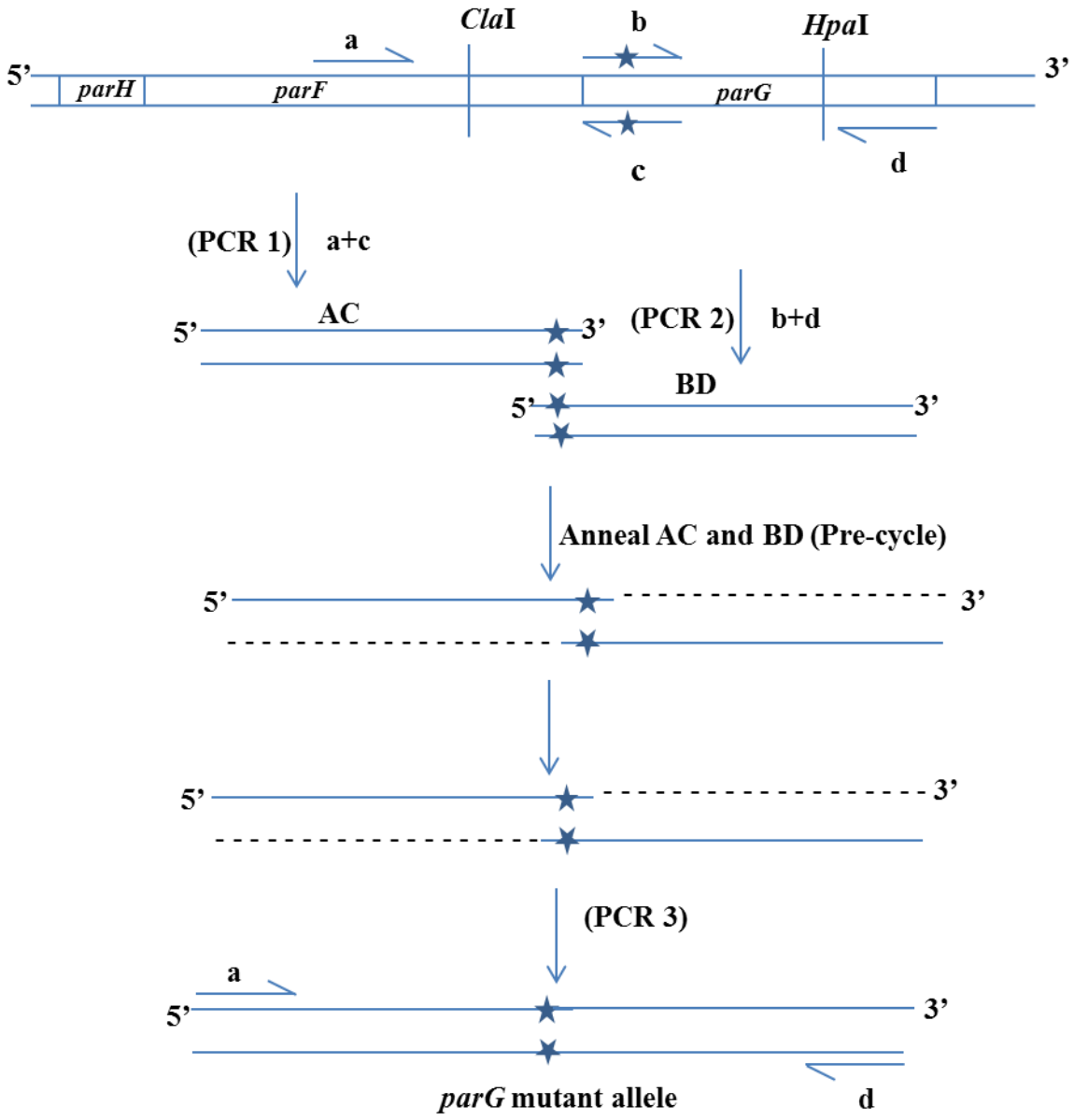

Figure 2.1. Schematic representation of overlap extension mutagenesis.

Three PCR reactions are carried out to generate *parG* mutant allele. The primers used are a- ParF *Cla*I Forward primer (External primer), b- ParG Mutant Forward primer (internal primer), c- ParG Mutant Reverse primer (Internal primer), d- ParG2 Reverse primer (external primer).

2.3.3 Cloning of the *parG* mutant gene in vector pBM20

Vector pBM20 contains the partition cassette *parFGH* and has the *mCherry* gene cloned in frame with *parG* in it. To clone a mutant *parG* allele into the pBM20 restriction digestion was carried out. The partition vectors containing mutant *parG* alleles and the vector pBM20, were digested with *Bst*XI (Promega) and *Hpa*I. The mutant *parG* allele fragment was swapped into the digested vector pBM20 and transformed into DH5α cells. Transformants were screened using a restriction digestion screen and confirmed by DNA sequencing.

2.4 Expression and purification of recombinant proteins

2.4.1 Overproduction and purification of ParF

The His-tagged ParF protein was overproduced in *E. coli* BL21(DE3). Around 8-10 transformants were inoculated in ~8 ml of LB with ampicillin in a 125 ml conical flask. ParF was grown at 30ºC with shaking at 180 rpm, for two-three hours until the culture started to become turbid. This starter culture was then inoculated into 300 ml of pre-warmed LB with ampicillin and grown till it reached an OD_{600} = 0.8 – 0.9. The culture was induced with isopropyl-beta-D-thiogalactopyranoside (IPTG) (Melford) at a final concentration of 1 mM and incubated for a further 3 hours. Cells were then harvested at 15303 g for 5 minutes at 4ºC and pellets were stored at -80ºC. The protein was purified by Ni^{2+} affinity chromatography as per the Novagen technical manual as follows. ParF containing cell pellets were re-suspended in 15 ml of 1X binding buffer (Table 2.10) and an EDTA free protease inhibitor tablet (Roche), 150 µl of lysozyme (10 mg/ml) (Sigma) and 150 µl of phenylmethylsulphonyl fluoride (PMSF; 100 mM in ethanol) were added. This mixture was incubated for 15 minutes at 30ºC, then an additional aliquot of 150 µl of lysozyme solution was added followed by a further incubation for another 15 minutes. The pellets were sonicated 12 times for 30 seconds each with 1 minute interval on ice. The sonicated mixture was centrifuged for 35-40 minutes at 11,000 rpm at 4ºC and the supernatant was collected. A column was prepared with His-binding resin (Novagen) with a 2.5 ml bed volume. The resin was charged with 1X 50 mM $NiSO_4$ and equilibrated with 1X binding buffer. The extract supernatant was loaded on this column in a close circuit for 1 h and 30 minutes at a peristaltic pump flow rate = 3.0. The column was washed first with 30 ml of 1X binding buffer and

then with 70 ml of 1X washing buffer (Table 2.10). Elution was carried out by using 1X elution buffer (Table 2.10) and 12 fractions of 1 ml each were collected. DTT was added to 2 mM final concentration in each fraction. Protein fractions were quantified by Bradford assay using the Bio-Rad protein assay reagent (2.4.4) and highly concentrated fractions were buffer exchanged by using a 5 ml HiTrap desalting column (2.4.3) eluted and stored in the storage buffer (Table 2.10).

Table 2.10 The composition of buffers used in ParF purification.

1X ParF Binding Buffer	**1X ParF Wash Buffer**	**1X ParF Elution Buffer**
50 mM Tris, pH 7.5-8.0	50 mM Tris, pH 8.0	50 mM Tris, pH 8.0
500 mM NaCl	1 M NaCl	150 mM NaCl
15 mM imidazole	85 mM imidazole	300 mM imidazole
10% Glycerol	10% Glycerol	10% Glycerol
Storage ParF Buffer	All buffers were pH checked and filtered prior to use.	
30 mM Tris, pH 7.5-8.0		
100 mM KCl		
10% Glycerol		
2 mM DTT		

2.4.2 Overproduction and purification of ParG and mutant proteins

The *parG* gene (wild type and mutant) was cloned into the expression vector pET-22b. The His-tagged proteins were overproduced in *E. coli* BL21(DE3). Around 8-10 transformants were inoculated in ~8 ml of LB with ampicillin and grown at 37ºC, shaking at 180 rpm for two-three hours until the culture started to become turbid. This starter culture was then inoculated into 300 ml of pre-warmed LB with ampicillin and grown at 37ºC on shaker at 180 rpm till it reached an OD_{600} = 0.8 – 0.9. The culture was induced with IPTG at a final concentration of 1 mM and incubated at 37ºC on shaker at 180 rpm for a further 2 hours. Cells were then harvested at 15303 g for 5 minutes at 4^{o}C. Pellets were stored at -80ºC. Proteins were purified by Ni^{2+} affinity chromatography according to the Novagen technical manual as follows. ParG and ParG mutants containing cell pellets were resuspended into 10 ml of 1X binding buffer (Table 2.11) and 100 µl of soybean trypsin inhibitor (1 mg/ml), 100 µl of lysozyme (10 mg/ml) and 100 µl of PMSF were added. This

mixture was incubated for 15 minutes at 30ºC, then additional 100 µl of lysozyme solution were added, and further incubated for another 15 minutes. The pellets were sonicated 12 times for 30 seconds each with 1 minute interval on ice and then this mixture was centrifuged for 1 h at 16,000 rpm at 4ºC. The supernatant was collected. The column was prepared with 2.5 ml of His-binding resin. The resin was charged with 1X $NiSO_4$ (50 mM) and equilibrated with 1X binding buffer. The cleared extract was loaded onto this column in a close circuit for 1 h and 15 minute at a peristaltic pump flow rate = 3.0. Then the column was washed, first with 30 ml of 1X binding buffer and then with 70 ml of 1X washing buffer (Table 2.11). Elution was carried out by using 1X elution buffer (Table 2.11) and 12 fractions of 1 ml each were collected. Protein fractions were quantified by Bradford assay using the Bio-Rad protein assay reagent (2.4.4) and highly concentrated fractions were buffer exchanged by using a 5 ml HiTrap desalting column (2.4.3), eluted and stored in the storage buffer (Table 2.11).

Table 2.11 The composition of buffers used in ParG purification.

1X Binding Buffer	**1X Wash Buffer**	**1X Elution Buffer**
20 mM Tris, pH 7.5-8.0	20 mM Tris, pH 8.0	20 mM Tris, pH 8.0
500 mM NaCl	1 M NaCl	500 mM NaCl
15 mM imidazole	90 mM imidazole	400 mM imidazole
Storage Buffer	All buffers were pH checked and filtered prior to use.	
50 mM Tris, pH 7.5-8.0		
50 mM KCl		
2mM DTT		

2.4.3 Buffer exchange using the HiTrap column

A syringe was filled with ParF/ParG storage buffer. The stopper on the top of the HiTrap column (GE healthcare) was removed and connected to the syringe while the buffer was dripping. The column was equilibrated with 10 ml of storage buffer. Protein fractions with high concentrations were applied to the column in batches of 1.5 ml. After loading each batch of 1.5 ml, protein was eluted in ParF/ParG storage buffer in two 1 ml fractions. Protein concentration was determined and fractions were analysed on SDS-PAGE. The fractions were aliquot into 100 µl volume and flash frozen in liquid nitrogen.

2.4.4 Protein concentration determination

Protein concentrations were determined by using Bradford assay. Bovine serum albumin (BSA) was used as a protein standard in the concentration range of 0.4, 1, 2, 4 and 6 µg/ml. Each one ml of reaction contained 1 part of Bradford reagent and 4 parts of Milli-Q water. The reaction was incubated for 5 minutes. The absorbance was measured at 595 nm. A graph of protein concentration versus absorbance (A_{595}) was plotted and a standard curve was obtained. The amount of 5 µl of the unknown protein was added to 795 µl of water and then 200 µl of Bradford reagent were added and the absorbance at 595 nm was recorded. Samples were tested in triplicate.

2.5 Sodium dodecyl sulfate-polyacrylamide gel electrophoresis (SDS-PAGE)

2.5.1 Gels and buffers

Gels were prepared by assembling the glass plate sandwich as per the manufacturer's instructions. The resolving gel (15%) solution was prepared as described in Table 2.12. The APS and TEMED solutions were added at the end and the solution was mixed gently to avoid formation of bubbles. The solution was poured between the glass plates to 3/4 of height leaving space for the stacking gel. The top of the resolving gel was covered with 70% isopropanol and the gel was allowed to solidify. The isopropanol was discarded and the gel was washed gently with water. The stacking gel solution was prepared as described in Table 2.13 and poured onto the resolving gel.

Table 2.12 Composition of 15% resolving gel.

Components	Volume for 10 ml resolving gel solution for 15% gel
Deionised water	3.4 ml
30% Acrylamide mix	7.5 ml
1.5 M Tris (pH 8.8)	3.8 ml
10% SDS	0.15 ml
10% Ammonium persulfate (APS)	0.15 ml
TEMED	0.006 ml

Table 2.13 Composition of stacking gel.

Components	Volume for 5 ml stacking gel solution
Deionised water	2.7 ml
30% Acrylamide mix	0.67 ml
1 M Tris (pH 6.8)	0.5 ml
10% SDS	0.04 ml
10% Ammonium persulfate (APS)	0.04 ml
TEMED	0.004 ml

2.5.2 Sample preparation

Each protein sample of 10 µl was added to 10 µl of 2X SDS loading buffer (100 mM Tris (pH 6.8), 200 mM DTT, 4% SDS, 0.2% Bromophenol Blue and 20% Glycerol). The mixture was then heated to 95°C for 5 minutes and quickly spun down. A PageRuler Prestained Protein Ladder (Thermo Scientific) was used to allow the molecular weight of proteins to be estimated.

2.5.3 Electrophoresis

Gels were run using the Mini-PROTEAN (Bio-Rad) system and the apparatus was assembled according to the manufacturer's instructions. Gels were put into the tank and then the tank was filled with 1X SDS running buffer (Table 2.14). Protein samples and a molecular weight marker were loaded and the gel was run for approximately 1 h (or till the blue dye front reached the bottom) at 25 mA.

Table 2.14 Components of 5X SDS running buffer.

Components	Concentration
Tris	125 mM
Glycine	1.25 M
SDS	0.5%

2.5.4 Staining of SDS gels

Staining of the SDS gels to detect proteins was carried out using Coomassie Brilliant Blue dye. The stain was prepared by adding 1.25 g dye into 250 ml methanol, 50 ml acetic acid and 250 ml sterile water. Gels were rinsed with water and then placed on

a rocker in the stain for 1 h. Gels were removed from the stain and placed into the destain solution overnight. The destain solution was prepared by adding 250 ml of methanol to 100 ml of water, followed by adding 50 ml of acetic acid and adjusting the final volume to 500 ml with water.

2.6 Plasmid partition assay

The efficiency of plasmid partition was tested by performing partition assays (Figure 2.2). Plasmids harbouring no partition cassette (pFH450), wild type partition cassette (pFH547) and a mutant version of the partition cassette (pMB series having mutation in ParG N-terminal end) were transformed into the strain BR825 with selection for chloramphenicol resistance on LB medium. Ten transformants were selected and streaked on a sterile LB medium plates containing chloramphenicol and incubated at 37°C overnight. One colony from each of these streaks was streaked on a sterile LB plates without antibiotics and incubated at 37°C overnight. Streaking on LB plates without antibiotics was repeated for one more day. This streaking on non-antibiotic media provides about 25 generation of non-selective growth. The following day, from each streak, 10 isolated colonies were stabbed onto LB plates with and without antibiotics which gives 100 colonies for each samples. The percentage of colonies which retain the plasmid was determined. Assays were performed at least in triplicate.

2.7 Chemical cross-linking

ParG mutant's dimerization was studied by chemical cross-linking. The cross-linker used in this experiment is dimethyl pimelimidate (DMP) (Sigma) which is an amine-reactive imidoester type of crosslinker. Imidoester crosslinkers react with primary amines to form amidine bonds. ParG and mutant proteins were used at a final concentration of 20 µM and DMP was added at increasing concentration of 0, 0.5, 1 and 10 mM. A buffer (50 mM Hepes-KOH pH 8.5, 50 mM KCl, 5 mM $MgCl_2$) was used. The final reaction volume was 15 µl. The reactions were incubated for 1 h at 37°C and then stopped by the addition of 1 µl of 0.5 M Tris-HCl pH 6.8. This was followed by addition of 1X SDS loading buffer. The samples were heated at 95°C for 5 minutes and analysed by SDS-PAGE.

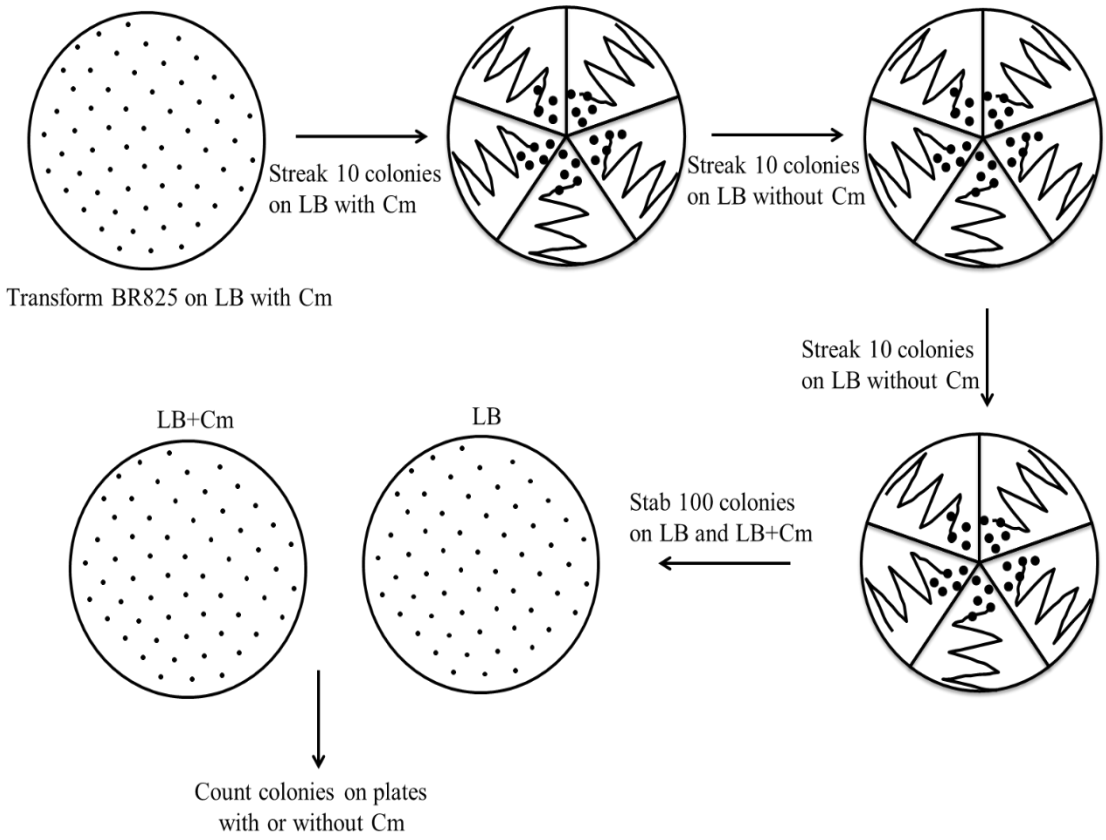

Figure 2.2. Schematic representation of plasmid partition assay.

On the first day BR825 cells were transformed with separate partition probe vectors which contain either no partition elements or wild type or mutant partition cassette. On day 2, 10 colonies were streaked onto two LB with chloramphenicol containing plates. The streaking was carried out for the next two days on plates without antibiotics. On the 5th day 100 isolated colonies were stabbed onto LB plates with and without chloramphenicol. On day 6, colonies were counted which indicated the percentage of plasmid retention.

2.8 Electrophoretic mobility shift assay (EMSA)

2.8.1 Generating biotinylated DNA fragment

EMSA was carried out to check the binding of ParG N-terminal mutant proteins to the *parFG* promoter sequence. The forward primer was designed to have a biotin label at the 5' end and the sequence flanking the *parFG* promoter. The PCR was set up as per Table 2.7, pFH547 as DNA template, Phusion polymerase (NEB) and 5X high fidelity Phusion buffer were used. The thermocycler was programmed as per Table 2.15. The PCR product was analysed on agarose gel and purified by the gel extraction method. The DNA concentration was determined by using the Nanodrop.

Table 2.15 Thermocycler programme for PCR.

Steps	Temperature (^{o}C)	Time (seconds)
1. Initial denaturation	98	30
2. Denaturation	98	10
3. Annealing	42	30
4. Extension	72	15
5. Repeat steps 2-4 for 29 cycles		
6. Final extension	72	6 minutes
7. Hold	10	∞

2.8.2 Preparation of samples and gel electrophoresis

A reaction mixture of 20 µl was prepared in which 0.5 nM biotinylated DNA (*parFG* promoter sequence) and an increasing concentration (100 to 1000 nM) of ParG or ParG mutant proteins were added. The reaction mixture also contained poly(dI-dC) (1 µg/µl), 50% glycerol (1 µl), 100 mM $MgCl_2$ (1 µl), 10X buffer (2 µl) and water to make it up to 20 µl volume. Reactions were incubated for 20 minutes at 25^{o}C. A 6% native gel (Table 2.16) was used which was pre-run for 20 minutes at 100 V. All the samples were loaded onto the gel and run with 0.5X TBE buffer (Table 2.17) at 100 V until the dye front reached 3/4th of the gel.

Table 2.16 Composition of 6% native gel.

Components	**Volume**
5X TBE	1.2 ml
30% Acrylamide	2.4 ml
10% APS	70 µl
TEMED	10 µl
Distilled water	8.4 ml

Table 2.17 Composition of 5X TBE buffer.

Components	**Quantity**
Tris base	54 g
Boric acid	27.5 g
0.5 m EDTA, pH 8.0	20 ml
Distilled water	To make 1000 ml

2.8.3 DNA transfer onto a positively-charged nylon membrane

DNA from the gel was transferred on to a positively charged membrane in an electrophoresis tank. A nylon membrane (Roche), 3 MM Whatman paper and sponges (Bio-Rad system) were cut to the size of the gel and soaked in 0.5X TBE buffer. In a transfer cassette (Bio-Rad system), one sponge and two pieces of Whatman 3MM paper were placed and then the gel was placed on Whatman paper. The nylon membrane was placed on top of gel avoiding air bubbles. Two pieces of Whatman 3MM paper and sponge were placed on the membrane. The sandwich was inserted in the cassette and placed in a tank to transfer the DNA to the positively-charged membrane. The DNA transfer was carried out at 380 mA for 30 minutes in 0.5X TBE buffer. The sandwich was then disassembled and the membrane was removed carefully and the position of the wells were marked. The membrane was dried on paper towel, wrapped in Saran wrap. The DNA was cross-linked to the membrane by placing DNA side down onto a UV transilluminator for 5 minutes.

2.8.4 Detection of Biotinylated DNA using the LightShift™ Chemiluminescent EMSA kit (Pierce)

The blocking buffer and the 4X wash buffer were warmed to 37-50^{o}C in a water bath until all the particulate material was completely dissolved. The membrane was placed in a clean tray and 20 ml of blocking buffer were added and then it was incubated for 15 minutes on a shaker. The blocking buffer was discarded and the membrane was placed in a conjugate/blocking buffer solution in a tray for 15 minutes on a shaker. The Conjugate/Blocking buffer solution was prepared by adding 1 µl streptavidin-horseradish peroxidase conjugate (Sigma-Aldrich) to 10 ml blocking buffer. 80 ml of 1X wash buffer were prepared by adding 40 ml of 4X wash buffer to 120 ml dH_2O. The membrane was transferred to a new tray and washed with 20 ml of 1X wash buffer four times (5 minutes each). The membrane was then transferred to a new container containing 30 ml of equilibration buffer and incubated for 5 minutes on a shaker. The membrane was then removed and placed on paper towel to remove the excess buffer. The substrate solution was prepared by adding 1 ml of luminol/enhancer solution to 1 ml stable peroxide solution and transferred to a small clean tray. The membrane was placed in the substrate solution with DNA side facing down and incubated for 5 minutes with gentle shaking. The membrane was

then removed and any excess of buffer was removed by tissue paper. The membrane was then placed in a film cassette and covered with an acetate sheet. After 10 minutes, the membrane was exposed to a X-ray film first for 30 seconds, and then for longer or shorter time periods as appropriate.

2.9 Catechol 2, 3-dioxygenase (CDO) reporter assay

For the CDO reporter assay, two plasmids were used; the pDM3.0 plasmid in which the *parFG* promoter-operator region was cloned upstream of the *xylE* reporter gene and pET22b derivatives expressing the *parG* gene (wild type or mutant). *E. coli* BL21 (DE3) cells were co-transformed with pDM3.0 and pET22b derivatives and selected for kanamycin (pDM3.0) and ampicillin (pET22b) resistance. A single transformant colony was inoculated on 50 ml of LB broth containing ampicillin (100 μg/ml) and kanamycin (50 μg/ml), and incubated at 37^{o}C until the mid-logarithmic phase was reached (OD_{600} = 0.5). The cells were centrifuged and the pellets were resuspended in 10 ml of 100 mM potassium phosphate buffer, pH 7.4, with 10% acetone. Resuspended pellets were sonicated on ice with five 15 second bursts. The lysate was cleared by centrifugation. The protein concentration in the supernatant was determined using the Bradford Assay (2.4.4). Samples were diluted to a protein concentration of 0.05 mg/ml. A 1ml aliquot of protein sample was transferred in a cuvette and 20 μl catechol (10mM) (Sigma) were added. After 1 minute, absorbance at 375 nm was recorded (measurements performed at least in triplicate, each from an independent culture containing the plasmids). Cell extracts containing the *xylE* product become yellow within seconds in the presence of catechol. Catechol is a colourless substrate that is converted into a yellow coloured product, 2-hydroxymuconic semialdehyde by catechol 2,3-dioxygenase. CDO units were determined by using the following equation:

$$\text{CDO units} = \left[\frac{A_{375\,nm}}{\varepsilon}\right] \text{X } 1000$$

where A is absorbance, ε is the extinction coefficient. One CDO (μmol/ml) unit is the amount of enzyme that oxidizes 1 μmol of catechol per minute at 24^{o}C.

2.10 Dynamic light scattering (DLS)

The Malvern Zetasizer Nano system was used to determine ParF polymerization by dynamic light scattering. Proteins to be analysed were centrifuged for 30 minutes at 13,000 rpm in a refrigerated microcentrifuge. The supernatant was collected and quantified by Bradford assay (2.4.4). Proteins (ParF, ParG wild type and mutant) were diluted to 50 ng/µl using the ParF/ParG storage buffer and kept on ice. In the DLS assay, 46.25 µl of the ParF protein (final concentration 2.16 µM) were added to a 50 µl quartz cuvette and placed in a Zetasizer chamber at 30^{o}C. Twenty readings were taken for the intensity of light scattering from which the hydrodynamic radius (Z-average) can be inferred. The cuvette was taken out of the chamber and $MgCl_2$ (final concentration 5 mM) and ATP (final concentration 500 µM) was added to a final volume of 50 µl. The cuvette was again placed into the chamber and further readings were taken for the intensity of light scattering. Approximately by 60th readings a plateau was reached. The cuvette was again taken out of the chamber and 2.16 µM ParG wild type or mutant protein was added. The solution was mixed by pipetting. The cuvette was returned to the chamber and further readings were taken till a plateau was reached. The intensity of scattered light is proportional to size and the concentration of the particles present in the solution.

2.11 Sedimentation assay

ParF polymerization stimulated by ParG was analysed by sedimentation assay in the absence and presence of nucleotides. ParF and ParG or mutant proteins (8 µM final concentration) were incubated at 30^{o}C for 30 minutes in buffer F (Table 2.18) in 60 µl reaction volume. ATP 2 mM and $MgCl_2$ 5 mM were added wherever indicated. After incubation, reactions were centrifuged at 14,000 rpm for 30 minutes at 4^{o}C. The supernatant was collected, and to a 20 µl aliquot, 10 µl of 2X SDS loading buffer were added. The pellets fractions were dried by heating at 30^{o}C for 5 minutes and resuspended in 15 µl of sterile water. To the resuspended pellets, 10 µl of 2X SDS loading buffer were added. Both the supernatant and the pellets were denatured at 95^{o}C for 5 minutes and then analysed by SDS-PAGE and Commassie blue staining. On each gel, 100% of the pellet and 33% of the supernatant were loaded.

The bands were quantified with ImageJ (National Institutes of Health, Bethesda, MD).

Table 2.18 Composition of Buffer F.

Buffer F
30 mM Tris, pH 8.0
100 mM KCl
2 mM DTT
10% glycerol

2.12 Bacterial two-hybrid assay

E. coli SP850 cells were co-transformed with the two plasmids containing T18 and T25 fusions of interest (pT18 and pT25, pT18-zip and pT25-zip, pT18-ParG/mutants and pT25-ParF). Single colonies were inoculated into 5 ml of LB broth with appropriate antibiotics and 0.5 mM IPTG and the cultures grown at 30ºC overnight. Cultures were cooled down on ice for 20 minutes and diluted 1:5 with M63 medium (Table 2.19). A_{600} was recorded for all cultures. For each culture, three 1 ml aliquots were taken and centrifuged for 20 minutes at 13000 rpm. The supernatants were removed and the pellets were resuspended into 700 µl of buffer Z (Table 2.20). To this solution 20 µl of $CHCl_3$ and 0.1% SDS were added and vortexed for 1 minute. These samples were incubated at 28ºC to equilibrate and then 200 µl of O-Nitrophenyl-β-D-Galactopyranoside (ONPG) (4 mg/ml) (Sigma) were added. The time taken to develop yellow colour was noted and the reaction was stopped by adding 500 µl of 1M Na_2CO_3. Samples were spun for 1 minute to remove any debris and A_{420} and A_{550} were recorded for the supernatants. Miller units were calculated by using the following equation:

$$MU = 1000 \times \frac{(A_{420\,nm} - (1.75 \times A_{550\,nm}))}{t \times V \times A_{600\,nm}}$$

where MU is Miller units, A is absorbance, t is time and V is volume.

Table 2.19 Composition of M63 medium.

5X M63 medium[1]
10 g $(NH_4)_2SO_4$
68 g KH_2PO_4
2.5 mg $FeSO_4.7H_2O$
Dissolved in 1 litre dH_2O and adjust to pH 7 with KOH

1 The above medium was sterilized by autoclaving and then 1 ml 1M $MgSO_4$ and 10 ml 20% maltose (filter sterilized) were added.

Table 2.20 Composition of Z buffer.

Z buffer [1]
0.06 M $Na_2HPO_4.7H_2O$
0.04 M $NaH_2PO_4.H_2O$
0.01 M KCl
0.001 M $MgSO_4$
Make to 1 litre with dH_2O and adjust to pH 7

1 To 20 ml of Z-buffer, 54 µl (0.05 M) β-mercaptoethanol (Sigma) were added just prior to use.

2.13 ATPase assay

ATPase assays were performed using thin layer chromatography (TLC). A polyethyleneimine (PEI)-cellulose plate (Macherey-Nagel) was pre-run in Milli-Q water in a TLC tank until the liquid reached the top of the plate. The plate was allowed to dry on the bench. The ParF ATPase activity was assessed in the presence of wild type and mutant ParG using [α^{35}S] ATP (Perkin Elmer, UK). In a 16 µl reaction, 0.5 µM ParF was incubated separately with increasing concentrations (0.5, 1, 2 and 5 µM) of wild type and mutant ParG protein fractions. [α- ^{35}S] ATP was added at a final concentration of 50 nM together with 4 µl of 4X ATPase buffer (Table 2.21) and the volume was made up with dH_2O. As a control all the ParG fractions were also run without ParF. The reactions were incubated for 1 h at 30ºC. 5 µl aliquots of the reaction mixtures were loaded on the PEI plate ~1 cm apart from one another. The samples were applied ~2 cm from the bottom of the plate using standard filtered tips. The spots were allowed to dry in air. The plate was then run in

0.5 M KH_2PO_4, pH 3.5, in a TLC tank until the buffer reached the top of the plate. The plate was then dried in fumehood. The dried plate was placed in a cassette and exposed to a BIOMAX MR Kodak flim for a suitable time. The ADP and ATP spots were quantified by using the Bio-Rad Phosphomager. The stimulation of ParF ATPase activity in the presence of wild type ParG (5 μM) was considered as 100% and that promoted by the ParG mutant proteins was calculated as relative ATPase stimulation.

Table 2.21 Composition of 4X ATPase assay buffer.

4X ATPase Buffer	Prepare 1ml aliquots and store at -20^{o}C
120 mM Tris, pH 7.5	
400mM KCl	
20 mM $MgCl_2$	
8 mM DTT	

2.14 Microscopy

2.14.1 Confocal microscopy

BW25113 *E. coli* cells were co-transformed with pBAD-ParF and pBM20 derivatives. The transformants were grown in 1 ml of M9 glucose medium with ampicillin (100 μg/ml) and chloramphenicol (30 μg/ml) for 1 hour at 37°C and then induced with 3 μl of 10% arabinose (final concentration 0.03%) for 3 hours at 30°C. The cells were harvested at 8000 rpm for 1 minute and the pellets were resuspended in 20 μl M9 medium without antibiotics. Agarose (1.2% in M9 medium with glucose) pads were prepared on a microscopy slide by using geneframes (ABgene). 0.4 μl of the cell suspension was placed on the agarose pad and covered with a glass coverslip. 4',6-diamidino-2-phenylindole (DAPI) was used at 2 μg/ml concentration wherever indicated. Confocal microscopy was performed using a Zeiss LSM710 and 488 nm and 561 nm lasers for eGFP and mCherry respectively. Images were analysed using the Volocity software (Perkin Elmer).

2.14.2 3D-Structured Illumination Microscopy

To study ParF localisation and its appearance *in vivo* on greater detail and at a higher level of resolution, super resolution 3 Dimensional-Structured Illumination

Microscopy (3D-SIM) was exploited The protocol applied was based on that described in (Schermelleh *et al.*, 2008). The cells were grown and the microscopy slides were prepared by using the same protocol as in 2.14.1. Images were acquired at SULSA, University of Dundee, using a 100x 1.4NA, oil immersion objective lens (Olympus, Center Valley, PA) and an electron-multiplying charge - coupled device (EMCCD) cameras (Photometrics, Tucson, AZ) on the OMX version 3 system (Applied Precision) equipped with 405-, 488-, and 593-nm solid-state lasers. Samples were illuminated by a coherent scrambled laser light source that had passed through a diffraction grating to generate the structured illumination by interference of light orders in the image plane to create a 3D sinusoidal pattern, with lateral stripes approximately 0.2 µm apart. Raw images were processed and reconstructed to reveal structures with greater resolution implemented on SoftWorx, ver. 6.0 (Applied Precision, Inc.). The channels were then aligned in x, y and rotationally. The images were analysed by 3D opacity using the Volocity software (Perkin Elmer).

Chapter 3: Residues crucial for the partition of plasmid TP228 were identified in the N-terminal tail of ParG

3.1 Introduction

The large, low copy number, multidrug resistant plasmid TP228 harbours the *parFGH* partition cassette, which consists of the two partition genes, *parF* and *parG*, and the *cis*-acting centromere sequence *parH*. ParF is a Walker-type ATPase, which forms polymers upon binding to ATP and acts as a motor to segregate plasmid DNA. ParG is a site-specific DNA-binding protein that associates to the centromere site *parH,* which is located upstream of the partition genes and recruits ParF to the segrosome to carry out plasmid segregation (Barillà *et al.*, 2005). ParG also acts as a transcriptional repressor of the *parFG* genes. ParG is a dimer and each of its monomers consists of a folded C-terminal domain containing a ribbon-helix-helix (RHH) motif, whereas the first 32 amino acids of the N-terminus form a flexible tail (Figure 3.1) (Golovanov *et al.*, 2003).

Although the ParG N-terminal end is unstructured, it is involved in various functions implicated in the partition of plasmid TP228. They are as follows:

1. the transcriptional repressor function of the ParG protein is modulated by its N-terminal end. Similarly, the binding affinity of ParG for the partition site is altered by the N-terminal end (Carmelo *et al.*, 2005, Wu *et al.*, 2011a).
2. ParG enhances ParF polymerization possibly by bundling ParF filaments or stabilizing the proto-filaments and the N-terminal tail of ParG appears to be involved in this activity (Barillà *et al.*, 2005).
3. the ATP hydrolysis of ParF is augmented by ParG and this is attributed to the arginine finger motif present in the ParG N-terminal end (Barillà *et al.*, 2007).

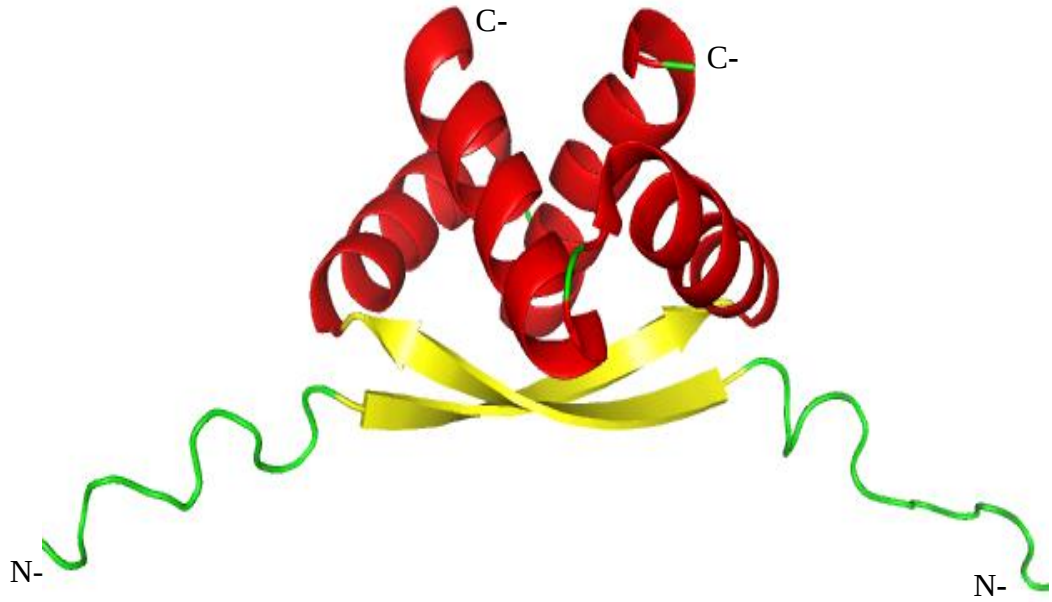

Figure 3.1. Structure of the ParG dimer.

The two β-sheets are arranged in an anti-parallel fashion into a β-ribbon (yellow) and four α-helices are tightly packed together (red). N-terminal tails are shown in green. The structure was generated by using PyMol (DeLano, 2002).

Chapter 3

Conventionally it is expected that the protein function is related to its tertiary structure and the unstructured region of protein is not functionally active (Dyson and Wright, 2005). However, it has been recently observed in various proteins that the unfolded regions are also involved in a variety of functions. It has been suggested that disordered domains present three advantages that appear to be universal for any protein with such regions (Dafforn and Smith, 2004). The first advantage is accessibility gained by protein using the flexible regions during binding the partner protein or cellular targets. While gaining lateral advantage it also gives spatial efficiency compared to the globular regions. The third advantage is cooperativity as protein might present more binding sites with the help of unstructured and flexible regions. If the interaction is weak due to the flexible region, this might ease assembly and disassembly, which is an added advantage for some proteins. The translocation domain of colicin E9, a bacterial toxin, is disordered and mobile (Collins *et al.*, 2002). The flexibility conferred by the unstructured region may assist the colicin to bind its partner proteins or outer membrane receptors during translocation, which eventually help to exert cytotoxic effect. Many proteins involved in regulation, recognition and cell signalling show presence of intrinsically disordered regions which might act as an identifying feature for such proteins (Uversky *et al.*, 2005). Disordered regions are also reported to form a substantial part of the eukaryotic transcriptional factors (Miller, 2009). Even though the long stretches of flexible regions are not found in prokaryotic transcriptional factors like in their eukaryotic counterparts, transcriptional repressors like MetJ and Arc also exhibit short N-terminal flexible regions, which make important DNA backbone contacts. In the argument for using flexible regions it has been suggested that the flexible regions of these proteins allow them to adapt to the conformational changes induced by for example bending of operator DNA (Raumann *et al.*, 1994). The flexible region may also fold against the phosphate backbone of DNA which could reduce non-specific binding to retain a stable complex (Raumann *et al.*, 1994). ParG is a member of the MetJ/Arc transcription repressor superfamily. The N-terminus of ParG might be involved in making DNA contacts as well as interactions with the partner protein ParF.

The aim of this project was to study the ParG N-terminal region and establish the role played by individual amino acids of this flexible tail. This was achieved by

using alanine-scanning mutagenesis. Alanine is a widely utilised choice of substitution as it is non-bulky residue and conformational change in the protein due to alanine substitution is considerably less (Ziolkowska *et al.*, 2006). The efficiency of an active partition system can be tested by employing a plasmid partition assay. In the absence of antibiotic selective pressure, low copy number plasmids are retained due to an active segregation process (Hayes, 2000). Partition assays were performed for all of the ParG N-terminal mutants to determine their partition efficiency. If plasmids carrying any of the mutant *parG* alleles show a retention rate lower than that of plasmids containing the wild type partition cassette this indicates that the residue change in the flexible tail of ParG plays a role in plasmid segregation.

3.2 Results

3.2.1 Construction of mutants in the N-terminal tail of ParG

3.2.1.1 Experimental setup

A stability probe vector, pALA136 was used in the past to identify the elements responsible for plasmid segregation (Macartney *et al.*, 1997). Plasmid pALA136 is a pBR322 derivative having two origins of replication i.e. P1, for low copy number and ColE1, for medium copy number. Under conditions that support only low copy number replication, vector pALA136 is highly unstable. If partition genes are introduced into pALA136, its stability increases. In this project, two vectors were used viz. pFH450 (7510 bp) and pFH547 (8972 bp), which were derived from pALA136. Plasmid pFH450 was generated by introducing multiple cloning sites into pALA136 . While screening for the segregation stabilising region in plasmid TP228, a partition locus was identified and then cloned into pFH450 using the restriction sites *Sal*I and *Eco*RI to generate pFH547 (Hayes, 2000). This locus was later characterised as the *parFGH* partition cassette of plasmid TP228.

The pFH547 construct containing the wild type *parFGH* partition cassette was used as the template for mutagenesis in this project (Figure 3.2). Two restriction sites, *Cla*I in the *parF* gene and *Hpa*I in the *parG* gene, were used to swap the wild type region with a fragment carrying a mutation in the 5’ end of *parG*.

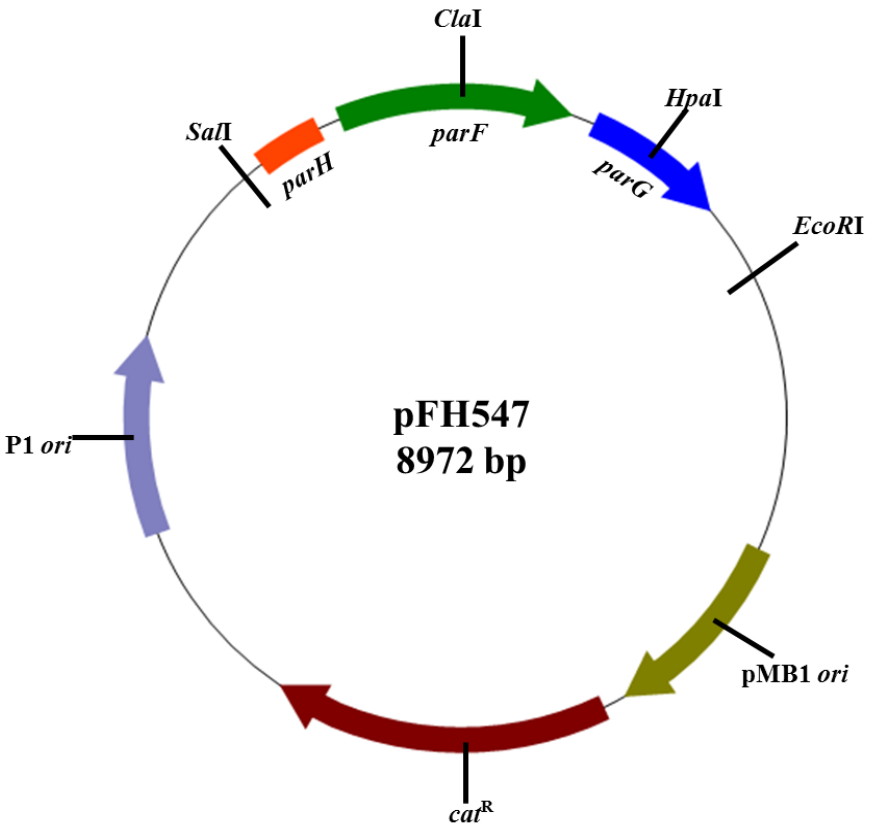

Figure 3.2. Vector map of pFH547.

Plasmid pFH547 harbouring the wild type *parFGH* partition cassette contains the chloramphenicol resistance gene and exhibits two origins of replication for low and medium plasmid copy number. The restriction sites used for generating mutations in the N-terminal end of ParG were *Cla*I and *Hpa*I.

3.2.1.2 Amplification and cloning of mutant *parG* alleles

Overlap extension PCR was carried out as outlined in the section 2.3.1, using two sets of external and internal primers to introduce mutations in the 5' end of *parG*. The external forward primer contained a *Cla*I restriction site and the external reverse primer contained a *Hpa*I restriction site. The internal forward and reverse primers were designed to contain the desired mutations. In PCR reaction 1, forward external primer and reverse internal primers were used to generate a 224 bp PCR fragment. In PCR reaction 2, the forward internal primer and reverse external primers were used to amplify a fragment around 254 bp in size. As an example, the PCR products leading to the construction of the mutant allele encoding ParG-M13A are shown in Figure 3.3.

The two fragments generated in separate PCR reactions display overhangs due to the overlapping sequence in the internal primers used in the amplification. These two PCR fragments were incubated together, allowed to anneal and the single strands extended in the absence of primers. Subsequently PCR 3 was carried out with the external forward and reverse primers to amplify the whole DNA fragment, which was approximately 434 bp. As an example, the product of PCR 3 leading to the construction of the mutant allele encoding ParG-N18A is shown in Figure 3.4A.

The DNA product of PCR 3 was digested with *Cla*I and *Hpa*I, which generated two fragments of 260 and 120 bp, of which the 260 bp one contained the *parG* mutation. This fragment was then cloned into pFH547 vector (Figure 3.4B). *E. coli* DH5α cells were transformed with the ligation mixture and a few colonies were picked to screen for positive clones by colony PCR (Figure 3.5). The same external primers used in PCR 3 were also used for colony PCR. Colonies containing potential positive clones were inoculated over-night in LB medium. Plasmid DNA extraction was carried out and the clones were screened by digesting the plasmid with *Cla*I and *Hpa*I.

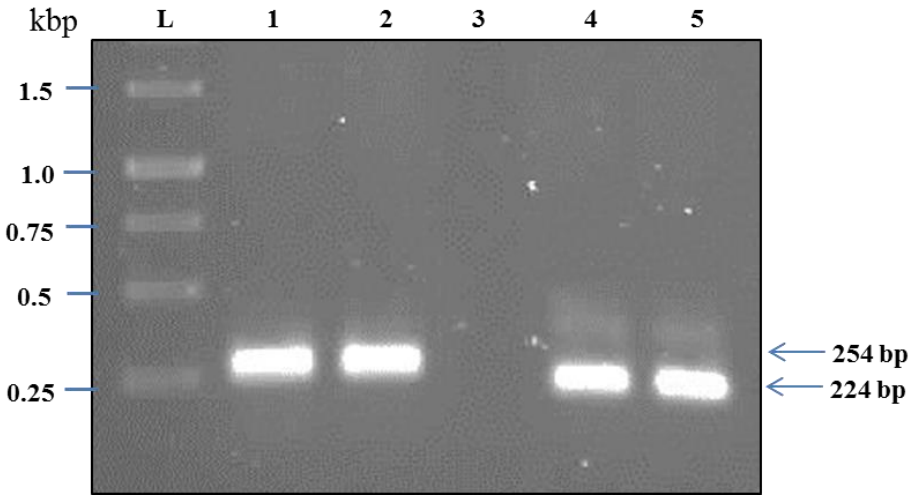

Figure 3.3. A representative agarose gel showing the products of PCR 1 and PCR 2 used for *parG* mutagenesis.

DNA fragments were subjected to electrophoresis on a 1.2 % agarose gel. Lanes: L, Gene ruler 10 kbp ladder; 1 and 2, products of PCR 1 (254 bp); 4 and 5, DNA products of PCR 2 (224 bp).

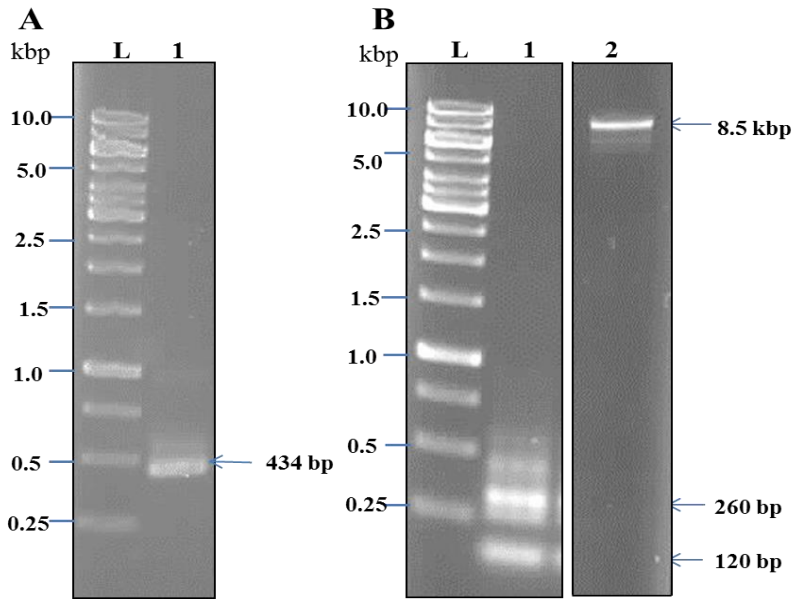

Figure 3.4. Representative agarose gels showing the product of PCR 3 and those of the restriction digest of PCR fragment and pFH547 vector used for *parG* mutagenesis.

A. Previously generated DNA fragments from PCR 1 and 2 are incubated together and subsequently amplified to obtain the DNA fragment with the desired mutation. Lanes: L, Gene ruler 10 kbp ladder and 1, PCR 3 product (434 bp). **B.** Both PCR DNA fragment and vector were digested with *Cla*I and *Hpa*I and run on a 1.2% agarose gel. Lanes: L, Gene ruler 10 kbp ladder; 1, digested products of PCR 3, generating two fragments of 260 and 120 bp; 2, digested pFH547 vector (~8.5 kbp).

Potential positive clones were sent for sequence analysis to GATC Biotech. The resulting sequencing data was analysed to identify mutant alleles (Figure 3.6). The constructed plasmids containing the correct mutations were named as pMB along with the change of amino acid and its position e.g. pMBS2A.

The ParG protein contains two alanines at positions 6 and 27. They were not changed. Several attempts were made to mutate the valine and aspartic acid residues at position 10 and 20 respectively, but they were unsuccessful. Other lab members had already constructed the F15A, R19A and R23A ParG mutants. An overview of the entire mutagenesis plan is given in Figure 3.7.

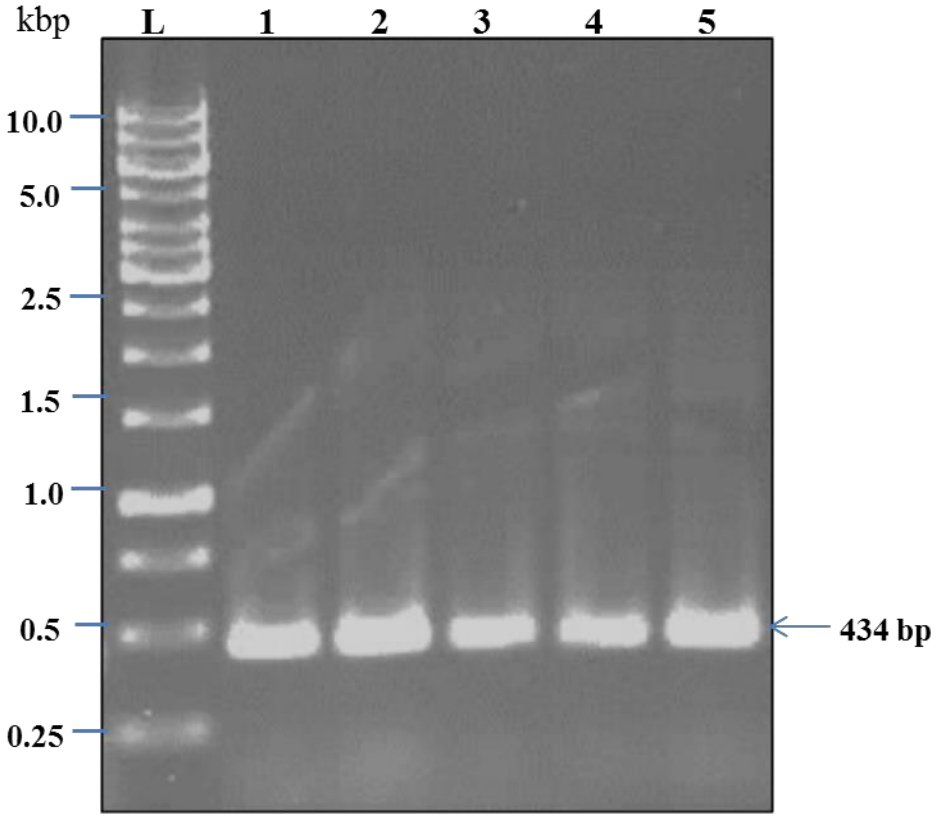

Figure 3.5. Representative agarose gels showing colony PCR products and restriction digestion screen of pFH547 plasmids potentially harbouring the desired mutation. Colony PCR was carried out on five samples. Lanes: L, Gene ruler 10 kbp ladder; 1 to 5, colony PCR product of five candidates.

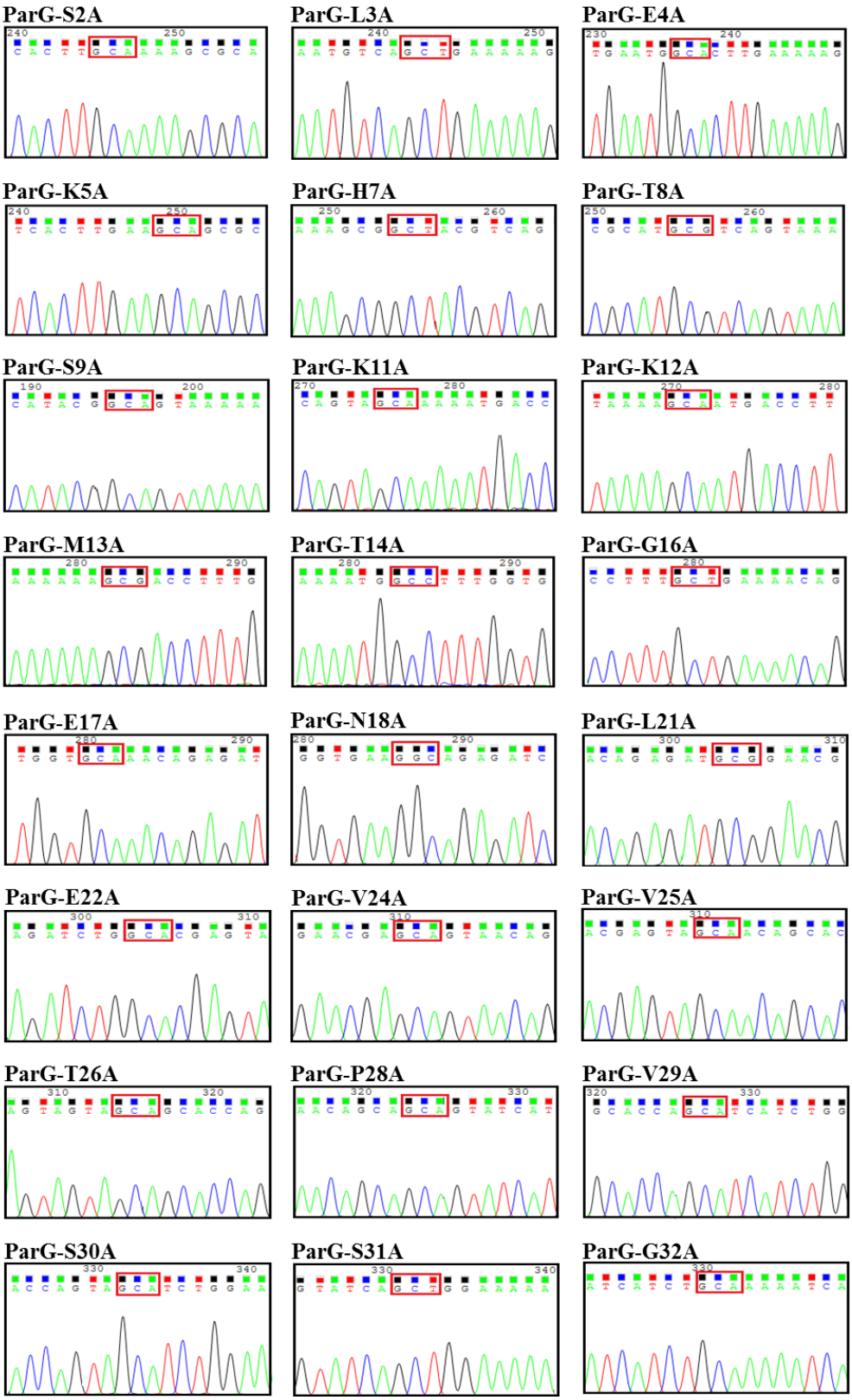

Figure 3.6. Sequences traces of mutant *parG* alleles.

ABI sequencing data of individual *parG* mutations obtained from GATC was analysed with Chromas software. Each mutated codon is highlighted with a red box.

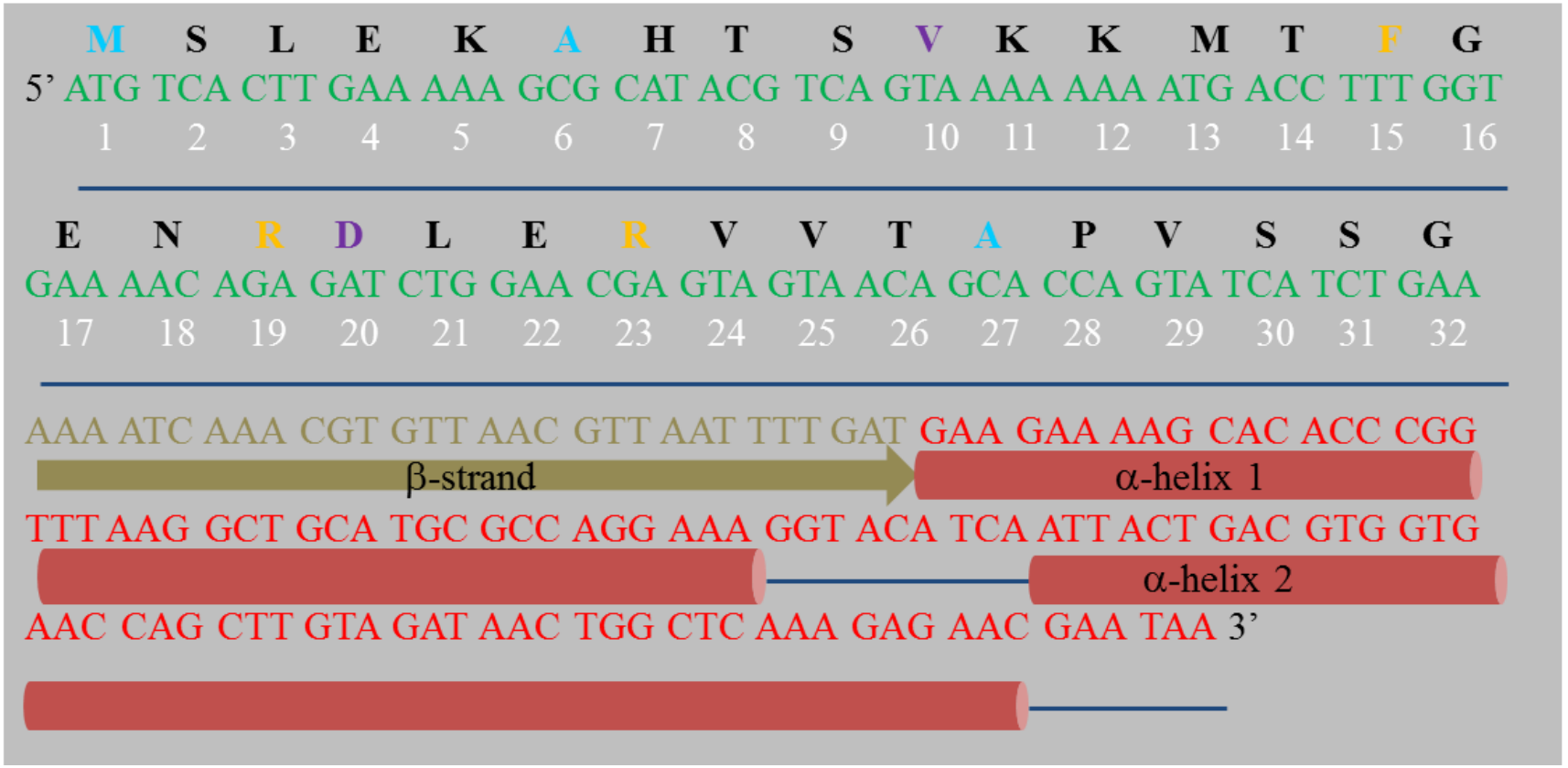

Figure 3.7. The *parG* gene and aligned protein amino acid sequence.

The *parG* wild type gene sequence is shown above. Nucleotides in green encode the N-terminal flexible region, whereas yellow and red nucleotides encode the folded C-terminal region. The secondary structure of the different regions of the ParG is drawn below the sequence. The unstructured N-terminal region is indicated by line. Amino acids in black were changed to alanine, those in cyan were not changed, those in orange had already been changed by other lab members and those in magenta proved refractory to convert to alanine.

3.2.2 Identification of amino acids crucial for plasmid segregation

Once mutations were constructed, it was determined whether they had an *in vivo* phenotype, i.e. any impact on plasmid retention. This was achieved by performing a partition assay using *E. coli* BR825, which is a *polA* strain whose defective DNA polymerase I supports replication only from the P1 low copy number origin. The partition assay is based on the principle that if BR825 cells are transformed with low copy number plasmids and grown in the absence of antibiotics, plasmids are retained after multiple generations only if they contain an active partition cassette. The partition assay was performed for all the plasmids harbouring the *parG* mutants to determine their plasmid partition efficiency. Two controls used in this assay were plasmid pFH450, which harbours no plasmid partition genes, and plasmid pFH547, which contains the wild type *parFGH* partition cassette from plasmid TP228. Together with these controls, all the pMB plasmids encoding *parG* mutants, were tested at least in triplicate. Plasmid retention was assessed by replica plating on solid agar medium with and without antibiotics after a time interval corresponding to about twenty-five generations. As the plasmid stabilising sequence is absent in FH450, the plasmid became very unstable and on average showed plasmid retention of ~8%. Plasmid pFH547 showed a higher retention of 65%. This is due to the presence of the wild type *parFGH* partition cassette. If plasmid retention decreased to less than 40%, it was assumed that the mutation had affected the partition process.

Mutations leading to amino acid changes in the 3rd, 5th, 11th, 12th, 13th, 18th and 21st residues of ParG resulted in lower plasmid retention, indicating that changes in these positions affect the partition system (Figure 3.8). ParG-N18A was shown to be the least efficient in plasmid retention (0%), whereas lowered plasmid retention was observed for ParG-L3A (8%), ParG-K5A-(30%), ParG-K11A (41%), ParG-K12A (16%), ParG-M13A (12%) and ParG-L21A (32%). It had been previously established that changes in the 15th residue (F15A) reduced partition efficiency considerably (13%, unpublished data), similarly a change in the 19th residue (R19A) resulted in a 34.7% plasmid retention, indicating an important role for this residue in plasmid TP228 segregation (Barillà *et al.*, 2007). The mutation leading to the change R23A had no effect on plasmid retention (Barillà *et al.*, 2007). These partition

deficient mutants were selected for further analysis to elucidate the role of the N-terminus in plasmid segregation.

The role of these amino acids in various functions of ParG such as activation of ParF ATP hydrolysis, enhancement of ParF polymerization, centromere binding and transcriptional repression of the *parFG* genes will be examined in the following chapters.

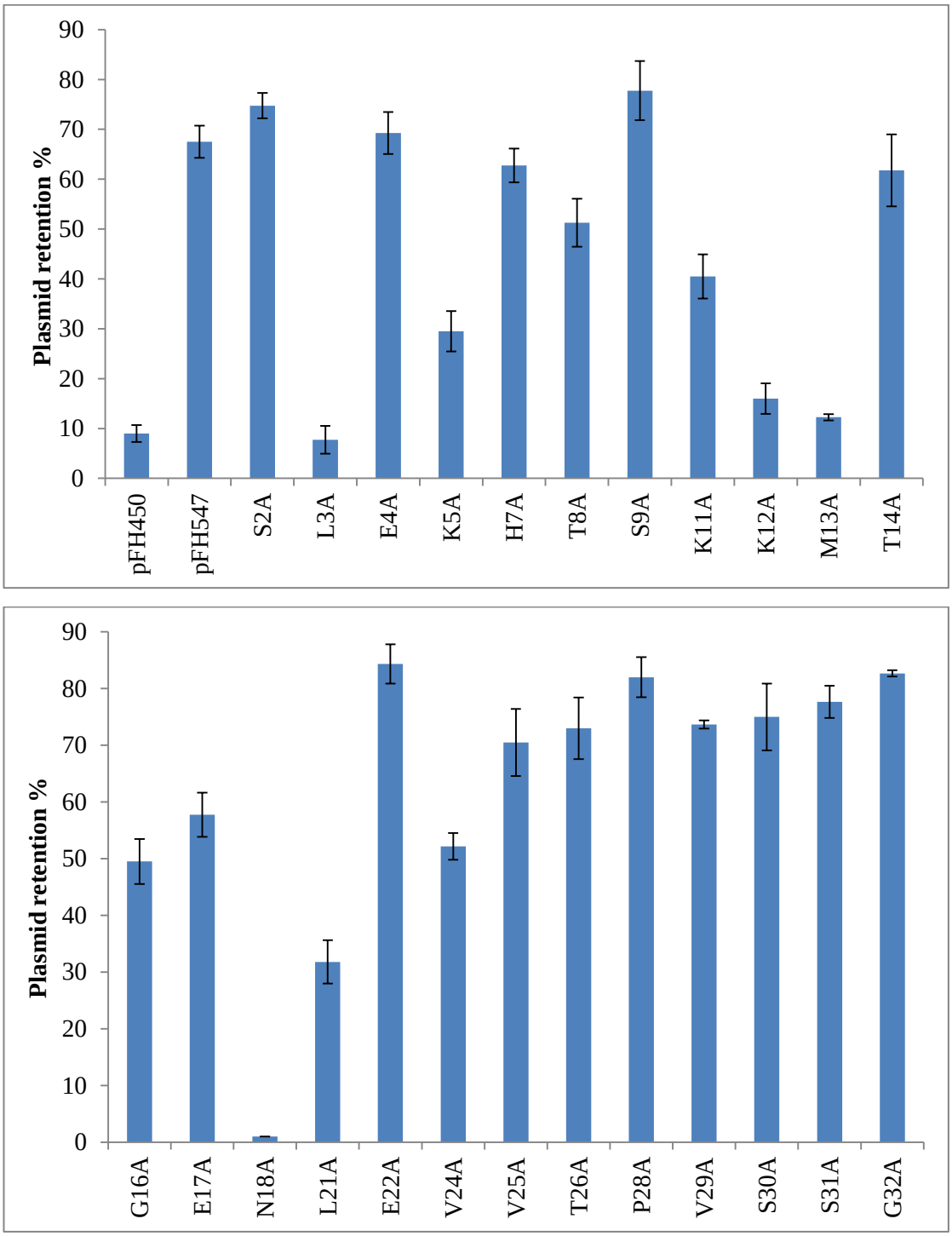

Figure 3.8. Plasmid retention percentage of ParG N-terminal mutants.

Plasmid pFH450 lacks a partition cassette and pFH547 harbours wild type partition cassette. Percentages of plasmid retention were determined after performing assay for empty plasmid, wild type cassette containing plasmid and each mutant encoding plasmid at least in triplicate. Error bars represent the standard error of mean.

3.3 Conclusions

Each amino acid in the unstructured ParG N-terminal tail was converted to alanine to elucidate the role played in plasmid segregation. Plasmid pFH547, which contains the wild type partition cassette *parFGH,* was used as a parent vector for the mutagenesis. With the exception of two alanines at positions 6 and 27, valine at 10 and aspartate at 20, all the other amino acids were successfully converted to alanine. A plasmid partition assay was carried out to study the effect of changes in the ParG N-terminal end on the segregation process. In the assay, the *E. coli* BR825 strain that supports only low copy number replication was used, making it necessary for plasmids to have an active segregation process for their survival. Although the ParG N-terminal tail is flexible, even a single amino acid change in this region can alter the partition efficiency (Figure 3.9). Leucine at position 3 and 21 and lysine at position 5, 11 and 12 lowered plasmid stability, when changed to alanine. The positively charged lysines may be involved in DNA-binding and hence altering the partition function of ParG. ParG is a type I transcriptional repressor of RHH family where basic residues are present at the beginning of the β-strand (Golovanov *et al.*, 2003). The pair of basic residues KK in the flexible N-terminal region at position 11 and 12 may help in additional DNA binding. Mutation of methionine at position 13 also showed reduced plasmid retention. When asparagine at position 18 was mutated to alanine, plasmid partition was found to be reduced almost to zero. Asparagine 18 is part of the arginine finger motif harboured in the flexible tail and thus its conversion to a different amino acid might affect the motif and alter ParG functions such as stimulation of ParF ATPase activity or enhancement of ParF polymerization. Here amino acids that are crucial for the partition of plasmid TP228 have been identified. However, the exact role played by these residues can only be determined by performing further biochemical assays.

Figure 3.9. Structure of ParG dimer showing the position of amino acids located in the N-terminal tail, which are crucial for plasmid partition.

Residues in the N-terminal flexible tail of ParG, whose change cause plasmid segregation defects, are highlighted. The structure was generated with PyMol (DeLano, 2002).

Chapter 4: ParG N-terminal mutant proteins are dimers, bind to DNA and act efficiently as transcriptional repressors of the putative *parFG* operon

4.1 Introduction

Mutations in the region of the *parG* gene encoding the N-terminal flexible region (L3A, K5A, K11A, K12A, M13A, F15A, N18A, R19A and L21A) affect the plasmid partition function of the ParG protein, as the stability of plasmids carrying these mutations is lower (Chapter 3). Here the mutant proteins were purified as recombinant polypeptides from *E. coli* using affinity chromatography. In this section, three questions will be addressed pertaining to ParG and its role in plasmid partitioning. The first is: do these mutations compromise the ability of ParG to dimerize? The second is: how do they affect the DNA binding function of ParG? And the third is: are these mutant proteins able to act as a transcriptional repressor of the putative *parFG* operon?

The partition protein ParG exhibits a folded domain consisting of a RHH motif at the C-terminal end and a flexible tail at the N-terminal end. The folded domains of two ParG monomers interlace to form a dimer. Molecular hydrophobicity potential (MHP) contact plots revealed that the inter-monomeric hydrophobic contacts are stronger than the intra-monomeric hydrophobic contacts. Amino acid residues V37, V39, F41, K45, R48, F49, V64, L67, V68, W71 and L72 of the C-terminal domain are implicated in ParG dimerization (Golovanov *et al.*, 2003). ParG is a member of the MetJ/Arc repressor family and a number of proteins from this family also show the conserved hydrophobic residues at similar positions. The ParG N-terminus (residues 1-32) is unstructured, but residues 17 - 23 form transient secondary structures (Golovanov *et al.*, 2003). Even though the flexible region is not involved in dimerization, it was important to establish whether the mutant ParG proteins can still form dimers.

ParG, a centromere binding protein (CBP), is functionally analogous to other ParB proteins like P1 ParB and RK2- KorB but it is structurally unrelated to them. Type Ia CBPs contain a N-terminal Helix-turn-helix (HTH) fold whereas type Ib, e.g. ParG, and type II, e.g. ParR, CBPs contain a RHH fold. Members of this functionally diverse superfamily regulate the transcription of genes that are involved in various cellular processes, including cell division and control of plasmid copy number. Structural analysis of MetJ and Arc proteins bound to their cognate DNA binding

site have shown that the antiparallel N-terminal β strands of the dimers are positioned in the DNA major groove (Somers and Phillips, 1992). Similarly, ParG makes contact with the DNA at the major groove through its antiparallel β-sheet.

ParG binds DNA at the operator site of the *parFG* genes initially as a dimer of dimers and then as a pair of tetramers. Tetramer binding to DNA has been observed for other RHH transcriptional repressors in their protein crystal structures (Gomis-Ruth *et al.*, 1998, Raumann *et al.*, 1994, Somers and Phillips, 1992). The flexible ParG N-terminal tail makes transient contact with DNA, facilitating the formation of a stable nucleoprotein complex. Deletion mutants in ParG N-terminus decreased the transcriptional repressor activity of ParG (Carmelo *et al.*, 2005). The *parFG* operator site is "fine-tuned" for optimal ParG binding to attain *parFG* regulation. The flexible N-terminal tail modulates ParG interaction with the operator site (Zampini *et al.*, 2009). The DNA sequence upstream of the *parFG* genes comprises of 20 degenerate repeats with AT rich spacers. The first 12 repeats make the centromere site *parH*, whereas the later eight repeats form the operator site (O_F) of the *parFG* genes. Both *parH* and O_F have comparable centromere activity and ParG binds to them with similar affinity. A comprehensive analysis of the interaction of ParG with whole (full-length) and partial *parH* site was recently reported (Wu *et al.*, 2011). ParG showed differential affinities to the sub-parts of the *parH* site. The N-terminal ParG deletion mutant Δ30, demonstrated strong binding to the whole *parH* sequence but showed less affinity to partial sequences (Wu *et al.*, 2011a). ParG loses the specificity in the absence of the flexible tail, which testifies the multiple roles played by the ParG N-terminal end.

In a variety of proteins, the unstructured domains perform prominent roles, which contradict the protein paradigm of "structure is equal to function". Type I CBPs, ParB in plasmid P1and KorB in RK2 show disordered N-terminal regions along with HTH motif in the C-terminus (Rajasekar *et al.*, 2010, Surtees and Funnell, 1999). Another type Ib CBP homologous to ParG, protein omega (ω) from plasmid pSM19035 shows an unstructured N-terminal region (Weihofen *et al.*, 2006). Type II CBP, ParR from plasmid R1, contains a flexible tail in the C-terminus (Salje *et al.*, 2010). Transcriptional repressors like Arc, Mnt and MetJ also show small disordered region in the N-terminal end, which assist in establishing DNA contact and also

confer DNA binding specificity (Knight and Sauer, 1988, Knight and Sauer, 1989). The presence of disordered domains and the flexibility conferred by them, might give advantage to the CBPs and repressor proteins in carrying out functions like DNA binding, gene regulation and interacting with partner proteins (Rajasekar *et al.*, 2010).

The flexible tail of ParG is implicated in DNA binding and determining specificity. In this chapter, the effects of the changes introduced in the N-terminal tail on ParG-DNA interactions will be investigated.

4.2 Results

4.2.1 Cloning of mutant *parG* alleles into the expression vector pET22b

ParG N-terminal mutant proteins were obtained using the pET expression system and tested in a number of biochemical assays. Each mutant *parG* gene was amplified by using a forward primer containing a *Nde*I restriction site and a reverse primer harbouring the *Xho*I site. The PCR product was a DNA fragment of around 250 bp. To amplify each mutant allele for cloning into the pET vector, the respective mutant partition plasmid (i.e. pMB plasmid series) was used as template DNA. The amplified DNA was then subjected to digestion with *Nde*I and *Xho*I, generating a 250 bp fragment (Figure 4.1).

These DNA fragments were then ligated into *Nde*I and *Xho*I digested pET22b vector and the recombinant plasmids selected on LB plates containing ampicillin. Plasmid DNA was isolated, screened by digestion with *Nde*I and *Xho*I to verify whether it contained the expected insert and potentially positive clones were sent for sequencing to GATC Biotech (Figure 4.2). On confirmation of the correct sequence these constructs were named as pET-MBL3A, pET-MBK5A, pET-MBK11A, pET-MBK12A, pET-MBM13A, pET-MBN18A and pET-MBL21A. Plasmid pET-ParGF15A had already been constructed and pET-ParF, pET-ParG and pET-ParGR19A plasmids were part of the laboratory plasmid collection.

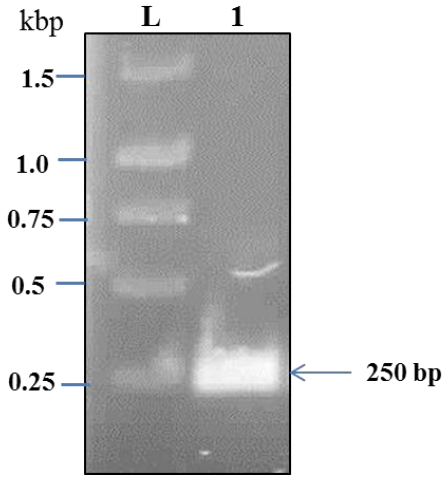

Figure 4.1. Representative agarose gel showing the restriction digestion of the PCR amplified *parG* mutant gene.

The *parG* mutant gene fragment was obtained by PCR amplification and then digested with restriction enzymes *Nde*I and *Xho*I. The digested DNA material was run on 1.2% agarose gel. Lanes: L, Gene ruler 10 kbp and 1, a digested fragment of 250 bp, indicated by the arrow.

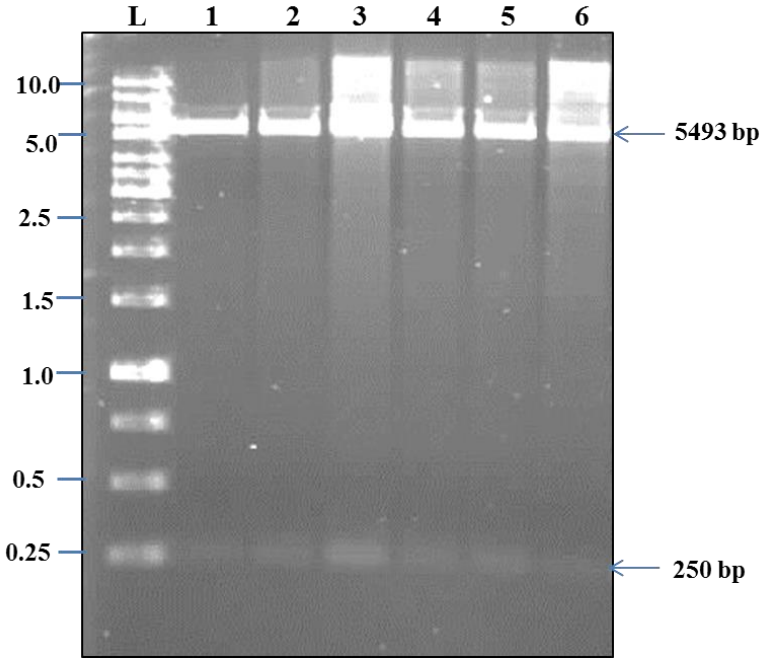

Figure 4.2. A representative agarose gel showing products of the restriction digest screen of pET-*parG* plasmids harbouring mutations.

Restriction analysis of plasmids was performed by digestion with restriction enzymes *Nde*I and *Xho*I. Lanes: L, Gene ruler 10 kbp and 1-6, digested DNA of clones isolated for screening.

4.2.2 Partition deficient mutant proteins were overproduced and purified

Proteins were overproduced by using the pET expression system. His-tagged ParF, ParG and mutant ParG-L3A, ParG-K5A, ParG-K11A, ParG-K12A, ParG-M13A, ParG-F15A, ParG-N18A, ParG-R19A and ParG-L21A proteins were purified by Ni^{2+} affinity column. It has been previously reported that His-tagged partition proteins support plasmid partition *in vivo* as efficiently as native proteins (Barillà and Hayes, 2003).

4.2.2.1 The ParF protein was purified by Ni^{2+} affinity chromatography

The $(His)_6$-tagged ParF protein is characterized by a molecular weight (MW) of 23 kDa. The purification was carried out by using the protocol described in the section 2.4.1 and the standard result is briefly outlined below. Pilot experiment estimated 3h as a suitable induction time for achieving a considerable level of *parF* gene overexpression. ParF was found to be soluble and bound to the Ni^{2+}-charged resin. The eluted fractions were buffer-exchanged and quantified by Bradford assay, showing concentrations ranging between 0.3 mg/ml and 0.1 mg/ml. The purity of the fractions was analysed by SDS-PAGE (Figure 4.3).

4.2.2.2 Purification of wild type ParG and the N-terminal mutant proteins by Ni^{2+} affinity chromatography

The recombinant His-tagged ParG and the mutant proteins have a MW of 9.6 kDa. They were purified from the *E. coli*. by following the protocol described in the section 2.4.2. Two hours induction with IPTG was optimised to obtain a good yield of ParG protein. His-tagged ParG and mutant proteins bound to the Ni^{2+} column efficiently. The mutations did not affect solubility as all the mutant proteins were found to be stable in solution similar to wild type ParG. Typical concentration of ParG protein fractions ranged from 0.4 mg/ml to 0.9 mg/ml. All mutant proteins were separated without any major impurities. As representative examples, SDS gels for wild type ParG and ParG-L21A purification are shown in Figure 4.4 and 4.5, respectively. Transformation of BL21(DE3) with pET-*parGF15A* was not successful on several attempts hence ParG-F15A protein was not purified.

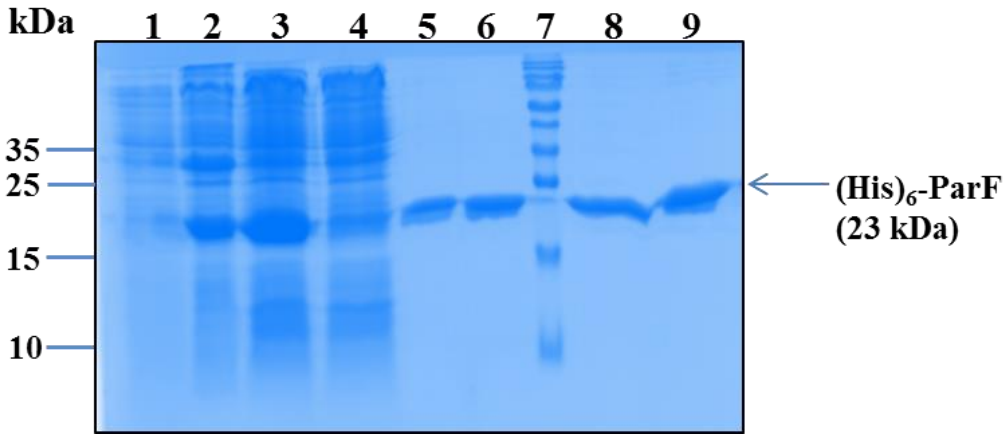

Figure 4.3. ParF protein was purified on Ni^{2+} affinity column.

SDS-polyacrylamide gel showing various fractions collected during ParF protein purification process. Lanes: 1, un-induced cell culture sample before addition of IPTG; 2, pellets after centrifugation of sonicated induced culture; 3, the cell extract containing total soluble protein from the induced culture; 4, flow through; 5,6,8,9, buffer exchanged elution fractions of the ParF protein; 7, PageRuler Prestained Protein Ladder. His-tagged ParF is indicated by the arrow.

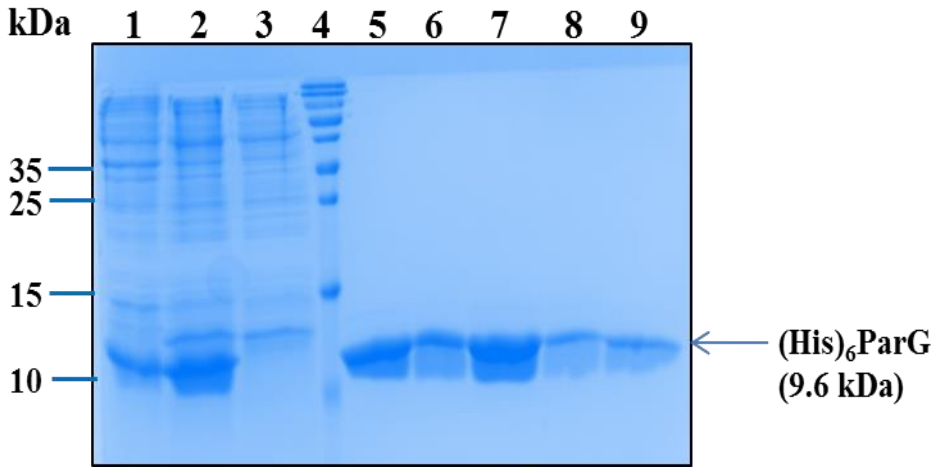

Figure 4.4. ParG was purified on Ni^{2+} affinity column.

SDS-polyacrylamide gel showing various fractions collected during ParG protein purification process. Lanes: 1, pellet fraction after centrifugation of sonicated culture; 2, cell extract containing total soluble protein; 3, flowthrough; 4, PageRuler Prestained Protein Ladder; 5-9, buffer exchanged elution fractions of the ParG protein. His-tagged ParG is indicated by the arrow.

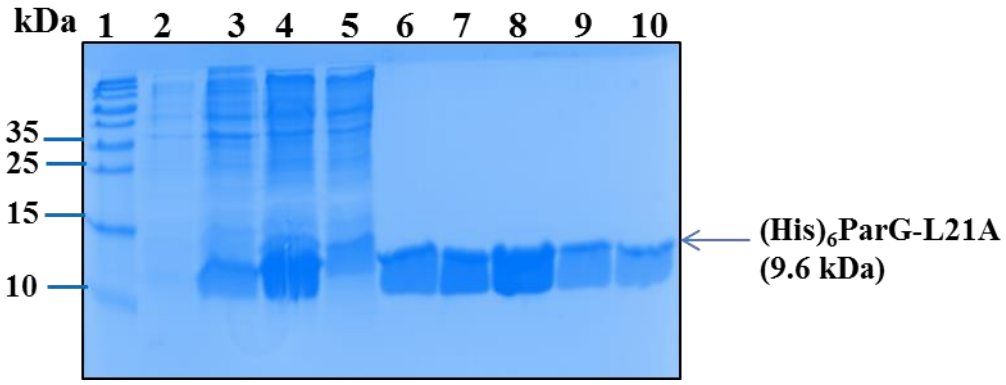

Figure 4.5. ParG-L21A purification.

SDS-polyacrylamide gel showing various fractions collected during ParG-L21A protein purification process. Lanes: 1, PageRuler Prestained Protein Ladder; 2, uninduced cell culture sample saved before addition of IPTG; 3, pellet fraction after centrifugation of sonicated culture; 4, cell extract containing total soluble protein from the culture; 5, flowthrough; 6-10, buffer exchanged elution fractions of the ParG-L21A protein. His-tagged ParG-L21A is indicated by the arrow.

4.2.3 ParG N-terminal mutant proteins form dimers

Dimerization of ParG mutants was studied by chemical cross-linking. Chemical cross-linking can detect both temporary and steady interactions, as covalent bonds are formed between two proteins. In this technique bi-functional reagents are used which contain reactive groups reacting with functional groups of proteins such as primary amines of amino acids. If two proteins are cross-linked, this indicates that they interact. The cross-linker used in this study was dimethyl pimelimidate (DMP) which is an amine-reactive imidoester-type cross-linker. Imidoester cross-linkers react with primary amines to form amidine bonds.

ParG and mutant proteins were included in the cross-linking reactions at a final concentration of 20 µM and increasing concentrations of DMP were added ranging from 0 to 10 mM. Wild type ParG is a dimer (Golovanov *et al.*, 2003). In the absence of DMP, ParG and all the mutant proteins ran as monomers in denaturing SDS-gels. When the proteins were incubated with DMP and then run on SDS-gels, all the proteins except ParG-K12A showed dimer formation and, at the highest DMP concentration, tetramers were visible (Figure 4.6). ParG-K12A failed to dimerize even at the highest concentration of DMP.

When incubated with increasing concentrations of DMP, the dimerization pattern observed for ParG-R19A was not similar to that of other mutant proteins. At the highest concentration of DMP (10 mM), ParG-R19A showed a faint dimeric band (Figure 4.7A). With the exception of ParG-K12A, the remaining mutants displayed dimer formation in the presence of as little as 0.5 mM DMP. When ParG-R19A was incubated with DMP for a longer interval, it was possible to observe a band corresponding to dimeric proteins, but the extent of dimerization was not as strong as that seen for the other mutants (Figure 4.7B).

The ParG-K12A residue change is in the flexible N-terminal end of ParG and is not expected to have any effect on ParG dimerization. To further investigate the apparent dimerization defect of ParG-K12A, a longer incubation with DMP was carried out. ParG-K12A at a concentration of 20 µM was used with 10 mM DMP, samples were incubated at 37°C for 1, 2 and 3 hours. ParG-K12A appeared unable to dimerize

even after extended incubation with DMP. After 3 hours no dimer formation was observed, whereas WT ParG dimers were visible after one hour (Figure 4.8A and 4.8B).

To further investigate whether ParG-K12A is impaired in dimerization, WT ParG and ParG-K12A mutant protein were analysed by Size Exclusion Chromatography associated with Multi Angle Laser Light Scattering (SEC-MALLS). The SEC-MALLS data indicated that the elution profile of both WT and mutant protein was comparable. The molecular weight estimates were similar for WT and mutant protein. The determined mass was 20.4 kDa and it corresponded to the molecular weight of a dimer. No significant evidence of monomeric protein was found for either of the proteins (Figure 4.9). Thus, the SEC-MALLS analysis established that ParG-K12A is dimeric.

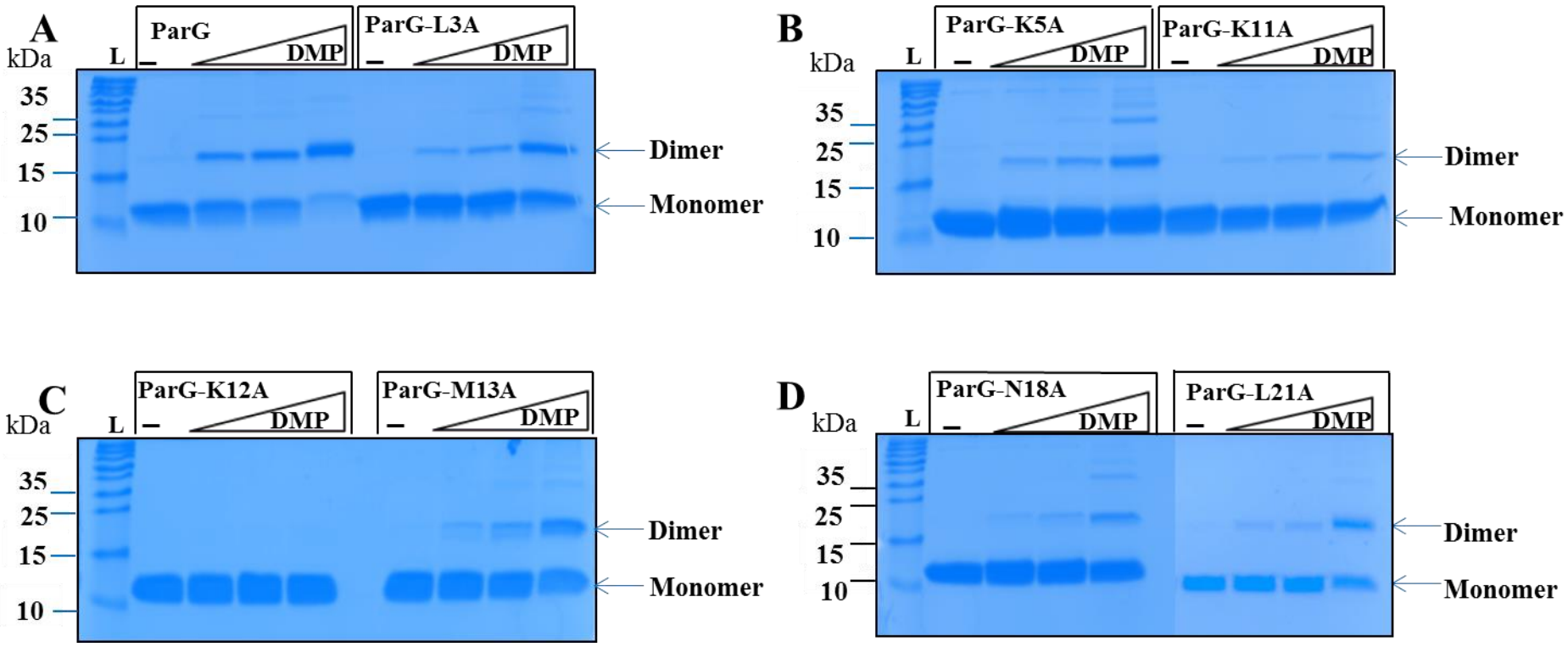

Figure 4.6. ParG mutant proteins are able to dimerize.

SDS-polyacrylamide gels showing cross-linked products of WT and mutant ParG proteins following 1 h incubation at 37°C with and without increasing concentrations of DMP, i.e. 0.5, 1 and 10 mM. **A**. ParG and ParG-L3A **B**. ParG-K5A and ParG-K11A. **C**. ParG-K12A and ParG-M13A **D**. ParG-N18A and ParG-L21A. The protein concentration is 20 µM. L is PageRuler Prestained Protein Ladder in all gel images.

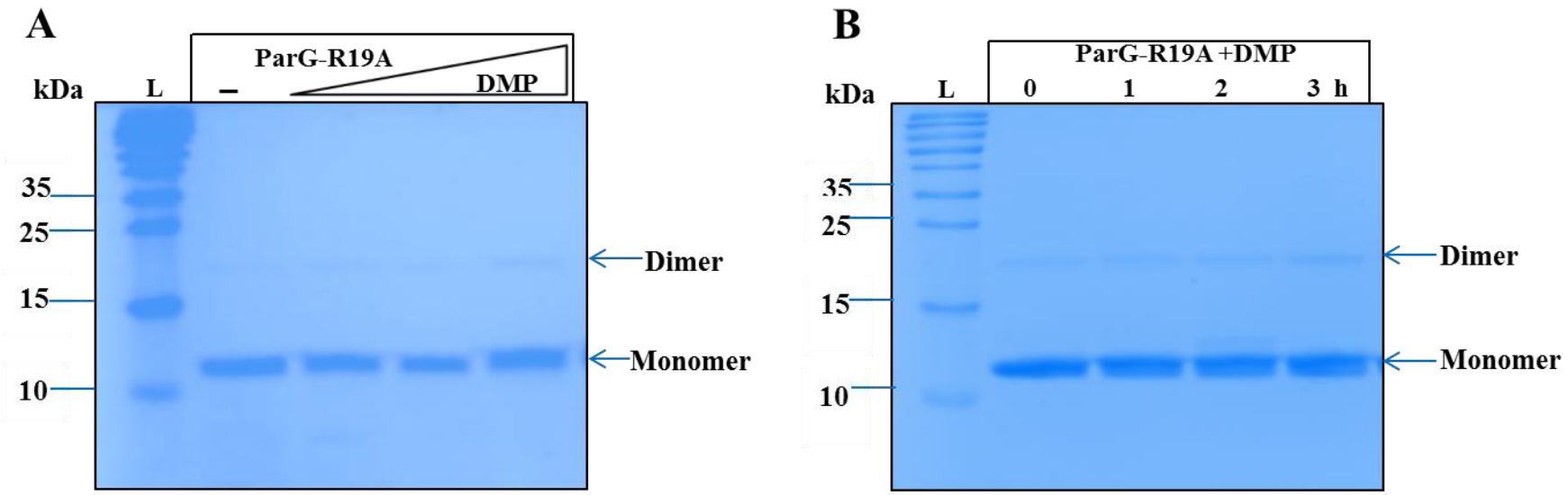

Figure 4.7. ParG-R19A forms dimers less efficiently.

A. SDS-polyacrylamide gel showing the products of the incubation of ParG-R19A at 37°C for 1 h with and without increasing concentration of DMP i.e. 0, 0.5, 1 and 10 mM. **B.** SDS-polyacrylamide gel showing the products of reactions in which DMP (10 mM) was added to 20 µM protein and incubated at 37°C for indicated time points. L is PageRuler Prestained Protein Ladder in all gel images. Monomer and dimer are indicated by the arrow on the right of each gel.

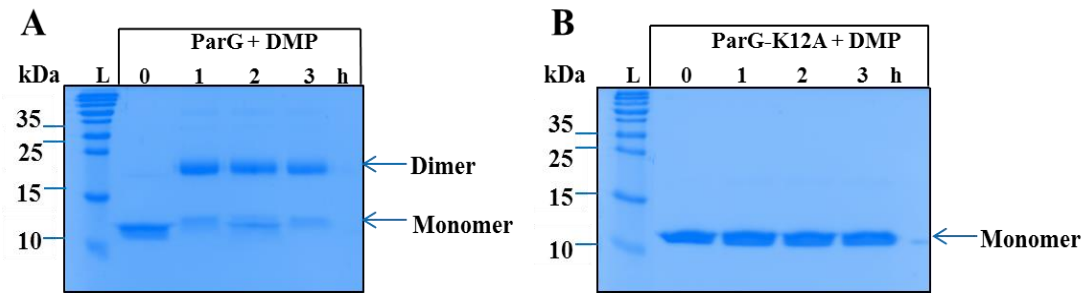

Figure 4.8. ParG-K12A does not show dimerization even after longer incubation with cross-linker.

Reaction containing DMP (10 mM) and ParG-K12A (20 µM) were incubated at 37°C and run on SDS-polyacrylamide gels. **A.** ParG WT **B.** ParG-K12A. Lanes: L, PageRuler Prestained Protein Ladder in all gel images. Monomer and dimer are indicated by arrow on right of each gel.

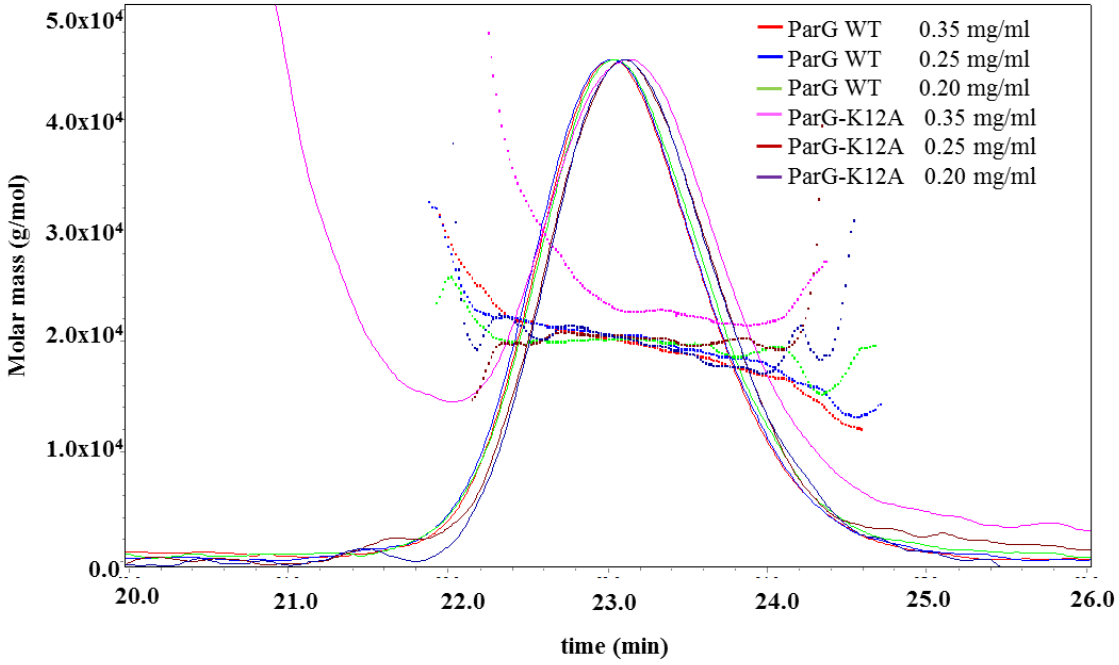

Figure 4.9. ParGK-12A is a dimer as established by SEC-MALLS.

The protein samples with indicated concentrations were injected into a Superdex S75 column. The Rayleigh ratio (light scattering signal, LS) is shown as a solid line and the MW traces are shown as a dashed line. The Astra software was used to estimate the MW from the RI (Refractive index) trace (proportional to concentration, not shown on the plot) and the LS signal by the standard Zimm fit. The experiment was performed and graph was prepared by Dr. Andrew Leech, Technology Facility, University of York

.

4.2.4 Partition deficient N-terminal mutants bind to the putative *parFG* operator

ParG is a centromere binding protein (CBP) that specifically recognizes the *parH* site. The centromere *parH* is made up of 12 degenerate repeats. Alongside *parH*, a *parFG* operator site is present upstream of the *parF* gene sequence. The operator site O_F (Figure 4.11), consists of 8 degenerate repeats (3 direct and 5 inverted sequence) of 5' ACTC- 3'. The tetramer motifs are separated by 4 bp, AT rich spacers (Zampini *et al.*, 2009). ParG binds to the operator site and acts as a transcriptional repressor. The DNA binding ability of ParG mutant proteins was tested by electrophoretic mobility shift assays (EMSA) using a DNA fragment harbouring the operator site of the *parFG* genes.

The 123 bp operator sequence upstream of *parF* was amplified by using a biotinylated forward primer (Figure 4.10). DNA binding can be studied by incubating different concentrations of protein with the same amount of DNA and running these complexes on native gel. Migration of these complexes depends on the size of the protein-nucleic acid complex.

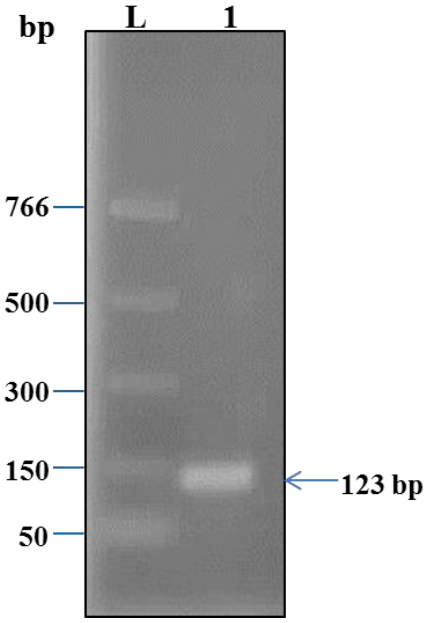

Figure 4.10. Agarose gel showing amplified *parFG* operator DNA sequence.

The *parFG* operator sequence was amplified by PCR and run on 1.2% agarose gel. Lanes: L, PCR marker and 1, PCR product of operator sequence DNA, size 123 bp.

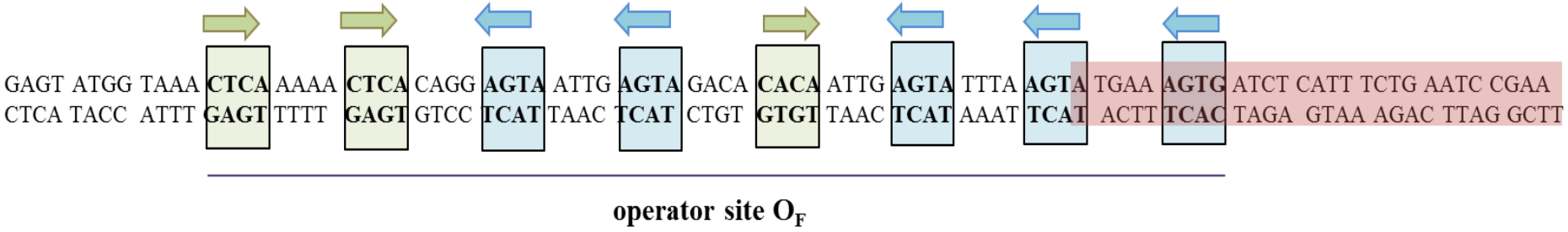

Figure 4.11. Operator of the *parFG* genes.

The repeats present in the operator sequence are boxed and denoted by arrows. Start of *parF* gene is shaded in red. The green arrows indicate direct repeats whereas the blue arrows indicate inverted repeats.

EMSAs were performed using the biotinylated 123 bp DNA fragment (0.5 nM). ParG and mutant proteins at different concentrations ranging from 100 to 1000 nM were incubated with the DNA fragment and shift of the complexes was examined (Figure 4.12). ParG binds as a dimer of dimers on the two adjacent tetramer boxes in the operator site and produces a single nucleoprotein complex. As the concentration of the protein increases, ParG spreads over the entire operator site and assembles into a larger nucleoprotein complex. It has been observed previously that eight ParG dimers were required to cover the entire operator site (Zampini *et al.*, 2009). DNA binding of ParG-L3A and ParG-K5A resembled the pattern observed for WT ParG with the exception of the reaction containing 100 nM protein which showed some unbound DNA. ParG-K11A did not shift all of the operator DNA until it reached a concentration of 400 nM, which may suggest a lower binding affinity. However, a further increase in protein concentration resulted in the formation of a nucleoprotein complex identical to that observed for WT ParG and other mutant proteins. ParG-K12A, ParG-M13A, ParG-N18A and ParG-R19A also showed a complete shift of the DNA at the lowest concentration of 100 nM similarly to WT ParG. ParG-L21A exhibited a lower DNA binding affinity as some unbound DNA was still visible up to a protein concentration of 700 nM. At higher concentrations, ParG-L21A bound to all the DNA in the reaction and a complete shift was visible on the gel.

Overall, these findings suggest that the N- terminal mutation do not adversly affect the DNA binding activity. However the behaviour of the mutant proteins at concentration below 100 nM was not tested for DNA binding and whether ParG mutants show altered binding still needs to be investigated. It has been reported that the deletion of the entire ParG N-terminal tail improves binding of ParG to the full length centromere as well as resulting in the loss of substrate specificity (Wu *et al.*, 2011a). It is possible that the ParG mutants described here may also be invoved in determing DNA binding specificity.

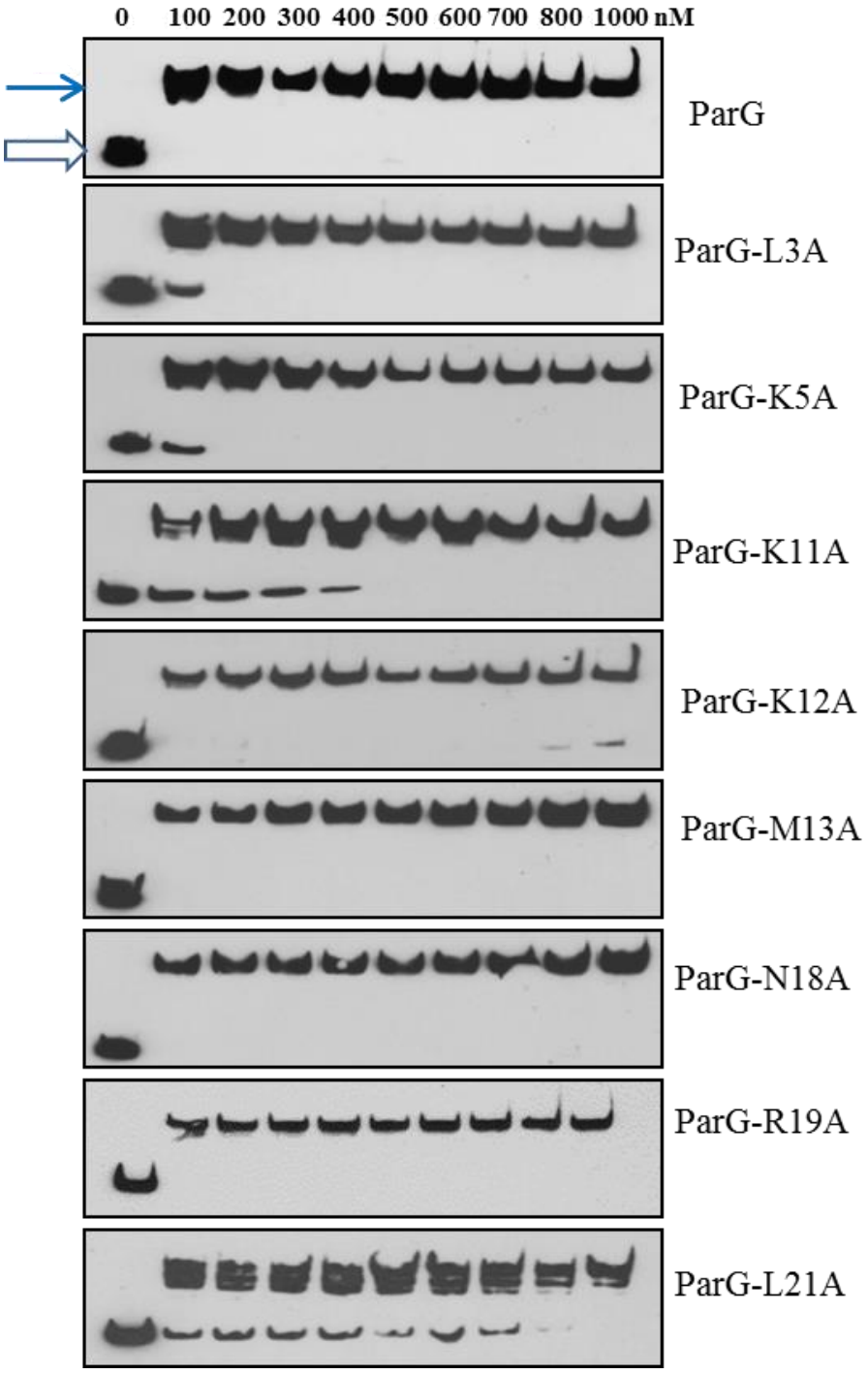

Figure 4.12. ParG mutant proteins retain the ability to bind DNA.

Increasing concentrations of WT and mutant ParG proteins were incubated with the 123 bp DNA fragment (0.5 nM) harbouring the *parFG* operator and subjected to EMSA. Unbound DNA is indicated by a hollow arrow and the filled arrow indicates the shifted nucleoprotein complexes.

4.2.5 Partition deficient ParG N-terminal mutants are still proficient in transcriptional repression of the putative *parFG* operon

To analyse the transcriptional repressor function of wild type and mutant ParG, a catechol 2-3 dioxygenase (CDO) reporter assay was carried out. This assay is based on the production of catechol 2, 3-dioxygenase encoded by the *Pseudomonas putida* TOL plasmid gene *xylE*. The pDM3.0 plasmid (Macartney *et al.*, 1997) used in this assay contained x*ylE*, cloned downstream of the *parFG* promoter region in order to have its expression modulated by ParG (Figure 4.13). This plasmid was transformed into *E. coli* cells together with *parG* expressing plasmids. Cell extracts containing the *xylE* product become yellow within seconds upon addition of catechol (Zampini *et al.*, 2009). Catechol is a colourless substrate that is converted into a yellow coloured product, 2-hydroxymuconic semialdehyde by CDO. One CDO unit is the amount of enzyme that oxidizes 1 µmol of catechol per min at 24ºC.

In this assay pET-MB ParG mutant constructs generated for protein production were used to express *parG*. BL21(DE3) cells were co-transformed with *xylE* containing pDM3.0 separately with pET22b, pET-ParG and pET-MB ParG mutant. Cells co-transformed with pDM3.0 and pET22b vector showed 100% expression of the *xylE* gene, co-transformation of pDM3.0 and pET-ParG resulted in transcriptional repression of *xylE,* whereas co-transformation of pDM3.0 and pET-MB ParG mutants affected the expression of *xylE* depending on the consequence of the change of N-terminal end residues on ParG transcriptional repression activity. When pDM3.0 was co-transformed with pET22b, the expression of *xylE* resulted in approximately 1800 CDO units, but on co-transformation with WT pET-ParG, *xylE* expression was repressed and less than 100 CDO units were produced. It was observed that all the partition deficient ParG N-terminal mutants were not affected in their transcriptional repressor activity, as the CDO units generated did not vary much as compared to those obtained with WT ParG (Figure 4.14). The CDO units for ParG-L3A, ParG-K5A, ParG-K11A, ParG-R19A and ParG-L21A were similar to those observed for WT ParG. ParG-K12A, ParG-M13A and ParG-N18A showed a level of repression that was half of that displayed by WT ParG. However they were still proficient in *xylE* repression. This demonstrated that, even though all these mutants are deficient in plasmid segregation, they all are still able to repress

transcription. These results are in agreement with the finding that the partition deficient mutants are efficient to bind the *parFG* operator DNA and hence the transcriptional repression action is not altered.

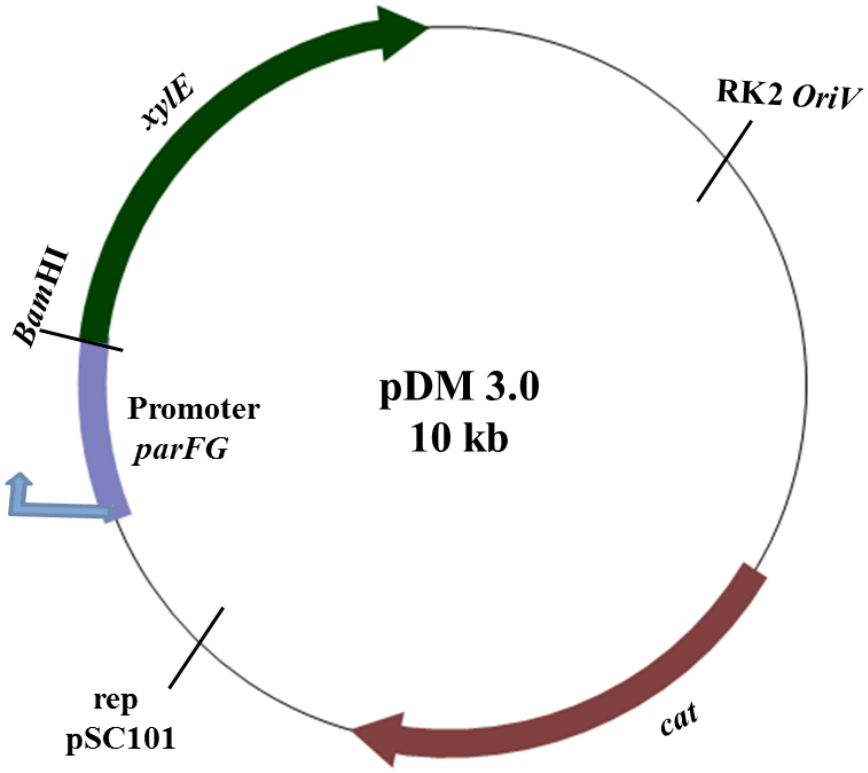

Figure 4.13. Vector map of pDM 3.0.

Plasmid pDM 3.0 contains *xylE* reporter gene cloned downstream of the *parFG* promoter sequence.

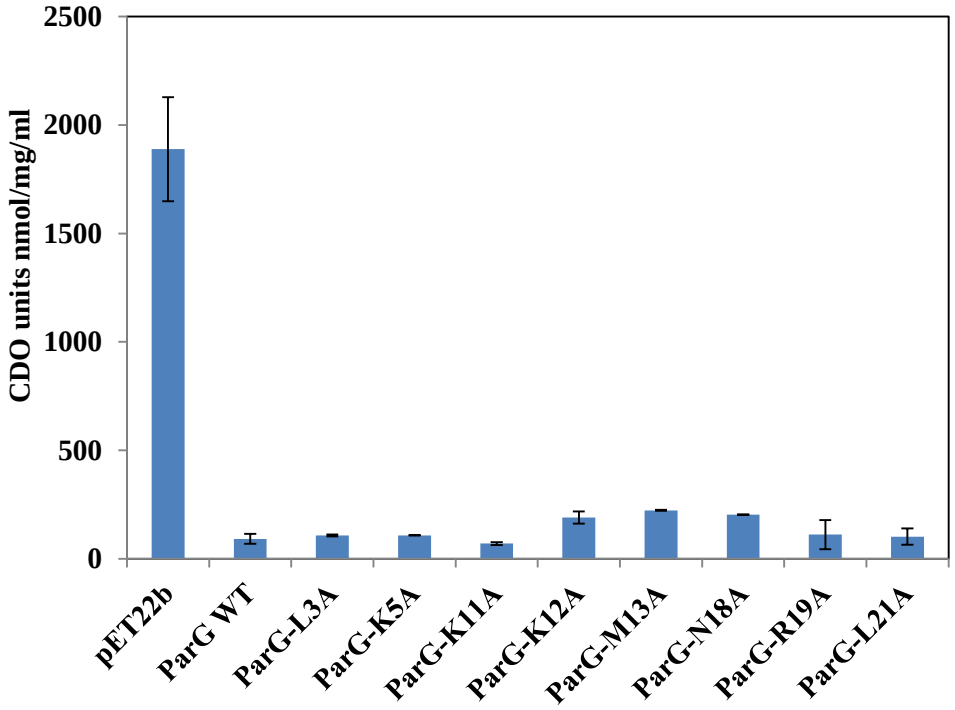

Figure 4.14. The ParG N-terminal mutants retain their *in vivo* transcriptional repressor function.

The repressor activity of WT ParG and mutant proteins was tested by CDO reporter assays. The results are averages of three experiments performed in triplicates and error bars represent the standard error of the mean, SEM.

4.3 Discussion and Conclusion

ParG is a dimer and the antiparallel β-strands of this dimer make direct contacts with the major groove of DNA. As ParG dimer formation is necessary for DNA binding, the first step was to test the ability of the partition deficient proteins to form dimers. This was also necessary to rule out the possibility that, the observed plasmid partition defect was due to the impairment in dimerization of the mutant proteins. When tested by chemical cross-linking, except ParG-K12A and ParG-R19A, other mutant proteins appeared dimeric in nature, similar to WT ParG. Imidoester cross-linkers react with primary amines to form amidine bonds. The DMP is not very stable and efficicent at higher pH and the amidine bond formed can be reversible. The cross-linker reacts with primary amine (-NH2) and in case of ParG-K12A, it appeared that DMP was not able to cross-link the protein in the absence of lysine and hence the reaction could not occur. However, with the SEC-MALLS experiment it was established that ParG-K12A was indeed a dimer. It is possible that the dimer formation in case of ParG-R19A was not very stable as weak bands were observed. The DNA binding and transcriptional repressor activities of ParG-R19A were not found altered. This may indicate that the eventhough cross-linking failed to demonstrate ParG-R19A dimerization; R19 has no prominent role in dimerization. The results obtained here support the previous finding that the ParG N-terminal domain has no detectable role in ParG dimerization.

ParG binds as a dimer of dimers to the operator sites (Zampini *et al.*, 2009) which results in the formation of a nucleoprotein complex in the EMSA experiments for ParG mutant proteins (Figure 4.12). When investigated for DNA binding function, overall the partition deficient ParG mutants showed no significant change in this activity at higher protein concentrations. However, the DNA binding was not tested below 100 nM protein concentration. ParG-K11A showed less affinity to the DNA at below 500 nM concentrations. Whereas ParG-L21A appeared the most affected mutant. L21 residue is in the region of a tail that may form transient secondary structure and involved in DNA binding. The change in L21 may lead to abolishing the DNA binding activity but it needs to be probed further. The dimerization and transcriptional repression activity of ParG-L21A was found to be similar to WT

ParG hence the aleteration in DNA binding and its implication on plasmid partition need to be examined in further details.

When partition deficient ParG mutants were tested for the transcriptional repressor function, none of the mutants showed alleviation of the repression. It is speculated that the abundance of positively charged residues in the N-terminal end helps in binding to negatively charged DNA. As a result, a single amino acid change is unlikely to alter the DNA binding and repression function. Hence, the mutant proteins showed efficient DNA binding and retained the transcriptional repression function.

The partition deficiency shown by ParG N-terminal mutants was not related to their DNA binding or transcriptional repressor function, hence their effect on activating ParF polymerisation and enhancing ParF ATPase activity were tested as the next step.

Chapter 5: ParG N-terminal tail is important for interaction with the partner protein ParF and stimulation its ATPase activity

5.1 Introduction

The focus of this project is on the unstructured and multifunctional N-terminal end of ParG. It has been reported in Chapter 3 that the mutations in the L3, K5, K11, K12, M13, N18, R19 and L21 of the ParG N-terminal end decreased the efficiency of plasmid partition. The partition deficient ParG mutant proteins were still able to form dimers, bind DNA efficiently and act as transcriptional repressors of the *parFG* operon (Chapter 4). The flexible N-terminal tail of ParG is involved in enhancement of ParF polymerization. In addition an arginine finger motif in the N-terminus has been shown to be responsible for the stimulation of ParF ATPase activity (Barillà *et al.*, 2007). To further probe the consequences of these mutations on plasmid partition, the mutants were tested for their efficiency in stimulating ParF polymerization and ATPase activity and the results are reported in this chapter.

Cellular organization in eukaryotes is attributed to cytoskeletal proteins like actin, tubulin and intermediate filaments. Recently, the prokaryotic homologues of these proteins were reported in various bacteria. The cell division protein FtsZ is a tubulin homologue whereas the shape determining protein MreB in rod-shaped bacteria is an actin homologue. In bacteria, there is another type of cytoskeletal proteins which have no eukaryotic counterparts and they are known as Walker A Cytoskeletal ATPases (WACAs) (Ingerson-Mahar and Gitai, 2012). Members of the WACA group fall under the superclass of P-loop NTPases. Nucleotide-dependent polymerization by NTPases plays an important role in fundamental processes like cell division, which are essential for the propagation of living species (Schumacher, 2008).

Previous investigations on ParF in the presence of ATP by negative-stain electron microscopy revealed that ParF forms a filamentous structure *in vitro* (Barillà *et al.*, 2005). Recently the crystal structure of ParF dimer was solved in the presence of non-hydrolysable ATP analogue, AMPPCP (Schumacher *et al.*, 2012). ParF-AMPPCP crystal structure showed the striking feature of polymer formation. The building block of the linear ParF polymer was shown to be a dimer-of-dimer unit. The polymer formation appeared as a stacking of one dimer-of dimer unit over the second dimer-of dimer unit where tip of the one unit notches into the second unit

(Schumacher *et al.*, 2012). ParG promotes ParF polymerization possibly through two mechanisms i.e. nucleation and bundling (Figure 5.1). When ParG binds to ParF in the absence of a nucleotide, it might bridge adjacent ParF monomers by employing the two N-terminal flexible tails present in the ParG dimer (Barillà *et al.*, 2007). It is possible that the mobile extensions of ParG act as sticky tentacles binding to the ParF monomers in solution, assisting and stabilizing the formation of the nucleus critical for filament growth. This function can be designated as 'nucleation'. ParF polymerizes upon binding ATP. When ParG is added to this ParF-ATP complex, multiple ParG dimers might associate with the ParF polymers along their length and might cross-link adjacent filaments. We refer to this ability of ParG as a 'bundling' function (Barillà *et al.*, 2005). ParG mutants were tested for both nucleation and bundling activities to determine the exact role played by the ParG flexible tail in ParF polymerization.

ParF polymerization is promoted by ATP and is inhibited by ADP. The nucleotide bound state may be a key factor in elucidating the underlying partition regulatory mechanism *in vivo* (Hayes and Barillà, 2006b). ParF is a weak ATPase and ParG stimulates this activity. The arginine finger motif in the ParG N-terminal tail is implicated in stimulating ParF ATPase activity (Barillà *et al.*, 2007). The residues at position 3, 5, 11, 12 and 13 are not part of the arginine finger but still crucial for plasmid partition. These mutant proteins will be tested to investigate if they are still able to stimulate ParF ATPase activity.

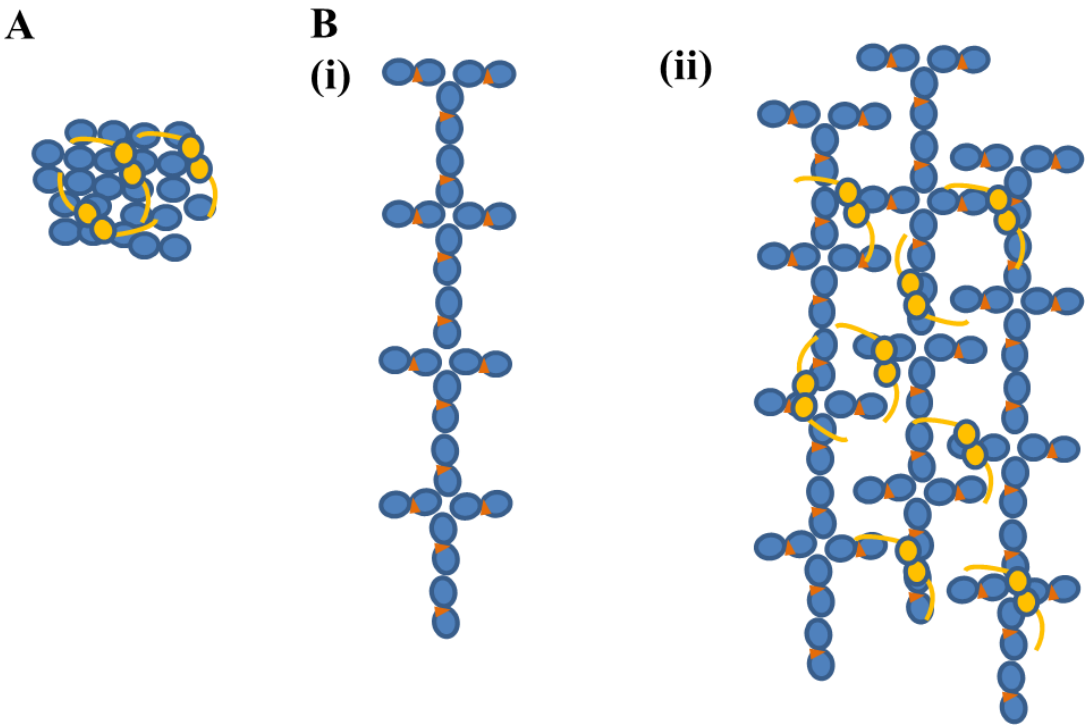

Figure 5.1. Two potential mechanisms by which ParG might promote ParF polymerization i.e. nucleation and bundling.

ParF monomers are shown as blue circles, ATP as orange triangle and ParG dimer with mobile tails as yellow ovals. **A**. Nucleation process: ParG dimers with their mobile N-terminal tails bind ParF monomers and form a nucleus which serves as a starting point for polymerization. **B**. Bundling process. **(i)**, Diagrammatic representation of ParF structure. ParF forms dimer on ATP binding and the dimers of ParF dimers get packed to generate polymers (Schumacher *et al.*, 2012). **(ii)**, ATP bound ParF proto-filaments are cross-linked by ParG and an extended mesh is formed.

5.2 Results

5.2.1 Partition deficient ParG N-terminal mutants are able to stimulate ParF polymerization

The effect of ParG on the polymerization of ParF was monitored in real time by Dynamic Light Scattering (DLS). DLS is different from static light scattering as it measures the hydrodynamic radius of the protein. Particles in solution follow Brownian motion and in DLS the measurement of this motion can be used to determine the size of the particles. The radius is denoted as hydrodynamic because DLS measures how a particle diffuses within the fluid. In DLS the intensity of the scattered light is also recorded. The changes in this intensity and particle size were analysed to study ParF polymerization.

In a typical DLS experiment, ParF (2.16 µM) was monitored for a few minutes to obtain a baseline which also exhibits dispersed nature of ParF in the absence of nucleotide. On addition of ATP (500 µM), ParF started to polymerise extensively, which triggered an increase in the intensity of light scattering (6000 to 12000 kct/s) and a simultaneous increase in the size of the particles in solution. When a plateau was reached for ATP-induced polymerization, WT ParG (2.16 µM) was added. A steep increase in the intensity of light scattering was observed (~ 20000 kct/s), as polymerization was enhanced by ParG (Figure 5.2A). The instantaneous enhancement in ParF polymerization suggests that ParG might cross-link ParF proto-filaments. In contrast, the particle size showed a steady increase rather than a swift change (Figure 5.2B). Particles of around 1000 nm were observed. ParF filament bundles observed by EM in the past showed a length of around 650 nm (Barillà *et al.*, 2005). All the buffers, solutions of ATP, $MgCl_2$ and fractions of WT and mutant ParG protein were tested separately in DLS experiment as a control to check if there was any residual or inherent polymerization associated with them. None of these components showed any increase in light scattering, which means that in the ParF polymerization reaction they do not contribute to the increased intensity of light scattering.

The ability of ParG N-terminal mutant proteins to promote ParF polymerization was analysed. After defining the baseline for ParF and then recording ATP induced ParF

polymerization, ParG mutants (2.16 µM) were separately added to the reaction. All the mutants (ParG-L3A, ParG-K5A, ParG-K11A, ParG-K12A, ParG-M13A, ParG-N18A and ParG-L21A) showed the same efficiency as WT ParG in enhancing ParF polymerization and showed the same pattern of sudden increase in intensity of light scattering (in the range of ~20000 to 30000 kct/s) and a steady increase in the particle size (Figure 5.2A and B). The increase in the intensity was speculated to be due to the bundling of adjacent ParF polymers by ParG, which may still not accelerate polymer growth *per se*. It has already been reported that the ParG-R19A induces a steep increase in ParF polymerization, as an increase of scattered light similar to that triggered by WT ParG was recorded hence the experiment was not repeated here (Barillà *et al.*, 2007).

It was previously shown that Δ9, Δ19 and Δ30 ParG N-terminal truncated proteins fail to stimulate ParF polymerization beyond the level induced by ATP. This may indicate that stimulation of ParF polymerization is not dependent on individual amino acids in the ParG tail, but it is a cumulative effect, exerted by the flexible tail possibly acting like 'sticky tentacles' as previously proposed (Barilla, *et al.* 2007).

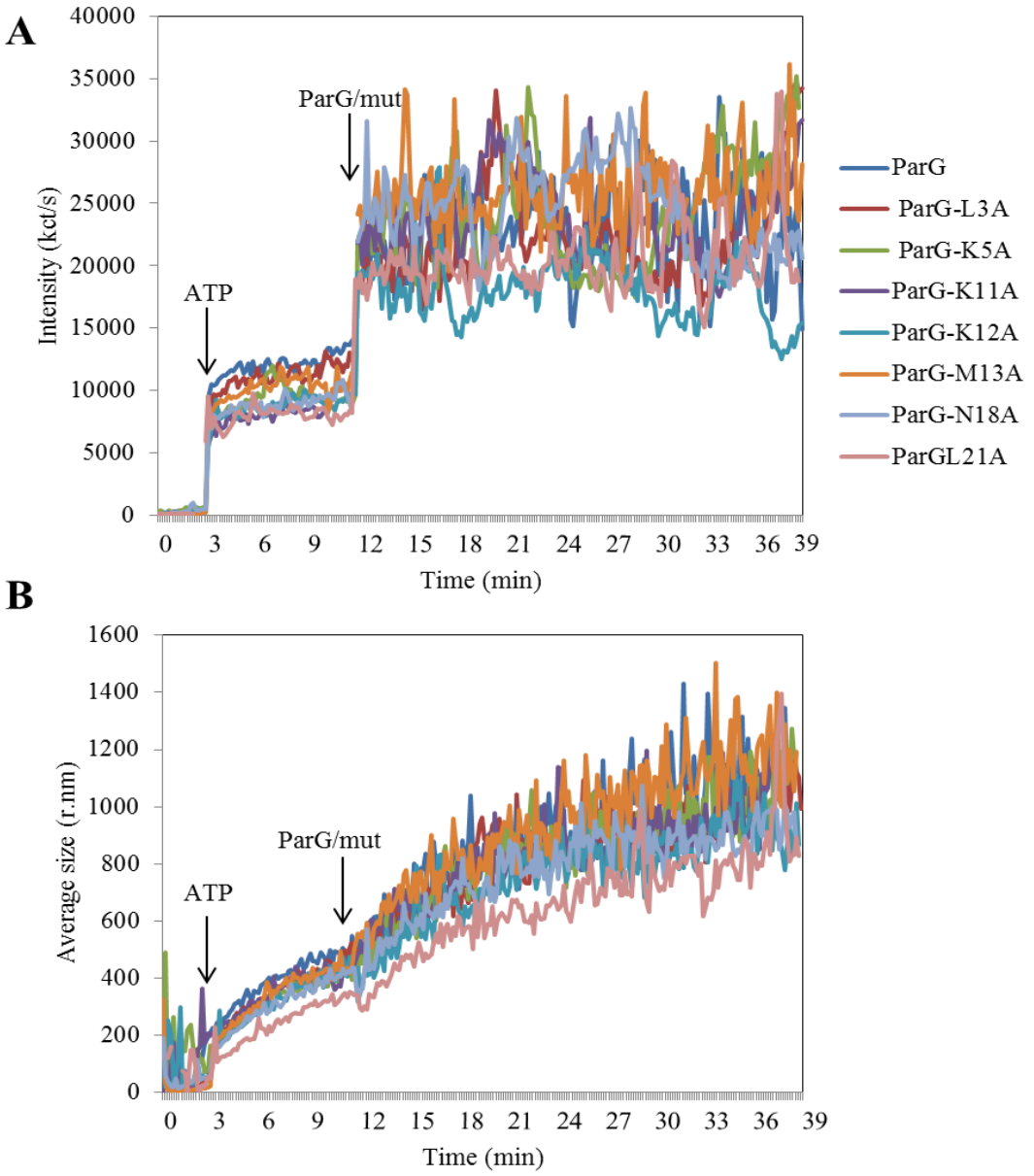

Figure 5.2. Partition deficient ParG N-terminal mutant proteins are still proficient in enhancing ParF polymerization.

A. DLS experiment in which the increase in the light scattering intensity (kct/s) was recorded for wild type ParG and all the mutants, whose profile is shown according to the colour code. For the first 3 minutes, the intensity of light scattered by ParF (2.16 μM) was recorded and a baseline obtained. Then ATP (500 μM) and $MgCl_2$ (5 mM) were added and ParF polymerization was observed. Readings were taken for the next 9 minutes and then WT or mutant ParG proteins (2.16 μM) were individually added in a 1:1 molar ratio and reaction was observed further for around 30 minutes. **B**. The size of the particles (nm) was recorded at the same time as the intensity of scattered light. The order of addition of ligands to the reaction is the same as in A. The data shown are representative examples of experiments performed in triplicate.

5.2.2 Partition deficient ParG-L3A and ParG-K12A mutant proteins failed to nucleate ParF polymerization

As previously mentioned, ParG may promote ParF polymerization in the absence of ATP and this activity may be described as nucleation. To evaluate the ability of the ParG mutants to nucleate ParF polymers, a DLS experiment was designed and set up following a different protocol. To begin with, monomeric ParF (2.16 µM) was monitored to obtain a baseline and then WT ParG was added to the reaction at an equal concentration (2.16 µM) allowing ParF-ParG interaction in the absence of a nucleotides. An increase in the intensity of scattered light was immediately observed (500 to 3000 kct/s), although this was more modest, when compared to the polymerization occurring as a result of ParF-ATP interaction. To the ParF-ParG reaction mixture, $MgCl_2$ (5 mM) and ATP (500 µM) were added and the reaction was monitored for 10 further minutes. The ParF-ParG nucleation core responded to the ATP and a second steep increase in the intensity of scattered light was observed (6000 to 9000 kct/s) (Figure 5.3). This confirmed the ability of ParG protein to nucleate ParF molecules in the absence of ATP. Although the overall intensity of scattered light recorded during the nucleation process was less pronounced, compared to that recorded during the bundling activity.

All the mutant proteins were tested for the ability to nucleate ParF using the same protocol. ParG-N18A showed a nucleation pattern identical to that of WT ParG. It stimulated ParF polymerization, in the absence of ATP, to the same level of WT ParG and the core formed by ParF-ParGN18A, which responded to ATP, showed a similar increase in intensity of light scattering. ParG-K5A, ParG-K11A, ParG-M13A, ParG-R19A and ParG-L21A showed comparable nucleation activity, as a similar increase in intensity was observed (500 to 3000 kct/s). However, when ATP was added, the increase in intensity of scattered light was less than that observed for the reaction containing WT ParG. This may indicate that the core formed by ParF-ParG mutants was not able to respond to ATP in the same manner as that containing WT ParG. ParG-L3A and ParG-K12A showed a very small increase in intensity (~1000 kct/s), when added to ParF compared to other mutants and there was no increase in intensity at all on the addition of ATP (Figure 5.3).

The size of ParF polymers increased gradually in the presence of WT and mutant ParG proteins, however the maximum size was 400 nm compared to a particle size of 1000 nm seen during the ParF bundling by ParG and its mutants (Figure 5.4). The data for the particle size also appeared very noisy, indicating the formation of mixed populations of ParF oligomers of different sizes.

Based on these results, the nucleation activity of ParG mutants can be divided into three categories: high, medium and low levels of nucleation. All the ParG N-terminal partition deficient mutant proteins are efficient in bundling ParF and stimulate polymerization, but they are dissimilar in nucleation. ParG-L3A and ParG-K12A are impaired in the nucleation of ParF thus giving a phenotype that can be summarized as bundling (+)/nucleation (-). ParG-K5A, ParG-K11A, ParG-M13A, ParG-R19A and ParG-L21A have not lost their nucleation activity completely, but they are not as efficient as WT ParG showing the phenotype bundling (+)/nucleation (+) whereas ParG-N18A showed the same high nucleation and bundling activity as that of WT ParG and exhibits a bundling (+)/nucleation (++) phenotype (Table 5.1).

Table 5.1 ParG mutants are categorised depending upon their ability to carry out nucleation and bundling of ParF.

Mutants	Nucleation	Bundling
ParG WT	+ +	+
ParG-L3A	-	+
ParG-K5A	+	+
ParG-K11A	+	+
ParG-K12A	-	+
ParG-M13A	+	+
ParG-N18A	+ +	+
ParG-R19A	+	+
ParG-L21A	+	+

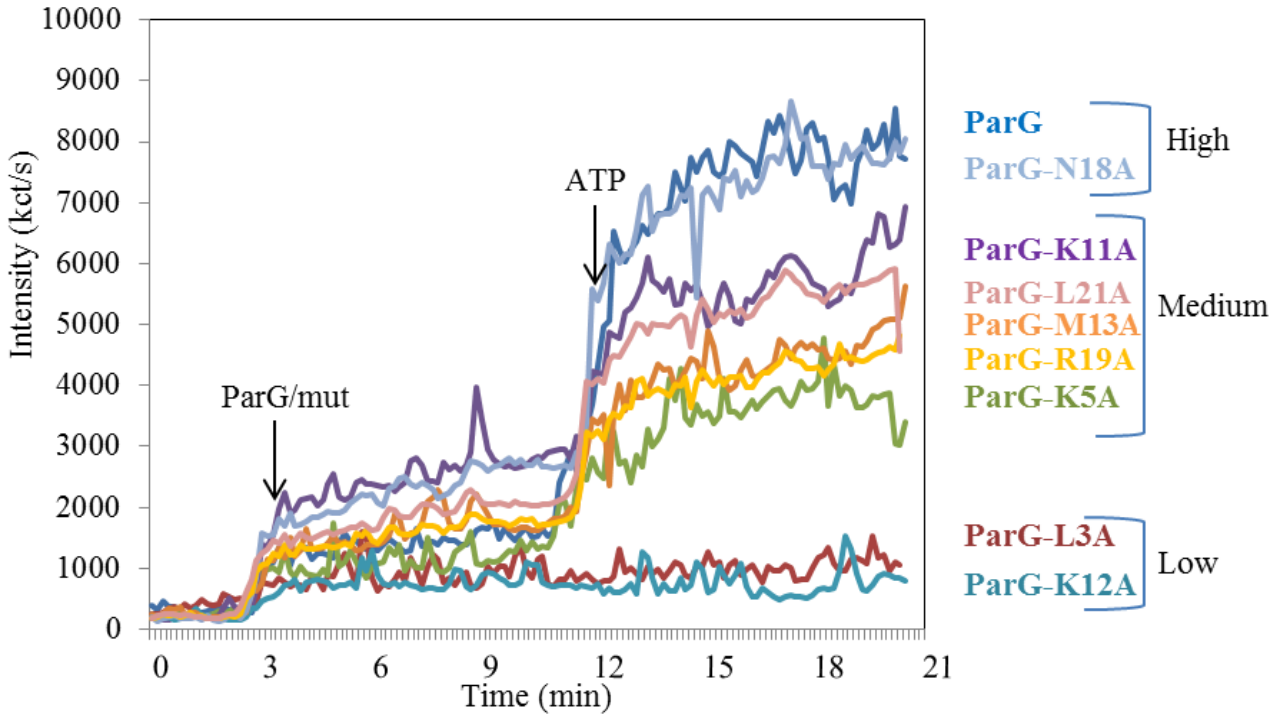

Figure 5.3. ParG mutant proteins show dissimilar performance in nucleation function.

DLS experiment in which the increase in the light scattering intensity (kct/s) was recorded for wild type ParG and all the mutants, whose profile is shown according to the colour code. For the first 3 minutes, the intensity of light scattered by ParF (2.16 μM) was recorded and a baseline obtained. Then WT or mutant ParG proteins (2.16 μM) were individually added in a 1:1 molar ratio and ParF polymerization by nucleation function was observed. Readings were taken for the next 9 minutes and then ATP (500 μM) and $MgCl_2$ (5 mM) were added. Reaction was observed for further 12 minutes. Depending upon the intensity signal, mutants are categorised into high, medium and low nucleation, as shown on right hand side. Data shown is the average intensity calculated from six different experiments.

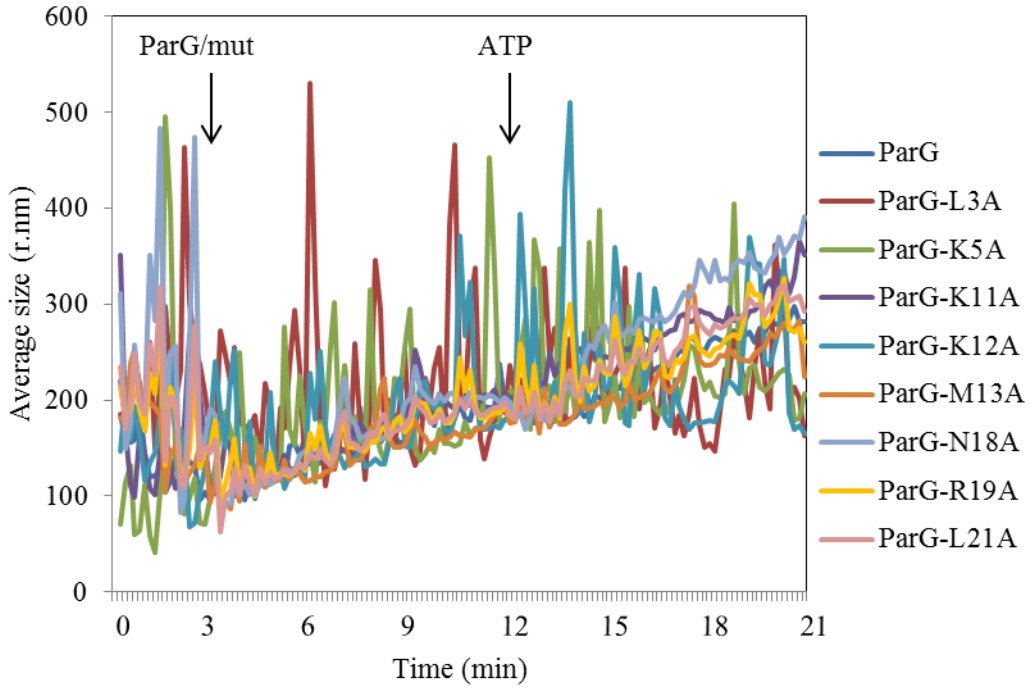

Figure 5.4. Change in particle size was observed during ParF polymerization caused by nucleation activity of ParG/mutant proteins.

DLS experiment in which the increase in the average size (nm) was recorded for wild type ParG and all the mutants, whose profile is shown according to the colour code. The order of addition of ligands is indicated by arrow and is same as in Figure 5.3 Data shown is average size calculated from six different experiments.

5.2.3 Partition deficient ParG N-terminal mutant proteins behave differently in nucleating ParF proto-filaments

Results obtained from DLS experiments show that the ParG N-terminal mutants might behave differently in nucleating ParF (nucleotide-independent ParF polymerization stimulated by ParG). Nucleation and bundling activity can be analysed together experimentally by performing a sedimentation assay. In this assay, ParF and ParG are incubated together before centrifuging and separating the pellet and supernatant. The polymerized protein sediment into a pellet. Polymerized and un-polymerized ParF fractions were resolved by loading 100% of the pellet and 33% of the supernatant, on a 15% SDS gel, which provides an insight into the process of ParF polymerization and the role of ParG.

5.2.3.1 Experimental set up to study bundling and nucleation activities by sedimentation assay

To evaluate the effect of WT ParG and mutants in ParF nucleation and bundling activities, three different types of reactions were set up (Figure 5.5). In reaction number 1, bundling activity was analysed. ATP (2 mM final) was added to ParF (8 µM) and incubated for 30 minutes allowing ATP dependent ParF polymerization. To this mixture, ParG or the mutant proteins (8 µM, dimer) were added and incubated for further 30 minutes. Then the reaction mixture was centrifuged and the protein pellet and supernatant were separated and loaded onto a SDS gel. In the second and the third reactions, nucleation activity was studied systematically. In the second reaction, ParF and ParG/mutant proteins were incubated without ATP for 30 minutes and separated into pellet and supernatant and resolved on the gel. This determines how much ParF polymerization is promoted by ParG/mutant proteins in the absence of ATP. In the third type of reaction, samples were set up in the same way as for reaction 2, but after 30 minutes, ATP was added to the mixture and further incubation was carried out for 30 minutes. The fraction of pellet and supernatant were separated and analysed on gel. The response to ATP of the core formed by ParF-ParG/mutant proteins was investigated by this reaction.

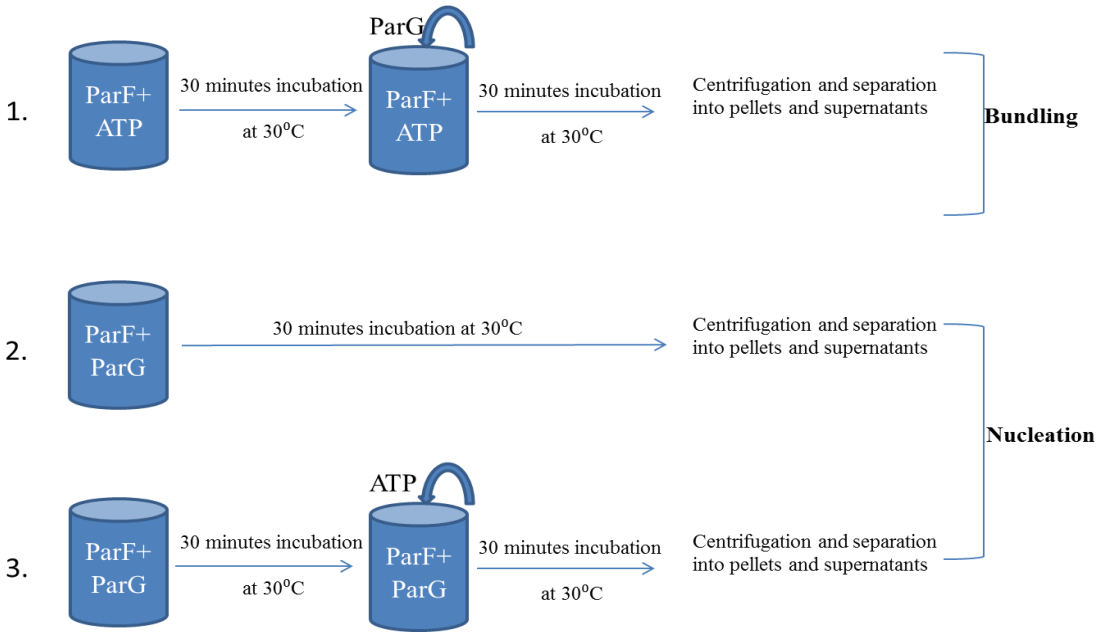

Figure 5.5. Three different types of reactions were set up to analyse bundling and nucleation activity of ParG and mutants.

Reaction number 1 tests the bundling activity as ParG is added to the ParF-ATP complex. Reaction 2 and 3 probes nucleation activity as formation of the ParF-ParG/mutant nucleus and its response to addition of ATP is analysed.

5.2.3.2 Partition deficient ParG mutants efficiently bundle ParF polymers

When ParF alone was analysed by the sedimentation assay in the absence of ATP around 30% of ParF was seen in the pellet, revealing the inherent self- association tendency of the protein. When ATP was added to ParF, almost 50% of ParF was seen in the pellet, as ATP binding initiates extensive ParF polymerization (Figure 5.6A), although this value is more modest than that previously recorded (Barilla' et al., 2005). In reaction set up one, when WT ParG was added to previously incubated ParF-ATP complex, ParF was recovered in the pellet and ParG co-sedimented with it, which reconfirmed that ParG was involved in ParF bundling. In this reaction, the amount of ParF in the pellet was more than 80% and that of the co-sedimented ParG was around 50% (lanes under bundling panel in Figure 5.6B). In the same type of reaction, in the presence of all the ParG mutant proteins ParF was similarly observed in the pellet (50-80%), which indicated that these mutants are efficient in ParF bundling activity, although the quantity of ParG mutants co-sedimented with ParF was not as much as WT ParG (lanes under bundling panels in Figure 5.6C - 5.6J).

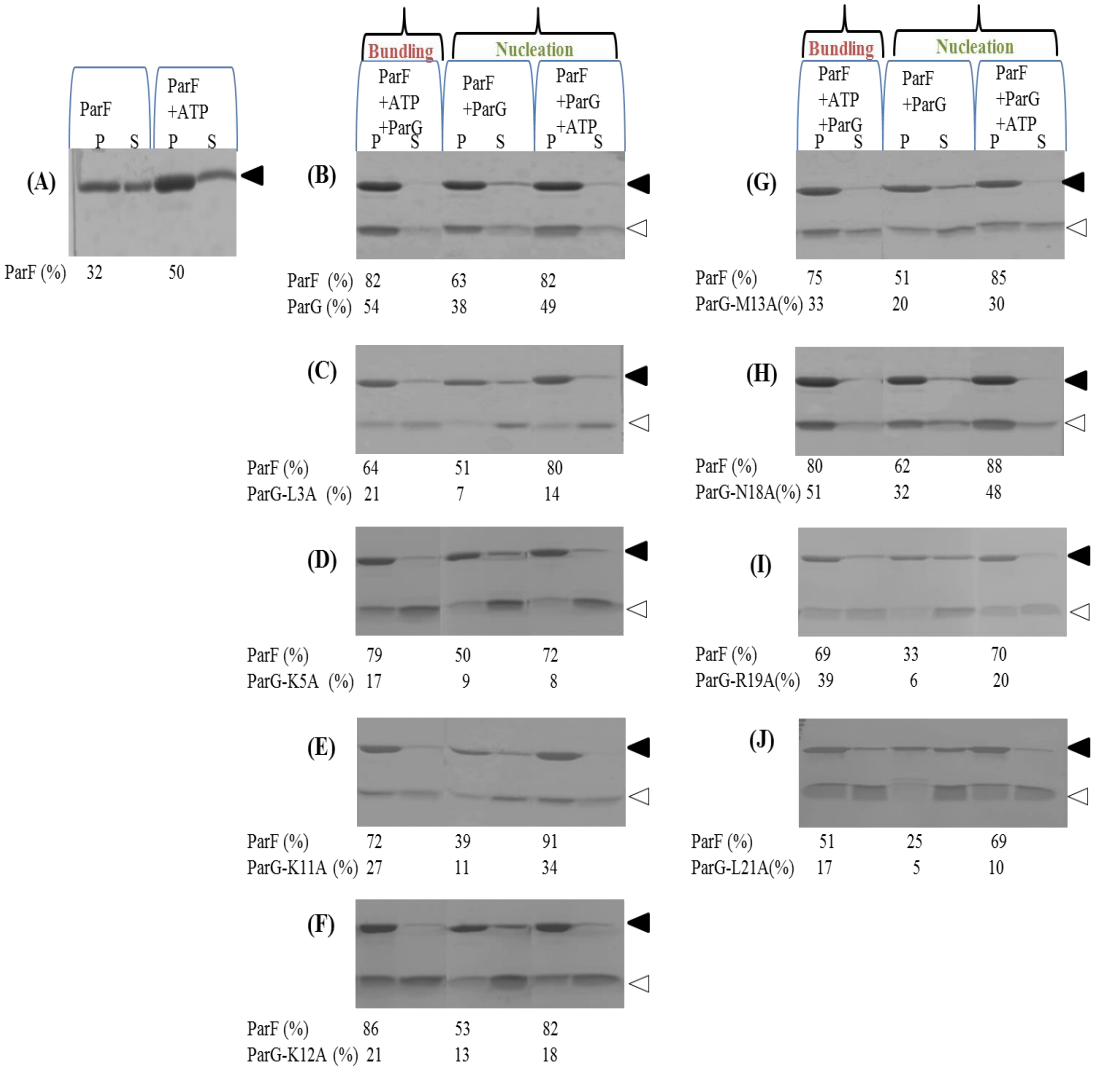

Figure 5.6. ParG N-terminal mutant proteins show variations in nucleation and bundling functions.

A. ParF (8 µM) incubated with and without nucleotide and separated on 15% SDS gel. **B-J**. ParG and N-terminal mutant proteins (8 µM) were incubated with ParF (8 µM) in the presence and absence of ATP (2 mM) in three different types of reaction setups as labelled at the top of the gels. 100% of pellet (p) fraction and 33% of supernatant (s) fractions were resolved on gels. The black and white arrowheads show ParF and ParG/mutant proteins respectively in all gels. Percentage of ParF and ParG/mutant protein in pellet fractions are given at the bottom of each gel. Gels and data shown are representative examples for WT and each mutant ParG protein from sedimentation assays performed in triplicate.

5.2.3.3 Partition deficient ParG mutants show variations in nucleating ParF polymers

In the second type of reaction, when ParG interacted with ParF in the absence of ATP, ParG was still able to stimulate ParF polymerization, as shown by 63% of ParF found in the pellet. When ATP was added after the ParF-ParG incubation (reaction 3), more than 80% of ParF was recovered in the pellet and ParG showed around 50% co-sedimentation. The pattern of ParF and ParG sedimentation in reaction 1 and 3 is very similar, suggesting that ParG equally promotes ParF bundling and nucleation. ParG-N18A performed in the same way as WT ParG in reactions 2 and 3 and the amount of ParF recovered in the pellet in the presence of ParG-N18A was very similar in the presence of that found with WT ParG (lanes under nucleation panel Figure 5.6B and 5.6H). This indicates that Asn18 does not appear to have specific role in the nucleation activity.

When rest of the ParG mutants were analysed by the second type of reaction and added to ParF without nucleotide, ParF showed polymerization as around 50% of the ParF was found in the pellet. However, more than 80% of the ParG mutant proteins remained in the supernatant fractions. In the third type of reaction, the ParF-ParG mutant core responded to added ATP, which led to an escalation in ParF polymerization and pulled more than 80% of ParF in the pellet. But during this process also, more than 70% of ParG mutant proteins remained in the supernatant. The inability of ParG mutants to co-sediment with ParF might be related to the change in ParF-ParG interaction. The nucleus produced with this interaction although responded to the ATP and showed ParF polymerization, the nature of ParF polymers need to be examined in future. The presence of ATP was found to be helpful only to increase ParF polymerization and not to promote ParF-ParG interaction. The pattern observed during the sedimentation assay, reflects the findings from DLS, which indicated that, with the exception of ParG-N18A, the other mutant proteins are affected in nucleation function and display variable activity.

In control sedimentation assays, ParG and the N-terminal mutant proteins (8 μM) were incubated on their own, with and without ATP. In both conditions, ParG and mutant proteins were found only in the supernatant, which indicated that ParG and

the mutant proteins do not self-associate in the presence or absence of ATP (data not shown). Thus, when ParG or the mutants are observed in the pellet in ParF-containing reactions, it is because of the association with ParF.

5.2.4 Partition deficient ParG N-terminal mutant proteins exhibit a weaker interaction with ParF

DLS experiments and sedimentation assays showed that the ParG partition deficient mutants behave differently in stimulating ParF polymerization in the absence of ATP. This observation prompted an investigation of the interaction of the ParG mutants with ParF to elucidate the precise role of these amino acids in plasmid partition. It has been speculated that both the flexible N-terminal tails and RHH motif of the ParG dimer contribute to ParF interaction (Carmelo *et al.*, 2005, Golovanov *et al.*, 2003). ParF-ParG/mutants interaction was studied by using a bacterial two-hybrid system and quantified by performing β-galactosidase assays (Dobruk-Serkowska *et al.*, 2012). The bacterial two-hybrid system allows a study of functional interactions between two proteins based on complementation of CyaA (adenylate cyclase) fragments. *cyaA* encodes the toxin adenylate cyclase produced by *B. pertussis* in a calmodulin-dependent manner. The catalytic domain of this protein, that consists of 400 amino acids, is proteolytically cleaved into two complementary fragments, T25 and T18. In the absence of calmodulin, T25 and T18 cannot interact. *E. coli* lacks calmodulin, so when T18 and T25, fused with interacting proteins are expressed in a Cya-deficient *E. coli* strain, they re-associate resulting in cAMP synthesis. cAMP binds to the catabolite gene activator protein, CAP. The cAMP/CAP complex then can recognise the promoters of catabolic operons and switch on the transcription of the corresponding genes (Karimova *et al.*, 1998).

Wild type *parF* and *parG* genes cloned into vectors pT25 and pT18 respectively. Constructs pT18ParG and pT25ParF were available in the laboratory plasmid collection. Mutant alleles *parG-L3A* and *parG-K5A* were cloned in pT18ParG by Benjamin Rodway and pT18ParG-K11A, pT18ParG-K12A, pT18ParG-M13A, pT18ParG-N18A, pT18ParG-R19A and pT18ParG-L21A were constructed as a part of this project. When the interacting proteins were not present and empty pT25 and

pT18 were co-transformed, the Miller units obtained in the assay were merely 70. Whereas WT ParG and ParF interaction generated more than 1200 Miller units. When ParF-ParG mutants interaction was tested, all partition deficient ParG N-terminal mutant proteins showed reduced interaction with ParF as compared to WT ParG (Figure 5.7), as none of the interaction generated more than 800 Miller units. ParG-K11A and ParG-K12A exhibited the lowest interaction (less than 400 Miller units) amongst the mutants. This indicates that a change in these amino acids, in the flexible N-terminal end of ParG, affects the interaction with ParF more drastically. The weakened interaction of ParG mutant proteins with ParF may contribute to partition deficiency, either by affecting nucleation activity or by impairing stimulation of ParF ATPase activity or formation of the segrosome.

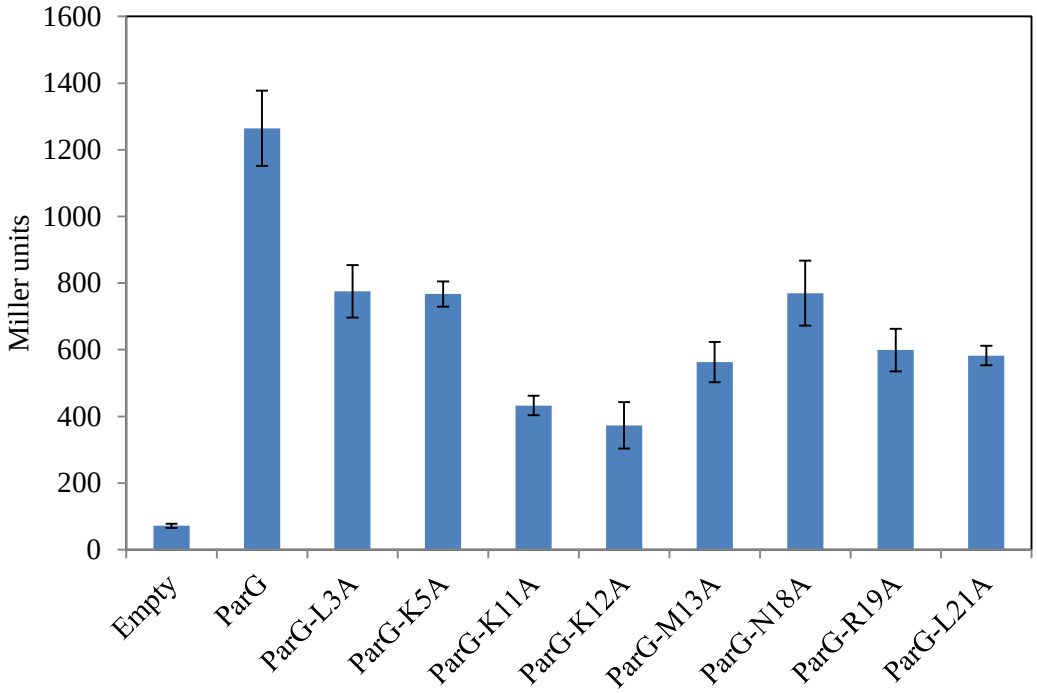

Figure 5.7. ParG N-terminal mutant proteins display a weaker interaction with ParF. ParF-ParG/mutant interaction was quantified using the β-galactosidase assays. Empty indicates the strain containing pT18 and pT25 vectors harbouring no genes, thus serving as the negative control. Plasmid pT25ParF was co-transform separately with plasmid pT18ParG/mut. The results are an average of three experiments carried out in triplicates and error bars represent the standard error of mean.

5.2.5 ParG N-terminal mutant proteins are impaired in triggering ParF ATPase activity

ParF is an intrinsically weak ATPase and relies on its partner protein ParG for activating ATP hydrolysis. So far, evidence has been obtained indicating that the ParF-ParG interaction might be compromised when certain amino acids are changed in the ParG N-terminal tail. The change in these residues was detrimental to plasmid partition. It remains to be determined if these mutant ParG proteins are able to stimulate ParF ATPase activity. The effect of mutant ParG proteins on stimulating ParF ATPase activity was studied by employing thin layer chromatography (TLC) as explained in section 2.13. In this assay, when ParF is incubated with radioactive ATP, ATP and its hydrolysis product ADP are separated using TLC. The ATP and ADP spots can be visualised on autoradiography films and quantified using a phosphorimager. When ParG is added to this reaction, the increase in ATP hydrolysis results in generation of more ADP, which can also be seen and quantified. Similarly, N-terminal end mutant proteins can be added and the effect on ParF ATPase activity can be investigated.

In the assay, ParF was incubated with [α^{35}S] ATP, along with increasing concentrations of ParG at 30°C. Increasing amounts of ParG resulted in augmentation of ATP hydrolysis by ParF (Figure 5.8). All the ParG N-terminal mutant proteins tested in the assay were found to be impaired in stimulating ParF ATP hydrolysis. Even when the concentration was increased to 5 µM, the proteins were not able to enhance ParF ATPase activity beyond 30% of the stimulation produced by the WT ParG (Figure 5.9). ParG-L3A, ParG-K5A and ParG-K11A showed some intrinsic ATPase activity in the absence of ParF which is likely due to the presence of some contaminating ATPases in the purified protein preparations. This was normalised during quantitation of their relative ATPase activity. In the past ParG-R19A demonstrated the similar impairment and at a concentration of 5 µM less than 20% relative ATPase stimulation was reported (Barillà *et al.*, 2007).

ParG-N18A showed the lowest level of stimulation amongst all the mutants. This could be due to the fact that N18 is part of the arginine finger motif and a mutation at this position affects ParG function more than mutations more distant from the finger-

motif. This result suggests that the defect in segregation shown by these mutants is related to a decrease in ParF ATPase stimulation. Interestingly, the ability of these mutants to repress transcription, to bind DNA and to enhance ATP dependant ParF polymerization was unaltered as suggested by results reported here and in previous chapters. This suggests that the N-terminal tail of ParG is involved in various functions.

It was not possible to draw any conclusion for the ability of ParG-L21A to stimulate ParF ATPase activity. On all three occasions, WT ParG showed variation in stimulating ATP hydrolysis making it difficult to compare the stimulation caused by the mutant protein. ParG-L21A also showed variation and did not display any consistency (Figure 5.10). Although it sometimes appeared that the ATP hydrolysis was diminished in the presence of this mutant protein, the collective data analysis failed to suggest a definite effect.

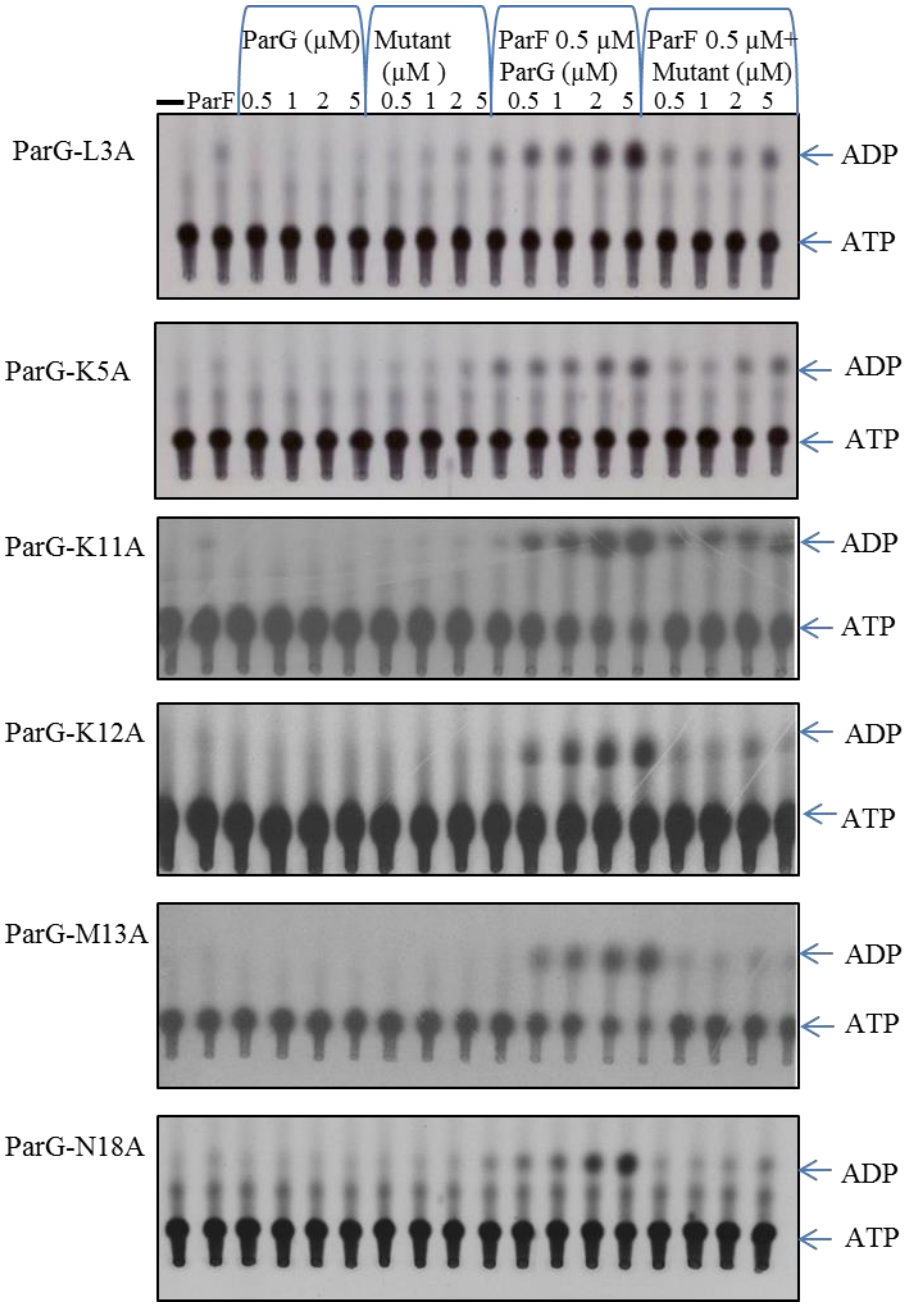

Figure 5.8. The ParG mutants are impaired in stimulation of ParF ATP hydrolysis. Autoradiographic images showing the results of ATPase assays in which radioactive ATP ([α^{35}S] ATP) was incubated with ParF and ParG/mutant proteins. ATP and its hydrolysed product (ADP) were separated by TLC. ParG protein fractions were tested without ParF to check for the presence of potential contaminating ATPase. ATP and ADP are indicated by arrows in all the images. WT ParG was run every time along with the mutant proteins to calculate the relative stimulation. Representative images are shown for each mutant from experiments performed in triplicate.

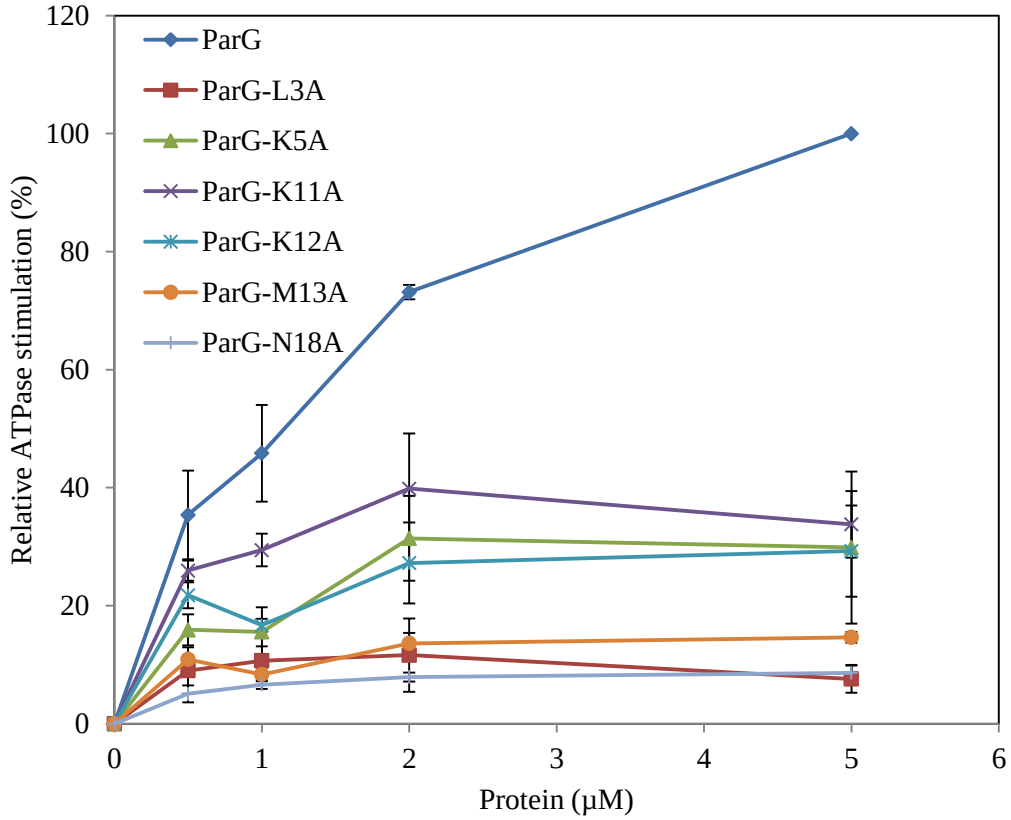

Figure 5.9. ParG N-terminal mutant proteins are impaired in stimulating ParF ATPase activity.

ATPase assays of ParF in the presence of ParG/mutant proteins harbouring the changes in L3A, K5A, K11A, K12A, M13A and N18A. Relative stimulation of ParF ATPase activity promoted by ParG/mutants plotted against protein concentration. The results are an average of three experiments. The error bars represent the standard error of mean.

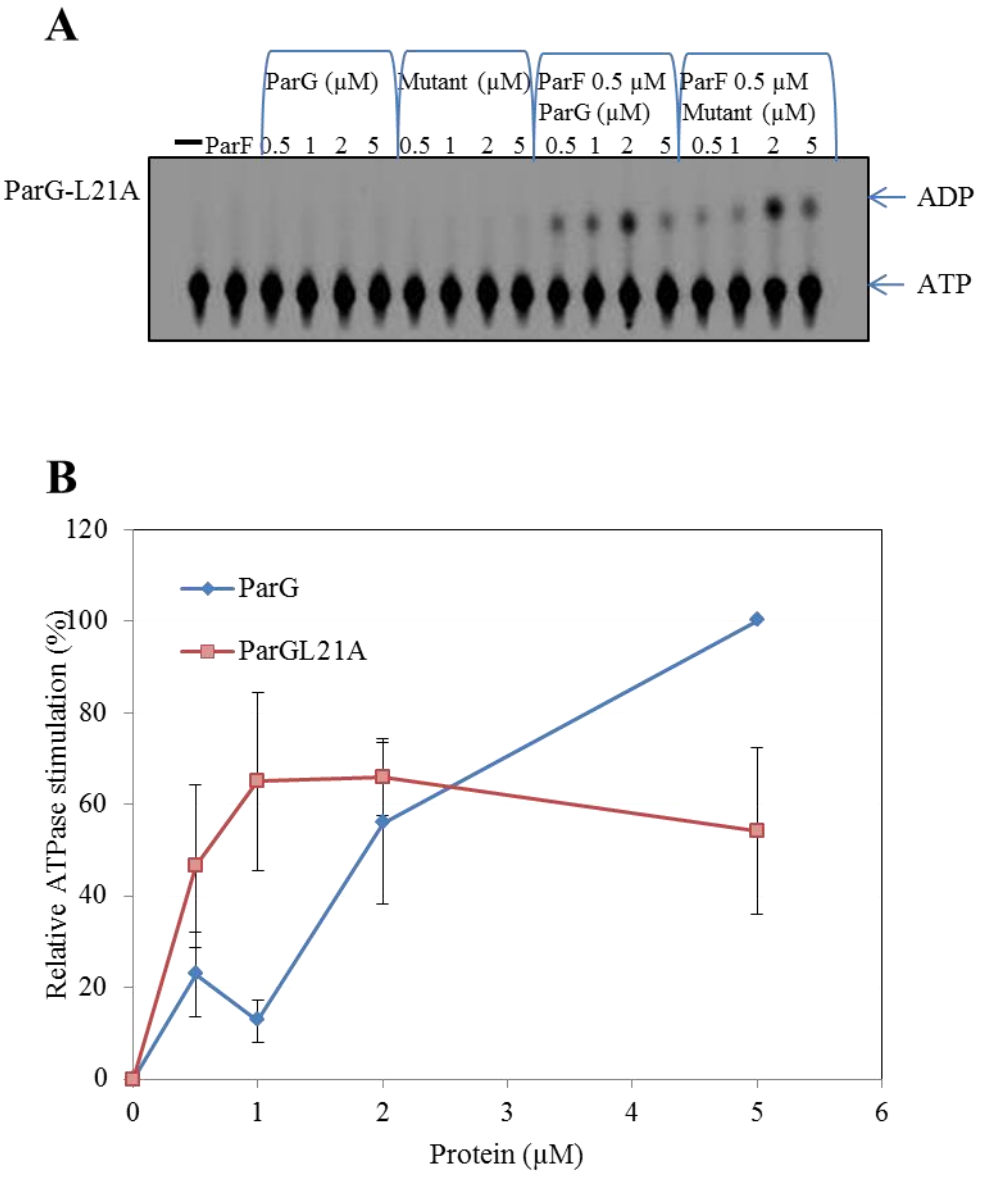

Figure 5.10. ParG-L21A exhibits inconsistent stimulation of ParF ATPase activity.

A. scan of the autoradiographic film showing the signal for ATP and its hydrolysis product ADP. **B**. The relative ATPase stimulation was plotted against the protein concentration. Both WT and mutant ParG showed variation in the ATPase stimulation. The results are an average of three experiments. The error bars represent the standard error of mean.

5.3 Conclusion

ParG stimulates ParF polymerization in the absence and the presence of ATP. For the purpose of this study, these activities of ParG have been referred to as nucleation and bundling respectively. To investigate how ParG N-terminal mutant proteins affect these two functions of ParG, DLS and sedimentation assays were performed. In DLS experiments, ParG mutant proteins deficient in plasmid partitioning showed similar augmentation of ParF polymerization as that triggered by WT ParG in an ATP-dependent manner. Similarly, in the sedimentation assays, incubation of ParG mutant proteins with ParF and ATP resulted in ParF being pelleted, indicating these mutants are still proficient in somehow bundling ParF filaments. Interestingly, even though ParG mutants were able to bundle ParF polymers, they displayed differences. WT ParG and ParG-N18A co-precipitated with ParF, but other ParG mutant proteins failed to co-sediment with ParF.

It was found that ParG could increase ParF polymerization by directly binding to monomeric ParF, even in the absence of nucleotides. ParG mutant proteins demonstrated variation in promoting ATP independent ParF polymerization. ParG-N18A protein displayed very similar nucleation activity as that of WT ParG in DLS and sedimentation assays. In DLS experiments, among the other mutant proteins, ParG-L3A and ParG-K12A showed diminished nucleation activity as ParF polymerization was neither increased by ParF-ParG-L3A/K12A interaction nor on further addition of ATP. The rest of the mutant proteins caused an increase in ParF polymerization, but less substantial than that promoted by WT ParG. In the sedimentation assay, all these mutants brought ParF into the pellet by promoting ParF polymerization, but the percentage of ParF protein in the pellet was always less pronounced than that observed with WT ParG. In addition, the ParG mutant proteins (except ParG-N18A) did not co-sediment with ParF during nucleation type of reaction.

As ParG mutant proteins showed a gradient in terms of nucleation activity, an investigation of the ParF-ParG interaction was conducted. The β-galactosidase assay used to analyse protein-protein interaction showed that all the ParG mutant proteins were compromised in the interaction with ParF. All the partition-deficient ParG N-

terminal mutant proteins showed impairment in stimulating ParF ATPase activity. Along with altered ParF interaction, the diminished ParF ATPase activity could be the reason behind partition defects.

Chapter 6: The ParG N-terminus is essential for *in vivo* ParF oscillation over the nucleoid

6.1 Introduction

In order to establish the role of the flexible ParG N-terminal tail in plasmid partition, various mutations were constructed. Crucial residues in the ParG N-terminal end (L3, K5, K11, K12, M13, N18, R19 and L21) have been identified; amino acid substitutions in these positions result in a defect in plasmid partition (Chapter 3). The ParG N-terminal mutant proteins were able to dimerise, bind DNA efficiently and act as a transcriptional repressor of the *parFGH* genes (Chapter 4). It was also observed that all of these mutant proteins were able to bundle the ParF proto-filaments and promote ParF polymerization. However, the ParF-ParG interaction appeared to be compromised due to a change in these residues. The major finding of this study so far has been the impairment in stimulation of ParF ATPase activity by the ParG mutant proteins (Chapter 5). This might explain the way these mutations confer the deficiency in plasmid partition, however to see a broader picture and to understand what happens *in vivo*, localisation of these proteins and analysis of plasmid positioning *in vivo* were investigated.

There have been several efforts to determine the intracellular localization of ParA proteins. In numerous bacteria, ParA proteins and other Walker-type ATPases play an important role in the correct positioning and segregation of chromosomal and plasmid DNA within the cell (Lutkenhaus, 2012). The selection of the division site in *E. coli* is governed by the Min proteins. MinD, an ATPase, represents a dynamic cellular element and exhibits rapid pole to pole oscillation in the cell (Raskin and de Boer, 1999). MinD associates with the membrane at the pole and alternatively with its partner proteins MinC (an inhibitor of FtsZ polymerization) or MinE (a site specific suppressor of division inhibition). It has been shown previously that MinE stimulates MinD ATPase activity which results in the dissociation of MinD from the membrane (Hu *et al.*, 2002). This dependence on the partner protein MinE is instrumental in MinD oscillation (Park *et al.*, 2011). A chromosomal ParA protein Soj, from *Bacillus subtilis* on DNA binding forms nucleoprotein complexes that dynamically relocate in the cell (Marston and Errington, 1999). The relocation of Soj is attributed to ATP hydrolysis which is dependent on partner protein Spo0J (Leonard *et al.*, 2005). ParA protein of plasmid pB171 forms cytoskeletal-like structures. In the presence of ParB and *parC* encoded by the *par2* locus of plasmid

pB171, ParA was shown to dynamically relocate over the nucleoid. The N-terminal residue Arg-26 of ParB, is essential for the ParA dynamics and changes to this conserved residue abolish ParA dynamics (Ringgaard *et al.*, 2009). Similarly, the partition protein SopA of F plasmid in *E. coli* is a member of the P-loop ATPases and in the presence of the partner protein SopB and partition site *sopC,* assembles into spindle like structures (Lim *et al.*, 2005). SopA was shown to be dynamic *in vivo* owing to its polymerization and depolymerization cycle and thus playing an important role in plasmid positioning and segregation (Lim *et al.*, 2005). However, in a cell-free system, the F plasmid partition was attributed to the concentration gradient of SopA protein and to a diffusion ratchet mechanism (Vecchiarelli *et al.*, 2013).

It has been observed that ParF polymers are dynamic and when they bind to the ParG-DNA cargo, the dynamic relocation of ParF polymers facilitates the segregation of plasmids (McLeod, B. unpublished data). It has been observed that ParF oscillates over the nucleoid in the presence of the entire *parFGH* system (B. McLeod unpublished data). It becomes essential then to analyse the phenotype of the ParG N-terminal partition deficient mutants with respect to ParF oscillation. The effect of ParG N-terminal mutant proteins on ParF localisation and oscillation is reported in this chapter in order to propose a broader role for the unstructured ParG N-terminus in plasmid partitioning.

Confocal microscopy was used as one of the methods for visualisation of ParF and ParG proteins *in vivo*. Light microscopy has always suffered from diffraction limitations since its conception, but recently new methods have been developed to overcome this constraint. These methods together are known as super resolution microscopy. To study ParF localisation and appearance in more detail *in vivo,* super resolution microscopy was conducted using an OMX microscope. The combined results from these two methods have been instrumental in understanding the segregation process of plasmid TP228 *in vivo*.

6.2 Results

6.2.1 The partition gene *parF* and partition cassette *parFGH* were cloned into vectors suitable for *in vivo* imaging

A fluorescent tagging system was used to study *in vivo* localisation of the partition proteins. The two plasmid vectors employed in the microscopy study were pBAD*parF* and pBM20, which were provided by Brett McLeod (Daniela Barilla` group, University of York) (Figure 6.1). In the vector pBAD*parF,* the fluorescent tag enhanced Green Fluorescent Protein (eGFP) encoded by the *egfp* gene was cloned in frame with *parF,* under the control of the arabinose-inducible promoter P_{BAD}. The vector pBM20 is a derivative of the partition probe vector pFH547 containing the *parFGH* cassette. The *mCherry* gene, which encodes for the mCherry fluorophore was cloned in frame with *parG* in vector pBM20. Vector pBM20 has been shown to be stable in plasmid partition assays (B. McLeod, unpublished data). Both the partition proteins fused with the fluorescent tags were found to be functional (B. McLeod, unpublished data). In the localisation study, the pBAD*parF* supplies ParF-EGFP in *trans* and it was established that in the presence of this vector the stability of pBM20 was not altered. It was also established that the signal from ParG-mCherry co-localises with the plasmid, as ParG binds to the centromere and operator sequences of the *parFGH* cassette (B. McLeod, unpublished data).

The mutant *parG* alleles, responsible for plasmid partition defects, were cloned into the vector pBM20 by digesting the mutant partition vectors (i.e. pMBL3A and all the others) with restriction enzymes *Bst*X1 and *Hpa*I and ligating the resulting 456 bp fragment into the digested vector pBM20. Screening of the clones was carried out by restriction digestion of plasmid DNA with enzymes *Hpa*I and *Bst*X1. Clones were confirmed by sequencing and named according to the mutation encoded e.g. pBM20-parGL3A. Digestion of the plasmid pMBL21A and cloning of *parG-L21A* fragment into pBM20 vector are shown in Figure 6.2 as an example, which led to the construction of the pBM20-L21A.

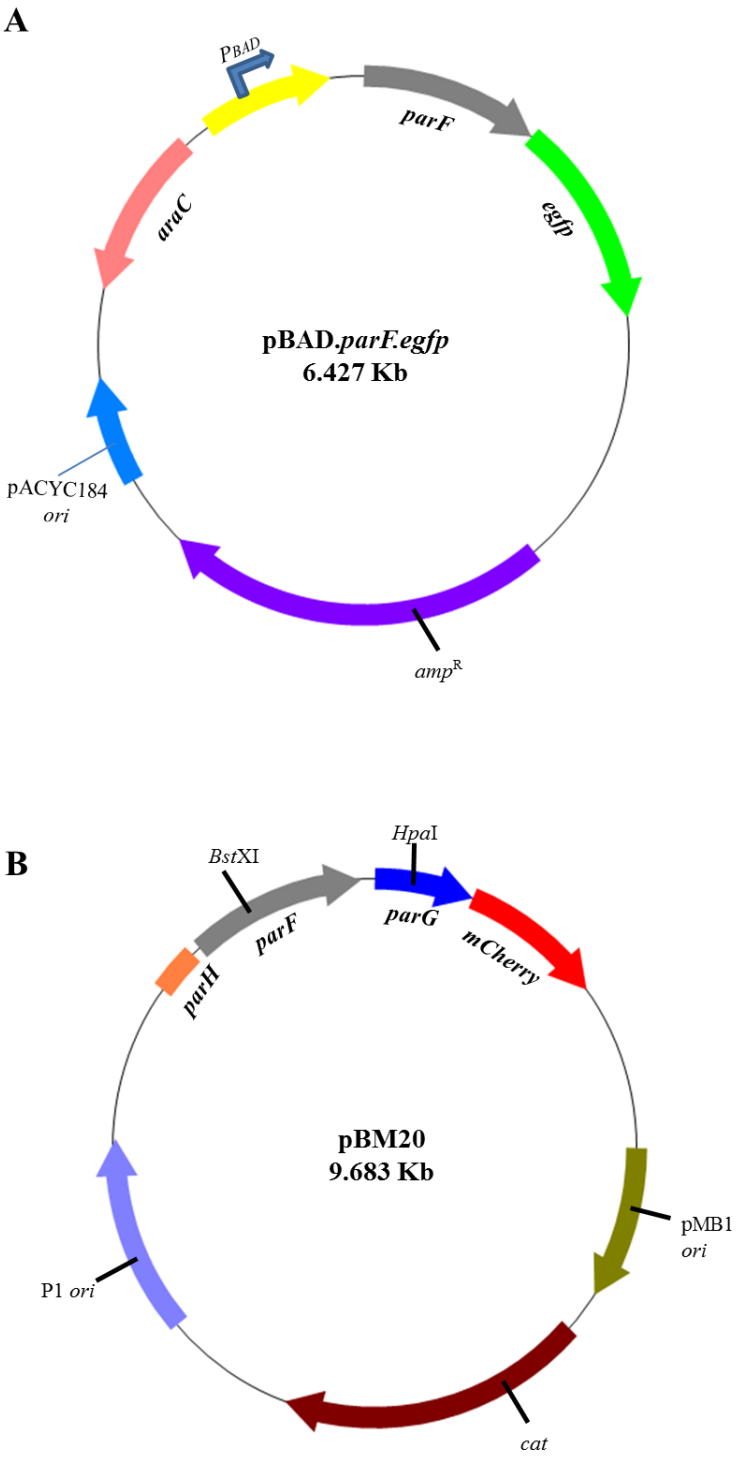

Figure 6.1. Plasmids used in the localisation of ParF and ParG proteins *in vivo*.

A. Vector pBAD-*parF* contains fusion gene *parF-eGFP* under the control of the P_{BAD} promoter. **B.** Vector pBM20 contains the wild type *parFGH* cassette and the mCherry encoding gene is cloned in frame with *parG*.

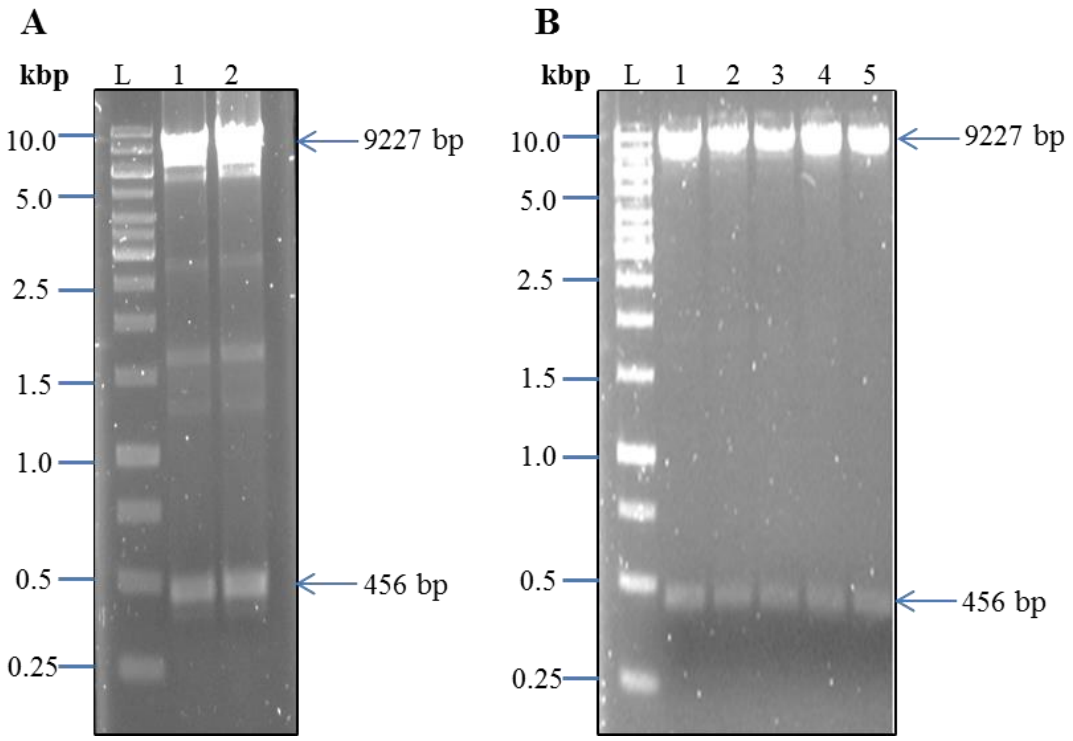

Figure 6.2. Representative agarose gels showing the digested mutant *parG* allele and the restriction digestion screen of pBM20 plasmids potentially harbouring the desired *parG* mutation.

A. Mutant *parG* fragment of 456 bp size was cleaved and cloned into pBM20 vector. Lanes: L, Gene ruler 10 kbp ladder; 1 and 2, DNA fragment generated on digestion of pMB-L21A. **B**. Restriction digest of five pBM20 constructs potentially containing the mutant *parG* allele. Lanes: L, Gene ruler 10 kbp ladder and 1-5, digested plasmids from five candidates.

6.2.2 Localisation of ParF in the cell in the presence of the ParG WT/N-terminal mutant proteins

In order to analyse how ParF drives plasmid segregation and how ParG supports this active partitioning, the dynamics of the intracellular localisation of these proteins were observed by confocal fluoroscence microscopy. *E. coli* cells (BW25113) were co-transformed with pBAD-*parF* and pBM20/pBM20-*parG* mutants and microscopy analysis was carried out. This strain supports the medium copy number plasmid replication. The cells were grown in the presence of antibiotic pressure to retain the plasmid. The analysis thus elucidate the localisation and dynamics of the partition elements rather than the actual partition process of low-copy number plasmids. It has been recently observed that ParF binds to the nucleoid *in vivo* (B. McLeod, unpublished data). To visualise the localisation of ParG, ParG mutants and ParF, with respect to the nucleoid, DAPI staining was used.

When cells were co-transformed with pBAD-*parF* and pBM20, the distribution of ParF-eGFP appeared asymmetrical over the nucleoid, as the green signal was concentrated at either side of the nucleoid. The ParG-mCherry red signal was found to be rather diffuse and present throughout the cell (Figure 6.3A). Occasionally tight foci (1, 2 or 3) were observed at various positions such as the mid-cell, near the poles, 1/4 (one quarter) or 3/4 (three quarter) of the cell length. In the presence of ParG mutant proteins, a stark contrast was observed for the ParF-eGFP signal compared to results observed in the presence of WT ParG. ParF-eGFP was distributed evenly throughout the nucleoid rather than localised at one side. ParG mutant proteins were observed predominantly as tight red foci (Figure 6.3B-I). An interesting pattern was observed with ParG-N18A. In the presence of this mutant protein, ParF formed a compact green focus overlapping with the similarly compact red focus of ParG-N18A (Figure 6.3G).

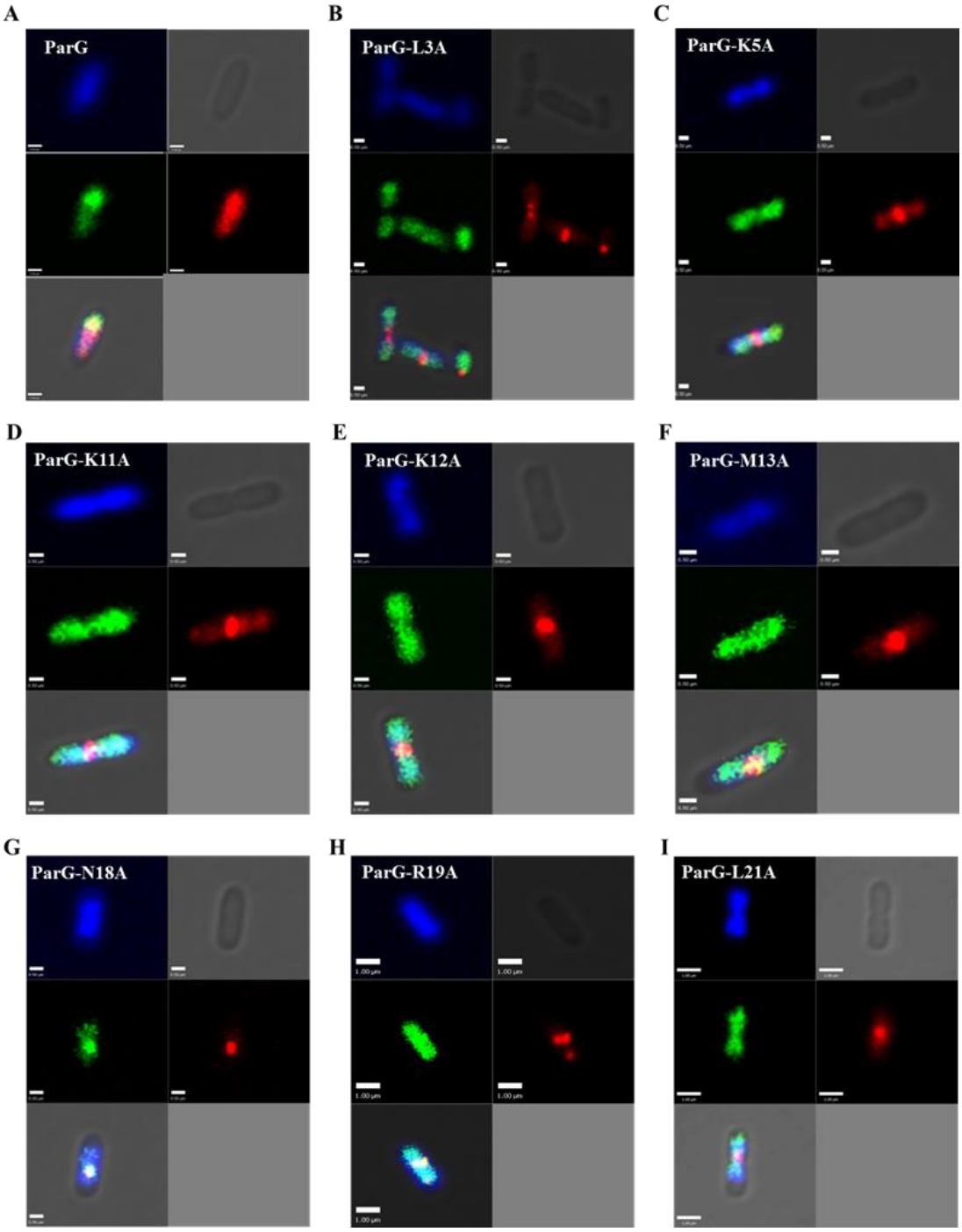

Figure 6.3. Localisation of ParF in the presence of ParG WT/ N-terminal mutant proteins over the nucleoid visualised by confocal microscopy.

Individual channels for DAPI (top-left), bright field (top-right), ParF-eGFP (middle-left), ParG-mCherry (middle-right), and merged (bottom-left) are shown. **A.** WT ParG, **B.** ParG-L3A, **C.** ParG-K5A, **D.** ParG-K11A, **E.** ParG-K12A, **F.** ParG-M13A, **G.** ParG-N18A, **H.** ParG-R19A and **I.** ParG-L21A. Scale bar=0.5 µm in A, B, C, D, E, F, G and 1 µm in H and I.

The localisation of ParF was also studied in the absence of the partner protein. When *E. coli* cells were transformed only with the pBAD-*parF* vector (thus in the absence of the full partition system), the ParF-eGFP signal appeared diffuse throughout the nucleoid (Figure 6.4A). This indicated that a functional ParG protein along with the partition site *parH* is responsible for the asymmetric distribution of ParF *in vivo*. When WT ParG and ParG mutants were analysed in the absence of ParF-eGFP by transforming *E. coli* with vector pBM20/mutant only, wild type ParG formed multiple foci over the nucleoid (Figure 6.4B), whereas the mutant proteins appeared as single, compact red foci (Figure 6.4C). The appearance of tight foci for ParG mutants was observed both in the presence and absence of ParF-eFGP. The *parFGH* cassette in pBM20 expressed the wild type ParF under the native promoter, hence absence of pBAD-*parF* does not result in lack of ParF protein in the cell.

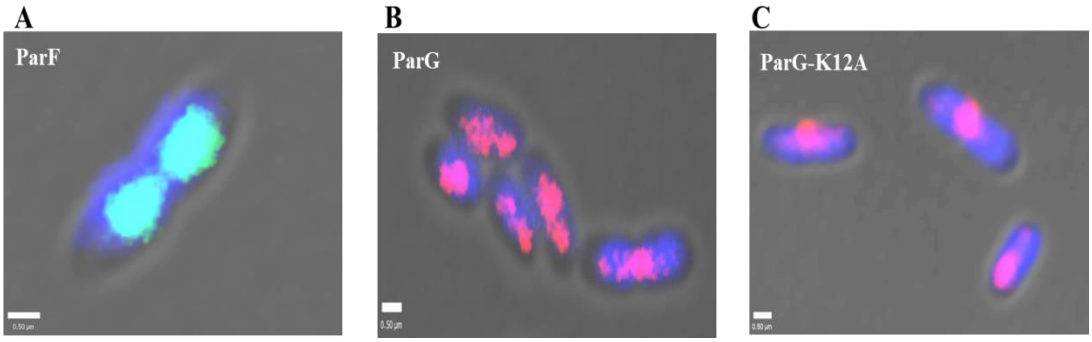

Figure 6.4. Individual localisation of ParF, ParG and ParG mutants observed by confocal microscopy.

A. *E. coli* cells harbouring only pBAD-*parF* vector show ParF spread over the whole nucleoid. **B.** *E. coli* cells harbouring only pBM20 vector show diffuse ParG. **C.** *E. coli* cells harbouring pBM20-K12A show a tight red focus. In all the images the merge of green/red signal, DAPI staining and bright field is shown. The images are representative example from the set of at least 100 cells analysed for each sample. Scale bar = 0.5 µm.

6.2.3 ParG N-terminal mutations alter the positioning of plasmid in the cell

Once the localisation of ParF and ParG proteins was determined *in vivo*, the positioning of the plasmid was scrutinised. Association of ParG with the plasmid partition site allowed tracking of the plasmid position by monitoring the ParG-mCherry red signal. Plasmid segregation is a multi-step process during which the plasmid is first located at mid-cell during replication and subsequently segregated to 1/4 or 3/4 positions of the cell, which will eventually serve as mid-cell position of the future daughter cells (Ebersbach and Gerdes, 2005). In the presence of ParF, ParG formed 1-4 foci per cell (Figure 6.5A). Although these foci looked distinct, they were diffuse. Most of the cells showed either 1 or 2 ParG foci. When there was only one focus, it appeared mostly at the mid-cell. In a cell population when two foci were observed, they were mainly located at the one quarter or three quarter location in the cell, probably taking up their position on the verge of segregation (Figure 6.5A).

The effect of partition deficient ParG N-terminal mutations on the positioning of the plasmid was also analysed (Figure 6.5Bi). Variable patterns were observed for the mutants. In the presence of ParG mutations L3A, K5A, K11A, M13A, R19A and L21A, cells with 1 to 4 red foci were observed in similar proportion. However, ParG-K12A containing cells showed mainly one or two foci in equal proportion, similarly to the pattern of wild type ParG. An unusual pattern was observed for ParG-N18A that showed over 60% of the cells harbouring a single focus, around 30% of cells showed double foci and a negligible number of cells showed 3 or 4 foci.

Whenever the cells containing plasmid with the mutations of ParG-L3A, M13A, R19A and L21A showed a single focus, it was observed that the plasmid was positioned along the entire cell length with less pronounced preference for mid-cell location as compared to cell harbouring wild type ParG. This suggested that the positioning of the plasmid was disturbed due to the effect of the mutations, when compared with wild type ParG. In the case of double foci, the plasmid localisation looked more disorganised for ParG-L3A, but ParG-R19A, ParG-M13 and ParG-L21A showed a pattern similar to that of wild type ParG.

When plasmids encoding ParG-K5A, ParG-K11A and ParG-K12A mutations coalesced as a single focus, they were positioned in a fashion similar to wild type ParG encoding plasmids i.e. at the mid-cell. In the double foci scenario, K5A resembled the pattern of wild type ParG, with plasmids at the 1/4 and 3/4 positions. However, the localisation of double foci of ParG-K11A and ParG-K12A appeared more disorganised. Plasmids harbouring ParG-N18A mutation showed the highest number of cells with single focus at mid-cell similar to wild type ParG, however the double foci scenario was not very similar to that of wild type ParG (Figure 6.5Giii, iv).

Plasmids harbouring ParG N-terminal mutations appear to be distributed more randomly along the cell length. It is possible that the movement from mid-cell to the quarter cell positions after replication and before segregation is affected. Majority of plasmids failed to reach their final destination. The randomness found in plasmid positioning suggested that plasmid transport was disrupted because of the mutation in the ParG N-terminal tail.

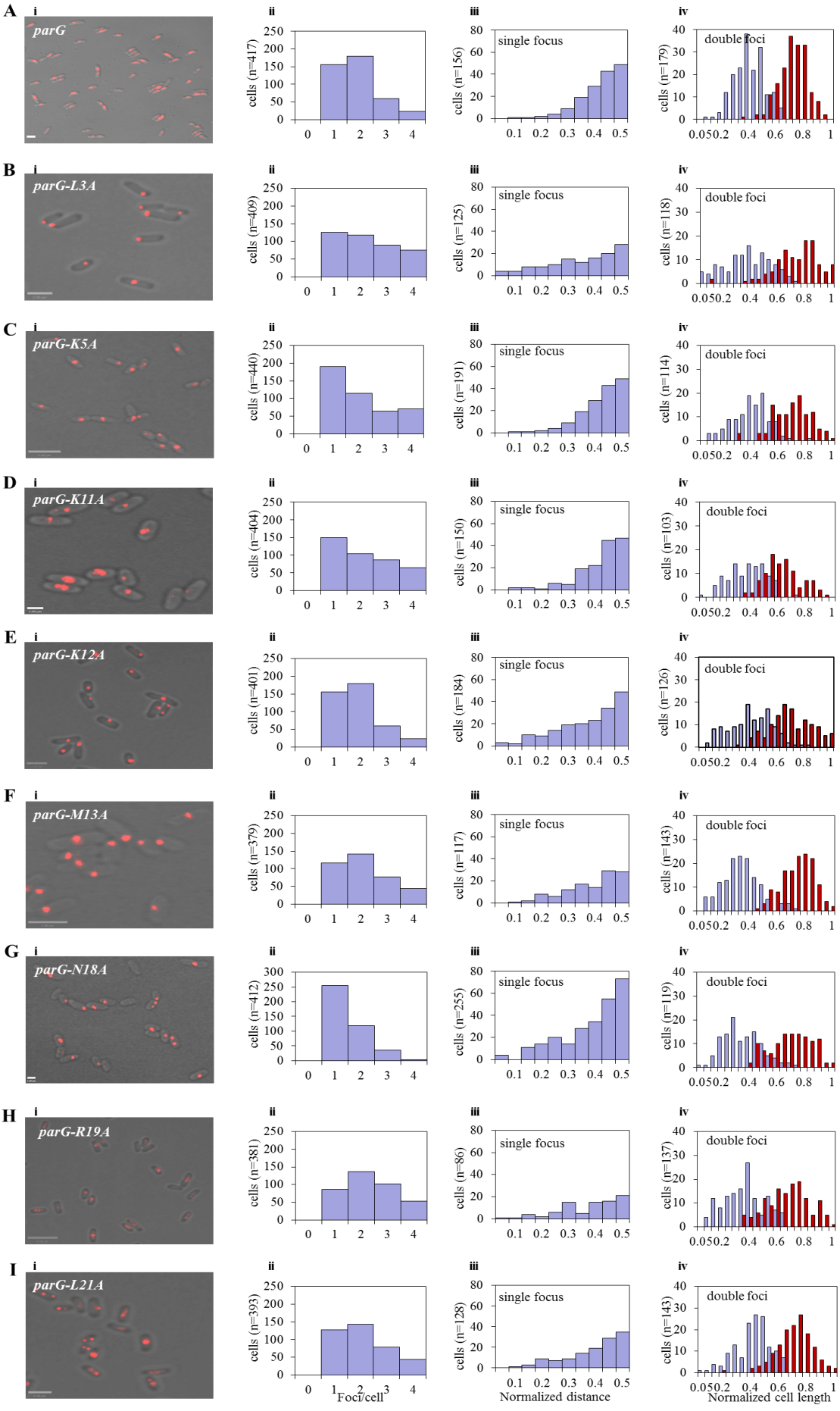
A
B
C
D
E
F
G
H
I
i
ii
iii
iv
parG
parG-L3A
parG-K5A
parG-K11A
parG-K12A
parG-M13A
parG-N18A
parG-R19A
parG-L21A
cells (n=417)
cells (n=409)
cells (n=440)
cells (n=404)
cells (n=401)
cells (n=379)
cells (n=412)
cells (n=381)
cells (n=393)
single focus
cells (n=156)
cells (n=125)
cells (n=191)
cells (n=150)
cells (n=184)
cells (n=117)
cells (n=255)
cells (n=86)
cells (n=128)
double foci
cells (n=179)
cells (n=118)
cells (n=114)
cells (n=103)
cells (n=126)
cells (n=143)
cells (n=119)
cells (n=137)
cells (n=143)
Foci/cell
Normalized distance
Normalized cell length

Figure 6.5. Effect of ParG N-terminal mutations on positioning of the plasmid containing the *parFGH* partition cassette.

Confocal microscopy snapshots of cells containing the plasmid harbouring wild type *parG* or the mutant allele and quantitative analysis of the ParG-mCherry foci localisation. The cells were co-transformed with pBAD.*parF* and pBM20-*parG*/mutant as indicated on the panels. **(i)** Snapshot of the cells from a population used for quantitative analysis. Scale bar = 1 µm in D and G, 2 µm in A, B, E, F and I, 4 µm in C and H. **(ii)** Number of ParG-mCherry foci per cell, counted for approximately 400 cells for each mutant. **(iii)** Position of single focus displayed on X-axis by taking the normalized distance from the pole in the population of cells shown in panel ii. **(iv)** Position of double foci displayed on X-axis by taking the normalised cell length in the population of cells shown in panel i.

6.2.4 ParF oscillation is abolished in the presence of ParG N-terminal mutant proteins

To examine the dynamics of the ParF-ParG localisation *in vivo*, time-lapse microscopy was employed. Cells were observed over 20 minutes and snapshots were taken at one minute intervals. Individual channels showing the ParF-eGFP and ParG-mCherry signals were aligned and are presented here to show the dynamics of the system (Figure 6.6). Over time, ParF appeared to move from one side of the nucleoid to the opposite (Figure 6.6A and movie 6.1) and this oscillation pattern was observed in approximately 70% of the cells. At the beginning (first three frames i.e. for 3 minutes) ParF-eGFP appeared to be localised at one side of the nucleoid. In the next two frames (4 and 5 minutes), the green signal gradually moved to the other side and eventually localised near the other nucleoid pole. ParF remained at this position for around 7 minutes and then began to migrate back to the opposite side of the cell. In the frames (14-19 minutes), the green signal slowly moved to the other side of the cell and before the end of 20 minutes, ParF had migrated back to the position observed at the start of the time-lapse series. Along with ParF-eGFP, the ParG-mCherry signal also relocated. (Figure 6.6B). This signal always lagged behind the ParF-eGFP green signal, which may indicate that ParF pulls the ParG-plasmid cargo during partitioning (Movie S1). ParG also appeared to be co-localised with ParF-eGFP at the start of the time sequence. After the 7^{th} minute, two ParG red foci were observed and the focus on the left side remained still till the end of the time-lapse experiment. This might suggest that ParF has placed this plasmid at its final position before cell division.

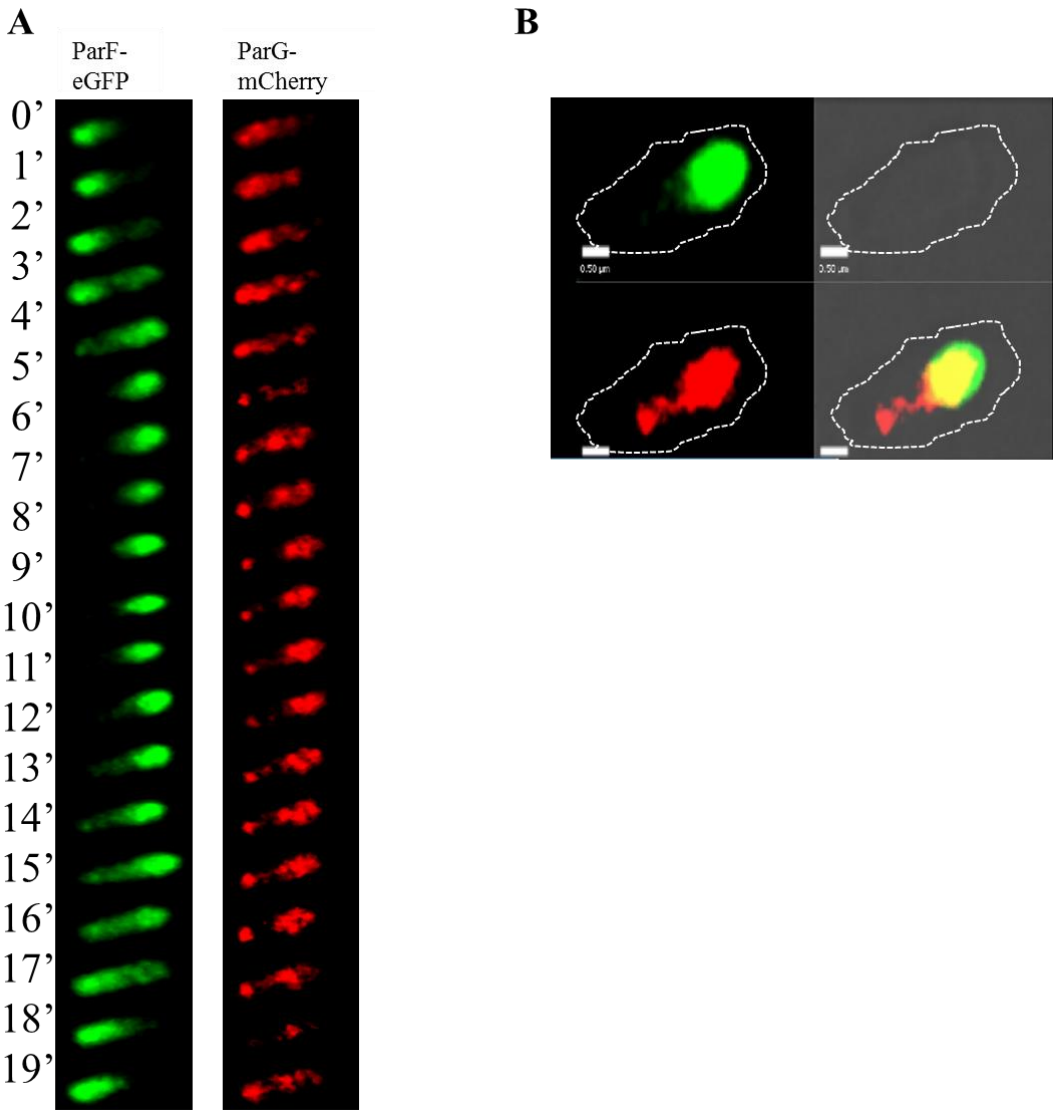

Figure 6.6. Localisation and dynamics of ParF and ParG during time-lapse microscopy.

A. A representative 20 minutes time-lapse experiment, the first column shows the ParF-eGFP signal and the second displays the ParG-mCherry signal. **B.** Snapshot of the cell during a time-lapse experiment with bright field (top-right), merged (bottom-right), mCherry (bottom- left) and eGFP (top-left) image. Scale bar = 0.5µm.

The effect of ParG N-terminal mutations on ParF oscillation was investigated by performing time-lapse experiments for each mutant. Approximately 100 cells were observed for each mutant and kymographs were generated for the ParF-eGFP signal to determine the presence of oscillation. All the movies from the 20 minute time-lapse experiments, carried out for wild type and N-terminal ParG mutants are provided as supplementary files (Movies S1-S9). Due to photo-bleaching the green signal looked weaker at later time intervals; hence sometimes the signal has to be corrected for photo-bleaching. Bacterial cells displace from their original position on agarose pad over time of 20 minutes of time-lapse experiment hence while processing the data to create time-lapse movie the displacement of the cell needs to be corrected by using Volocity software.

ParF oscillation was severely impaired in the presence of ParG mutant proteins and abolished in most of the cells containing the plasmid harbouring *parG* mutations. In comparison, 67% of the cells showed ParF oscillation in the presence of wild type ParG, whereas the percentage of cells showing ParF oscillation was much lower for the strains carrying the mutant N-terminal ParG proteins. The number of cells exhibiting ParF oscillation ranged from 1% in the presence of ParG-M13A to 15 % in the presence of ParG-K11A (Figure 6.7). ParF appears to be recruited into the defective segrosome and to remain locked in this complex displaying no movement.
The movies, S2-S9, show that ParF-eGFP did not oscillate in the presence of mutant ParG proteins. The evenly spread localisation of the ParF-eGFP signal, which is presumably bound to the nucleoid as in the snap-shots in Figure 6.3, was observed throughout the 20 minute time span for all the mutants. Even though the overall pattern was lack of ParF-eGFP oscillation, the localisation pattern of mutant ParG proteins over time was different. In the presence of ParG-L3A, ParG-M13A, ParG-R19A and ParG-L21A, ParF-eGFP was evenly distributed on both the sides over the nucleoid and made contact with mutant protein. Mutant ParG-plasmid complex was present at mid-cell without any movement towards the pole (movies S2, S6, S8 and S9). In case of ParG-K5A, ParG-K11A and ParG-K12A containing plasmids, ParF-eGFP did not co-localise with these mutant ParG proteins although sometimes ParF polymers reorganised and relocated over the nucleoid as seen in the movies S3, S4 and S5, but still ParF failed to transport the plasmid away from the mid-cell position. ParF-eGFP localisation was distinctive in the presence of ParG-N18A (movie S7).

Even though ParF-eGFP was distributed over the nucleoid, a substantial amount of ParF-eGFP co-localised with the ParG-N18A into a compact focus. This focus remained static over time and no movement was observed for plasmid and ParF. As a representative example, of the pattern displayed by the mutants, a snapshot and time-lapse of a cell harbouring the ParG-N18A mutant are shown in Figure 6.8.

Movies legend

Movies S1-S9. ParF-eGFP oscillation is disrupted in the presence of the ParG N-terminal mutant proteins *in vivo*. *E. coli* cells harbouring plasmids pBAD-*parF* and pBM20-*parG/mutant* were imaged for 20 minutes in time-lapse experiment and displayed in movies with individual bright field, red and green channels. **(S1)** ParG WT, scale bar = 1 µm. (**S2)** ParG-L3A, scale bar = 0.5 µm (**S3)** ParG-K5A, scale bar = 0.5 µm (**S4)** ParG-K11A, scale bar = 0.9 µm (**S5)** ParG-K12A, scale bar = 1 µm (**S6)** ParG-M13A, scale bar = 0.6 µm (**S7)** ParG-N18A, scale bar = 0.7 µm (**S8)** ParG-R19A, scale bar = 0.5 µm (**S9)** ParG-L21A, scale bar = 0.9 µm.

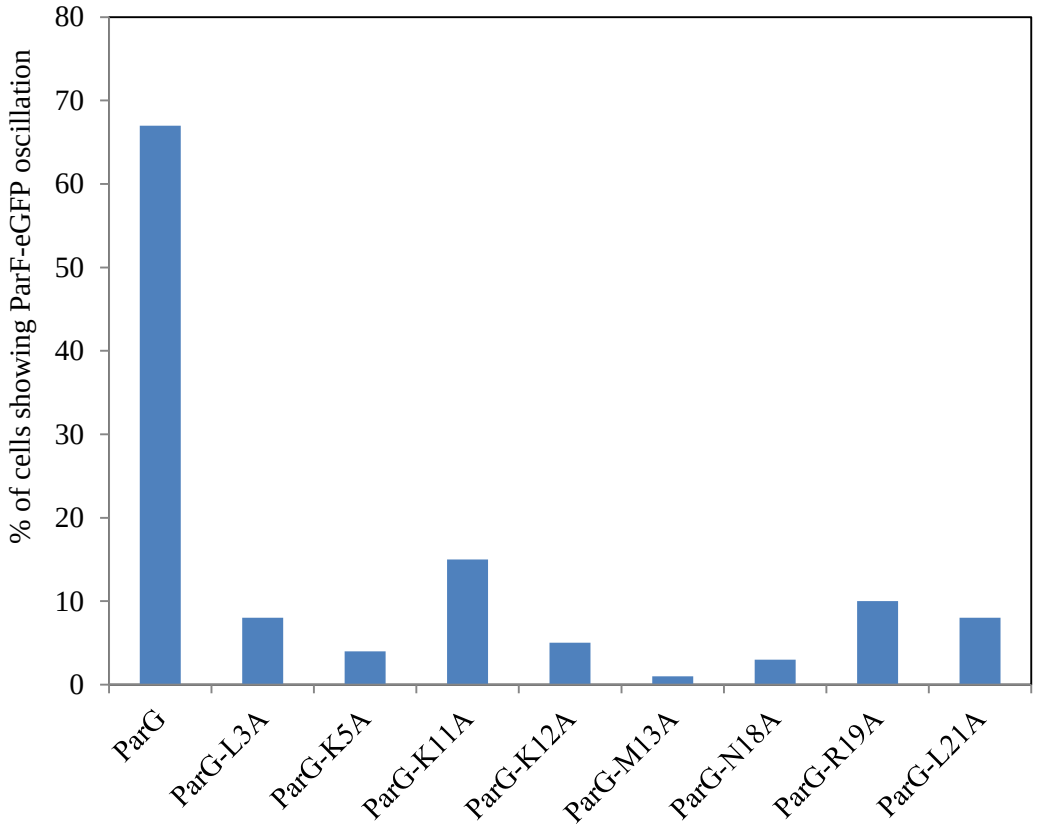

Figure 6.7. ParF does not dynamically relocate in the presence of the N-terminal ParG mutants.

Histogram showing the percentage of cells displaying ParF oscillations. The movement of the ParF signal was monitored by generating kymographs. Approximately 100 cells from at least three separate experiments were analysed for each mutant.

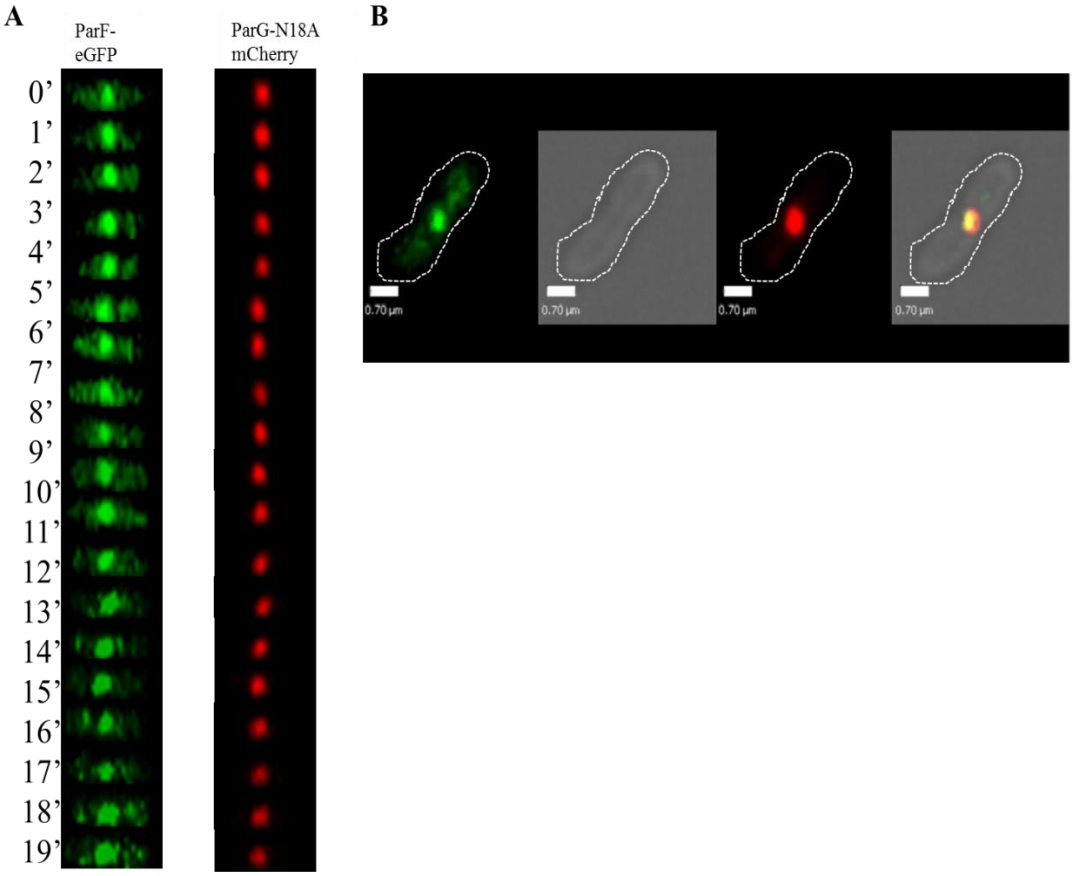

Figure 6.8. Localisation and dynamics of the ParF and ParG-N18A proteins.

A. A 20 minute time-lapse experiment. The first column shows the ParF-eGFP signal and the second is ParG-N18A-mCherry. **B.** A Snapshot of the cell from the time-lapse experiment showing eGFP, bright field, mCherry and merge channels from left to right. Scale bar = 0.7µm.

A kymograph was obtained for the ParF-eGFP green signal during the 20 minute time interval, which helped to give a graphical representation of the spatial and temporal movement of ParF (Figure 6.9). In the presence of wild type ParG, ParF showed oscillation, which produced a wave-like appearance in the kymograph. On the contrary, in the presence of ParG N-terminal mutant proteins the ParF was static and failed to show any oscillation resulting in a stationary kymograph.

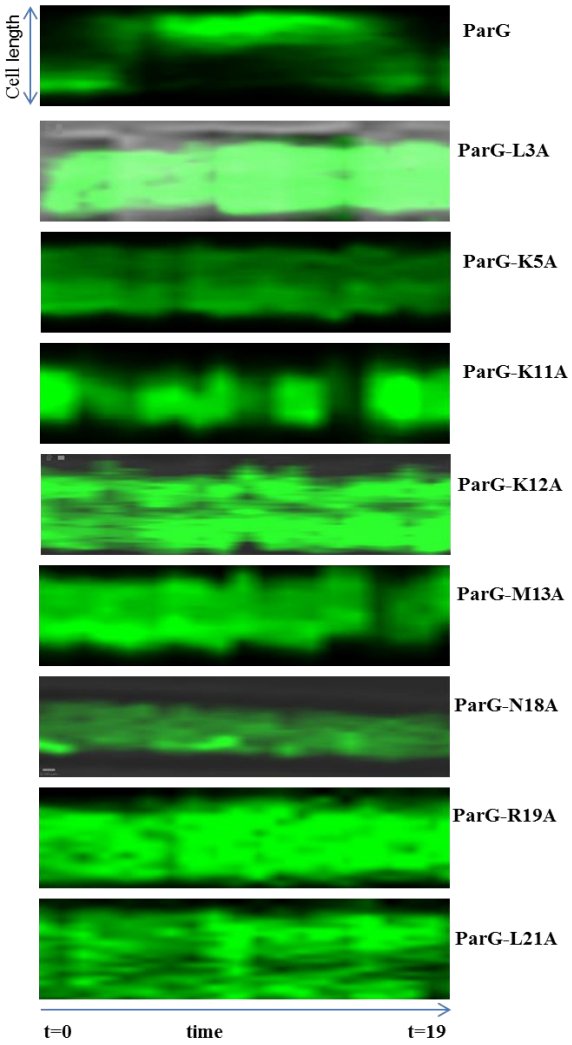

Figure 6.9. Kymograph analysis of the ParF-eGFP signal in the presence of ParG N-terminal mutant proteins during time-lapse experiment.

The movement of the ParF-eGFP signal along the cell length over time in an *E. coli* cell containing pBAD-*parF* and pBM20-*parG/mutant* plasmids is displayed. The kymographs were constructed using the same time-lapse sequence which are displayed as movies S1-S9 respectively.

6.2.5 Super resolution microscopy reveals that ParF forms a meshwork of polymers over the nucleoid

Because of the limitation of resolution, confocal microscopy does not provide fine morphological details of the proteins hence three dimensional structured illumination microscopy (3D-SIM) was employed by using an OMX (Optical Microscopy eXperimental) microscope to investigate the features of the ParF structures *in vivo*. OMX set up includes isolated components for light source, imaging, microscope control and tracing the sample (Dobbie *et al.*, 2011). In this microscopy, the lasers are beamed on the sample at multiple angles and in phases of the stripes to acquire and build up a compound image. The images have twice the resolution in the XY and Z planes after processing. Thus super resolution microscopy enhances resolution up to 100 nm in both axial and lateral directions. Approximately 50 cells were observed for each of wild type and mutant ParG containing plasmids. The images were analysed by 3D opacity using Volocity software (Perkin Elmer). As OMX microscope scans the sample for a longer interval, the photo-bleaching effect becomes a limiting factor.

The pattern of the ParF-eGFP localisation observed by OMX was found to be similar to those observed in the confocal images. When wild type ParG was present, the ParF-eGFP was distributed asymmetrically over the nucleoid (Figure 6.10). Images obtained from 3D-SIM showed ParF as a meshwork with various ParF polymers forming cable-like inter-wined structures distributed over the nucleoid. Wild type ParG-mCherry bound plasmids were located along the ParF cables. The co-localisation of multiple ParG-mCherry foci with ParF-eGFP appeared as beads on strings. A representative example of wild type ParG containing cells and the presence of ParF meshwork is given in Figure 6.10.

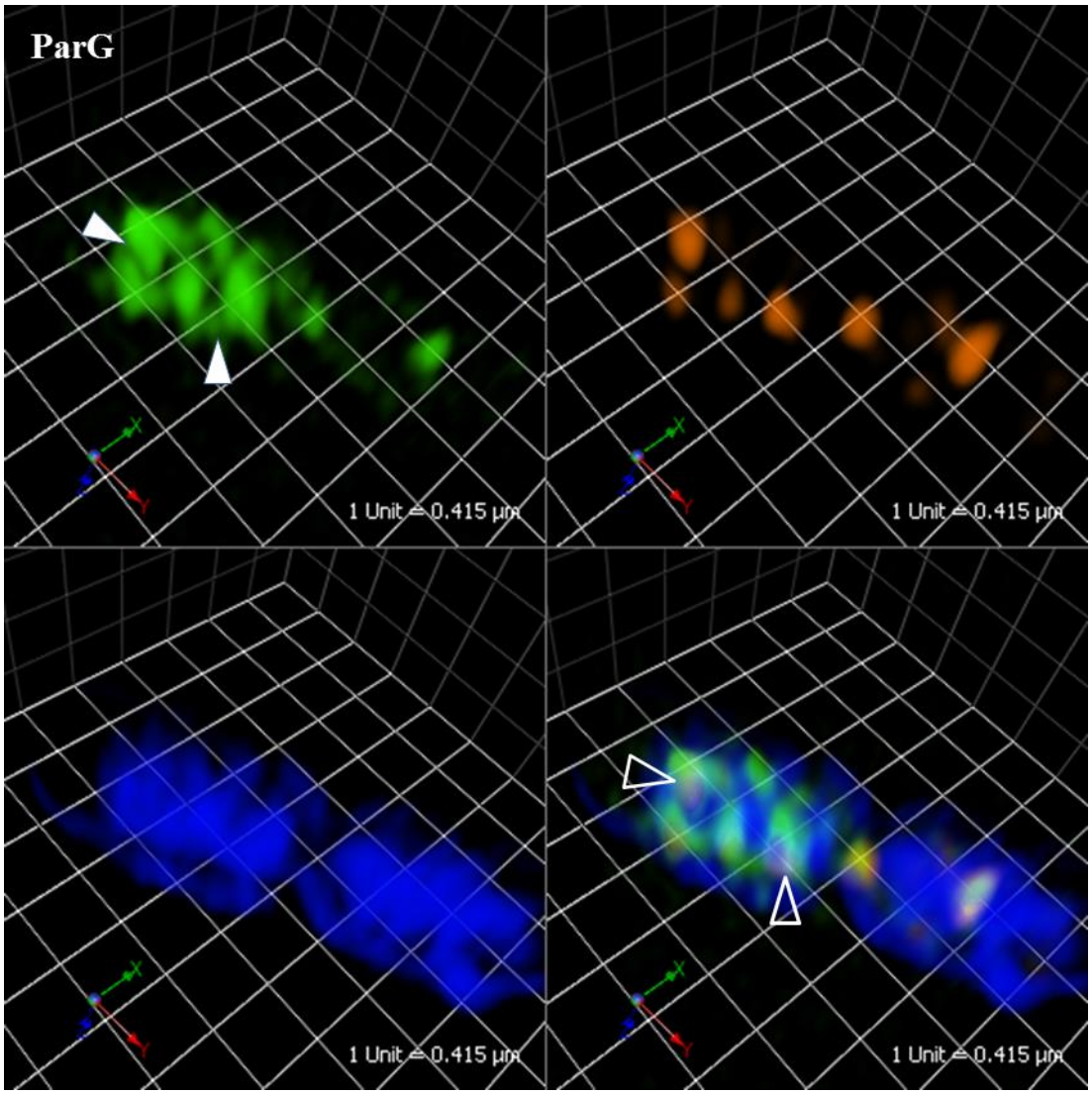

Figure 6.10. Structured illumination microscopy image of the ParF and ParG signal in *E. coli* cells.

ParF-eGFP forms an asymmetric mesh of elongated structures over the nucleoid and ParG-mCherry bound plasmids appear as compact foci along the ParF cables. The filled white arrowheads show ParF cables. Empty arrowheads show co-localisation of ParF and ParG. The channels shown are ParF-eGFP (top-left), ParG-mCherry (top-right), DAPI (bottom-left) and merged (bottom-right). Scale bar, 1 unit = 0.415 µm.

The cable-like ParF structures were also observed in the presence of ParG mutant proteins. ParG mutant proteins appeared as tight foci mainly at mid-cell position. ParG N-terminal partition deficient mutants were not impaired in promotion of ParF polymerization, hence it was not surprising to see the cable-like structure of ParF in the presence of these mutants in OMX images. Images of *E. coli* cells containing plasmids with ParG mutations were analysed by 3D opacity using Volocity software and representative examples are shown in Figure 6.11 and 6.12. Sometimes asymmetrical distribution was observed as shown for ParG-K12A. The images obtained using 3D-SIM are also shown as movies (Supplementary files, movies S10-S18). In the movies a rotation along the long axis suggests that the mesh forming cable-like ParF structures permeate the nucleoid.

Mutant ParG-mCherry bound plasmids were found at a fixed position. ParF-eGFP was evenly distributed over the nucleoid. The meshwork of ParF was visible in the presence of all the ParG mutant proteins except ParG-M13A and ParG-N18A. The absence of ParF meshwork in case of ParG-M13A cannot be established quantitatively as the sample size was small. In case of ParG-N18A, the compact focus of ParF-eGFP and lack of meshwork feature was frequently observed. This mirrors the observation made during the confocal imaging where ParF and ParG-N18A co-localised into a tight focus (Movie S7). In case of ParG-K11A sometimes two adjacent foci were observed at the mid-cell which might have arisen after replication. ParF-eGFP was spread around these ParG-K11A foci. In case of ParG-K5A and ParG-K12A, although ParF meshwork was observed over the nucleoid, the area around the plasmid was devoid of ParF-eGFP signal. During time-lapse experiment in confocal imaging, less overlap was observed between ParF-ParG-K5A and ParF-ParG-K12A (Movies S3 and S5). This might indicate towards the altered interaction between ParF and these ParG mutants. In case of ParG-R19A and ParG-L21A, co-localisation of ParF-ParG was observed. In the presence of ParG-R19A, long cables of ParF-eGFP were seen rather than a meshwork.

Chapter 6

Movies legend

Movies S10-S18. The ParF-eGFP meshwork over the nucleoid shows variation depending upon the ParG mutants. *E. coli* cells containing plasmids pBAD-*parF* and pBM20-parG/mutant were imaged on OMX microscope and displayed as a movie. **(S10)** ParG WT, Scale bar 1 unit = 0.316 µm; **(S11)** ParG-L3A, Scale bar 1 unit = 0.419 µm; **(S12)** ParG-K5A, Scale bar 1 unit = 0.581 µm; **(S13)** ParG-K11A, Scale bar 1 unit = 0.415 µm; **(S14)** ParGK12A, Scale bar 1 unit = 0.45 µm; **(S15)** ParGM13A, Scale bar 1 unit = 0.478 µm; **(S16)** ParGN18A, Scale bar 1 unit = 0.577 µm; **(S17)** ParGR19A, Scale bar 1 unit = 0.233 µm; **(S18)** ParGL21A Scale bar 1 unit = 0.517 µm.

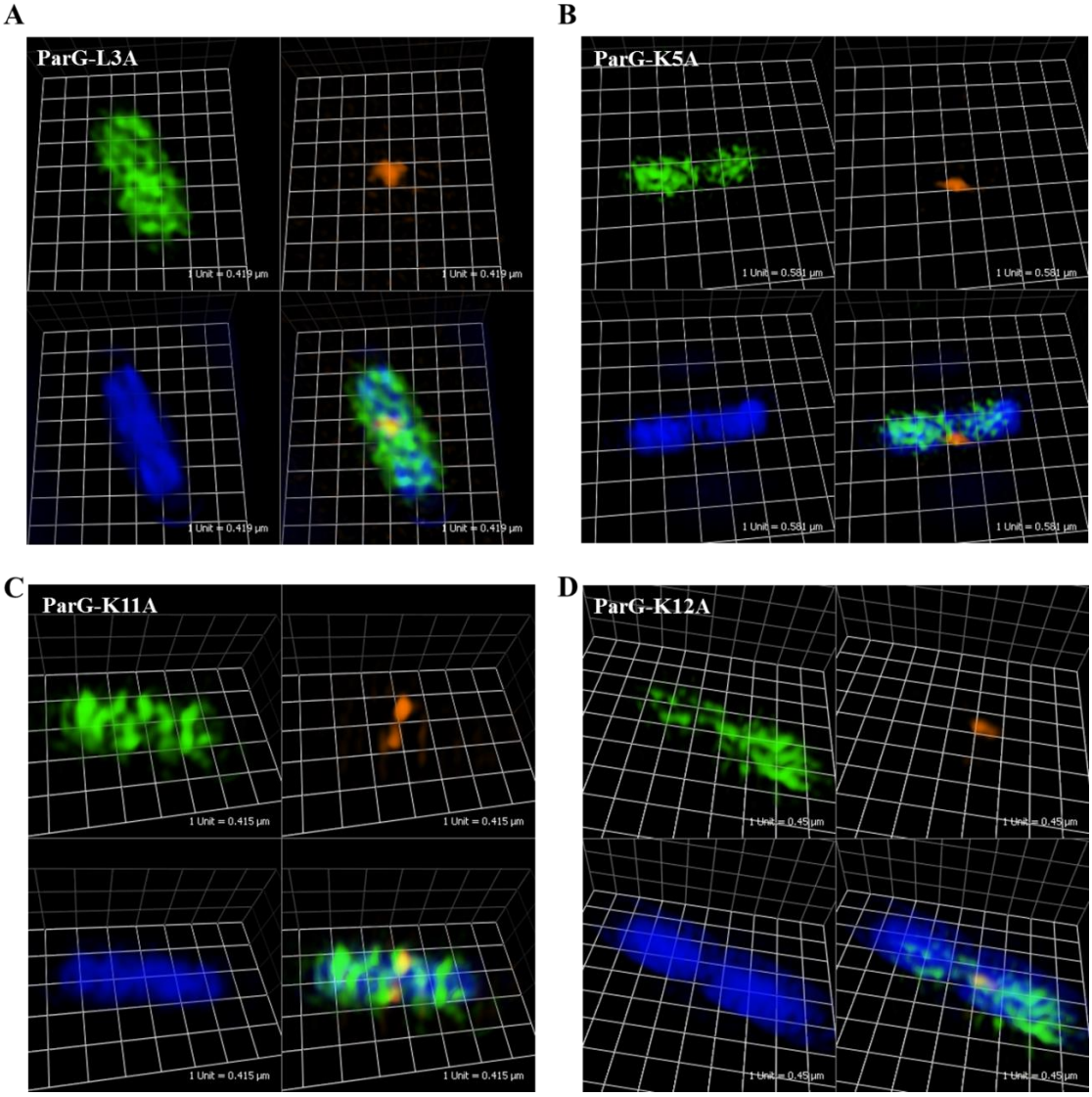

Figure 6.11. Structured illumination microscopy images of the ParF distribution in the presence of ParG mutants inside *E. coli* cells.

The channels shown are green, red, DAPI and merged in all the images. **A.** ParG-L3A, **B.** ParG-K5A, **C.** ParG-K11A, **D.** ParG-K12A. In each pannel, the channels shown are ParF-eGFP (top-left), ParGmut-mCherry (top-right), DAPI (bottom-left) and merged (bottom-right). Scale bar, 1 unit = 0.415 µm.

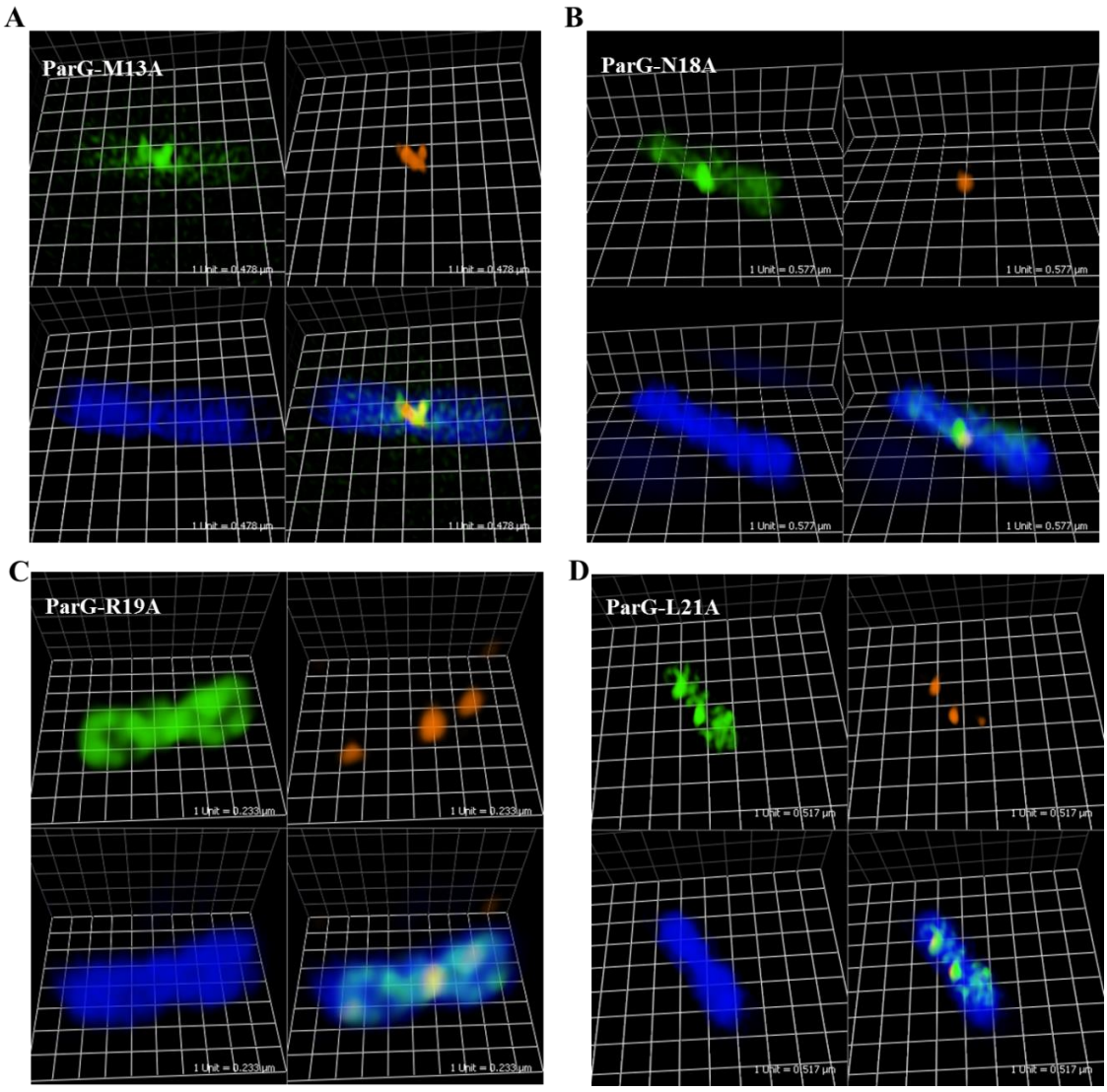

Figure 6.12. Structured illumination microscopy images of the ParF distribution in the presence of ParG mutants inside *E. coli* cells.

The channels shown are green, red, DAPI and merged in all the images. **A.** ParG-M13A, **B.** ParG-N18A, **C.** ParG-R19A, **D.** ParG-L21A. In each pannel, the channels shown are ParF-eGFP (top-left), ParGmut-mCherry (top-right), DAPI (bottom-left) and merged (bottom-right). Scale bar, 1 unit = 0.415 µm.

6.3 Conclusion

The orchestration of plasmid segregation was investigated by microscopy. ParF-eGFP appeared asymmetrically distributed over the nucleoid and ParG-mCherry appeared distinct but diffuse and located either at the mid-cell (in case of a single focus) or at 1/3 or 3/4 position. ParF-eGFP was visualised as an oscillating entity over the nucleoid during time-lapse experiment. While performing its dynamic movement ParF also transported the ParG-plasmid cargo and placed it at a site ready for segregation which indicates that ParF oscillation drives plasmid segregation. In the presence of ParG N-terminal mutants, ParF localisation was altered and it was distributed evenly throughout the nucleoid. ParG mutant proteins appeared as tight red foci and disorganised in the positioning compared to wild type ParG. The partition defective ParG N-terminal mutations caused detrimental effects on ParF oscillation. In the presence of the ParG mutant proteins, ParF polymers were locked and the oscillation was stalled. The compact nature of mutant foci pointed towards the inertness of the plasmid, as a consequence of lack of ParF oscillation. When bound to ATP, ParF dimerises and ParG stimulates the assembly of ParF into higher order structures. Partition deficient ParG N-terminal mutant proteins are able to promote ParF polymerization, hence the ParF-eGFP signal and localisation was similar in all cases. Polymeric ParF assembles onto the nucleoid, however, in the absence of stimulation of its ATPase activity by the ParG mutants, no dynamic relocation is observed. The enhancement of ParF ATP hydrolysis is likely to be a prerequisite for polymer remodelling and disassembly. Thus when this stimulation is missing, no turnover of ParF polymers and no oscillation are detected.

It was not possible to determine the effect of ParG-L21A on stimulation of ParF ATPase activity (Figure 5.10). However, as the ParF oscillation was abolished in the presence of ParG-L21A, it indicated that like other ParG mutants ParG-L21A might be impaired in stimulating ParF ATPase activity.

3D-SIM was instrumental in exploring the structural features of the ParF protein and showed ParF polymers as a mesh of inter-wined cables going through the nucleoid. The super resolution images displayed ParG mutants as tight foci.

Chapter 7: Discussion and future work

7.1 Discussion

Genome replication and segregation with high precision is a prerequisite for all living cells. Large, low copy number plasmids ensure stable inheritance of the genetic material in the daughter cells via active partition system. The partition system of plasmid TP228 investigated in this work is evolutionarily different from the P1 and F plasmids. The segregation locus *parFGH* of plasmid TP228 encodes for partition proteins ParF and ParG and the centromere-like site *parH*. ParF is a Walker-type ATPase from a ParA superfamily and it is more closely related to cell division protein MinD than P1 ParA. The centromere binding protein ParG is also unrelated to other ParB-like proteins. ParG enhances ParF polymerization and stimulates ParF ATPase activity through its unstructured N-terminus (Barillà *et al.*, 2007). The present study dissected further the role of ParG N-terminal flexible tail in the partition of plasmid TP228 and interplay between ParF and ParG proteins.

7.1.1 Single amino acid changes in the flexible ParG N-terminus affect plasmid partition

It has been previously established that the N-terminal flexible tail is necessary for ParG functions, but the importance of several individual amino acids in the flexible region is a significant finding of this study. When plasmids carrying ParG N-terminal mutations were tested for partition efficiency, residues L3, K5, K11, K12, M13, N18, R19 and L21 were found to be crucial for plasmid partition (Figure 3.8). Spectral density function calculations have shown that the first six to ten residues of the ParG N-terminus are part of the most flexible region (Golovanov *et al.*, 2003). Leucine at position 3 and lysine at position 5 fall in this region. The pair of lysines at position 11 and 12 forms an important cluster of positively charged residues in the tail along with methionine at position 13. Secondary structure prediction programmes have suggested that the region of residues 17-23 might form an α-helix with limited movement (Golovanov *et al.*, 2003). The crucial residues for plasmid partition N18, R19 and L21 are part of this less mobile region of the tail. The arginine finger formed by R19 is located in the same region and is implicated in partition (Barillà *et al.*, 2007). Depending upon their location, these crucial residues can be grouped into three clusters (Figure 7.1) -

1. Residues in the most flexible region- L3 and K5

2. Residues in the linker region- K11, K12 and M13

3. Residues in the arginine finger motif region- N18, R19 and L21

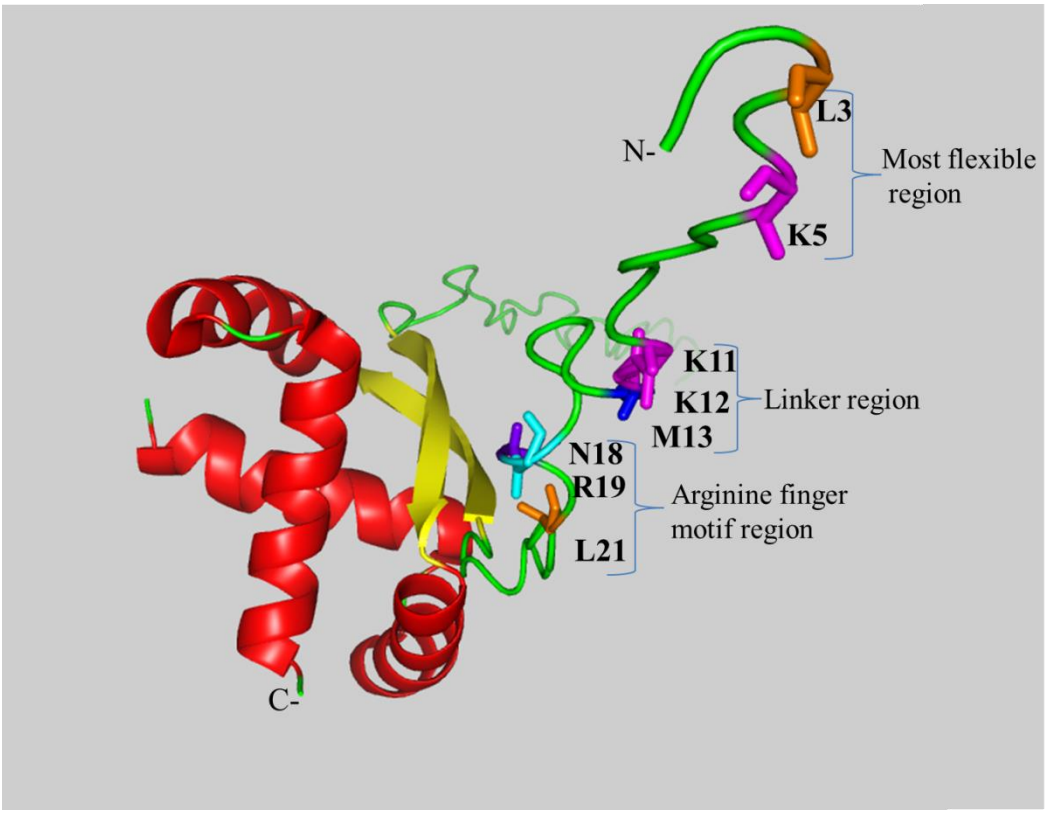

Figure 7.1. The flexible N-terminal end of ParG harbours crucial residues for plasmid partition.

The residues that cause plasmid partition defect are shown as sticks in the ribbon diagram of ParG dimer. The residues in the flexible tail (green) region can be classified into three groups depending upon their location as displayed. The structure was generated by using PyMol (DeLano, 2002).

7.1.2 ParG does not rely upon single amino acids in the N-terminus for DNA-binding and transcriptional repression functions

Across the different partition systems, the centromere binding ParB proteins and their functional homologues e.g. P1 ParB, SopB from plasmid F, omega from pSM19035, ParR from plasmid R1 and TubR from pBtoxis are present as a dimer (Moller-Jensen *et al.*, 2007, Mori *et al.*, 1989, Ni *et al.*, 2010, Surtees and Funnell, 1999, Weihofen *et al.*, 2006). ParG, like other CBPs, forms a dimer and the dimerization which is carried out by C-terminal RHH domain is required for DNA binding. The ParG N-terminal mutant proteins were also found to be able to dimerize and all the purified mutant proteins were observed as dimers although with different abilities (Figure 4.6, 4.7 and 4.9). At higher protein concentration, the ParG N-terminal mutants did not show any alteration to DNA binding (Figure 4.12). As the anti-parallel β-strands at ParG C-terminus are known to insert in the DNA major groove, the residues in the flexible region may not be required for DNA binding. ParG binding to the partition site *parH* was not tested, but as the centromere site contains repeats similar to those in the operator site, the centromere binding activity of ParG mutants is not expected to differ (Wu *et al.*, 2011a). An auto-regulatory circuit maintains the partition proteins at optimal concentration and prevents plasmid loss that may result from an excess of partition proteins (Surtees and Funnell, 2003). The ParG N-terminal tail is reported to be involved in transcriptional repression as deletion mutations in the tail resulted in decreased repression of the *parFG* promoter (Carmelo *et al.*, 2005). However, single amino acid changes in the tail did not alter the transcriptional repression activity of ParG as none of the N-terminal mutants was impaired as shown by gene reporter assays (Figure 4.14).

ParG is a sequence-specific DNA binding protein and the N-terminus region is responsible for determining the sequence specificity (Carmelo *et al.*, 2005). Unlike other DNA binding proteins in which the mobile tails become structured on DNA binding, the ParG N-terminal tail is reported to remain flexible and make transient DNA contact (Carmelo *et al.*, 2005). The chemical shift mapping of ParG-DNA interaction did not report any change in non-specific DNA interaction but specific DNA interaction for K11, K12, M13, N18 and R19 showed an increased magnitude of change indicating their role in specific DNA sequence binding (Carmelo *et al.*,

2005). In the ParB homologue, SopB from F plasmid, positively charged arginine (R219) is shown to be an essential centromere binding determinant apart from the DNA binding HTH domain. It has been proposed that the extra DNA binding domain in ParB proteins may confer high specificity (Sanchez *et al.*, 2013). On the same line, it is possible that the residues implicated in partition defect even though displaying efficient DNA binding and transcriptional repressor activity may be involved in sequence specificity. It can be speculated that the advantage of the ParG flexible region depends on the entire domain and not on a single amino acid for DNA binding and transcriptional repression functions.

7.1.3 Importance of ParG N-terminal flexible domain in enhancement of ParF polymerization and interaction with ParF

Polymerising ParA proteins are mainly involved in genome segregation in bacteria (Schumacher, 2012). Various Walker-type ParA ATPases have shown a switch in the function depending upon their ADP/ATP bound state. ParA proteins dimerise on ATP binding whereas the ADP-bound form is monomeric. Some ParA proteins in complex with ATP undergo polymerization and display a nucleoid association. ATP hydrolysis may lead to depolymerization which facilitates the transport of DNA cargo by ParA polymers (Leonard *et al.*, 2005, Lim *et al.*, 2005, Ringgaard *et al.*, 2009). In case of ParF, ATP binding results in dimerization and polymerization which is further enhanced by ParG. Interestingly, the ParF mutants that are inefficient in polymerization are responsive to ParG (Barillà *et al.*, 2005, Dobruk-Serkowska *et al.*, 2012). Thus ParF polymerization by ATP and ParG are independent of each other but are found to be additive (Dobruk-Serkowska *et al.*, 2012).

ParG bundles polymers formed due to ParF-ATP complex and none of the partition deficient single amino acid ParG mutant proteins exhibited any adverse effect on ATP-dependent ParF polymerization i.e. bundling (Figure 5.2). If ATP is absent, ParG is still able to stimulate ParF self-assembly and we defined this activity of ParG as nucleation. In the absence of ATP, ParG mutants showed a different ParF polymerization pattern. ParG-L3A and ParG-K12A lost their ability to increase ParF polymerization in the absence of ATP (Figure 5.3 and 5.6 C and F). The exact

mechanism by which leu3 and lys12 facilitate ATP independent ParF polymerization is still elusive. Moreover, ParG-K12A also showed the weakest interaction with ParF among all the mutants tested (Figure 5.7). Due to the reduced ParF-ParG-K12A interaction, ParF may be unable to form a nucleus that responds to ATP in a suitable manner leading to polymerization. When in protein sedimentation assay, ParF and ParG mutants were incubated together, the amount of ParG mutants co-precipitated with ParF was found to be less (except ParG-N18A) than that of wild type ParG (Figure 5.6). This indicated that the residues implied in the partition defect might be involved in a ParF interaction. It was also observed that the presence of ATP enhanced ParF polymerization but did not assist in facilitating the ParF-ParG interaction. The level of ParF polymerization by nucleation activity was always found to be less compared to the bundling activity. The physiological relevance of the nucleation activity of ParG is not yet established. Nevertheless, this analysis helped us to explore the ParF-ParG interaction.

In the presence of ATP, ParG enhances ParF polymerization and to do so ParG does not rely upon a single, specific residue of the N-terminal tail. ParG might use the flexible N-terminal as tentacles to bundle the ParF polymers formed by the ParF-ATP complex (Barillà *et al.*, 2007). Another RHH protein ParR from the R1 plasmid also shows a disordered tail at the C-terminus and plays an important role in stabilising ParM polymers. The flexible domain interacts with ParM and probably enforces conformational changes in the ParM polymers favourable for filament formation (Salje *et al.*, 2010). It appears that the extensions in ParB proteins might perform a architectural role in facilitating and stabilising polymerization of the partner protein.

In plasmid segregation, ParB proteins bound to the plasmid via the partition site interact with ParA proteins and form the segrosome (Hayes and Barillà, 2006b). Thus the ParA-ParB interaction is crucial step in plasmid segregation. The N-terminus of a number of other ParB proteins is implicated in interaction with ParA proteins (Leonard *et al.*, 2005, Ravin *et al.*, 2003, Surtees and Funnell, 1999). The limited flexible region containing residues 17-23 in ParG is also speculated to be a determinant of ParF interaction (Golovanov *et al.*, 2003). When ParG recruits ParF in the nucleoprotein complex to form the segrosome, it might use both C- and N-

terminal domains for ParF interaction. Thus, it seems there are multiple ParF-ParG interfaces and interactions that are used during the plasmid segregation process.

7.1.4 Stimulation of ParF ATPase activity is dependent on ParG N-terminal domain

Stimulation of nucleotide hydrolysis by the centromere binding partner is a unifying theme among ParA superfamily ATPases (Leonard *et al.*, 2005). The ParG N-terminal mutants showed impairment in stimulating ATP hydrolysis by ParF (Figure 5.9). ParG is predicted to provide the basic residues that intercalate into the nucleotide-binding pocket of ParF, thereby promoting ATP hydrolysis (Barillà *et al.*, 2007). The crucial basic residues identified in the ParG N-terminus K5, K11, K12 and R19 are located in the flexible tail, which may allow them to reach the ATP binding pocket of ParF during ATP hydrolysis. Arginine is also conserved in various other ATPase activators. In ParG, R19 acts as an arginine finger for stimulation of ParF ATPase activity (Barillà *et al.*, 2007). Residues N18 and L21 are in the region of the arginine finger motif hence altering them might change the alignment of the arginine finger loop and cause impairment in stimulation of ParF ATP hydrolysis. In MinD proteins of various bacteria, asparagine (N45 in *E. Coli* MinD) is conserved and acts to stabilise the transition state of ATP hydrolysis (Park *et al.*, 2012). It is tempting to suggest that the N18 in the ParG flexible region might be performing a similar role. How L3 and M13 are involved in stimulating ParF ATPase activity is not yet clear.

Eukaryotic RasGAPs perform a similar function in enhancing Ras GTPase activity with an invariant arginine finger residue (Resat *et al.*, 2001). Mutants of Ras are found in 25-30% of human tumours. Arg-789 of GAPs may play a dual role in generating the nucleophile as well as stabilizing the transition state for P-O bond cleavage (Resat *et al.*, 2001). The N-terminal regions of MinE and Spo0J are indicated in stimulating ATPase activity of MinD and Soj respectively and interestingly these regions are also unstructured (Ghasriani *et al.*, 2010, Leonard *et al.*, 2005). In *E. coli*, MinE might provide the basic residues (R21 and K19) for stimulating MinD ATPase activity. The basic residue near the γ-phosphate oxygen may stabilise the negative charge in a transition state (Hayashi *et al.*, 2001, Ma *et al.*,

2004). A peptide containing lysine and arginine residues stimulates the ATPase activity of Soj (Leonard *et al.*, 2005). In plasmid F, the ATPase activity of SopA was shown to be stimulated by the arginine finger R36 of partner protein SopB (Ah-Seng *et al.*, 2009). The N-terminal domain of ParB protein from plasmid pB171 is also involved in stimulation of ParA ATPase activity (Ringgaard *et al.*, 2009). The role of ParB proteins as an ATPase activator rather than a nucleotide exchanger is speculated to be favoured as it gives rise to monomeric ParA (Leonard *et al.*, 2005).

7.1.5 Role of the ParG N-terminus in ParF oscillation

Analysis of ParF localisation *in vivo*, suggested that the ability of ParF to polymerise is not the only requirement for the *parFGH* system to function, but the ability to relocate dynamically in the cell is also crucial. ParF dimerizes when bound to ATP and ParG stimulates ParF polymerization. For ParF dynamics, the next required step is the dismantling of ParF polymers. ATP hydrolysis may lead to ParF depolymerization. ParF-eGFP was shown to oscillate over the nucleoid (Figure 6.6 and movie S1). The cycle of assembly into polymers to carry plasmid and disassembly to release the cargo and relocate, is mediated by ParF oscillation. Due to the oscillation, ParF appeared asymmetrically distributed over the nucleoid in the presence of ParG bound plasmid. The plasmids were seen at 1/4 and 3/4 positions in case of wild type ParG, which indicates that the plasmids are placed at future mid-cell position by ParF (Figure 6.5A). The ParG-mCherry signal in the case of all the N-terminal mutations appeared static *in vivo* showing that the ParG bound plasmid is not transported by ParF polymers for segregation. The ParF-eGFP was evenly distributed on the nucleoid in the presence of these mutants and the level of oscillation decreased considerably compared to wild type ParG. In the absence of ParF oscillation, plasmids harbouring ParG N-terminal mutations were found to be more randomly distributed along the cell length hence ParF oscillation appeared to facilitate positioning of the plasmids at the cell quarters (Figure 6.5). ParF polymers appeared to be cable-like structures forming a mesh in 3D-SI microscopy. The ParF-eFGP mesh was spread evenly over the nucleoid around the plasmid foci in case of ParG mutants. The inert nature of plasmid when bound to mutant ParG (in the form of compact foci) was evident in both confocal and OMX microscopy experiments. Overall, similar to other ParA oscillating proteins, ParF exists in two forms, ADP-

bound and ATP-bound states. ParF–ATP may form following the exchange of ADP for ATP and ParF–ADP is formed by the hydrolysis. Combining all the observations, it can be concluded that the impairment in stimulating ParF ATPase activity demonstrated by ParG N-terminal mutants may lead to a dearth in the ParF oscillation which causes the plasmid partition defect.

Members of ParA/MinD type P loop ATPases form dimers on ATP binding which is required for anchoring them either to DNA or membrane (Hu *et al.*, 2002, Hwang *et al.*, 2013). In the case of MinD, the C-terminal amphipathic helix mediates membrane binding (Hu and Lutkenhaus, 2003), whereas the positively charged residues in the ParA proteins bind DNA non-specifically (Hester and Lutkenhaus, 2007). In the ADP-bound form, ParA/MinD proteins are shown to be monomeric and randomly diffuse in the cell. The partner proteins ParB/MinE are activators of the ATPase activity of ParA/MinD proteins (Bouet and Funnell, 1999, Hu and Lutkenhaus, 2001). ParA ATPases polymerise due to ATP, DNA or ParB interactions and *in vivo* these proteins are found to be dynamic because of the polymerization and depolymerization (Leonard *et al.*, 2005, Lim *et al.*, 2005, Ringgaard *et al.*, 2009). Chromosome segregation protein Soj in *Bacillus subtilis* is able to relocate on the nucleoid but in the absence of Spo0J, the movement ceases and Soj appears static on the nucleoid (Autret *et al.*, 2001). In plasmid pSM19035, the N-terminal region of ω is required to stimulate redistribution of δ-GFP from the nucleoid to the cell poles (Pratto *et al.*, 2008). The *E. coli* cell division regulator MinD exhibits similar oscillatory motion on a time scale of seconds due to membrane and MinE association (Raskin and de Boer, 1999). Thus, it can be supported that the movement of ParA proteins either by oscillation or by pattern formation is activated by ParB proteins.

7.1.6 How ParG N-terminus performs multiple functions

The data obtained for the residues crucial in plasmid partition reinforced that the ParG N-terminal tail is indeed multifunctional. The effect of point mutations in the ParG flexible tail on plasmid partition and on ParF related functions is presented in table 7.1.

The location of these residues within distinct clusters may indicate that ParG cleverly utilises its flexible tail to carry out multiple functions. ParG functions related to DNA-binding, transcriptional repression and enhancing ParF polymerization possibly require the entire N-terminus. The flexible domain may provide accessibility to the tail to reach its target of partition site, operator DNA sequence and the partner protein. The multifunctional nature of unstructured domain has also been reported in other ParB proteins e.g. P1 ParB and RK2 KorB (Rajasekar *et al.*, 2010, Schumacher and Funnell, 2005).

On the other hand, the role of ParG N-terminus in ParF interaction, stimulation of ParF ATPase activity and ParF oscillation appeared to be divided among its different clusters. The stimulation of ParF ATPase activity by ParG maybe a result of two effects, which are interaction and activation. The most flexible region at the tip of the tail may give the tail access to reach the ATP binding pocket of ParF. The basic residue K5 in this region may activate ATP hydrolysis by ParF. The residue L3 may be involved in ParF interaction as ParG-L3A failed to form a ParF-ParG nucleus responsible for ParF polymerization (Figure 5.3 and 5.6). The region with residues K11, K12 and M13 is a linker between the most flexible and least flexible region so this region may serve as a hinge, which may help anchoring the arginine finger motif near the ATP binding pocket of ParF. ParG-K12A showed weakest interaction with ParF (Figure 5.3, 5.6 and 5.7). Nevertheless, being basic residues, the role of K11 and K12 in activating ATP hydrolysis cannot be ruled out. Apart from stimulating ParF ATPase activity, the cluster of positively charged lysine (K11, K12) may perform additional roles. In *E. coli* MinE, the cluster of positively charged residues at positions 10-12 (RKK) is essential for membrane binding upon interaction with MinD (Hu *et al.*, 2002). In case of the Min system, the membrane acts as a scaffold, similarly, in the case of the plasmid, the nucleoid acts as a scaffold. Thus, it might be that the lysine cluster in ParG provides additional contacts with the nucleoid upon interaction with ParF. Further investigation is required now for the lysine doublet. The residues N18, R19 and L21 in the arginine finger might be direct activators of ATP hydrolysis by ParF. It is also possible that the conformational changes required for ParF interaction are brought up by the limited flexibility and formation of transient secondary structure by this region. The change in asparagine at position 18 showed the most detrimental effects on plasmid partition. The tight focus due to

ParF and ParG-N18A co-localisation *in vivo* might suggest the irreversible association between two proteins. It is possible that the residues in the ParG N-terminus are strategically placed to carry out interaction and activation functions towards the common goal of coordinated interplay with ParF for efficient plasmid segregation.

Table 7.22 Summary of the effect[1] caused by the ParG N-terminal mutants on various functions related to plasmid partition and ParF.

Mutants	Plasmid partition efficiency	Dimerization	DNA binding	Transcriptional repression	ParF bundling	ParF nucleation	ParF interaction	ParF ATPase stimulation	ParF oscillation
ParG-L3A	+++	+	+	+	+	+++	++	+++	+++
ParG-K5A	+++	+	+	+	+	++	++	+++	+++
ParG-K11A	+++	+	++	+	+	++	++	+++	+++
ParG-K12A	+++	++	+	+	+	+++	+++	+++	+++
ParG-M13A	+++	+	+	+	+	++	++	+++	+++
ParG-N18A	+++	+	+	+	+	+	++	+++	+++
ParG-R19A	+++	++	+	+	+	++	++	+++	+++
ParG-L21A	+++	+	+++	+	+	++	++	+++	+++

1 The effect of ParG mutations on various functions are indicated by traffic light colour scheme, where red corresponds to severely affected (+++), orange to moderately affected (++) and green to not affected (+).

7.1.7 Plasmid partition model

The presence of host factor in plasmid segregation has always been anticipated and now it has started emerging that the nucleoid could be that host factor which provides a scaffold for the orchestration of plasmid partition. Many ParAs bind nonspecific DNA in reversible fashion, which facilitates their movement on the nucleoid. The Par protein mediated plasmid segregation displays common features such as the use of a nucleoid as a scaffold, ADP or ATP bound form of ParA as a molecular function switch and use of disordered regions in the ParB proteins for stimulation of ParA ATPase activity. Discovery of the actin-type fold in type II ParA proteins (ParM) and tubulin-type fold in type III ParA proteins (TubZ) revealed the existence of bacterial cytoskeleton systems. These cytoskeletal-like proteins may provide the force required for plasmid segregation (Schumacher, 2012). The type I plasmid partition system is exemplified by ParA proteins which are Walker-type ATPases and proposed to be another class of cytoskeletal proteins, Walker A cytoskeletal ATPases (WACA) (Lowe and Amos, 2009). However, WACA proteins have no eukaryotic homologues. The segregation mechanism involved in the type I plasmid partition system mediated by ParA ATPases is still debated. As ParA is spread on the nucleoid, it pulls the plasmid in one direction but at the same time ParA depletion zone forms on the other side. Mathematical modelling has indicated that the continuous rounds of ParA assembly and disassembly are adequate for segregation of plasmids (Lutkenhaus, 2012). The assembly and disassembly has been demonstrated *in vivo* and *in vitro* but whether it is mediated by ParA polymerization or ParA gradient is still debated (Hwang et al., 2013; Ringgaard et al., 2009). The diffusion-ratchet mechanism is proposed for P1 plasmid partition whereas for the pB171 plasmid system a pulling model for segregation has been suggested. The presence of ParA polymers is also questioned in the P1 plasmid. In the present study, we reconfirmed the polymerization characteristic of ParF, but in contrast to the single filament reported for pB171 ParA protein, we found that ParF forms a web of cable-like polymers over the nucleoid. Based on the findings, a new model for plasmid partition is presented here (Figure 7.2).

Upon binding ATP, ParF dimerises and this may be the form favoured to bind the nucleoid. ParG binds to the partition site *parH* on the plasmid. When ParF in association with the nucleoid encounters the ParG-plasmid complex, ParF-ParG interaction results in segrosome formation. ParG may stimulate extensive ParF polymerization which might result into remodelling of ParF polymers in the form of a mesh. The ParG-plasmid cargo becomes embedded in the ParF mesh. ParG at low concentrations may enhances ParF polymerization but at high concentrations stimulates ParF ATPase activity (Barillà *et al.*, 2005). ParF has weak intrinsic ATPase activity and it needs ParG N-terminus for ATPase stimulation. Our data suggest that the lack of ParF ATPase activity abolishes ParF oscillation. ParF depolymerization results in the disassembly of the mesh and then ParF re-assembles on the other side of the nucleoid (Figure 7.2). The ParG-plasmid cargo follows ParF over the nucleoid and the cycle restarts. Thus, ParF oscillates from pole to pole on the nucleoid and transports the plasmid for segregation. ParG bound to the plasmid via the centromere site is required for ParF oscillation and in turn, oscillation helps the plasmid to be placed in a position suitable for segregation. According to our model, the ParF assembly and disassembly is mediated by the ParG N-terminus. Alterations in the N-terminus residues bring out the adverse changes in ParF localisation and oscillation. ParF polymers may remain distributed evenly on the nucleoid or are locked with ParG mutant protein as a compact body. Depending upon our data, we proposed that the functional ParG N-terminal tail is a prerequisite for ParF oscillation and plasmid segregation.

The importance of the unstructured domain in ParB proteins thus can be extended to the ParA oscillation or relocation in plasmid partition in various systems. The ParB proteins are structurally unrelated and their modes of action differ from each other for DNA binding and interaction with other partner factors. The presence of unstructured regions among ParB proteins emerges to be essential and common requirement for partitioning. The dynamics of plasmid segregation investigated in this study may also provide insights into chromosome segregation and may lead to the discovery of novel molecular targets to combat antibiotic resistance.

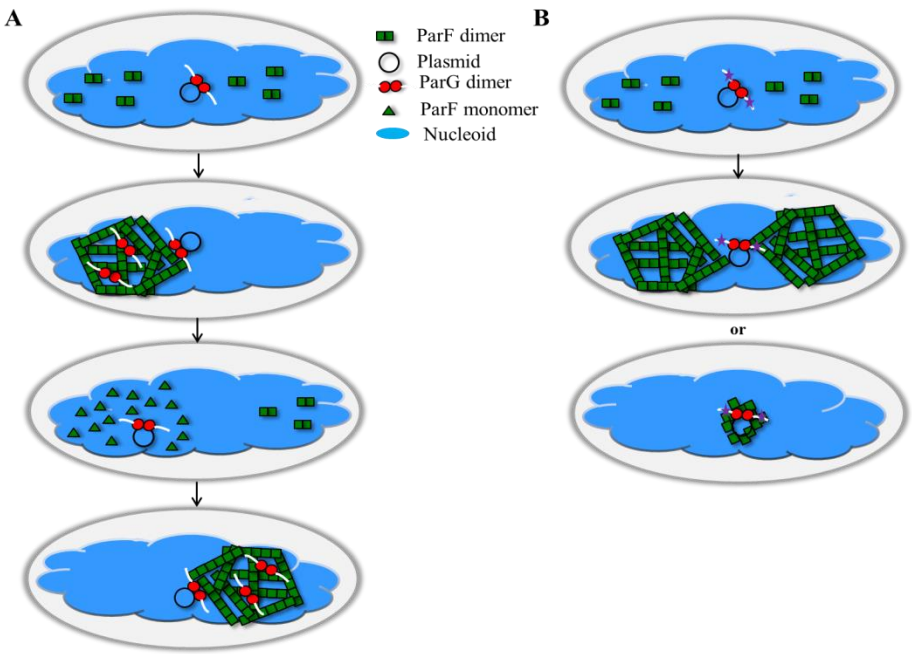

Figure 7.2. Plasmid partition model.

A. ParF in complex with ATP forms a dimer and may become associated with the nucleoid. ParG bound to the plasmid interacts with ParF and may enhance ParF polymerization and remodel ParF polymers to form a mesh. ParG stimulates ParF ATPase activity through the N- terminus, which may lead to disassembly of the ParF polymers and release of ParF-ADP. ParF again forms a complex with ATP and binds nucleoid on the other side. The ParG-plasmid cargo is transported from one side to the other on the nucleoid by ParF oscillation. **B.** If the ParG N-terminal residues are altered (denoted by purple stars) ParF polymers may distribute evenly on the nucleoid or maybe in some cases ParF is locked as an overlapping focus without any oscillatory movement hence lead to a stagnant plasmid.

7.2 Future work

The ParG N-terminal tail is multifunctional and utilises multiple mechanisms for carrying out these functions. To move forward with this acquired knowledge about the *parFGH* partition system, different aspects need to be investigated further.

DLS and sedimentation assays monitored ParF polymerization but the nature of the polymers formed was not detectable. High-magnification Electron Microscopy (EM) images showed that ParF fibres assembled in the presence of ParG were thicker and longer than those observed in its absence (Barillà *et al.*, 2005). Even though ParG mutants showed efficiency in stimulating ParF polymerization the ParF polymers formed in the presence of ParG mutant proteins might not be as thick as those assembled in the presence of WT ParG. In the absence of ATP, ParG stimulated ParF polymerization and some of the mutants showed small increase in ParF polymerization but whether the polymers formed are of the same nature or not is yet to be tested.

The ParF-ParG interaction is crucial step in plasmid segregation. The bacterial two-hybrid assay was able to indicate a weak interaction between ParF and ParG mutants in a semi-quantitative manner but to dissect the exact role of individual amino acid in plasmid partition, more detailed interaction studies need to be carried out. Initial attempts were made to check the ParF-ParG interaction by Surface Plasmon Resonance (SPR), Isothermal Titration Calorimetry (ITC) and MicroScale Thermophoresis (MST). The self-association of ParF and oligomerization of ParG posed critical problems in performing the interaction studies. However, optimising experimental conditions will assist in gaining more knowledge about the interaction pattern of the ParG mutants.

ParF has been shown to spread over the nucleoid, which indicates that ParF also binds DNA non-specifically. This additional factor in the ParF dynamics needs to be examined further by performing the ParF polymerization and ATPase activity studies in the presence of DNA. It will be interesting to find out the effect of DNA on the ParG mediated activation of ParF polymerization, ATPase activity and subsequently the influence on the functions of ParG N-terminus. This will help to gain more

insight into the mechanism of how the unstructured domain of ParG assists in plasmid partition.

The localisation of ParF and ParG investigated by using fluorescent tagging system was instrumental in this study to build a plasmid partition model. However there are still some questions that remain unanswered. The time required for actual plasmid segregation and how it is coupled with bacterial cell division has not yet been established. The set up still needs to be optimised to mimic the actual physiological conditions of plasmid maintenance in the cell. OMX contributed to find out the exact nature of ParF protein over the nucleoid. Time-lapse experiments can also be performed in OMX which can help to check and analyse ParF mesh over the time.

Abbreviations

E. coli - *Escherichia coli*

kbp - kilobase pairs

LZ - leucine zipper like

HTH - helix-turn-helix motif

θ - theta

TA - toxin-antitoxin

ATP - adenosine 5-triphosphate

CBP - centromere binding protein

RHH - ribbon-helix-helix

IHF - integration host factor

IR - inverted repeat

O_F - operator site

AMPPCP - phosphomethylphosphonic acid adenylate ester

EM - electron microscopy

LB - luria-bertani

dNTPs - deoxynucleotide triphosphates

BSA – bovine serum albumin

DLS - dynamic light scattering

ONPG - O-nitrophenyl-β-d-galactopyranoside

EMSA - electrophoretic mobility shift assay

SDS-PAGE - sodium dodecyl sulfate-polyacrylamide gel electrophoresis

kDa – kilo dalton

TLS - thin layer chromatography

DAPI - 4', 6-diamidino-2-phenylindole

3D-SIM - 3 dimensional structured illumination microscopy

MHP - molecular hydrophobicity potential

MW - molecular weight

SEC-MALLS - multi angle laser light scattering

DMP - dimethyl pimelimidate

CDO - catechol 2-3 dioxygenase

WACAs - walker A cytoskeletal ATPases

SPR - surface plasmon resonance

ITC - isothermal titration calorimetry

MST - microscale thermophoresis

References

Abeles, A. L., L. D. Reaves, B. Youngren-Grimes and S. J. Austin (1995). Control of P1 plasmid replication by iterons. *Mol Microbiol* 18(5) 903-912.

Actis, L. A., M. E. Tolmasky and J. H. Crosa (1999). Bacterial plasmids: replication of extrachromosomal genetic elements encoding resistance to antimicrobial compounds. *Front Biosci* 4 D43-62.

Ah-Seng, Y., F. Lopez, F. Pasta, D. Lane and J. Y. Bouet (2009). Dual role of DNA in regulating ATP hydrolysis by the SopA partition protein. *J Biol Chem* 284(44) 30067-30075.

Aravind, L., V. Anantharaman, S. Balaji, M. M. Babu and L. M. Iyer (2005). The many faces of the helix-turn-helix domain: transcription regulation and beyond. *FEMS Microbiol Rev* 29(2) 231-262.

Austin, S. and A. Abeles (1983). Partition of unit-copy miniplasmids to daughter cells. I. P1 and F miniplasmids contain discrete, interchangeable sequences sufficient to promote equipartition. *J Mol Biol* 169(2) 353-372.

Austin, S. and K. Nordstrom (1990). Partition-mediated incompatibility of bacterial plasmids. *Cell* 60(3) 351-354.

Austin, S., M. Ziese and N. Sternberg (1981). A novel role for site-specific recombination in maintenance of bacterial replicons. *Cell* 25(3) 729-736.

Autret, S., R. Nair and J. Errington (2001). Genetic analysis of the chromosome segregation protein Spo0J of Bacillus subtilis: evidence for separate domains involved in DNA binding and interactions with Soj protein. *Mol Microbiol* 41(3) 743-755.

Aylett, C. H., Q. Wang, K. A. Michie, L. A. Amos and J. Lowe (2010). Filament structure of bacterial tubulin homologue TubZ. *Proc Natl Acad Sci U S A* 107(46) 19766-19771.

Barillà, D., E. Carmelo and F. Hayes (2007). The tail of the ParG DNA segregation protein remodels ParF polymers and enhances ATP hydrolysis via an arginine finger-like motif. *Proc Natl Acad Sci U S A* 104(6) 1811-1816.

Barillà, D. and F. Hayes (2003). Architecture of the ParF*ParG protein complex involved in prokaryotic DNA segregation. *Mol Microbiol* 49(2) 487-499.

Barillà, D., M. F. Rosenberg, U. Nobbmann and F. Hayes (2005). Bacterial DNA segregation dynamics mediated by the polymerizing protein ParF. *EMBO J* 24(7) 1453-1464.

Biek, D. P. and J. Shi (1994). A single 43-bp sopC repeat of plasmid mini-F is sufficient to allow assembly of a functional nucleoprotein partition complex. *Proc Natl Acad Sci U S A* 91(17) 8027-8031.

Blomberg, P., E. G. Wagner and K. Nordstrom (1990). Control of replication of plasmid R1: the duplex between the antisense RNA, CopA, and its target, CopT, is processed specifically in vivo and in vitro by RNase III. *EMBO J* 9(7) 2331-2340.

Bouet, J. Y., Y. Ah-Seng, N. Benmeradi and D. Lane (2007). Polymerization of SopA partition ATPase: regulation by DNA binding and SopB. *Mol Microbiol* 63(2) 468-481.

Bouet, J. Y. and B. E. Funnell (1999). P1 ParA interacts with the P1 partition complex at parS and an ATP-ADP switch controls ParA activities. *EMBO J* 18(5) 1415-1424.

Bouet, J. Y., J. A. Surtees and B. E. Funnell (2000). Stoichiometry of P1 plasmid partition complexes. *J Biol Chem* 275(11) 8213-8219.

Bramhill, D. and A. Kornberg (1988). A model for initiation at origins of DNA replication. *Cell* 54(7) 915-918.

Carattoli, A. (2009). Resistance plasmid families in Enterobacteriaceae. *Antimicrob Agents Chemother* 53(6) 2227-2238.

Carmelo, E., D. Barillà, A. P. Golovanov, L. Y. Lian, A. Derome and F. Hayes (2005). The unstructured N-terminal tail of ParG modulates assembly of a quaternary nucleoprotein complex in transcription repression. *J Biol Chem* 280(31) 28683-28691.

Castaing, J. P., J. Y. Bouet and D. Lane (2008). F plasmid partition depends on interaction of SopA with non-specific DNA. *Mol Microbiol* 70(4) 1000-1011.

Clowes, R. C. (1972). Molecular structure of bacterial plasmids. *Bacteriol Rev* 36(3) 361-405.

Collins, E. S., S. B. Whittaker, K. Tozawa, C. MacDonald, R. Boetzel, C. N. Penfold, A. Reilly, N. J. Clayden, M. J. Osborne, A. M. Hemmings, C. Kleanthous, R. James and G. R. Moore (2002). Structural dynamics of the membrane translocation domain of colicin E9 and its interaction with TolB. *J Mol Biol* 318(3) 787-804.

Critchlow, S. E., M. H. O'Dea, A. J. Howells, M. Couturier, M. Gellert and A. Maxwell (1997). The interaction of the F plasmid killer protein, CcdB, with DNA gyrase: induction of DNA cleavage and blocking of transcription. *J Mol Biol* 273(4) 826-839.

Dafforn, T. R. and C. J. Smith (2004). Natively unfolded domains in endocytosis: hooks, lines and linkers. *EMBO Rep* 5(11) 1046-1052.

Davey, M. J. and B. E. Funnell (1994). The P1 plasmid partition protein ParA. A role for ATP in site-specific DNA binding. *J Biol Chem* 269(47) 29908-29913.

Davis, M. A., K. A. Martin and S. J. Austin (1992). Biochemical activities of the parA partition protein of the P1 plasmid. *Mol Microbiol* 6(9) 1141-1147.

del Solar, G., R. Giraldo, M. J. Ruiz-Echevarria, M. Espinosa and R. Diaz-Orejas (1998). Replication and control of circular bacterial plasmids. *Microbiol Mol Biol Rev* 62(2) 434-464.

Diago-Navarro, E., A. M. Hernandez-Arriaga, J. Lopez-Villarejo, A. J. Munoz-Gomez, M. B. Kamphuis, R. Boelens, M. Lemonnier and R. Diaz-Orejas (2010). parD toxin-antitoxin system of plasmid R1--basic contributions, biotechnological applications and relationships with closely-related toxin-antitoxin systems. *FEBS J* 277(15) 3097-3117.

Dmowski, M., I. Sitkiewicz and P. Ceglowski (2006). Characterization of a novel partition system encoded by the delta and omega genes from the streptococcal plasmid pSM19035. *J Bacteriol* 188(12) 4362-4372.

Dobbie, I. M., E. King, R. M. Parton, P. M. Carlton, J. W. Sedat, J. R. Swedlow and I. Davis (2011). OMX: a new platform for multimodal, multichannel wide-field imaging. *Cold Spring Harb Protoc* 2011(8) 899-909.

Dobruk-Serkowska, A., M. Caccamo, F. Rodriguez-Castaneda, M. Wu, K. Bryce, I. Ng, M. A. Schumacher, D. Barillà and F. Hayes (2012). Uncoupling of nucleotide hydrolysis and polymerization in the ParA protein superfamily disrupts DNA segregation dynamics. *J Biol Chem* 287(51) 42545-42553.

Dunham, T. D., W. Xu, B. E. Funnell and M. A. Schumacher (2009). Structural basis for ADP-mediated transcriptional regulation by P1 and P7 ParA. *EMBO J* 28(12) 1792-1802.

Dyson, H. J. and P. E. Wright (2005). Intrinsically unstructured proteins and their functions. *Nat Rev Mol Cell Biol* 6(3) 197-208.

Ebersbach, G. and K. Gerdes (2001). The double par locus of virulence factor pB171: DNA segregation is correlated with oscillation of ParA. *Proc Natl Acad Sci U S A* 98(26) 15078-15083.

Ebersbach, G. and K. Gerdes (2004). Bacterial mitosis: partitioning protein ParA oscillates in spiral-shaped structures and positions plasmids at mid-cell. *Mol Microbiol* 52(2) 385-398.

Ebersbach, G. and K. Gerdes (2005). Plasmid segregation mechanisms. *Annu Rev Genet* 39 453-479.

Ebersbach, G., S. Ringgaard, J. Moller-Jensen, Q. Wang, D. J. Sherratt and K. Gerdes (2006). Regular cellular distribution of plasmids by oscillating and filament-forming ParA ATPase of plasmid pB171. *Mol Microbiol* 61(6) 1428-1442.

Erdmann, N., T. Petroff and B. E. Funnell (1999). Intracellular localization of P1 ParB protein depends on ParA and parS. *Proc Natl Acad Sci U S A* 96(26) 14905-14910.

Funnell, B. E. (1991). The P1 plasmid partition complex at parS. The influence of Escherichia coli integration host factor and of substrate topology. *J Biol Chem* 266(22) 14328-14337.

Garcia de Viedma, D., R. Giraldo, G. Rivas, E. Fernandez-Tresguerres and R. Diaz-Orejas (1996). A leucine zipper motif determines different functions in a DNA replication protein. *EMBO J* 15(4) 925-934.

Garcia de Viedma, D., R. Giraldo, M. J. Ruiz-Echevarria, R. Lurz and R. Diaz-Orejas (1995a). Transcription of repA, the gene of the initiation protein of the Pseudomonas plasmid pPS10, is autoregulated by interactions of the RepA protein at a symmetrical operator. *J Mol Biol* 247(2) 211-223.

Garcia de Viedma, D., A. Serrano-Lopez and R. Diaz-Orejas (1995b). Specific binding of the replication protein of plasmid pPS10 to direct and inverted repeats is mediated by an HTH motif. *Nucleic Acids Res* 23(24) 5048-5054.

Garner, E. C., C. S. Campbell, D. B. Weibel and R. D. Mullins (2007). Reconstitution of DNA segregation driven by assembly of a prokaryotic actin homolog. *Science* 315(5816) 1270-1274.

Gerdes, K., M. Howard and F. Szardenings (2010). Pushing and pulling in prokaryotic DNA segregation. *Cell* 141(6) 927-942.

Gerdes, K. and S. Molin (1986). Partitioning of plasmid R1. Structural and functional analysis of the parA locus. *J Mol Biol* 190(3) 269-279.

Gerdes, K., P. B. Rasmussen and S. Molin (1986). Unique type of plasmid maintenance function: postsegregational killing of plasmid-free cells. *Proc Natl Acad Sci U S A* 83(10) 3116-3120.

Ghasriani, H., T. Ducat, C. T. Hart, F. Hafizi, N. Chang, A. Al-Baldawi, S. H. Ayed, P. Lundstrom, J. A. Dillon and N. K. Goto (2010). Appropriation of the MinD protein-interaction motif by the dimeric interface of the bacterial cell division regulator MinE. *Proc Natl Acad Sci U S A* 107(43) 18416-18421.

Golovanov, A. P., D. Barillà, M. Golovanova, F. Hayes and L. Y. Lian (2003). ParG, a protein required for active partition of bacterial plasmids, has a dimeric ribbon-helix-helix structure. *Mol Microbiol* 50(4) 1141-1153.

Gomis-Ruth, F. X., M. Sola, P. Acebo, A. Parraga, A. Guasch, R. Eritja, A. Gonzalez, M. Espinosa, G. del Solar and M. Coll (1998). The structure of plasmid-encoded transcriptional repressor CopG unliganded and bound to its operator. *EMBO J* 17(24) 7404-7415.

Hayashi, I., T. Oyama and K. Morikawa (2001). Structural and functional studies of MinD ATPase: implications for the molecular recognition of the bacterial cell division apparatus. *EMBO J* 20(8) 1819-1828.

Hayes, F. (2000). The partition system of multidrug resistance plasmid TP228 includes a novel protein that epitomizes an evolutionarily distinct subgroup of the ParA superfamily. *Mol Microbiol* 37(3) 528-541.

Hayes, F. (2003). Toxins-antitoxins: plasmid maintenance, programmed cell death, and cell cycle arrest. *Science* 301(5639) 1496-1499.

Hayes, F. and S. Austin (1994). Topological scanning of the P1 plasmid partition site. *J Mol Biol* 243(2) 190-198.

Hayes, F. and S. J. Austin (1993). Specificity determinants of the P1 and P7 plasmid centromere analogs. *Proc Natl Acad Sci U S A* 90(19) 9228-9232.

Hayes, F. and D. Barillà (2006a). Assembling the bacterial segrosome. *Trends Biochem Sci* 31(5) 247-250.

Hayes, F. and D. Barillà (2006b). The bacterial segrosome: a dynamic nucleoprotein machine for DNA trafficking and segregation. *Nat Rev Microbiol* 4(2) 133-143.

Hayes, F. and B. Kedzierska (2014). Regulating toxin-antitoxin expression: controlled detonation of intracellular molecular timebombs. *Toxins (Basel)* 6(1) 337-358.

Hayes, F., L. Radnedge, M. A. Davis and S. J. Austin (1994). The homologous operons for P1 and P7 plasmid partition are autoregulated from dissimilar operator sites. *Mol Microbiol* 11(2) 249-260.

Hester, C. M. and J. Lutkenhaus (2007). Soj (ParA) DNA binding is mediated by conserved arginines and is essential for plasmid segregation. *Proc Natl Acad Sci U S A* 104(51) 20326-20331.

Hirano, M., H. Mori, T. Onogi, M. Yamazoe, H. Niki, T. Ogura and S. Hiraga (1998). Autoregulation of the partition genes of the mini-F plasmid and the intracellular localization of their products in Escherichia coli. *Mol Gen Genet* 257(4) 392-403.

Hu, Z., E. P. Gogol and J. Lutkenhaus (2002). Dynamic assembly of MinD on phospholipid vesicles regulated by ATP and MinE. *Proc Natl Acad Sci U S A* 99(10) 6761-6766.

Hu, Z. and J. Lutkenhaus (2001). Topological regulation of cell division in E. coli. spatiotemporal oscillation of MinD requires stimulation of its ATPase by MinE and phospholipid. *Mol Cell* 7(6) 1337-1343.

Hu, Z. and J. Lutkenhaus (2003). A conserved sequence at the C-terminus of MinD is required for binding to the membrane and targeting MinC to the septum. *Mol Microbiol* 47(2) 345-355.

Hu, Z., C. Saez and J. Lutkenhaus (2003). Recruitment of MinC, an inhibitor of Z-ring formation, to the membrane in Escherichia coli: role of MinD and MinE. *J Bacteriol* 185(1) 196-203.

Hwang, L. C., A. G. Vecchiarelli, Y. W. Han, M. Mizuuchi, Y. Harada, B. E. Funnell and K. Mizuuchi (2013). ParA-mediated plasmid partition driven by protein pattern self-organization. *EMBO J* 32(9) 1238-1249.

Ingerson-Mahar, M. and Z. Gitai (2012). A growing family: the expanding universe of the bacterial cytoskeleton. *FEMS Microbiol Rev* 36(1) 256-266.

Ireton, K., N. W. t. Gunther and A. D. Grossman (1994). spo0J is required for normal chromosome segregation as well as the initiation of sporulation in Bacillus subtilis. *J Bacteriol* 176(17) 5320-5329.

Ivanov, V. and K. Mizuuchi (2010). Multiple modes of interconverting dynamic pattern formation by bacterial cell division proteins. *Proc Natl Acad Sci U S A* 107(18) 8071-8078.

Jensen, R. B. and K. Gerdes (1997). Partitioning of plasmid R1. The ParM protein exhibits ATPase activity and interacts with the centromere-like ParR-parC complex. *J Mol Biol* 269(4) 505-513.

Johnson, T. J. and L. K. Nolan (2009). Pathogenomics of the virulence plasmids of Escherichia coli. *Microbiol Mol Biol Rev* 73(4) 750-774.

Kalnin, K., S. Stegalkina and M. Yarmolinsky (2000). pTAR-encoded proteins in plasmid partitioning. *J Bacteriol* 182(7) 1889-1894.

Karimova, G., J. Pidoux, A. Ullmann and D. Ladant (1998). A bacterial two-hybrid system based on a reconstituted signal transduction pathway. *Proc Natl Acad Sci U S A* 95(10) 5752-5756.

Kiewiet, R., S. Bron, K. de Jonge, G. Venema and J. F. Seegers (1993). Theta replication of the lactococcal plasmid pWVO2. *Mol Microbiol* 10(2) 319-327.

Kim, S. K. and J. Shim (1999). Interaction between F plasmid partition proteins SopA and SopB. *Biochem Biophys Res Commun* 263(1) 113-117.

Knight, K. L., J. U. Bowie, A. K. Vershon, R. D. Kelley and R. T. Sauer (1989). The Arc and Mnt repressors. A new class of sequence-specific DNA-binding protein. *J Biol Chem* 264(7) 3639-3642.

Knight, K. L. and R. T. Sauer (1988). The Mnt repressor of bacteriophage P22: role of C-terminal residues in operator binding and tetramer formation. *Biochemistry* 27(6) 2088-2094.

Knight, K. L. and R. T. Sauer (1989). DNA binding specificity of the Arc and Mnt repressors is determined by a short region of N-terminal residues. *Proc Natl Acad Sci U S A* 86(3) 797-801.

Koonin, E. V. (1993). A superfamily of ATPases with diverse functions containing either classical or deviant ATP-binding motif. *J Mol Biol* 229(4) 1165-1174.

Lacatena, R. M. and G. Cesareni (1981). Base pairing of RNA I with its complementary sequence in the primer precursor inhibits ColE1 replication. *Nature* 294(5842) 623-626.

Larsen, R. A., C. Cusumano, A. Fujioka, G. Lim-Fong, P. Patterson and J. Pogliano (2007). Treadmilling of a prokaryotic tubulin-like protein, TubZ, required for plasmid stability in Bacillus thuringiensis. *Genes Dev* 21(11) 1340-1352.

Lederberg, J. (1952). Cell genetics and hereditary symbiosis. *Physiol Rev* 32(4) 403-430.

Leipe, D. D., Y. I. Wolf, E. V. Koonin and L. Aravind (2002). Classification and evolution of P-loop GTPases and related ATPases. *J Mol Biol* 317(1) 41-72.

Lemonnier, M., J. Y. Bouet, V. Libante and D. Lane (2000). Disruption of the F plasmid partition complex in vivo by partition protein SopA. *Mol Microbiol* 38(3) 493-505.

Leonard, T. A., P. J. Butler and J. Lowe (2005). Bacterial chromosome segregation: structure and DNA binding of the Soj dimer--a conserved biological switch. *EMBO J* 24(2) 270-282.

Li, Y. and S. Austin (2002a). The P1 plasmid in action: time-lapse photomicroscopy reveals some unexpected aspects of plasmid partition. *Plasmid* 48(3) 174-178.

Li, Y. and S. Austin (2002b). The P1 plasmid is segregated to daughter cells by a 'capture and ejection' mechanism coordinated with Escherichia coli cell division. *Mol Microbiol* 46(1) 63-74.

Libante, V., L. Thion and D. Lane (2001). Role of the ATP-binding site of SopA protein in partition of the F plasmid. *J Mol Biol* 314(3) 387-399.

Lim, G. E., A. I. Derman and J. Pogliano (2005). Bacterial DNA segregation by dynamic SopA polymers. *Proc Natl Acad Sci U S A* 102(49) 17658-17663.

Lim, H. C., I. V. Surovtsev, B. G. Beltran, F. Huang, J. Bewersdorf and C. Jacobs-Wagner (2014). Evidence for a DNA-relay mechanism in ParABS-mediated chromosome segregation. *Elife* 3 e02758.

Lioy, V. S., F. Pratto, A. B. de la Hoz, S. Ayora and J. C. Alonso (2010). Plasmid pSM19035, a model to study stable maintenance in Firmicutes. *Plasmid* 64(1) 1-17.

Loose, M., E. Fischer-Friedrich, J. Ries, K. Kruse and P. Schwille (2008). Spatial regulators for bacterial cell division self-organize into surface waves in vitro. *Science* 320(5877) 789-792.

Lowe, J. and L. A. Amos (2009). Evolution of cytomotive filaments: the cytoskeleton from prokaryotes to eukaryotes. *Int J Biochem Cell Biol* 41(2) 323-329.

Ludtke, D. N., B. G. Eichorn and S. J. Austin (1989). Plasmid-partition functions of the P7 prophage. *J Mol Biol* 209(3) 393-406.

Lutkenhaus, J. (2012). The ParA/MinD family puts things in their place. *Trends Microbiol* 20(9) 411-418.

Lutkenhaus, J. and M. Sundaramoorthy (2003). MinD and role of the deviant Walker A motif, dimerization and membrane binding in oscillation. *Mol Microbiol* 48(2) 295-303.

Ma, L., G. F. King and L. Rothfield (2004). Positioning of the MinE binding site on the MinD surface suggests a plausible mechanism for activation of the Escherichia coli MinD ATPase during division site selection. *Mol Microbiol* 54(1) 99-108.

Macartney, D. P., D. R. Williams, T. Stafford and C. M. Thomas (1997). Divergence and conservation of the partitioning and global regulation functions in the central control region of the IncP plasmids RK2 and R751. *Microbiology* 143 (Pt 7) 2167-2177.

Marston, A. L. and J. Errington (1999). Dynamic movement of the ParA-like Soj protein of B. subtilis and its dual role in nucleoid organization and developmental regulation. *Mol Cell* 4(5) 673-682.

Martin, K. A., S. A. Friedman and S. J. Austin (1987). Partition site of the P1 plasmid. *Proc Natl Acad Sci U S A* 84(23) 8544-8547.

Miller, M. (2009). The importance of being flexible: the case of basic region leucine zipper transcriptional regulators. *Curr Protein Pept Sci* 10(3) 244-269.

Moller-Jensen, J., J. Borch, M. Dam, R. B. Jensen, P. Roepstorff and K. Gerdes (2003). Bacterial mitosis: ParM of plasmid R1 moves plasmid DNA by an actin-like insertional polymerization mechanism. *Mol Cell* 12(6) 1477-1487.

Moller-Jensen, J., R. B. Jensen, J. Lowe and K. Gerdes (2002). Prokaryotic DNA segregation by an actin-like filament. *EMBO J* 21(12) 3119-3127.

Moller-Jensen, J., S. Ringgaard, C. P. Mercogliano, K. Gerdes and J. Lowe (2007). Structural analysis of the ParR/parC plasmid partition complex. *EMBO J* 26(20) 4413-4422.

Mori, H., A. Kondo, A. Ohshima, T. Ogura and S. Hiraga (1986). Structure and function of the F plasmid genes essential for partitioning. *J Mol Biol* 192(1) 1-15.

Mori, H., Y. Mori, C. Ichinose, H. Niki, T. Ogura, A. Kato and S. Hiraga (1989). Purification and characterization of SopA and SopB proteins essential for F plasmid partitioning. *J Biol Chem* 264(26) 15535-15541.

Murayama, K., P. Orth, A. B. de la Hoz, J. C. Alonso and W. Saenger (2001). Crystal structure of omega transcriptional repressor encoded by Streptococcus pyogenes plasmid pSM19035 at 1.5 A resolution. *J Mol Biol* 314(4) 789-796.

Neu, H. C. (1992). The crisis in antibiotic resistance. *Science* 257(5073) 1064-1073.

Ni, L., W. Xu, M. Kumaraswami and M. A. Schumacher (2010). Plasmid protein TubR uses a distinct mode of HTH-DNA binding and recruits the prokaryotic tubulin homolog TubZ to effect DNA partition. *Proc Natl Acad Sci U S A* 107(26) 11763-11768.

Nordstrom, K. and S. J. Austin (1989). Mechanisms that contribute to the stable segregation of plasmids. *Annu Rev Genet* 23 37-69.

Ogura, T. and S. Hiraga (1983). Partition mechanism of F plasmid: two plasmid gene-encoded products and a cis-acting region are involved in partition. *Cell* 32(2) 351-360.

Park, K. T., W. Wu, K. P. Battaile, S. Lovell, T. Holyoak and J. Lutkenhaus (2011). The Min oscillator uses MinD-dependent conformational changes in MinE to spatially regulate cytokinesis. *Cell* 146(3) 396-407.

Park, K. T., W. Wu, S. Lovell and J. Lutkenhaus (2012). Mechanism of the asymmetric activation of the MinD ATPase by MinE. *Mol Microbiol* 85(2) 271-281.

Popp, D., A. Narita, T. Oda, T. Fujisawa, H. Matsuo, Y. Nitanai, M. Iwasa, K. Maeda, H. Onishi and Y. Maeda (2008). Molecular structure of the ParM polymer and the mechanism leading to its nucleotide-driven dynamic instability. *EMBO J* 27(3) 570-579.

Pratto, F., A. Cicek, W. A. Weihofen, R. Lurz, W. Saenger and J. C. Alonso (2008). Streptococcus pyogenes pSM19035 requires dynamic assembly of ATP-bound ParA and ParB on parS DNA during plasmid segregation. *Nucleic Acids Res* 36(11) 3676-3689.

Quisel, J. D., D. C. Lin and A. D. Grossman (1999). Control of development by altered localization of a transcription factor in B. subtilis. *Mol Cell* 4(5) 665-672.

Rajasekar, K., S. T. Muntaha, J. R. Tame, S. Kommareddy, G. Morris, C. W. Wharton, C. M. Thomas, S. A. White, E. I. Hyde and D. J. Scott (2010). Order and disorder in the domain organization of the plasmid partition protein KorB. *J Biol Chem* 285(20) 15440-15449.

Raskin, D. M. and P. A. de Boer (1999). Rapid pole-to-pole oscillation of a protein required for directing division to the middle of Escherichia coli. *Proc Natl Acad Sci U S A* 96(9) 4971-4976.

Raumann, B. E., M. A. Rould, C. O. Pabo and R. T. Sauer (1994). DNA recognition by beta-sheets in the Arc repressor-operator crystal structure. *Nature* 367(6465) 754-757.

Ravin, N. V., J. Rech and D. Lane (2003). Mapping of functional domains in F plasmid partition proteins reveals a bipartite SopB-recognition domain in SopA. *J Mol Biol* 329(5) 875-889.

Resat, H., T. P. Straatsma, D. A. Dixon and J. H. Miller (2001). The arginine finger of RasGAP helps Gln-61 align the nucleophilic water in GAP-stimulated hydrolysis of GTP. *Proc Natl Acad Sci U S A* 98(11) 6033-6038.

Reyes-Lamothe, R., E. Nicolas and D. J. Sherratt (2012). Chromosome replication and segregation in bacteria. *Annu Rev Genet* 46 121-143.

Ringgaard, S., G. Ebersbach, J. Borch and K. Gerdes (2007). Regulatory cross-talk in the double par locus of plasmid pB171. *J Biol Chem* 282(5) 3134-3145.

Ringgaard, S., J. van Zon, M. Howard and K. Gerdes (2009). Movement and equipositioning of plasmids by ParA filament disassembly. *Proc Natl Acad Sci U S A* 106(46) 19369-19374.

Salje, J., P. Gayathri and J. Lowe (2010). The ParMRC system: molecular mechanisms of plasmid segregation by actin-like filaments. *Nat Rev Microbiol* 8(10) 683-692.

Sanchez, A., J. Rech, C. Gasc and J. Y. Bouet (2013). Insight into centromere-binding properties of ParB proteins: a secondary binding motif is essential for bacterial genome maintenance. *Nucleic Acids Res* 41(5) 3094-3103.

Schermelleh, L., P. M. Carlton, S. Haase, L. Shao, L. Winoto, P. Kner, B. Burke, M. C. Cardoso, D. A. Agard, M. G. Gustafsson, H. Leonhardt and J. W. Sedat (2008). Subdiffraction multicolor imaging of the nuclear periphery with 3D structured illumination microscopy. *Science* 320(5881) 1332-1336.

Schreiter, E. R. and C. L. Drennan (2007). Ribbon-helix-helix transcription factors: variations on a theme. *Nat Rev Microbiol* 5(9) 710-720.

Schumacher, M. A. (2007). Structural biology of plasmid segregation proteins. *Curr Opin Struct Biol* 17(1) 103-109.

Schumacher, M. A. (2008). Structural biology of plasmid partition: uncovering the molecular mechanisms of DNA segregation. *Biochem J* 412(1) 1-18.

Schumacher, M. A. (2012). Bacterial plasmid partition machinery: a minimalist approach to survival. *Curr Opin Struct Biol* 22(1) 72-79.

Schumacher, M. A. and B. E. Funnell (2005). Structures of ParB bound to DNA reveal mechanism of partition complex formation. *Nature* 438(7067) 516-519.

Schumacher, M. A., T. C. Glover, A. J. Brzoska, S. O. Jensen, T. D. Dunham, R. A. Skurray and N. Firth (2007). Segrosome structure revealed by a complex of ParR with centromere DNA. *Nature* 450(7173) 1268-1271.

Schumacher, M. A., K. M. Piro and W. Xu (2010). Insight into F plasmid DNA segregation revealed by structures of SopB and SopB-DNA complexes. *Nucleic Acids Res* 38(13) 4514-4526.

Schumacher, M. A., Q. Ye, M. T. Barge, M. Zampini, D. Barillà and F. Hayes (2012). Structural mechanism of ATP induced polymerization of the partition factor ParF: implications for DNA segregation. *J Biol Chem*.

Sherratt, D., P. Dyson, M. Boocock, L. Brown, D. Summers, G. Stewart and P. Chan (1984). Site-specific recombination in transposition and plasmid stability. *Cold Spring Harb Symp Quant Biol* 49 227-233.

Simpson, A. E., R. A. Skurray and N. Firth (2003). A single gene on the staphylococcal multiresistance plasmid pSK1 encodes a novel partitioning system. *J Bacteriol* 185(7) 2143-2152.

Somers, W. S. and S. E. Phillips (1992). Crystal structure of the met repressor-operator complex at 2.8 A resolution reveals DNA recognition by beta-strands. *Nature* 359(6394) 387-393.

Suefuji, K., R. Valluzzi and D. RayChaudhuri (2002). Dynamic assembly of MinD into filament bundles modulated by ATP, phospholipids, and MinE. *Proc Natl Acad Sci U S A* 99(26) 16776-16781.

Summers, D. K., C. W. Beton and H. L. Withers (1993). Multicopy plasmid instability: the dimer catastrophe hypothesis. *Mol Microbiol* 8(6) 1031-1038.

Summers, D. K. and D. J. Sherratt (1984). Multimerization of high copy number plasmids causes instability: CoIE1 encodes a determinant essential for plasmid monomerization and stability. *Cell* 36(4) 1097-1103.

Surtees, J. A. and B. E. Funnell (1999). P1 ParB domain structure includes two independent multimerization domains. *J Bacteriol* 181(19) 5898-5908.

Surtees, J. A. and B. E. Funnell (2003). Plasmid and chromosome traffic control: how ParA and ParB drive partition. *Curr Top Dev Biol* 56 145-180.

Tang, M., D. K. Bideshi, H. W. Park and B. A. Federici (2007). Iteron-binding ORF157 and FtsZ-like ORF156 proteins encoded by pBtoxis play a role in its replication in Bacillus thuringiensis subsp. israelensis. *J Bacteriol* 189(22) 8053-8058.

Tonthat, N. K., S. T. Arold, B. F. Pickering, M. W. Van Dyke, S. Liang, Y. Lu, T. K. Beuria, W. Margolin and M. A. Schumacher (2011). Molecular mechanism by which the nucleoid occlusion factor, SlmA, keeps cytokinesis in check. *EMBO J* 30(1) 154-164.

Uversky, V. N., C. J. Oldfield and A. K. Dunker (2005). Showing your ID: intrinsic disorder as an ID for recognition, regulation and cell signaling. *J Mol Recognit* 18(5) 343-384.

van den Ent, F., L. A. Amos and J. Lowe (2001). Prokaryotic origin of the actin cytoskeleton. *Nature* 413(6851) 39-44.

van den Ent, F., J. Moller-Jensen, L. A. Amos, K. Gerdes and J. Lowe (2002). F-actin-like filaments formed by plasmid segregation protein ParM. *EMBO J* 21(24) 6935-6943.

Vecchiarelli, A. G., Y. W. Han, X. Tan, M. Mizuuchi, R. Ghirlando, C. Biertumpfel, B. E. Funnell and K. Mizuuchi (2010). ATP control of dynamic P1 ParA-DNA interactions: a key role for the nucleoid in plasmid partition. *Mol Microbiol* 78(1) 78-91.

Vecchiarelli, A. G., L. C. Hwang and K. Mizuuchi (2013). Cell-free study of F plasmid partition provides evidence for cargo transport by a diffusion-ratchet mechanism. *Proc Natl Acad Sci U S A* 110(15) E1390-1397.

Vecchiarelli, A. G., K. C. Neuman and K. Mizuuchi (2014). A propagating ATPase gradient drives transport of surface-confined cellular cargo. *Proc Natl Acad Sci U S A* 111(13) 4880-4885.

Vecchiarelli, A. G., M. A. Schumacher and B. E. Funnell (2007). P1 partition complex assembly involves several modes of protein-DNA recognition. *J Biol Chem* 282(15) 10944-10952.

Walker, J. E., M. Saraste, M. J. Runswick and N. J. Gay (1982). Distantly related sequences in the alpha- and beta-subunits of ATP synthase, myosin, kinases and other ATP-requiring enzymes and a common nucleotide binding fold. *EMBO J* 1(8) 945-951.

Weihofen, W. A., A. Cicek, F. Pratto, J. C. Alonso and W. Saenger (2006). Structures of omega repressors bound to direct and inverted DNA repeats explain modulation of transcription. *Nucleic Acids Res* 34(5) 1450-1458.

Williams, J. J. and P. J. Hergenrother (2008). Exposing plasmids as the Achilles' heel of drug-resistant bacteria. *Curr Opin Chem Biol* 12(4) 389-399.

Wu, M., M. Zampini, M. Bussiek, C. Hoischen, S. Diekmann and F. Hayes (2011a). Segrosome assembly at the pliable parH centromere. *Nucleic Acids Res* 39(12) 5082-5097.

Wu, W., K. T. Park, T. Holyoak and J. Lutkenhaus (2011b). Determination of the structure of the MinD-ATP complex reveals the orientation of MinD on the membrane and the relative location of the binding sites for MinE and MinC. *Mol Microbiol* 79(6) 1515-1528.

Zampini, M., A. Derome, S. E. Bailey, D. Barillà and F. Hayes (2009). Recruitment of the ParG segregation protein to different affinity DNA sites. *J Bacteriol* 191(12) 3832-3841.

Zhou, H. and J. Lutkenhaus (2003). Membrane binding by MinD involves insertion of hydrophobic residues within the C-terminal amphipathic helix into the bilayer. *J Bacteriol* 185(15) 4326-4335.

Ziolkowska, K., P. Derreumaux, M. Folichon, O. Pellegrini, P. Regnier, I. V. Boni and E. Hajnsdorf (2006). Hfq variant with altered RNA binding functions. *Nucleic Acids Res* 34(2) 709-720.